

Raimund Sieder

Influence of Lengthwise Split Boards on the Mechanical Properties of Engineered Timber Products

TET 8

MONOGRAPHIC SERIES TU GRAZ
TIMBER ENGINEERING & TECHNOLOGY



Raimund Sieder

**Influence of Lengthwise Split Boards on the
Mechanical Properties of Engineered Timber Products**

Monographic Series TU Graz
Timber Engineering & Technology

Series Editors

G. Schickhofer

Institut für Holzbau und Holztechnologie

R. Brandner

Institut für Holzbau und Holztechnologie

Raimund Sieder

**Influence of Lengthwise Split Boards on the
Mechanical Properties of Engineered Timber Products**

This work is based on the dissertation “Influence of Lengthwise Split Boards on the Mechanical Properties of Engineered Timber Products”, presented at Graz University of Technology, Institute of Timber Engineering and Wood Technology in 2025.

Supervision / Assessment:

Reinhard Brandner (Graz University of Technology)
Andrea Frangi (ETH Zurich)

Cover Verlag der Technischen Universität Graz
Cover photo Wennerbrücke at St. Georgen, Styria / Austria
Source: Gerhard Schickhofer
Printed by Buchschmiede (DATAFORM Media GmbH)

2026 Verlag der Technischen Universität Graz
www.tugraz-verlag.at

Print

ISBN 978-3-99161-063-2

E-Book

ISBN 978-3-99161-064-9

DOI 10.3217/978-3-99161-063-2



This work is licensed under the Creative Commons Attribution 4.0 International (CC BY 4.0) license.
<https://creativecommons.org/licenses/by/4.0/deed.en>

This CC license does not apply to the cover, third party material (attributed to other sources) and content noted otherwise.

Preface of the Monographic Series

Composing a scientific work in terms of a dissertation constitutes a supremely personal concern of a cognition-oriented extension of knowledge. After having finalised and published such a work it is the aim to conduct a liberal, scientific discourse with an interested and objective scientific community. This circumstance together with the associated possibility to discuss this scientific work have to be accentuated especially in times where the amount of applied research is increasing. In this spirit: **The personal liberty in research starts at that point where the externally demanded applicability ends.**

With the monographic series **Timber Engineering & Technology (TET)** of the Institute of Timber Engineering and Wood Technology the publishers aim on providing the community with fundamental works of the area of expertise. With regards to content this is judged as a contribution for an outstanding and open-minded scientific discourse among experts. Citing B. von Chartes (freely translated): “...**we are like dwarfs on the shoulders of giants, so that we can see more than they, and things at a greater distance, not by virtue of any sharpness of sight on our part, or any physical distinction, but because we are carried high and raised up by their giant size.**”. Following this, today’s state-of-the-art together with the own scientific work counts as basis of the next generations, thereby providing those fundamentals what from innovations can be derived in succession.

Graz, February 2013, Univ.-Prof. Dipl.-Ing. Dr.techn. Gerhard Schickhofer

Danksagung

Ohne die Unterstützung meines Umfeldes wäre das Verfassen dieser Arbeit nicht möglich gewesen. Daher möchte ich im Folgenden all jenen danken, die mich auf diesem Weg begleitet und gestärkt haben.

Mein besonderer Dank gilt meinem Betreuer Assoc. Prof. Dipl.-Ing. (FH) Dr. techn. Reinhard Brandner, der mir mit seiner fachlichen Expertise stets zur Seite stand und wertvolle Diskussionen ermöglichte. Sein unermüdlicher Optimismus, seine gute Laune und seine ansteckende Motivation haben wesentlich dazu beigetragen, dass sich die Arbeit an diesem Thema nicht nur leichter, sondern auch mit Freude gestalten ließ.

Ebenso danke ich Herrn Univ.-Prof. Dipl.-Ing. Dr. techn. Gerhard Schickhofer, welcher mich durch die freundliche Aufnahme an seinem Institut für Holzbau und Holztechnologie hat erst die Möglichkeit gegeben die Forschung im Bereich Holzbau kennenzulernen. Für die Übernahme der Begutachtung und die motivierenden Worte in der finalen Phase danke ich herzlich Prof. Dr. Andrea Frangi.

Mein Dank gilt ebenso meinen ehemaligen Arbeitskolleginnen und -kollegen am Institut für Holzbau und Holztechnologie sowie der holz.bau forschungs GmbH für ihre Unterstützung, die anregenden Gespräche und die gemeinsam verbrachte Zeit.

Der größte Dank jedoch gebührt meinen Eltern, die mir diese Ausbildung ermöglicht und mir stets den notwendigen Rückhalt im Leben gegeben haben. Sie haben mir von Kindesbeinen an die Grundlagen für ein erfülltes und gesundes Leben vermittelt und mir alle Wege geöffnet, meinen eigenen Weg zu gehen.

Von Herzen danke ich auch meiner Frau Teresa, die mich in jeder Hinsicht unterstützt, mir den Raum geschaffen hat, mich ganz auf die Dissertation zu konzentrieren, und stets aufmunternde Worte fand, wenn diese nötig waren. Ein besonderer Dank gilt meinem Sohn Theodor – er war der letzte Anstoß, den ich brauchte, um dieses Werk zu vollenden.

Vielen Dank!

Abstract

The bending strength and elastic properties of structural engineered timber products, such as glulam (GLT) and cross laminated timber (CLT), are usually described via load-bearing models, where the tensile properties parallel to the grain of the base material boards and finger joints are used as input parameters. These models assume that the strength graded boards remain with their full cross-section in the final product. Nonetheless in some application cases, the structural timber products are lengthwise split, e.g. resawn glulam, or may contain an arbitrary share of lengthwise split lamellas, e.g. CLT beams or slabs. As a result of the splitting process of the boards or lamellas the previously assigned strength class and corresponding properties lose their validity. Such lengthwise split lamellas are also present within two novel structural products namely flex_GL T and flex_CL T which are cut from large dimensional multi-layered panels.

The first part of the thesis covers the derivation of a new probabilistic board model. This model is able to describe the distribution of knots within boards and their tensile properties parallel to the grain, not only for boards in full cross-section, but also of lengthwise split boards. The possibility to characterise such lengthwise split boards is a novelty. In combination with an additionally newly developed stochastic-numerical beam model, part two of the thesis, it enables calculating the load-bearing behaviour of beam and plate elements containing such split boards/lamellas. The new stochastic-numerical beam model allows to model the bending properties of various engineered timber products with unidirectional or orthogonal orientated boards/lamellas and is successfully validated by tests. Furthermore, the influence of lengthwise split boards/lamellas and system and size effects are analysed for each investigated product. Finally, load-bearing models and minimal geometric requirements for the newly developed flex_GL T-CL T products are presented.

Kurzfassung

Die Biegeeigenschaften von Holzbauprodukten wie Brettschichtholz (BSH; engl. GLT) und Brettsperrholz (BSP; engl. CLT) werden in der Regel mit Hilfe von Tragmodellen beschrieben, welche die Zugkenngrößen parallel zur Faser der Bretter und Keilzinkenverbindungen als Eingangsparameter nutzen. Diese Modelle gehen in der Regel davon aus, dass die festigkeitssortierten Bretter im Endprodukt in ihrem vollen Querschnitt erhalten bleiben. In einigen Anwendungsfällen sind die Holzbauprodukte jedoch längs aufgetrennt, z.B. aufgetrenntes Brettschichtholz, oder können einen zufälligen Anteil an längs aufgetrennten Brettern bzw. Lamellen enthalten, z.B. BSP als Träger oder Deckenelemente. Durch das längsweises Auftrennen der Bretter bzw. Lamellen verlieren diese ihre im Vollquerschnitt zugeordnete Festigkeitsklasse und damit verbundene Eigenschaften. Solche längs aufgetrennten Lamellen sind auch in zwei neuartigen Bauprodukten vorhanden, nämlich flex_GLT und flex_CLT, welche aus großen massiven Mehrschichtplatten gewonnen werden.

Der erste Teil der Arbeit befasst sich mit der Herleitung eines neuen probabilistischen Brettmodells. Das Modell ist in der Lage, die Verteilung der Äste in den Brettern und ihre Zugkenngrößen längs zur Faser zu beschreiben; dies für Bretter mit vollem Querschnitt, aber auch für nach der Festigkeitssortierung längs aufgetrennter Bretter. Die Charakterisierung von längs aufgetrennten Brettern ist ein Novum. In Kombination mit einem ebenfalls neu entwickeltem stochastisch-numerischen Trägermodell (Teil Zwei der Arbeit) ermöglicht es die Berechnung des Tragverhaltens von stabförmigen aber auch flächigen Holzbauprodukten, welche derartig aufgetrennte Bretter/Lamellen enthalten. Das neue stochastisch-numerische Trägermodell, erfolgreich validiert durch Versuchsergebnisse, erlaubt es die Biegeeigenschaften verschiedener Holzbauprodukte, aufgebaut aus unidirektional oder orthogonal orientierten Brettern / Lamellen zu modellieren. Darüber hinaus werden für jedes analysierte Produkt der Einfluss von aufgetrennten Brettern/Lamellen sowie System- und Größeneffekte analysiert. Schließlich werden Tragmodelle und geometrische Mindestanforderungen für die neu entwickelten flex_GLT-CLT-Produkte vorgestellt.

Content

CHAPTER 1: INTRODUCTION	1
1-1 MOTIVATION	2
1-2 OBJECTIVES.....	3
1-3 OUTLINE AND OVERVIEW	3
CHAPTER 2: PROBABILISTIC BOARD MODEL	4
2-1 INTRODUCTION AND OVERVIEW.....	5
2-2 MODEL SPECIFICATIONS.....	7
2-2.1 Weak Zones and Intermediate Zones	9
2-3 BOARD DATABASE.....	13
2-3.1 Overview.....	13
2-3.2 Sorting and Grading.....	15
2-4 GEOMETRIC PARAMETERS, DISTRIBUTIONS AND CORRELATIONS	18
2-4.1 Introduction and Overview.....	18
2-4.2 Boards in full Cross-Section Width.....	18
2-4.2.1 Influence of Board Thickness on the Geometric Parameters.....	18
2-4.2.2 Influence of the Board Width on the Geometric Parameters.....	20
2-4.3 Boards in Split Condition.....	23
2-4.3.1 Influence of lengthwise Splitting.....	23
2-4.3.2 Influence of the Position of Residual Board Pieces on the Geometric Parameters.....	26
2-4.4 Distributions of the Geometric Parameters.....	29
2-4.5 Comparison of Selected Model Parameters with the Literature	32
2-4.6 Correlation between Geometric Parameters.....	36
2-5 PROBABILISTIC REPRESENTATION OF TIMBER BOARDS	39
2-5.1 Concept of the Probabilistic Board Model.....	39
2-5.2 Model for the Geometric Parameters	41
2-5.2.1 Distributions and Hierarchical Models	41
2-5.2.2 Moments and Equi-correlation	42
2-5.2.3 Correlations between Model Parameters	46
2-5.3 Dynamic Modulus of Elasticity	49
2-5.4 Allocation of Material Properties	50
2-6 BOARD GENERATION PROCESS AND PROPERTIES.....	51
2-7 APPLICATION & VALIDATION OF THE PROBABILISTIC BOARD MODEL	54

2-7.1	Boards in Full Width.....	54
2-7.1.1	Influence of the Board Width w_b at Reference Board Length of $l_{b,ref} = 9 \cdot w_b$	55
2-7.1.2	Influence of the Board Width w_b at fixed Board Lengths	56
2-7.1.3	Influence of the Board Length.....	58
2-7.1.4	Influence of the Reference Board Length.....	59
2-7.2	Boards in Split Condition.....	61
2-7.2.1	Influence of Lengthwise Splitting of Boards	61
2-7.2.2	Validation of the Influence of Lengthwise Splitting of Boards.....	62
2-8	CHARACTERISATION OF FINGER JOINTS.....	65
2-8.1	Tensile Properties of Finger Joints	65
2-8.2	Positioning of Finger Joints.....	67
2-9	BENDING STRENGTH OF SIMULATED BOARDS	69
2-10	INTERMEDIATE CONCLUSIONS	70
	CHAPTER 3: STOCHASTIC-NUMERICAL BEAM MODEL.....	72
3-1	INTRODUCTION AND OVERVIEW	73
3-2	VIRTUAL PRODUCTION PROCESS.....	74
3-2.1	Multi-Layered Panels (MLP)	74
3-2.2	Beam Elements.....	76
3-2.3	Special Cases	77
3-3	STOCHASTIC-NUMERICAL BEAM MODEL	77
3-3.1	Basic Principles	77
3-3.2	Stochastic-Numerical Model for the Bending Strength.....	80
	CHAPTER 4: UNIDIRECTIONALLY LAMINATED ENGINEERED TIMBER PRODUCTS. 83	
4-1	OVERVIEW.....	84
4-2	GLULAM.....	84
4-2.1	Glulam – Flatwise Loaded Lamellas	84
4-2.1.1	Bending Properties of Glulam	84
4-2.1.2	Load-Bearing Models for the Bending Strength of Glulam Beams.....	88
4-2.2	Glulam – Edgewise Loaded Lamellas	91
4-2.3	Glulam – Flatwise vs. Edgewise Loaded Lamellas	95
4-2.4	Resawn Glulam	97
4-2.4.1	Glulam in Split Condition.....	97
4-2.4.2	Comparison with Previous Investigations	100
4-2.4.3	Load-Bearing Models for the Bending Strength of Resawn Glulam Beams.....	101

4-3	FLEX_GLT.....	104
4-3.1	Type A – Edgewise Loaded Lamellas.....	104
4-3.1.1	Bending Properties of flex_GLT type A.....	104
4-3.1.2	Load-Bearing Models for the Bending Strength of flex_GLT type A Beams	109
4-3.2	Type B – Flatwise Loaded Lamellas.....	112
4-3.2.1	Bending Properties of flex_GLT type B	112
4-3.2.2	Load-Bearing Models for the Bending Strength of flex_GLT type B Beams	116
4-4	INTERMEDIATE CONCLUSIONS.....	118
CHAPTER 5: ORTHOGONALLY LAMINATED ENGINEERED TIMBER PRODUCTS.....		121
5-1	OVERVIEW.....	122
5-2	FLEX_CLT	122
5-2.1	flex_CLT beams – Edgewise Loaded Lamellas.....	123
5-2.1.1	Bending Properties of flex_CLT beams	123
5-2.1.2	Load-Bearing Models for the Bending Strength of flex_CLT beams.....	128
5-2.2	flex_CLT slabs – Flatwise Loaded Lamellas	130
5-2.2.1	Bending Properties of flex_CLT slabs	130
5-2.2.2	Load-Bearing Models for the Bending Strength of flex_CLT slabs	134
5-3	INTERMEDIATE CONCLUSIONS.....	136
CHAPTER 6: SUMMARY, CONCLUSIONS AND OUTLOOK.....		139
6-1	SUMMARY AND CONCLUSIONS.....	140
6-2	OUTLOOK.....	142
CHAPTER 7: REFERENCES.....		143
ANNEX A: LIST OF NOTATIONS AND ABBREVIATIONS		A-1
A-1	LATIN UPPER-CASE LETTERS.....	A-2
A-2	LATIN LOWER-CASE LETTERS	A-3
A-3	GREEK LETTERS.....	A-6
ANNEX B: FORMULAS.....		B-8
B-1	HIERARCHICAL MODELS FOR DISTRIBUTIONS & STATISTICAL VALUES	B-9
B-1.1	Lognormal Distribution	B-9
B-1.2	Beta Distribution	B-9
B-1.3	Gamma Distribution.....	B-10
B-1.4	Coefficient of determination.....	B-10
B-2	CROSS-SECTION VALUES.....	B-11
B-2.1	Beams with Unidirectional Layers	B-11

B-2.2	Beams with Orthogonal Layers & Edgewise Loaded Boards	B-12
B-2.3	Slabs with Orthogonal Layers & Flatwise Loaded Boards.....	B-13
ANNEX C: PLOTS		C-15
C-1	PROBABILISTIC BOARD MODEL	C-16
C-1.1	Influence of the Board Thickness on the Model Parameters.....	C-16
C-1.2	Influence of the Board Width on the Model Parameters	C-19
C-1.3	Influence of lengthwise Splitting on the Model Parameters	C-22
C-1.4	Correlation of Model Parameters.....	C-25
ANNEX D: TABLES		D-30
D-1	PROBABILISTIC BOARD MODEL	D-31
D-1.1	Influence of the Board Thickness on the Model Parameters.....	D-31
D-1.2	Influence of the Board Width on the Model Parameters	D-33
D-1.3	Influence of lengthwise Splitting on the Model Parameters	D-35
D-1.4	Boards in Full Cross-Section Width.....	D-37
D-1.5	Boards in Split Condition.....	D-39
D-2	INPUT PARAMETERS FOR THE LOAD-BEARING MODELS	D-41
D-3	UNIDIRECTIONAL LAMINATED ENGINEERED TIMBER PRODUCTS	D-42
D-3.1	Glulam – Flatwise Loaded Lamellas	D-42
D-3.2	Flex_GLT – type A – Edgewise Loaded Lamellas	D-42
D-3.3	Flex_GLT – type B – Flatwise Loaded Lamellas	D-44
D-4	ORTHOGONALLY ENGINEERED TIMBER PRODUCTS	D-46
D-4.1	Flex_CLT – beams	D-46
D-4.2	Flex_CLT – slabs.....	D-48

Chapter 1: Introduction

1-1 Motivation

Timber is a naturally grown material featuring large uncertainties in many of its properties. To maintain a reliable and widely homogeneous quality for the application in engineered timber products, timber members have to be strength graded. For structural timber products, such as glued laminated timber (glulam; GLT) and cross laminated timber (CLT), the main strength and elastic properties are usually described via load-bearing models. These models are frequently based on the tensile properties parallel to the grain of the base material boards and finger joints. The load-bearing models are developed on the basis of experimental investigations but also on the basis of probabilistic-numerical simulations (e.g. [1–6]). The latter aim on characterising the serial, sub-parallel structure within these products represented by boards and finger joints.

All these load-bearing models assume that the boards are strength graded and that their full cross-sections remain within the final structural timber product. However, in some applications or use cases the total structural timber product gets split or during their production process parts of their components, the lamellas, are split lengthwise. Well-known examples for such structural timber products are resawn glulam and CLT; see **Figure 1-1 (a,b)**. Lengthwise split boards/lamellas also occur in new structural timber products called flex_GLt and flex_CLT, which have been thoroughly investigated in the FFG BRIDGE research project “flex_GLt-CLT-beams” (No. 877111); see **Figure 1-1 (c)**. Flex_GLt beams are cut from large-dimensional unidirectional, while flex_CLT beams are cut from large-dimensional orthogonal multi-layer plates. These multi-layer plates are manufactured in production lines normally used for the production of conventional CLT. Due to the cutting of beams at an arbitrary position within the multi-layer plates, arbitrary in width lengthwise split boards/lamellas occur to a random share within such beam elements. An additional unique feature of flex_GLt and flex_CLT is the load-bearing capacity of the glue-line between the narrow board edges, i.e. the structural edge bonding.

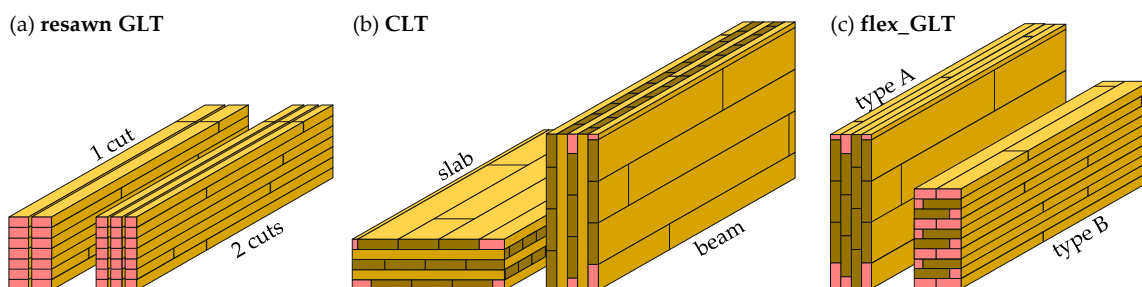


Figure 1-1: Examples of structural timber products featuring lengthwise split boards/lamellas (marked in red) within their cross-sections: (a) resawn GLT produced by one and two cuts, (b) CLT used as slab or beam element, and (c) flex_GLt beams type A and B.

The load-bearing capacity of these products depends fully or partially on the tensile properties of lengthwise split boards/lamellas. However, due to the splitting process the strength class and corresponding material properties assigned to the boards during strength grading in

full cross-section are no longer valid. This circumstance is also regulated in **EN 14081-1 [7]**, where the allowed reduction Δw_b in width after grading, without invalidating the assigned strength grade, is limited to $\Delta w_b \leq 5$ mm for board widths below $w_b = 100$ mm and $\Delta w_b \leq 10$ mm for board widths above or equal to $w_b \geq 100$ mm. Anyway, the magnitude of the change in the material properties of the boards/lamellas remains unknown so far. Nevertheless, to characterise the mechanical properties of engineered timber products containing lengthwise split boards/lamellas it seems inevitable to characterise finger joints, boards with full cross-section as well as boards arbitrary reduced in width. Furthermore, size and system effects for the engineered timber products such as flex_GLT beams are not yet quantified.

1-2 Objectives

The present thesis aims to develop a probabilistic board model to characterise boards and lengthwise split boards with focus on their tensile properties parallel to the grain. Furthermore, to gain further knowledge on the load-bearing behaviour of engineered structural timber products containing such lengthwise split boards, this board model, supplemented by a model for finger joints, is implemented within a newly developed three-dimensional stochastic-numerical beam model. Additionally, the influence of lengthwise split boards (i.e. residual board cross-section) on the load-bearing behaviour is analysed.

To summarise, the objectives of this thesis are:

- (i) to develop a probabilistic model for boards with full and residual cross-sections and for finger joints;
- (ii) to characterise the tensile properties parallel to the grain of lengthwise split boards;
- (iii) to develop a stochastic-numerical beam model for predicting the load-bearing behaviour of flex_GLT beams and other engineered structural timber products featuring lengthwise split boards;
- (iv) to analyse exemplarily the influence of lengthwise split boards on the load-bearing behaviour of investigated engineered structural timber products;
- (v) to quantify exemplarily size and system effects on the load-bearing behaviour of investigated engineered structural timber products.

1-3 Outline and Overview

The structure of this thesis follows the development of load-bearing models for engineered structural timber products in a logical manner. The probabilistic board model and its validation is presented in **Chapter 2**. The basis of the stochastic-numerical beam model is described in **Chapter 3**. The mechanical properties of unidirectionally laminated engineered structural timber products, such as glulam, resawn glulam and flex_GLT beams type A and B, are analysed in **Chapter 4**. **Chapter 5** is dedicated to the mechanical properties of orthogonally laminated engineered structural timber products like CLT as slab or beam elements. Finally, a summary and an outlook are presented in **Chapter 6**.

Chapter 2:

Probabilistic Board Model

This chapter is dedicated to the probabilistic board model and its application to predict the tensile parallel to grain properties of boards. At first, a short introduction and literature review is presented. This is followed by the definition of geometric parameters used in the new probabilistic board model and an outline of the board database used for the derivation of these geometric parameters is made. The allocation of the material properties and the board generation process are specified. The chapter ends with the validation of the new probabilistic board model by a successful application in predicting size effects for the tensile strength of boards and the impact of lengthwise splitting on the tensile properties. The probabilistic board model is supplemented by a probabilistic model for the finger joints. The new probabilistic board model is the basis for the stochastic-numerical beam model introduced in Chapter 3, of which the application is demonstrated in Chapter 4 & 5.

2-1 Introduction and Overview

Timber is a naturally and organically grown material featuring large uncertainties and variabilities in many of its material properties. These uncertainties can be identified on the scales of species, provenance, individual trees as well as between and within timber members. Within a single board the properties are influenced by growth features such as knots and grain deviations. The variability in properties, e.g. in the tensile strength and modulus of elasticity $\{f_{t,0,ij}; E_{t,0,ij}\}$, in longitudinal direction of a board are shown exemplarily in **Figure 2-1**.

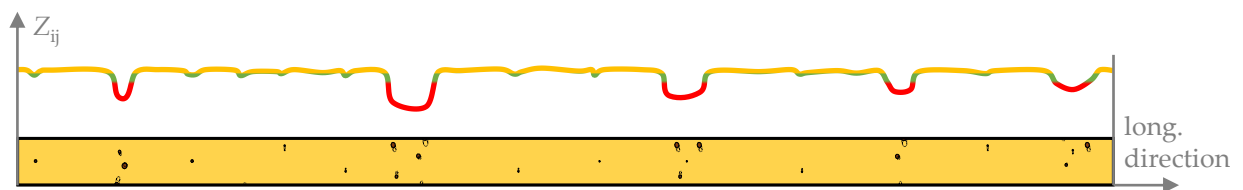


Figure 2-1: Variability in properties (e.g., tensile strength $f_{t,0,ij}$ or modulus of elasticity $E_{t,0,ij}$ parallel to grain) in longitudinal direction of a board.

In order to make use of timber in engineering applications, these uncertainties have to be addressed. This is usually achieved by grading and assigning a certain set of mechanical properties to the timber members. In Europe, these sets or strength classes are regulated in **EN 338 [8]**. The grading can be done either visually or by machines. Visual grading is done mostly by limiting the magnitude of local growth features, in particular knots or knot parameters (e.g. **DIN 4074-1 [9]**). In machine grading systems additional parameters like the density, ultrasonic runtime or eigenfrequency can be determined directly and used to predict the mechanical properties more accurately. Especially, the dynamic modulus of elasticity is well correlated with the “average” board properties and its determination can be seen as state-of-the-art for grading machines. However, strength properties, such as the tensile strength parallel to grain, are additionally determined by local growth features, in particular knots. By consideration of typical growth cycles in trees, in particular coniferous trees, the longitudinal distribution of knots is found to occur with some regularity (e.g. **[3, 10–12]**).

For the description of local properties, such as the modulus of elasticity and the tensile or bending strength along the longitudinal direction, numerous models can be found in the literature (e.g. **Fink [3]**, **Frese [4]**, **Blaß et al. [5]**, **Tapia [6]**, **Ehlbeck et al. [10]**, **Brandner [12]**). Most of these models use knot parameters as surrogates for the influence of local growth features on the mechanical properties of the boards. One example is the $tKAR$ -value (tension/total knot area ratio), which describes the ratio between projected knot area within a board segment of 150 mm length and the board cross-section; see **Isaksson [11]**. The geometrical position and magnitude of knots and knot clusters are defined by probabilistic models as well as the assignment of physical properties, e.g. via (multiple) regression models. These regression models make use of different sets of explanatory variables. For example, the regression models for assigning the strength and elastic properties in the “Karlsruher Rechenmodell” (see **[1, 4, 5]**) are

based on the oven-dry density and the $tKAR$ -value. The regression models from Fink [3] make use of a more recent indicator for the “average” board properties, the dynamic modulus of elasticity based on the eigenfrequency. For estimating the tensile strength parallel to the grain, this parameter is additionally combined with the $tKAR$ -value.

All these mentioned probabilistic board models are developed to predict the tensile properties parallel to grain of strength graded boards whose cross-sections (largely) remain unchanged throughout the production process in structural timber products such as glulam and CLT. The models are further used within stochastic-numerical beam models to predict the bending strength of glulam. As already mentioned in Chapter 1, in some applications and products, the cross-section (particularly the width) of a subset of boards/lamellas within engineered structural timber products may be reduced to a widely random extend. Due to the lengthwise splitting the distribution and pattern of properties along such residual boards change significantly. This circumstance is illustrated in Figure 2-2 (b) where one board is split into three equally wide residual boards. In doing so, the previously assigned strength class and its associated mechanical properties become invalid. As already mentioned in Section 1-1, EN 14081-1 [7] limits the reduction in width after grading, Δw_b , to $\Delta w_b \leq 5$ mm and $\Delta w_b \leq 10$ mm for boards featuring widths below and above $w_b = 100$ mm, respectively. The influence on the tensile properties parallel to grain of such arbitrary in width reduced boards is so far not covered by any probabilistic board model known to the author. Nevertheless, this information is inevitable for the prediction of the bending strength and also other mechanical properties via so-called load-bearing models for engineered structural timber products such as flex_GLT and flex_CLT, as already mentioned in Chapter 1.

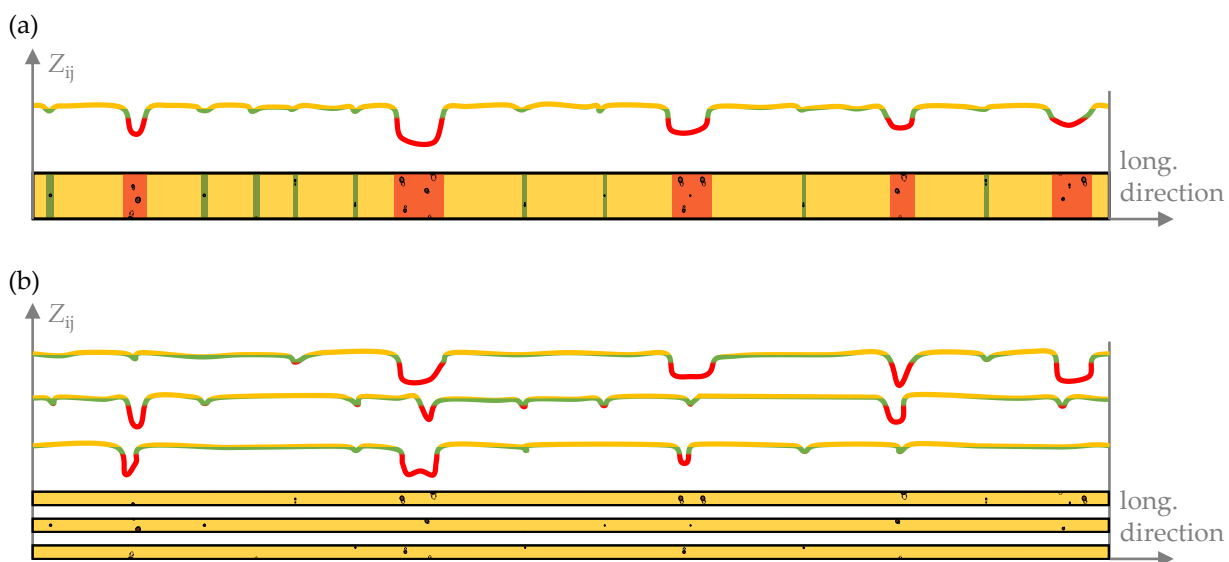


Figure 2-2: Qualitative changes in distribution and pattern of properties (e.g., tensile strength $f_{t,0,ij}$ or modulus of elasticity $E_{t,0,ij}$ parallel to grain) in longitudinal direction of one board: (a) board in full cross-section and (b) the same board split into three equally wide residual boards.

In the following, a novel probabilistic board model is presented. The main differences to so far existing models in the literature are elaborated at the individual parts of the board model. The new model also covers the impact of lengthwise splitting on the distribution of the knots within the residual parts and on the mechanical properties.

2-2 Model Specifications

The probabilistic board model aims on a generic representation of the distribution and magnitude of global and local growth characteristics in structural timber with board dimensions. Hereby, the focus is on boards of softwood species, in particular, because of its dominance in use and availability of data, of Norway spruce (*Picea abies*), as base material for laminated structural timber products like glulam and CLT. These products are usually characterised by means of the tensile properties parallel to the grain of the base material, the structural timber boards, and of the finger joints, which are used for joining boards and board segments lengthwise.

For the investigated wood species and strength classes the tensile properties are mainly governed by knots and knot clusters. Other local growth characteristics, like reaction wood, bark inclusions, local grain deviations or cracks, are only considered implicitly. Nonetheless, as the tensile strength of boards is usually determined by global indicators, such as the dynamic modulus of elasticity, and local indicator, such as knot-parameter, other local growth characteristics are covered implicitly via uncertainties of the predictive model. Following this, knots and knot clusters serve also as surrogates for the other local growth characteristics. As the tensile properties are highly influenced by local growth characteristics, the probabilistic model aims to represent the longitudinal extension and classification of these local growth characteristics widely realistically. The positioning and magnitude of knots and knot clusters is already defined to a certain extent by the branches within the tree; see **Figure 2-3 (a)**.

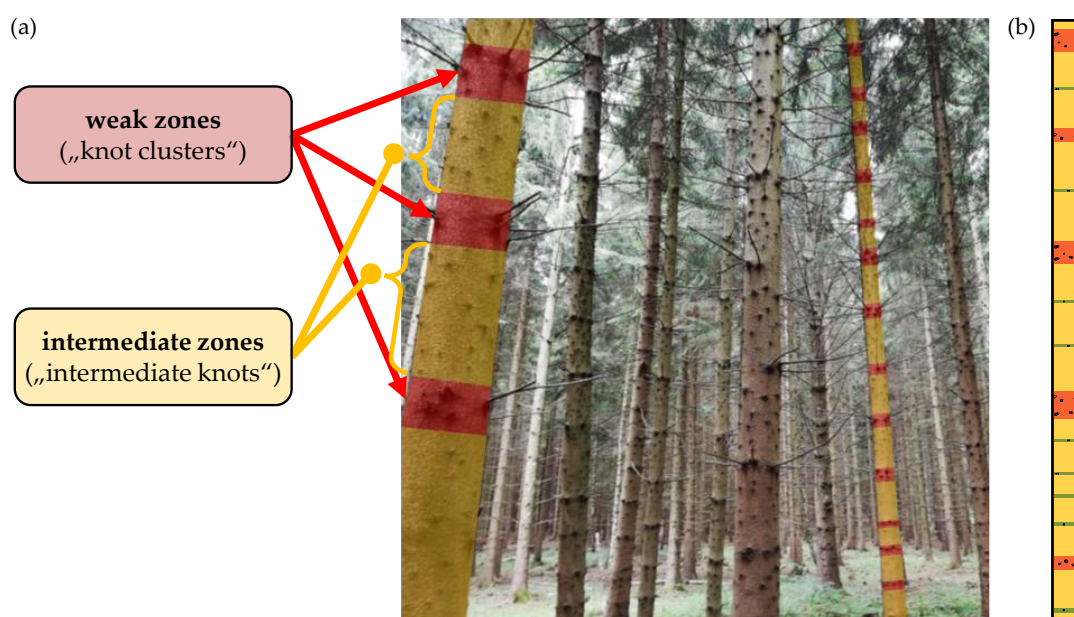


Figure 2-3: (a) Norway spruce trees with knot zones; (b) board with corresponding knot zones.

Analogue to the natural structure in trees, sawn boards are further separated in longitudinal direction into weak zones (WZ), intermediate knot zones (IZ) and knot free zones, so called “clear wood” (CW); see **Figure 2-3 (b)**. The same classification scheme of board segments was used by **Brandner [12]**. The corresponding geometric parameters describing the spacing and lengths of these zones are illustrated in **Figure 2-4**.

Figure 2-4 (a) shows all four surfaces (wide and narrow faces) of a board, in longitudinal direction divided in the three types of knot zones, specifically: knot clusters or weak zones “WZ” (marked in red), intermediate zones “IZ” (marked in green) and clear wood zones “CW” (unmarked; orange). Details regarding the length and spacing of WZ and IZ are illustrated in **Figure 2-4 (b)&(c)**, respectively.

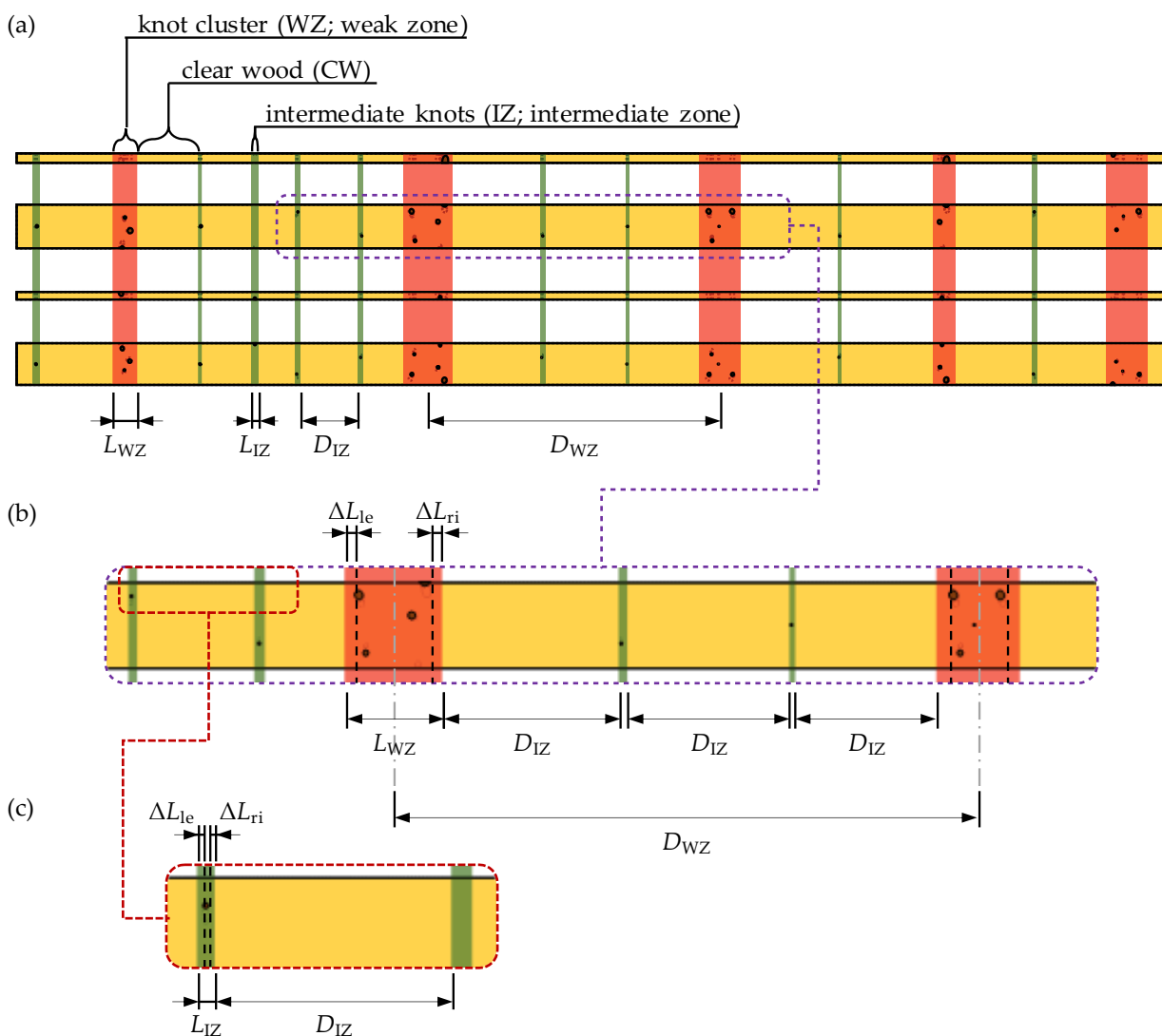


Figure 2-4: Geometric parameters for knot zones in boards: (a) definition of knot zones and spacings; (b) detail of the lengths of knot zones and their spacings; (c) detail of the length and spacings of the intermediate zones (IZ).

The methodology to differentiate them and the definitions of $\{L_{WZ}; L_{IZ}\}$ are described in detail in [Section 2-2.1](#). The distance between weak zones D_{WZ} is measured from the centre points of the neighbouring WZs; see [Figure 2-4 \(b\)](#). The same definition of the distances between weak zone was already used in the literature; see [Fink \[3\]](#), [Brandner \[12\]](#). The distance between intermediate knots D_{IZ} is defined as the clear spacing in-between; [Figure 2-4 \(c\)](#). This different modelling approach was necessary because D_{IZ} is also used to model the distance between WZ and neighbouring IZ. Otherwise, the significantly different length of the zones $\{L_{WZ}; L_{IZ}\}$ would falsify the statistics of D_{IZ} . Additionally, the definition of the distance D_{IZ} allows a simpler and more straightforward implementation in the board generation process; see [Section 2-6](#).

2-2.1 Weak Zones and Intermediate Zones

In most current probabilistic models, the length of knot zones (L_{KZ}) is kept constant with $L_{KZ} = 150$ mm ([Fink \[3\]](#), [Frese \[4\]](#), [Blaß et al. \[5\]](#)) or $L_{KZ} = 100$ mm ([Tapia \[6\]](#)). To calculate the knot parameter $tKAR$ (tension/total Knot Area Ratio), a segment with the corresponding length ($L_{cell} = L_{KZ}$) is moved over the board. The knot area within this region projected onto the respective board cross-section is used to derive the knot parameter, whereby overlapping areas are counted only once; see [Figure 2-5 \(a\)](#) and [Figure 2-6 \(d\)](#). Therefore, the length of the cell L_{cell} has a certain influence on the magnitude of the $tKAR$ -value. [Figure 2-5 \(b\)](#) shows the magnitude of the $tKAR$ in longitudinal direction of the board and for different cell lengths L_{cell} .

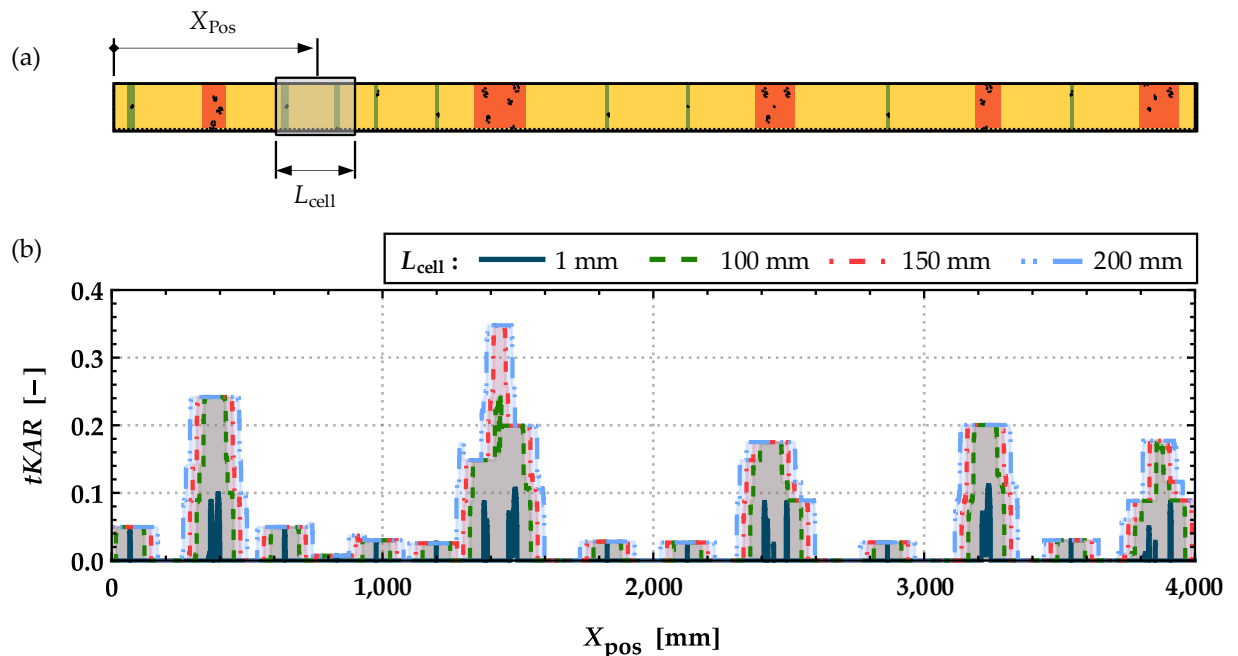


Figure 2-5: (a) Board with knot zones; (b) magnitude of $tKAR$ in longitudinal direction of the board calculated for different cell lengths L_{cell} .

According to [Brandner \[12\]](#) approximately 98 % of all knot clusters have a length $L_{KZ} \leq 150$ mm. Following this, a cell length of $L_{cell} = 150$ mm is sufficiently long enough to correctly estimate the $tKAR$ -value of nearly all board sections. Nonetheless, the lengths of knot clusters are

overestimated in most of the cases. Additionally, current probabilistic board models regard knots or knot clusters over a certain $tKAR$ -threshold as weak zones; knots and knot clusters below this threshold are neglected (e.g. [3, 4, 10]) and no differentiation between weak zones and intermediate zones is made.

For a more realistic representation of knots and knot clusters, which is also independent from a fixed cell length L_{cell} , a new model was developed based on the findings in Brandner [12]. The main advantages of the new approach are (i) a more realistic depiction of weak zones, (ii) a possibility to differentiate between weak zones and intermediate knot zones explicitly, and (iii) a minimised influence of the cell length on the $tKAR$ -value. Figure 2-6 shows the methodology used to determine knot zones and differentiate between weak zones (knot clusters) and intermediate knot zones. The steps are depicted for the detailed section of the board in Figure 2-6 (a).

In a first step, the length in longitudinal direction of each knot is extended by the lengths $\{\Delta L_{le}; \Delta L_{ri}\}$. This is done to take the grain deviations surrounding the knot into account. The background is, that the tensile strength perpendicular to the grain is about 1/30 of the strength parallel to the grain and even small grain deviations lead to a significant loss in tensile strength. Olsson et al. [13] stated that local grain distortions in the vicinity of knots decay after a distance in longitudinal direction of approximately 1.5 times the knot diameter. Based on this investigation and the assumption of a gradual decrease of the grain distortions, to account for the influence of knots on the mechanical properties the additional lengths $\{\Delta L_{le}; \Delta L_{ri}\}$ are fixed with 1.0 times the diameter of the knot; see Figure 2-6 (b). By assuming a gradual decaying influence of the local grain deviation starting from the outer diameter of the knot, this dimension corresponds to the distance of the centre of gravity.

In a second step, the in longitudinal direction of the board overlapping knot areas are grouped together and the length of each knot zone is determined; see Figure 2-6 (c). The $tKAR$ -value of each knot zone is calculated and multiplied with the length of the corresponding knot zone to receive a measure called “knot intensity”. Figure 2-6 (d) shows the “knot intensity” $L_{kz} \cdot tKAR_{kz}$ over the length of the selected board segment. By visual inspection of multiple boards, a plausible limit for the differentiation between weak zones (WZ) and intermediate zones (IZ) was found with a “knot intensity” of $L_{kz} \cdot tKAR_{kz} \geq 2.0$ for WZ. In addition to the knot intensity, a minimum distance of $\Delta D_{WZ} = 100$ mm between two weak zones was introduced. WZs with distances below this threshold were merged and the values L_{WZ} and $tKAR_{WZ}$ were determined as seen in Figure 2-6 (e).

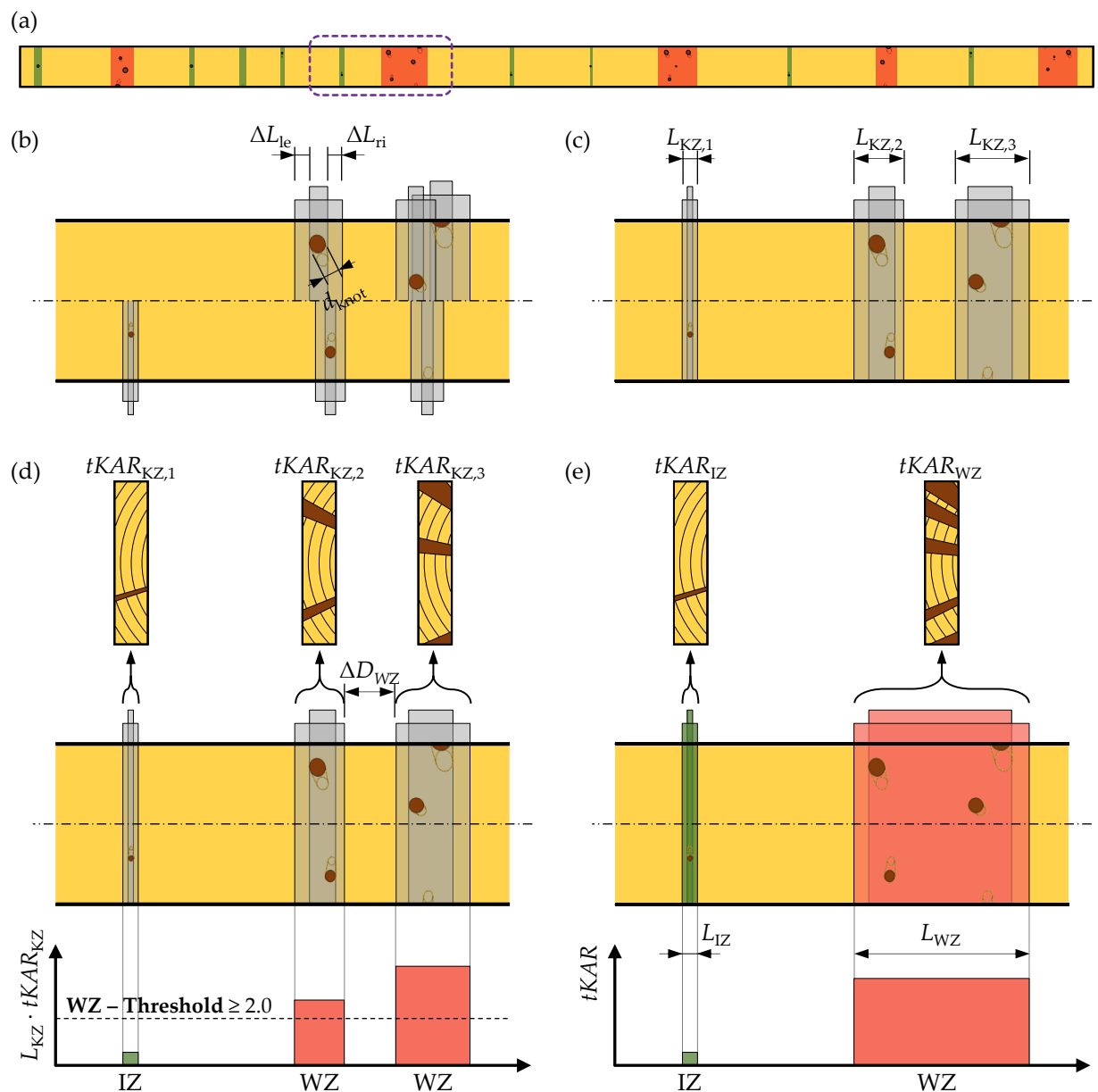


Figure 2-6: Differentiation in Weak Zones (WZ) and Intermediate Zones (IZ): (a) board with marked detail range; (b) detail of knots and assumed areas with local grain deviations; (c) detail clarifying the lengths of knot zones; (d) differentiation in weak zones (WZ) and intermediate zones (IZ) based on the “knot intensity” parameter ($L_{KZ} \cdot tKAR_{KZ}$); (e) detail clarifying the lengths and $tKAR$ -values of knot zones {IZ in green and WZ in red}.

A comparison between the new dynamic method and current methods using fixed lengths to characterise and describe knot zones is illustrated in **Figure 2-7**. In addition to the $tKAR$ -value in longitudinal direction of the board, the lengths of the weak zones are shown. The lengths of the knot zones and $tKAR$ -values for the four knot zones in **Figure 2-7** are summarised in **Table 2-1**. The new approach differs from current models in literature (e.g. **Fink [3]**, **Frese [4]**, **Ehlbeck et al. [10]**) in the following three aspects: (i) classification of weak zone and intermediate zones, (ii) dynamic length of the knot zones, and (iii) dynamic length for the determination of the $tKAR$ -value.

The differentiation of the knot zones via the threshold for the “knot intensity” of $L_{KZ} \cdot tKAR_{KZ} \geq 2.0$ and the $tKAR$ -value of ≥ 0.1 leads to the same classification of the knot zones into WZ and IZ. However, the length of the knot zones is captured more accurately by the new approach, in particular for the intermediate zones, featuring lengths of {32.0; 16.0} mm. For WZ₁ the new method results in a length of $L_{WZ} = 86$ mm and $L_{WZ} = 160$ mm for WZ₂. All other models would overestimate the length WZ₁. The lengths of $L_{KZ} = \{100; 150\}$ mm as used so far in the literature (e.g. [3, 4, 10]) would underestimate the length of WZ₂. The $tKAR$ -values determined by means of variable, individual lengths of knot zones are in good agreement with $tKAR$ -values determined by means of a fixed length. At a fixed cell length of $L_{cell} = 100$ mm the $tKAR$ -value for WZ₂ with $tKAR_{100} = 0.24$ is even lower than for all other approaches. In this case the influence of the knots on the tensile properties may be underestimated.

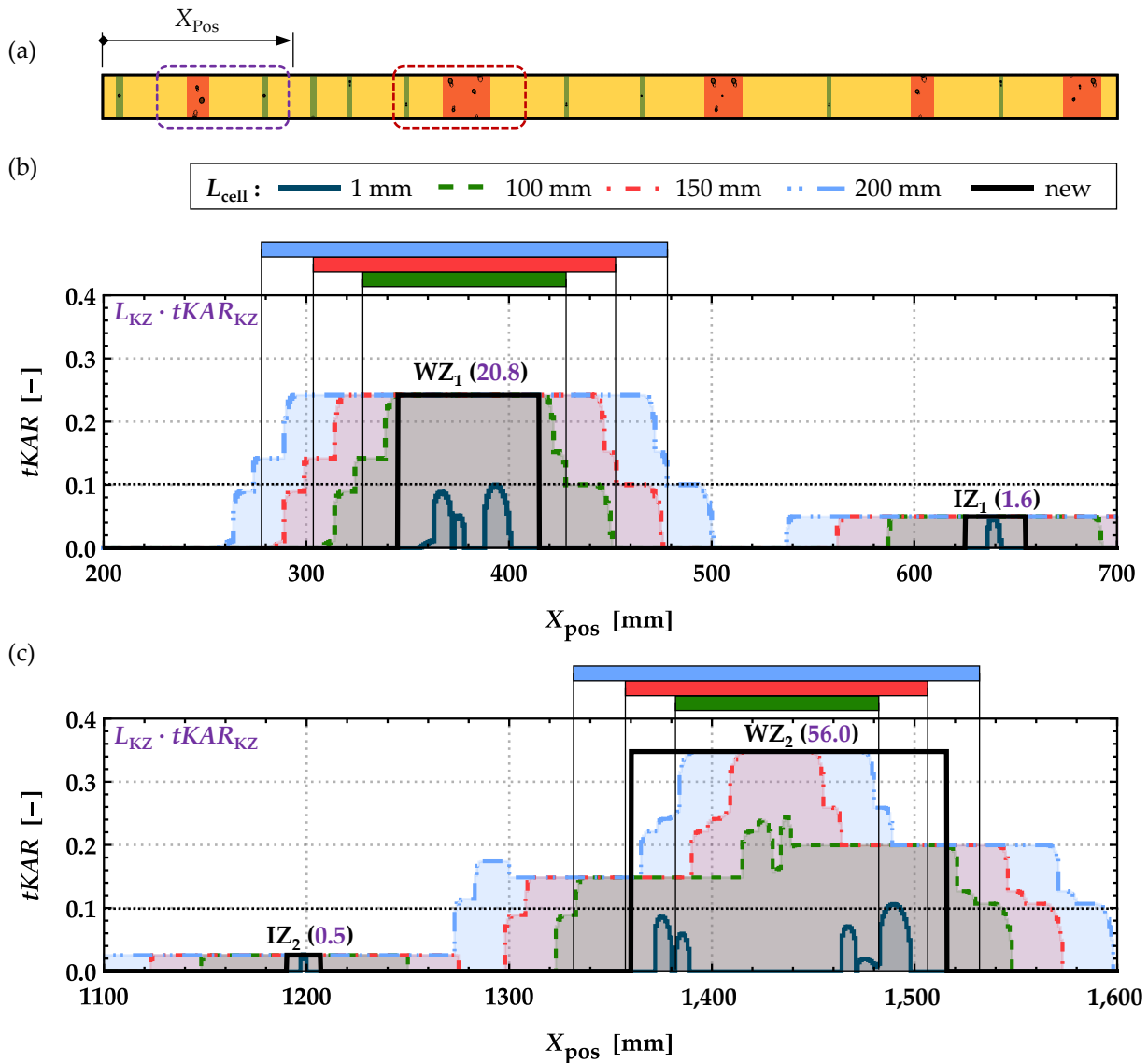


Figure 2-7: (a) board with marked detail range; (b/c) magnitude of $tKAR$ in longitudinal direction of selected board segments: comparison between approaches with fixed lengths of $L_{cell} = \{100; 150; 200\}$ mm and the new approach which uses a variable length L_{cell} .

Table 2-1: Length, $tKAR$ -value and “knot intensity” $L_{KZ} \cdot tKAR_{KZ}$ for the knot zones in **Figure 2-7**.

	WZ ₁	IZ ₁	WZ ₂	IZ ₂
$L_{KZ,new}$ [mm]	86.0	32.0	160.0	16.0
$tKAR_{new}$ [-]	0.24	0.05	0.35	0.03
$L_{KZ,new} \cdot tKAR_{new}$ [mm]	20.8	1.6	56.0	0.5
$tKAR_{100}$ [-]	0.24	0.05	0.24	0.03
$tKAR_{150}$ [-]	0.24	0.05	0.35	0.03
$tKAR_{200}$ [-]	0.24	0.05	0.35	0.03

Overall, the new model achieves similar $tKAR$ -values than most other probabilistic board models with a fixed length of $L_{WZ} = 150$ mm (e.g. **Fink [3]**, **Frese [4]**, **Ehlbeck et al. [10]**). Nevertheless, the new model is superior with respect to the real depiction of the knot zone lengths. This new flexibility in the knot zone length is seen to be essential especially for lengthwise split boards, where a single knot could become a weak section. In this Section, however, only the basic principles of the new approach are described, exemplarily shown and compared with models from the literature. A more detailed comparison between the new and existing probabilistic board models is presented in **Section 2-4.2**.

2-3 Board Database

2-3.1 Overview

For the validation of the distribution models which are further used to represent the physical and geometric properties as random variables within the probabilistic board model, as well as for the estimation of corresponding distribution parameters, correlations and relationships within and between random variables and main statistics, two databases comprising boards for the glulam production were analysed, namely from the research projects “INTELLIWOOD” (**Schickhofer & Augustin [14]**) and “separate” (**Kastner et al. [15]**). The databases contain knot data (position and dimension), other technological parameters, like annual ring width or radial distance to the pith, and physical properties like the dynamic modulus of elasticity based on eigenfrequency measurements, density at reference moisture content of $u_{ref} = 12$ % and the modulus of elasticity and strength in tension parallel to the grain, $\{E_{DYN,b}; Q_{12,b}; f_{t,0,b}; E_{t,0,loc,12,b}\}$, respectively, from more than 1,000 timber boards of Norway spruce (*Picea abies*), with provenance Central Europe; see **Table 2-2**. A complete dataset including the tensile strength parallel to the grain and more than one weak zone per board is only available for a subset of approximately 550 boards, which is also referred to as “censored board data”.

The current product standards for GLT and CLT (**EN 14080 [16]**, **EN 16351 [17]**) allow a board thickness of $t_b = 6 \div 45$ mm and the board width within $w_b = 80 \div 280$ mm. Nonetheless, for GLT boards with a thickness of $t_b = 40$ mm and for CLT $t_b = \{20; 30; 40\}$ mm are mostly used for production. The most common board is within $w_b = 120 \div 240$ mm for GLT and $w_b = 80 \div 200$ mm for CLT. The board thickness t_b in the databases ranges from 29 mm to 45 mm and the board

width w_b from 110 mm to 230 mm. Consequently, most of the previously mentioned board dimensions are covered within the database. A classification of boards in the databases in respect to their nominal dimensions is illustrated in **Figure 2-8**.

Table 2-2: Board databases – overview of main- & sub-series, nominal grading classes, quantity and dimensions based on **Schickhofer & Augustin [14]** & **Kastner et al. [15]**.

	main- & sub-series		assigned class ¹	quantity [-]		width w_b [mm]	thickness t_b [mm]	length l_b [mm]
				all	cen ²			
Schickhofer & Augustin [14]	I-CH	_1:semi:m	na ³	62	52	150	45	4,450
		_1:semi:s		62	45			
		_1:semi:ss		61	46		29	
	II-AT	_1:vis	S10	45	39	150	35	3,200 ÷ 4,000
		_2:vis	S13	45	33			
		_3:mach	MS13	45	40			
		_4:mach	MS17	41	33	230		
		_5:mach	MS13	16	14			
		_6:mach	MS17	14	8			
	III-AT	_1:vis	S10	45	38	110		
		_2:vis	S13	45	34			
		_3:mach	MS10	45	44			
		_4:mach	MS13	45	39			
		_5:mach	MS17	44	40			
Kastner et al. [15]	separate	I	rejects	5	0	170	45	4,000
		II	L25	383	33			
		III	L36	151	14			
			$\Sigma =$	1,154	552			

¹nominal grading classes according to **DIN 4074-1 [9]** and **EN 14081-1 [7]**

²censored board data; datasets with all data present $\{E_{DYN,b}; Q_{12,b}; f_{t,0,b}; E_{t,0,loc,12,b}\}$ and number of weak zones $\#wz > 1$

³no grading class assigned

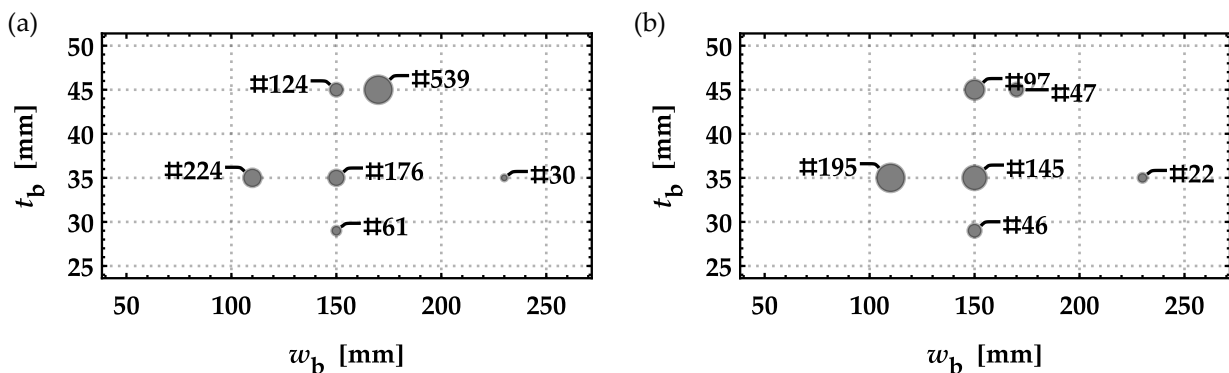


Figure 2-8: Number of boards classified by their nominal cross-section dimensions: (a) all boards and (b) the censored board data; datasets with all data present $\{E_{DYN,b}; Q_{12,b}; f_{t,0,b}; E_{t,0,loc,12,b}\}$ and number of weak zones $\#wz > 1$.

2-3.2 Sorting and Grading

The boards within the database were divided into two groups, GI and GII, based on the dynamic modulus of elasticity and the maximum *tKAR*-value. For the “INTELLIWOOD” database only measurements of the dynamic modulus of elasticity based on the ultrasonic runtime were available. This method results in higher values for the dynamic MOE and therefore had to be corrected via the linear model in **Equation (2.1)** which was derived from test data in **Fink & Kohler [18]**.

$$E_{DYN,b} = \begin{cases} 0.95 \cdot E_{DYN,US} - 2,000 \\ E_{DYN,F} \end{cases} \quad (2.1)$$

with

$E_{DYN,F}$ dynamic modulus of elasticity based on eigenfrequency [MPa]

$E_{DYN,US}$ dynamic modulus of elasticity based ultrasonic runtime [MPa]

The parameters applied for the allocation of the boards into the two groups are listed in **Table 2-3**. Hereby, the *tKAR*-value with a cell length of 150 mm was used, as it is an already well established parameter for grading timber boards. The limits of both classes were chosen based on a literature survey ([3, 5, 15, 19, 20]) and checked afterwards with results from the tensile tests parallel to the grain. The number of boards which could be allocated into one of both classes, grouped by their nominal cross-section dimensions, are shown in **Figure 2-9 (a)**. For a subset of these boards data from tensile parallel to the grain tests $\{E_{t,0,loc,12,b}; f_{t,0,b}\}$ were also available; see **Figure 2-9 (b)**. The majority of boards can be allocated to group GI; nevertheless, both groups are present at all dimensions.

Table 2-3: Parameters and their limit values applied in allocating boards into groups GI & GII.

	reject	GI (T14)	GII (T24)
$E_{DYN,b}^1$ [MPa]	< 9,500	9,500 ÷ 12,499	≥ 12,500
$tKAR_{150}$ [-]	> 0.50	≤ 0.50	≤ 0.35

¹.....see **Equation (2.1)**

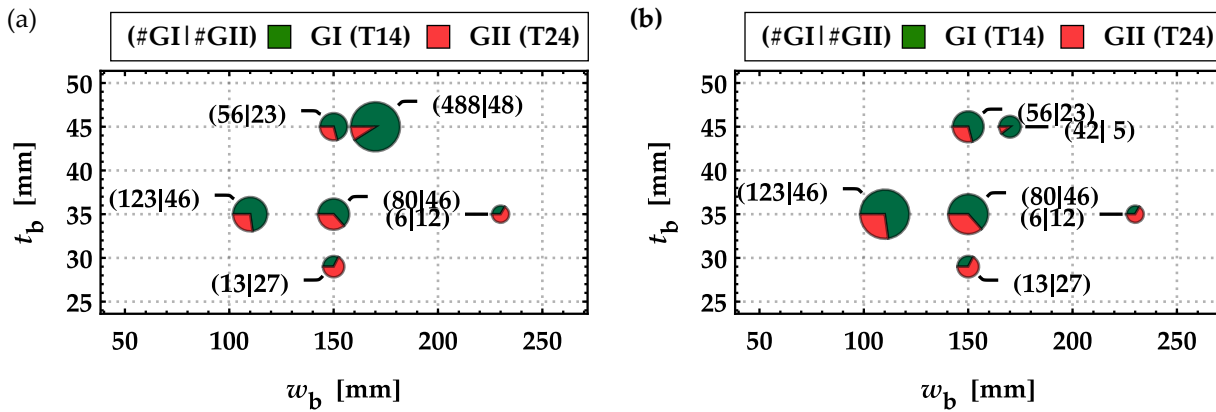


Figure 2-9: Number of boards in GI (T14) and GII (T24) classified by their nominal cross-section dimensions: (a) all boards and (b) boards with all data present $\{E_{DYN,b}; Q_{12,b}; f_{t,0,b}; E_{t,0,loc,12,b}\}$ (number of weak zones $\#wz > 1$).

The main statistics for the mechanical properties of all boards in **Figure 2-9 (b)** are listed in **Table 2-4**. According to **EN 338 [8]**, for the allocation of boards into the strength class T14, the following requirements have to be fulfilled: a characteristic density of $\rho_k = 350 \text{ kg/m}^3$, a tensile strength of $f_{t,0,k} = 14 \text{ MPa}$ and a modulus of elasticity of $E_{t,0,mean} = 11.0 \text{ GPa}$. For the allocation of boards to the strength class T24, the requirements are: a characteristic density of $\rho_k = 400 \text{ kg/m}^3$, a tensile strength of $f_{t,0,k} = 24 \text{ MPa}$ and a modulus of elasticity of $E_{t,0,mean} = 13.5 \text{ GPa}$. Based on the results in **Table 2-4** the boards in groups GI and GII, respectively, can be assigned to the strength classes T14 and T24 according to **EN 338 [8]**. Histograms and calibrated lognormal density functions for the physical/mechanical properties $\{f_{t,0,b}; E_{t,0,loc,12,b}; Q_{12,b}; E_{DYN,b}\}$ are shown in **Figure 2-10**.

Table 2-4: Main statistics for the physical/mechanical properties of the censored board data allocated to groups GI (T14) & GII (T24).

	GI (T14)				GII (T24)			
	$f_{t,0,b}$	$E_{t,0,loc,12,b}$	$E_{DYN,b}$	$Q_{12,b}$	$f_{t,0,b}$	$E_{t,0,loc,12,b}$	$E_{DYN,b}$	$Q_{12,b}$
#	320				160			
mean [MPa kg/m ³]	28.4	11,394	11,945	447	39.7	13,540	14,233	481
COV [%]	30.8	15.5	14.1	9.67	25.3	16.0	11.3	7.51
$\chi_{05,emp}$ [MPa kg/m ³]	15.5	8,954	9,826	394	24.2	9,194	12,550	431
$\chi_{05,LN}$ [MPa kg/m ³]	15.9	8,625	9,313	374	24.8	10,043	12,230	424
$\chi_{k,EN14358}$ [MPa kg/m ³]	15.6	–	–	372	24.2	–	–	421

A comparison between the physical/mechanical properties $\{E_{DYN,b}; Q_{12,b}\}$ of all boards and the censored board data is illustrated in **Figure 2-11**. With respect to the dynamic modulus of elasticity and the density both datasets show a similar distribution. Based on this observation all or as many as possible boards are used to derive the model parameters. The mean values and the coefficients of variation of the dynamic modulus of elasticity $E_{DYN,b}$ for GI and GII are summarised in **Table 2-5**.

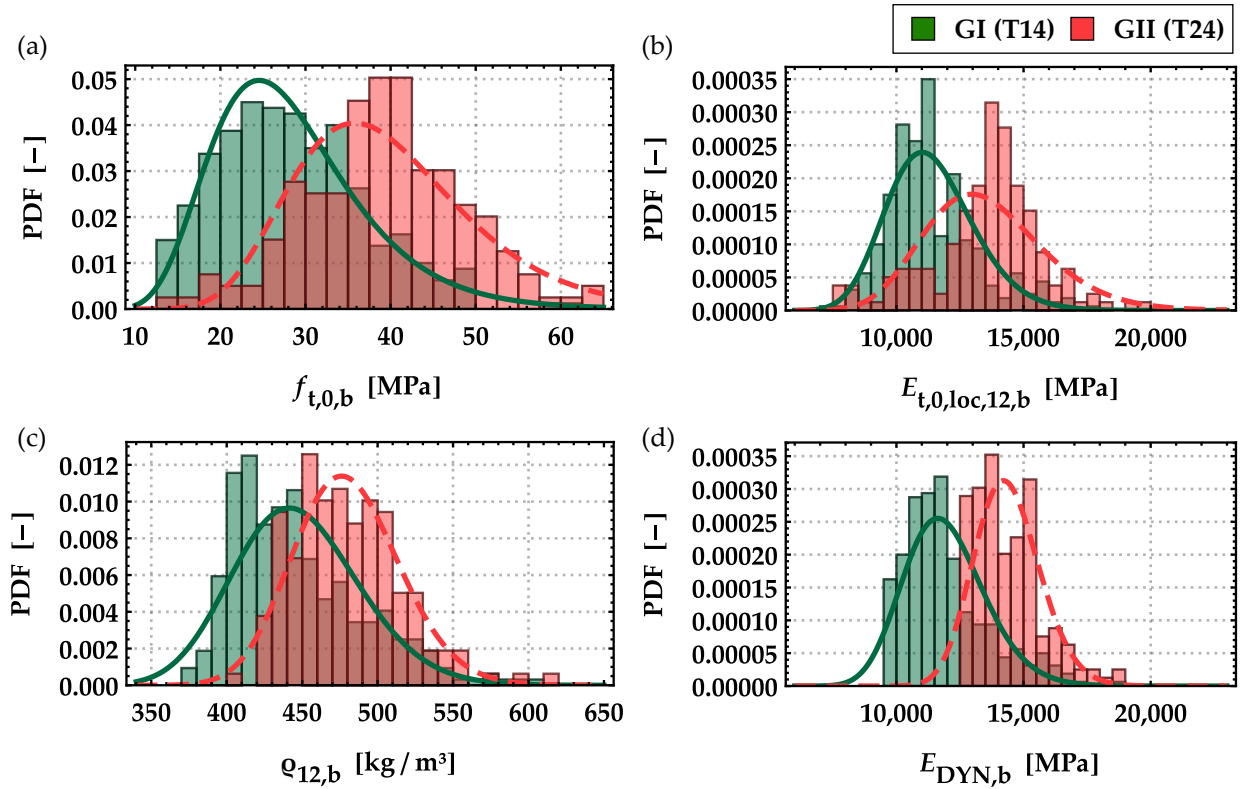


Figure 2-10: Histograms and calibrated lognormal density functions for the censored board data allocated to group GI (T14) and GII (T24) for (a) the tensile strength $f_{t,0,b}$ parallel to the grain in [MPa], (b) the local modulus of elasticity in tension $E_{t,0,loc,12,b}$ in [MPa], (c) the density $\rho_{12,b}$ in [kg/m³] and (d) the dynamic modulus of elasticity $E_{DYN,b}$ in [MPa].

Table 2-5: Main statistics for the dynamic modulus of elasticity considering all boards allocated to groups GI (T14) & GII (T24).

	GI (T14)	GI (T14) & GII (T24)
$E_{DYN,b,mean}$ [MPa]	11,680	14,140
$COV(E_{DYN,b})$ [%]	13.6	12.4

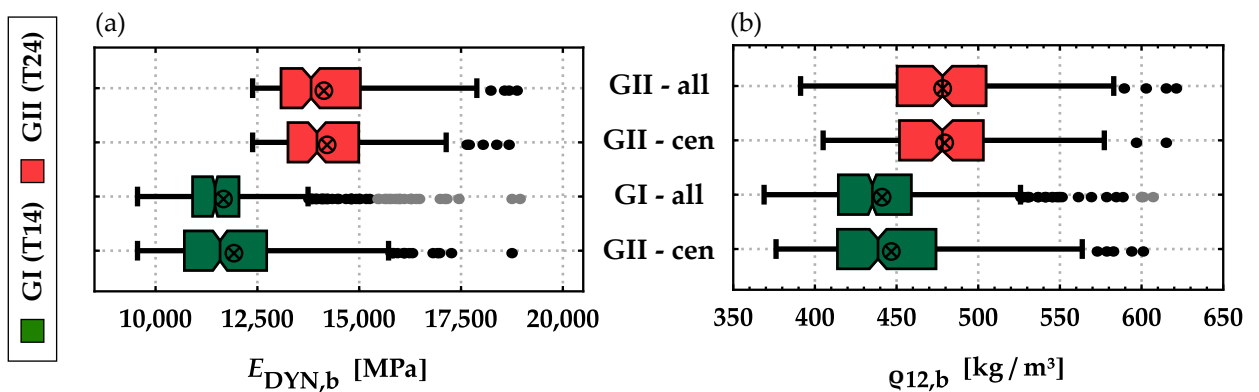


Figure 2-11: Comparison between the data sets comprising all boards and censored boards data for (a) the dynamic modulus of elasticity $E_{DYN,b}$ in [MPa] and (b) the density $\rho_{12,b}$ in [kg/m³].

2-4 Geometric Parameters, Distributions and Correlations

2-4.1 Introduction and Overview

The statistic of the geometric parameters $\{L_{WZ}; tKAR_{WZ}; D_{WZ}; L_{IZ}; tKAR_{IZ}; D_{IZ}\}$ introduced in **Section 2-1** were derived from two databases (**Schickhofer & Augustin [14]** and **Kastner et al. [15]**). To calculate all necessary parameters automatically the software tool **KnotInterpreter [21]** was used and **Mathematica [22]** for the statistical analysis of the parameters. In a first step, the statistics of the geometric parameters of boards in full cross-section were analysed for influences regarding the board thickness t_b and width w_b . In a second step, all boards were virtually split lengthwise into $\{2; 3; 5; 8\}$ equally wide pieces; see **Figure 2-12**. Hereby, the separation ratio η_s was introduced to describe the ratio of the residual width in relation to the original board width; see **Equation (2.2)**. Afterwards, the influence of the lengthwise splitting of boards (expressed by the separation ratio η_s) on the geometric parameters is investigated. The results of this section are the basis for the probabilistic board model presented in **Section 2-5**.

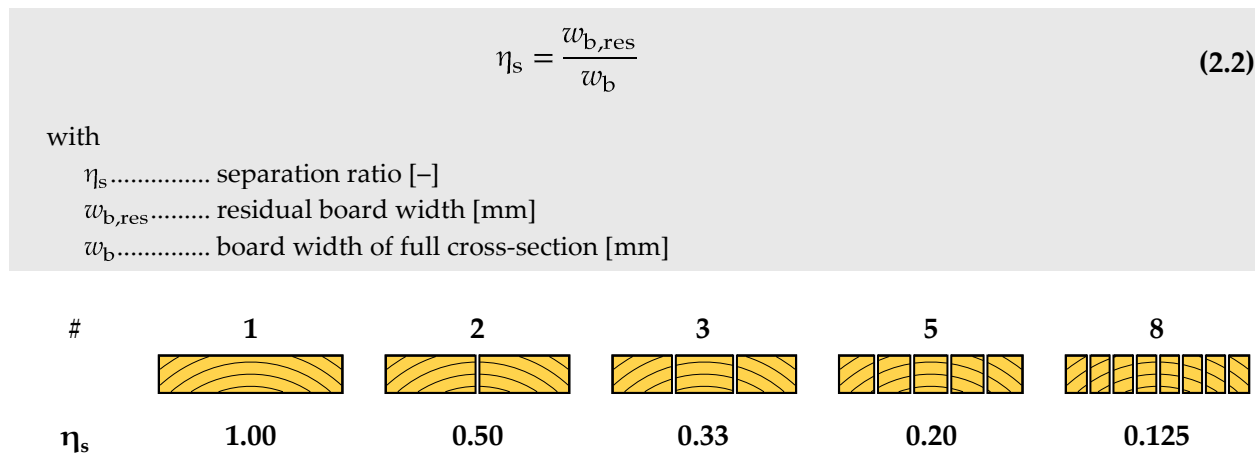


Figure 2-12: (from left to right) Board with full cross-section and its residual cross-sections after splitting lengthwise into $\{2; 3; 5; 8\}$ equally wide pieces realising separation ratios $\eta_s = \{0.50; 0.33; 0.20; 0.125\}$.

2-4.2 Boards in full Cross-Section Width

2-4.2.1 Influence of Board Thickness on the Geometric Parameters

At first, the influence of the board thickness t_b on the statistics of the geometric parameters $\{L_{WZ}; tKAR_{WZ}; D_{WZ}; L_{IZ}; tKAR_{IZ}; D_{IZ}\}$ is analysed. **Figure 2-13** shows the dimensions of the boards used in the analysis. For all cross-section dimensions, boards from both groups GI (T14) and GII (T24) are present within the data. The statistics of the geometric parameters of boards with dimension $w_b = 150$ mm and $t_b = \{29; 35; 45\}$ mm are summarised in **Table Annex D-1** & **Table Annex D-2**. Histograms with calibrated density functions for all board dimensions and geometric parameters are illustrated in **Annex C-1.1**.

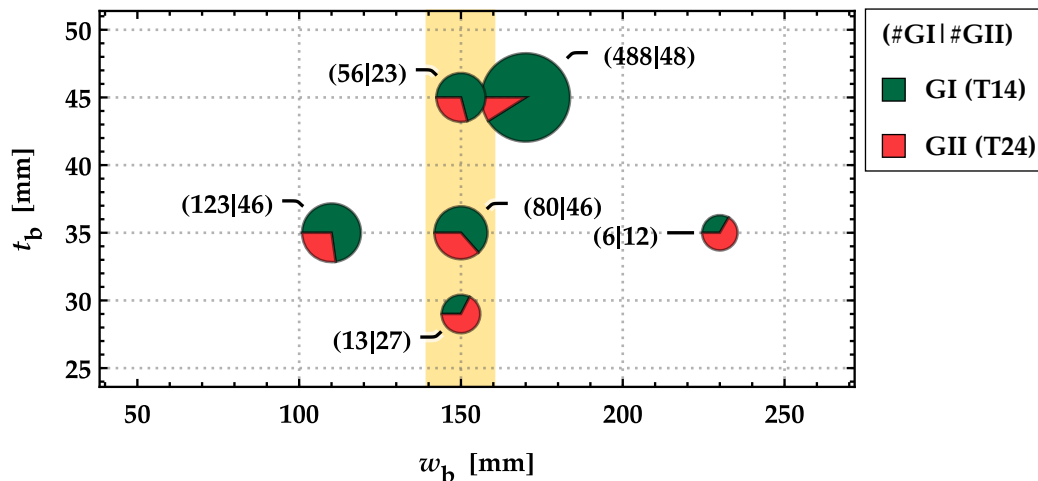


Figure 2-13: Number of boards classified by their nominal cross-section dimensions (marked in yellow) used to analyse the influence of the board thickness t_b on the geometric parameters.

Figure 2-14 shows the mean, 5 %- and 95 %-quantile values of the geometric parameters in dependency of the board thickness t_b . In interpretation of the outcomes it needs to be kept in mind that the range in thickness with $t_b = \{20; 35; 45\}$ mm is rather small. For each geometric parameter the following observations can be summarised:

- L_{wz} :**
 With increasing thickness t_b , the mean and the 95 %-quantile values of the length of the weak zone are slightly increasing for group GI (T14) and decreasing for group GII (T24). The 5 %-quantile values are not affected neither by the thickness nor by the group. Overall, the length of the weak zone is slightly higher for the group GI (T14), which seems reasonable as the number of knots and their diameter are expected to be higher within the lower strength class.
- D_{wz} :**
 The mean and both quantile values of the distance between the weak zones D_{wz} are almost constant for group GI (T14) and GII (T24). The distances between the WZs of group GII (T24) are slightly larger than in group GI (T14), which appears plausible for boards with a higher strength class.
- $tKAR_{wz}$:**
 The mean and both quantile values of the $tKAR$ of the weak zones $tKAR_{wz}$ are almost constant for group GI (T14) and GII (T24). The $tKAR_{wz}$ -values are larger in group GI (T14). This is again plausible as the knot parameter should be lower for higher strength classes and $tKAR_{150}$ was a parameter within the grading process as well.
- Intermediate Zones IZ:**
 For the parameters of the intermediate zones $\{L_{IZ}; tKAR_{IZ}; D_{IZ}\}$ the mean and the quantile values are almost at a constant level, i.e., no dependency on the board thickness is observed. This seems plausible as the intermediate knot zones consist mostly only of single small knots. A difference of on average 30 mm between the groups was found only for the distance between the IZs.

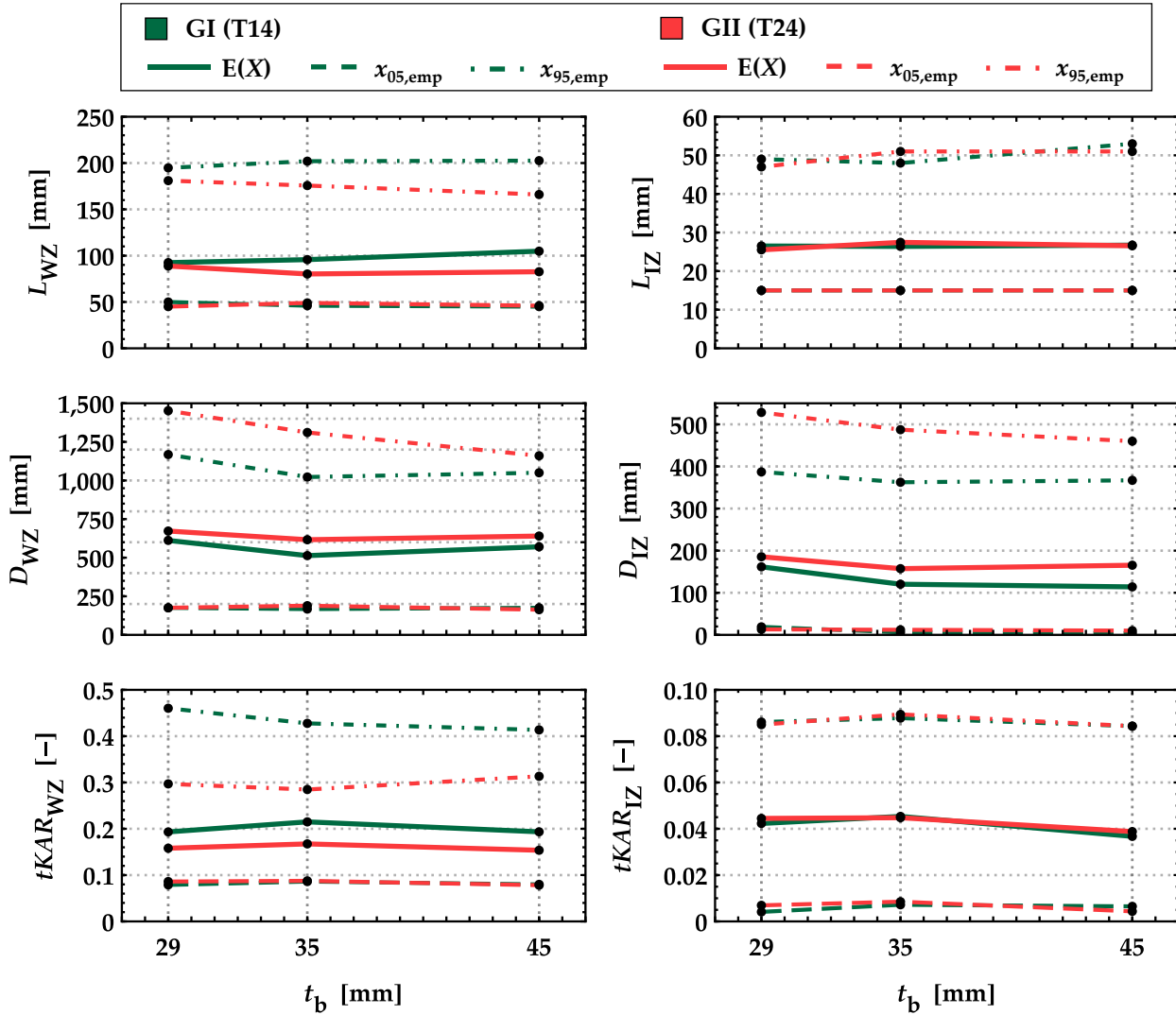


Figure 2-14: Mean, 5 %- and 95 %-quantile values of the geometric parameters $\{L_{WZ}; tKAR_{WZ}; D_{WZ}; L_{LZ}; tKAR_{LZ}; D_{LZ}\}$ in dependence of the board thickness t_b for group GI (T14) and GII (T24).

Overall, and within each group GI and GII the influence of the board thickness on the geometric parameters $\{L_{WZ}; tKAR_{WZ}; D_{WZ}; L_{LZ}; tKAR_{LZ}; D_{LZ}\}$ is rather small or has almost no influence at all. Nevertheless, statistics for some of the geometric parameters are different between the two groups, especially those for the weak zone parameters. For GI (T14) a smaller distance of the WZs is observed whereas the weak zone length and the $tKAR$ -values are larger. These differences between the groups GI (T14) and GII (T24) are as expected and/or intended by the grading process. Based on these observations, the geometric parameters are further treated partly dependent on the group (or board strength class) but independent on the board thickness. A comparison of the geometric parameters with the literature can be found in [Section 2-4.5](#).

2-4.2.2 Influence of the Board Width on the Geometric Parameters

In a second step, the influence of the board width w_b on the statistics of the geometric parameters $\{L_{WZ}; tKAR_{WZ}; D_{WZ}; L_{LZ}; tKAR_{LZ}; D_{LZ}\}$ is analysed. As already presented in the previous [Section 2-4.2.1](#), the board thickness can be neglected regarding the influence on the geometric

parameters. **Figure 2-15** shows the number and width of the boards independent of the thickness used in the analysis. For all cross-section dimensions boards from both groups GI (T14) and GII (T24) are present. The statistics of the geometric parameters of boards with dimension $w_b = \{110; 150; 170; 230\}$ mm are summarised in **Table Annex D-3** & **Table Annex D-4**. Histograms with calibrated density functions {LND; WD; BD; GD} for all board dimensions and geometric parameters are illustrated in **Annex C-1.2**.

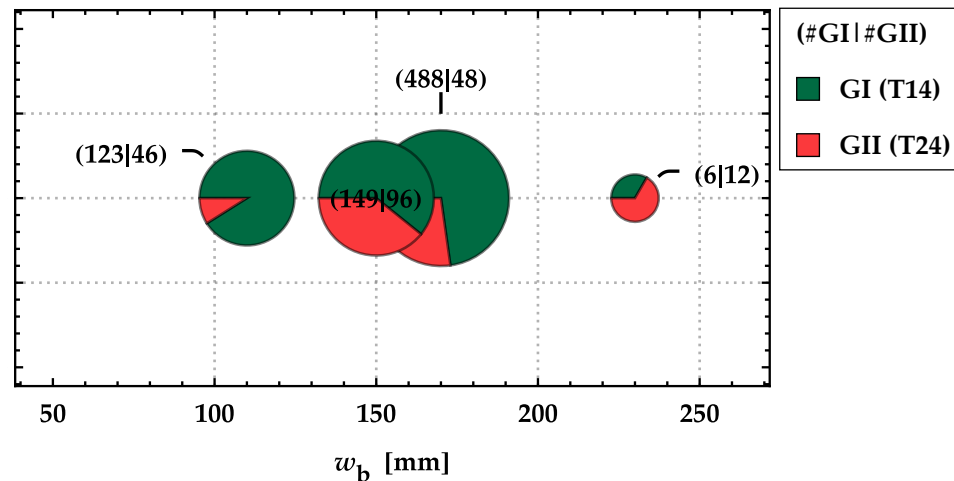


Figure 2-15: Number of boards classified by their nominal cross-section dimensions used to analyse the influence of the board width w_b on the geometric parameters.

Figure 2-16 shows the mean, 5 %- and 95 %-quantile values of the geometric parameters in dependence of the board width w_b . For each geometric parameter depending on the board width w_b the following observations can be summarised:

- **L_{wz} :**
 With increasing width w_b , the mean and both quantile values of the length of the weak zones are increasing for group GI (T14) and group GII (T24). Overall, the length of the weak zone is higher for the group GI (T14), which seems reasonable as the number of knots and their diameter are expected to be higher in lower strength classes.
- **D_{wz} :**
 Similar to L_{wz} , the mean and both quantile values of the distances between the weak zones D_{wz} are increasing with increasing board width in both groups GI (T14) and GII (T24). The distances between the WZs of group GII (T24) are slightly longer than in group GI (T14), which appears plausible for boards with a higher strength class.
- **$tKAR_{wz}$:**
 The mean and both quantile values of the $tKAR$ of the weak zones $tKAR_{wz}$ are decreasing with increasing board widths w_b in both groups GI (T14) and GII (T24). The same trend was also observed by **Burger [23]**. The $tKAR_{wz}$ -values are larger in group GI (T14). This is plausible as the knot parameter should be lower for higher strength classes and $tKAR_{150}$ was a parameter within the applied grading process as well.

• **Intermediate Zones IZ:**

For the parameters of the intermediate zones $\{L_{IZ}; D_{IZ}\}$ the mean and the 5 %-quantile values are almost at a constant level, while the 95 %-quantile values increase with an increasing board width. The mean and 95 %-quantile values of $tKAR$ of the intermediate zones $tKAR_{IZ}$ are decreasing with increasing board width w_b within both groups GI (T14) and GII (T24). Similar to [Section 2-4.2.1](#), a difference between the groups with on average 30 mm is only present for the distance between the IZs. Overall, no clear trends for the parameters of the intermediate zones $\{L_{IZ}; tKAR_{IZ}; D_{IZ}\}$ can be derived, which is partially due to the erratic data.

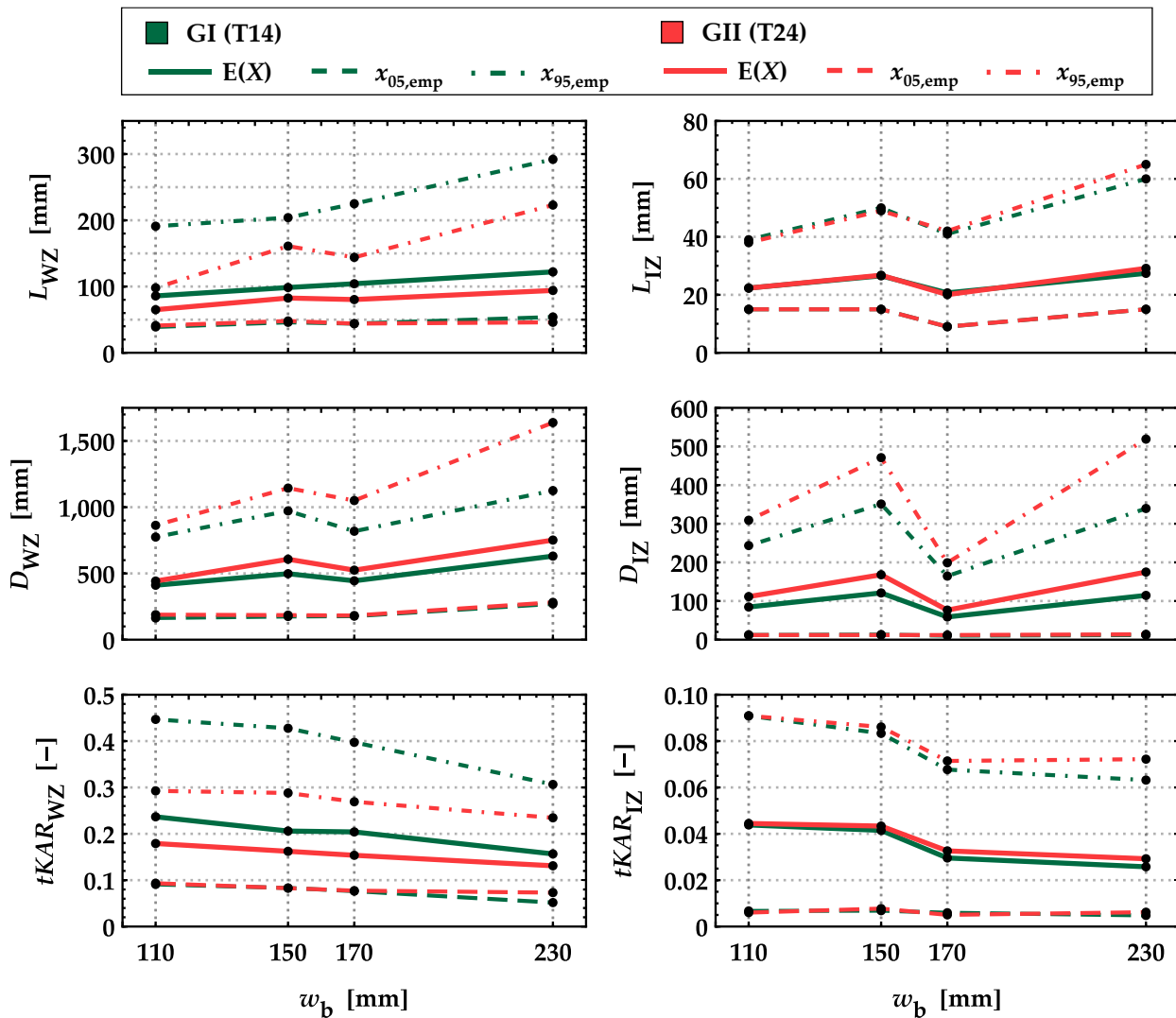


Figure 2-16: Mean, 5 %- and 95 %-quantile values of the geometric parameters $\{L_{WZ}; tKAR_{WZ}; D_{WZ}; L_{IZ}; tKAR_{IZ}; D_{IZ}\}$ in dependence of the board width w_b for group GI (T14) and GII (T24).

Based on these observations the following conclusions can be made: The board width has an influence on the geometric parameters of the weak zones $\{L_{WZ}; tKAR_{WZ}; D_{WZ}\}$. The differences (Δ) between the mean values from a board width of $w_b = 110$ mm to $w_b = 230$ mm are as follows: for the lengths of the weak zones $\Delta L_{WZ,GI} = 36.3$ mm and $\Delta L_{WZ,GII} = 29.1$ mm; for the $tKAR$ -value $\Delta tKAR_{WZ,GI} = -0.08$ and $\Delta tKAR_{WZ,GII} = -0.05$; and for the distance of the weak zone

$\Delta D_{WZ,GI} = 219$ mm and $\Delta D_{WZ,GII} = 308$ mm. In reference to a board width of $w_b = 110$ mm, these absolute differences amount to relative differences of $35 \div 45$ %.

As the tensile properties are mainly governed by the weak zones, it is of utmost importance to correctly depict them and to consider their relationships with the board width. For the intermediate zones, however, no clear trend was observed. By rating the influence of intermediate knots on the tensile properties of timber boards generally as small (at least for the investigated strength classes), possible influences from the board width are neglected in the ongoing investigation. Differences between the groups GI (T14) and GII (T24) are as expected and/or intended by the grading process. Based on these observations, the geometric parameters are assumed to be dependent on the assigned group and for the weak zone also on the board width. A comparison of the geometric parameters with the literature can be found in [Section 2-4.5](#).

2-4.3 Boards in Split Condition

2-4.3.1 Influence of lengthwise Splitting

An additional aspect of the probabilistic board model is the representation of boards, which were strength graded with full cross-section and lengthwise split afterwards. Due to the splitting process the positions of the knot zones, their lengths and relative change in magnitude; see [Figure 2-17](#).

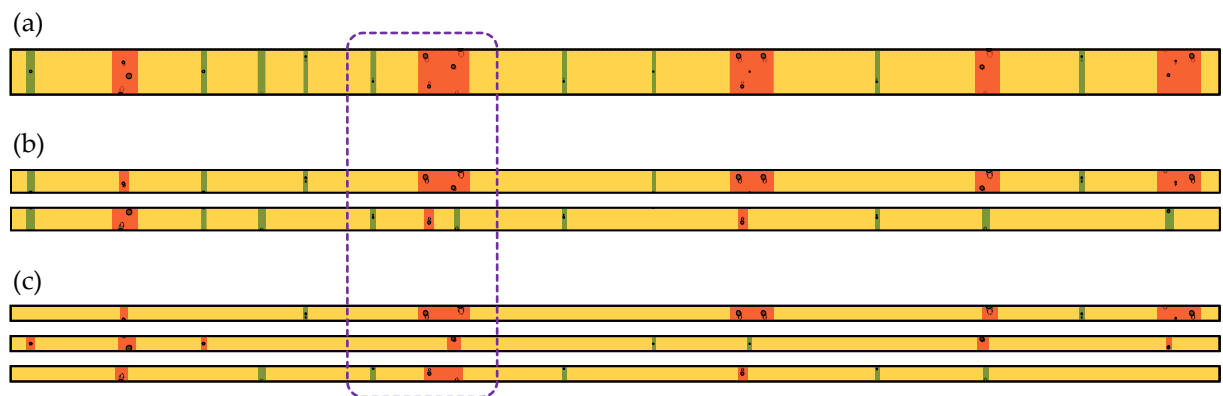


Figure 2-17: Knot zones within a board with full cross-section (a) and the same board split lengthwise into two (b) and three equally wide pieces (c).

[Figure 2-18](#) shows the $tKAR$ -value in longitudinal direction for the board segment highlighted in [Figure 2-17](#), in unsplit condition and after it got split in two and three equally wide pieces. Due to the lengthwise splitting, also the relative magnitude of the knot parameter $tKAR$ changes. In [Figure 2-18 \(b\)](#) the board is split into two equally wide pieces. The weak zone from the board with full cross-section is split up into one weak zone within the top board ([Figure 2-17 \(b\)](#)) and one weak zone and one intermediate zone within the bottom board. When the board is split into three equally wide pieces the magnitude of the weak zone, their length and classification change again; see [Figure 2-18 \(c\)](#). The newly introduced dynamical definition of

knot zones is capable of depicting the observed changes in their length, distance and magnitude. Probabilistic board models which consider weak zones by a fixed length (e.g. [3, 4, 10]) would give similar $tKAR$ -values but overestimate the length of knot zones significantly for some of the illustrated cases (Figure 2-18 (b) bottom board and Figure 2-18 (c) middle board).

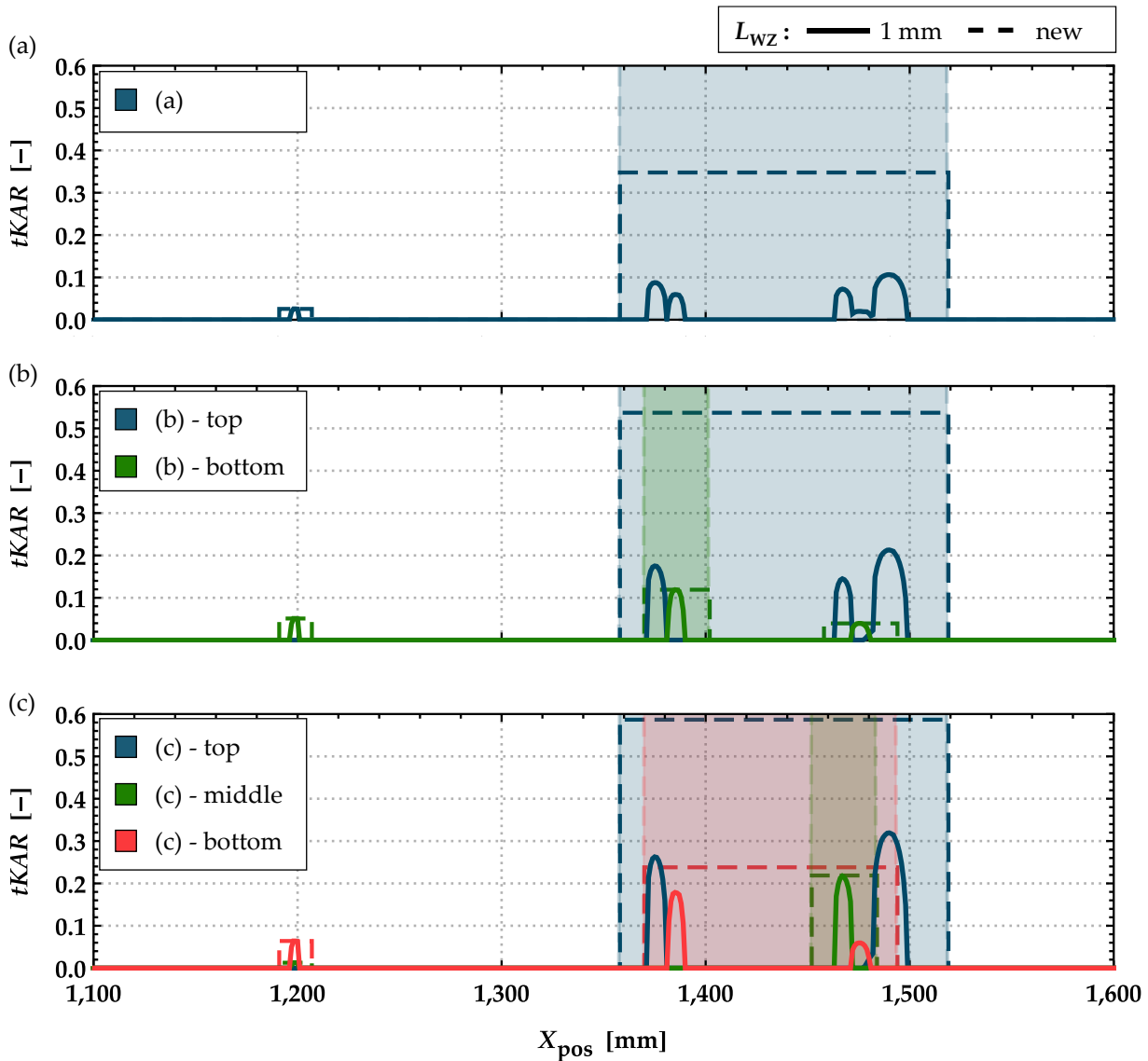


Figure 2-18: Detail of $tKAR$ -values of board segments from Figure 2-17 with a full board cross-section (a) and split lengthwise into two (b) and three equally wide pieces (c).

Following the observations in Figure 2-17 and Figure 2-18, the influence of lengthwise splitting of boards on the statistics of the geometric parameters $\{L_{WZ}; tKAR_{WZ}; D_{WZ}; L_{IZ}; tKAR_{IZ}; D_{IZ}\}$ is analysed. For the analysis boards with a width of $w_b = 150$ mm featuring a separation ratio of $\eta_s = \{1.00; 0.50; 0.33; 0.20; 0.125\}$ were used. For all cross-section dimensions boards from both groups GI (T14) and GII (T24) are present. The statistics of the geometric parameters of boards with dimension $w_b = 150$ mm and separation ratios of $\eta_s = \{1.00; 0.50; 0.33; 0.20; 0.125\}$ are summarised in Table Annex D-5 & Table Annex D-6. Histograms with calibrated density functions for all board dimensions and geometric parameters are illustrated in Annex C-1.3.

Figure 2-19 shows the mean, 5 %- and 95 %-quantile values of the geometric parameters in dependence of the separation ratios η_s . The following conclusions are made:

- **L_{wz} :**
With a decreasing separation ratio η_s , the mean and both quantiles of the length of the weak zone are decreasing for group GI (T14) and group GII (T24). This trend seems plausible as knot clusters within boards in full cross-section width are split up into smaller clusters or even single knots. For group GI (T14) the length of the weak zone is higher as for GII (T24), which is true for all separation ratios.
- **D_{wz} :**
For the distance between the weak zones D_{wz} , the mean and 95 %-quantile are increasing with decreasing separation ratios for both groups GI (T14) and GII (T24), while the 5 %-quantile stays constant. This tendency appears plausible given the possibility that knot clusters are split up into single knots which consequence that the distance between remaining weak zones increases. The distances between WZs of group GII (T24) are slightly larger than of group GI (T14) which is found to be independent of the separation ratio.
- **$tKAR_{wz}$:**
The $tKAR_{wz}$ -values are larger in group GI (T14) than in group GII (T24) at full cross-section width. This is due to the grading process of the boards. The mean and both quantile values of the $tKAR$ of the weak zone $tKAR_{wz}$ are increasing with decreasing separation ratios η_s within both groups GI (T14) and GII (T24). Both groups converge with lower separation ratios to common mean value and variation. This seems plausible, as the initial grading of the boards is lost due to the lengthwise splitting and both groups converge to the natural occurrence of knots in unsorted boards.
- **L_{iz} :**
Similar to the length of the weak zone, also the length of the intermediate zone is slightly decreasing with decreasing separation ratio η_s . No differences between the groups GI (T14) and GII (T24) are observed.
- **D_{iz} :**
For the distance between the weak zones D_{iz} , the mean and 95 %-quantile values are increasing with lower separation ratios for both groups GI (T14) and GII (T24), while the 5 %-quantile stays constant. This tendency appears plausible, as intermediate knots in boards with full cross-section width may vanish from certain board parts after the lengthwise splitting. Consequently, the distance between IZs is increasing as shown in **Figure 2-17**. The distances between intermediate zones of group GII (T24) are slightly larger than in group GI (T14) which is independent of the separation ratio.
- **$tKAR_{iz}$:**
Within both groups GI (T14) and GII (T24) the mean and the 95 %-quantile values of the $tKAR$ of the intermediate zone $tKAR_{iz}$ are increasing with decreasing separation ratios η_s , while the 5 %-quantile values stay constant. For the $tKAR_{iz}$ -values no differences are observed between both groups GI (T14) and GII (T24).

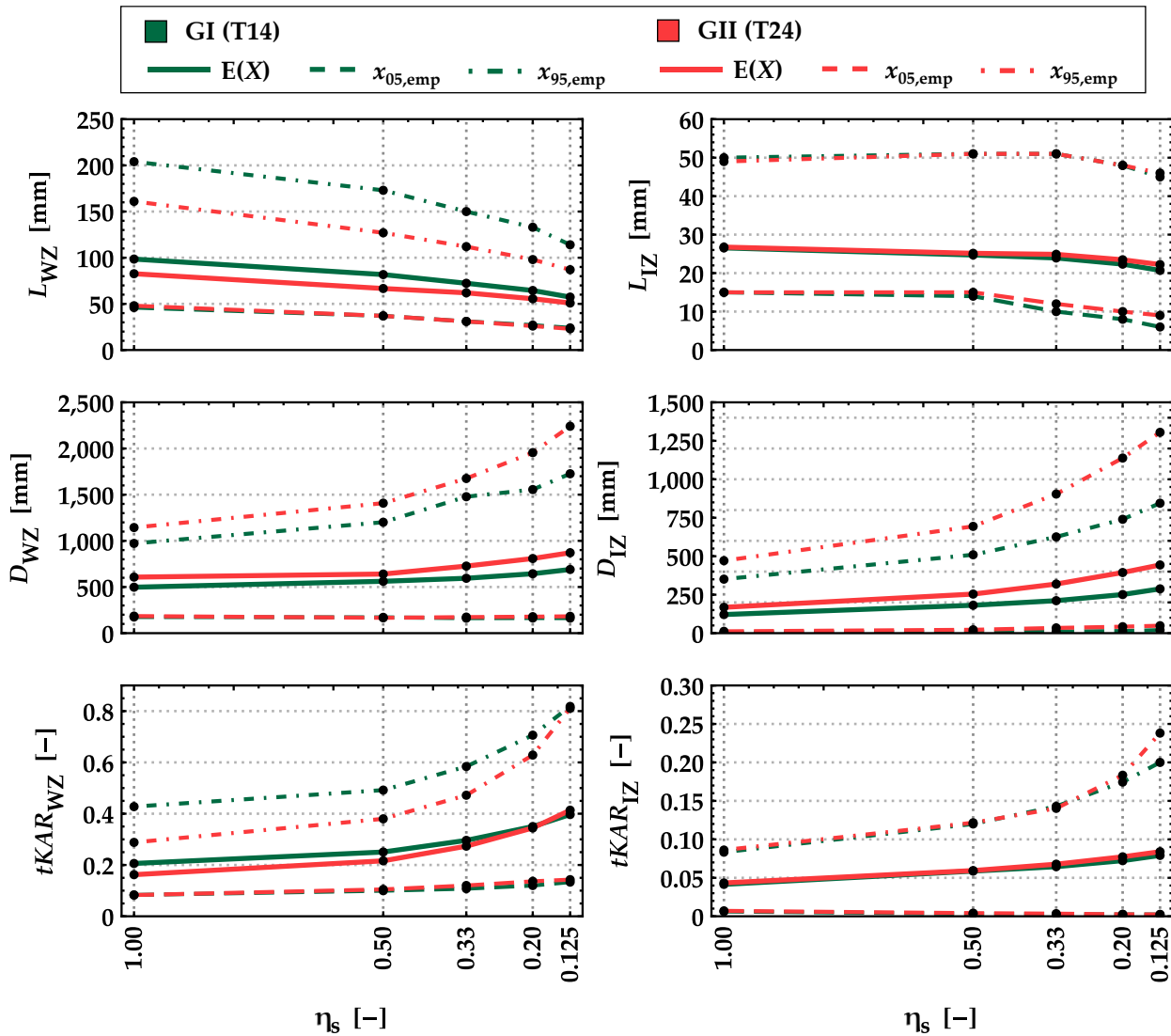


Figure 2-19: Mean, 5 %- and 95 %-quantile values of the geometric parameters $\{L_{WZ}; tKAR_{WZ}; D_{WZ}; L_{IZ}; tKAR_{IZ}; D_{IZ}\}$ in dependency of the separation ratio η_s for groups GI (T14) and GII (T24).

As expected, the separation ratio η_s has a significant influence on all geometric parameters $\{L_{WZ}; tKAR_{WZ}; D_{WZ}; L_{IZ}; tKAR_{IZ}; D_{IZ}\}$. The differences between the groups GI (T14) and GII (T24) are as expected and/or intended by the grading process. Based on these observations the geometric parameters are further treated as dependent on the assigned group and separation ratio.

2-4.3.2 Influence of the Position of Residual Board Pieces on the Geometric Parameters

So far, all necessary parameters $\{L_{WZ}; tKAR_{WZ}; D_{WZ}; L_{IZ}; tKAR_{IZ}; D_{IZ}\}$ were calculated with the software tool **KnotIntertpreter** [21]. Thereby, the boards within the database were virtually split lengthwise into $\{2; 3; 5; 8\}$ equally wide pieces. In calculating the parameters for each separation ratio, the data of all pieces was used to derive the statistics. This approach is suitable for resawn glulam. As seen in **Figure 2-20 (a)**, within the resawn glulam beams all lengthwise board pieces are present (outer and middle pieces of the board). In other engineered timber

products, like CLT, flex_GLT or flex_CLT, however, usually only the outer pieces of the lengthwise split boards are within the final product, i.e. the boards are split lengthwise only once but at an arbitrary position so that the widths of the residual pieces are random; see **Figure 2-20 (b)**. By considering this, in the following the statistics of the geometric parameters $\{L_{wz}; tKAR_{wz}; D_{wz}; L_{lz}; tKAR_{lz}; D_{lz}\}$ are analysed for the two cases (i) all board pieces and (ii) only the outer board pieces are within the final product, **Figure 2-20 (a & b)**. Both cases are compared whether a unified approach for the geometric parameters is possible.

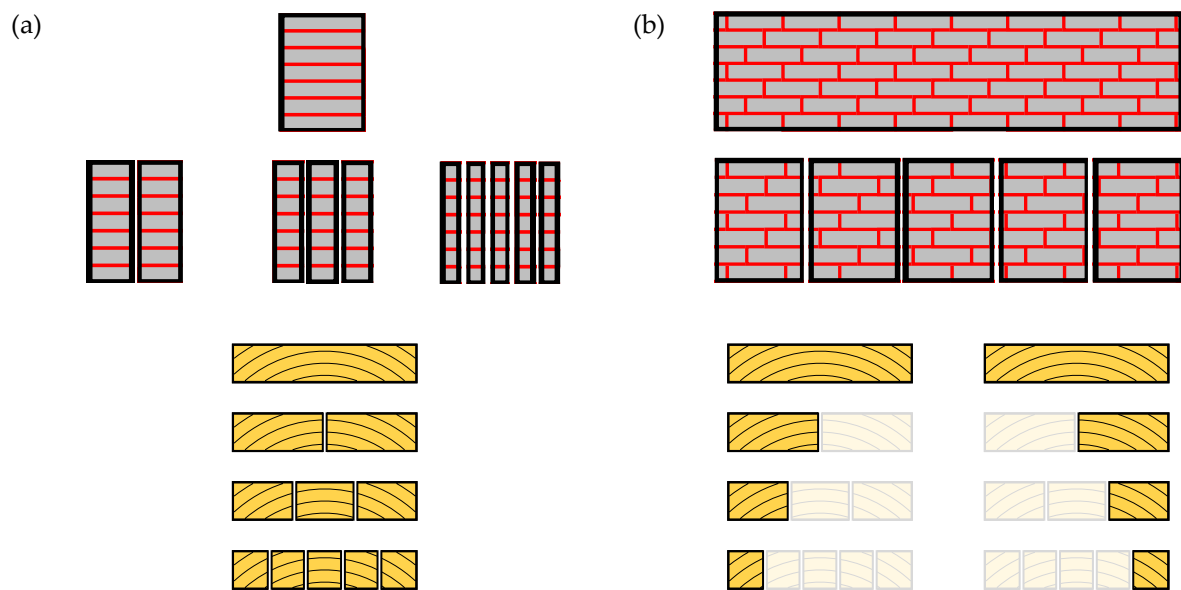


Figure 2-20: Residual board pieces in different engineered structural timber products: (a) resawn glulam with all residual board pieces present in the final product {case (i)} and (b) flex_GLT containing only outer pieces of residual boards within the product {case (ii)}.

Figure 2-21 shows P-P plots of the empirical distributions of (i) all residual board pieces versus (ii) only the outer residual board pieces for the parameters of the weak zones $\{L_{wz}; tKAR_{wz}; D_{wz}\}$, the separation ratios of $\eta_s = \{0.33; 0.20; 0.125\}$ and boards from groups GI (T14) and GII (T24). For the parameters of the weak zones $\{L_{wz}; tKAR_{wz}; D_{wz}\}$ the deviations between the empirical distributions of the outer residual board parts and all residual board parts are minor. Therefore, in the following no differentiation in the representation of the weak zones is made between both cases.

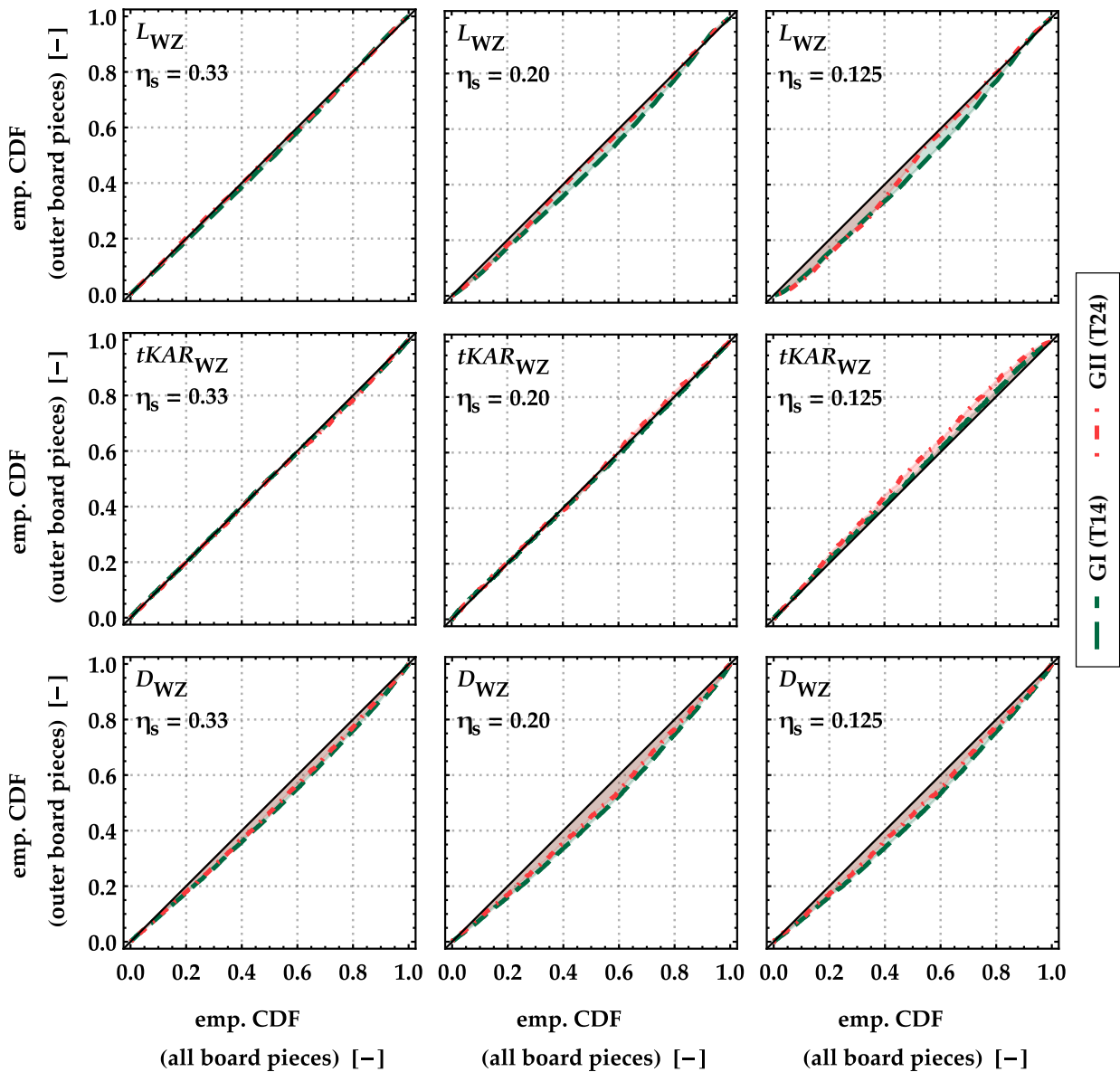


Figure 2-21: P-P plots of the empirical distributions of all residual board pieces versus that of the outer residual board pieces for the geometric parameters $\{L_{WZ}; tKAR_{WZ}; D_{WZ}\}$ and the separation ratios of $\eta_s = \{0.33; 0.20; 0.125\}$ allocated to groups GI (T14) and GII (T24).

Figure 2-22 shows P-P plots of the empirical distributions of (i) all residual board pieces versus (ii) only the outer residual board pieces for the parameters of the intermediate zones $\{L_{IZ}; tKAR_{IZ}; D_{IZ}\}$, the separation ratios of $\eta_s = \{0.33; 0.20; 0.125\}$ and boards from groups GI (T14) and GII (T24). For the parameters of the intermediate zone $\{L_{IZ}; tKAR_{IZ}; D_{IZ}\}$ higher deviations between the empirical distributions of the outer residual board parts and all residual board parts are observed than for $\{L_{WZ}; tKAR_{WZ}; D_{WZ}\}$. The deviations increase with decreasing separation ratios. The overall high uncertainty within the data of intermediate zones (see [Section 2-4.4](#)) supersedes the observed deviations regarding the positions of the residual board. Hence, the influence of the position of residual board pieces is neglected in the ongoing investigation and no differentiation between the two cases in [Figure 2-20](#) regarding the intermediate zones is made.

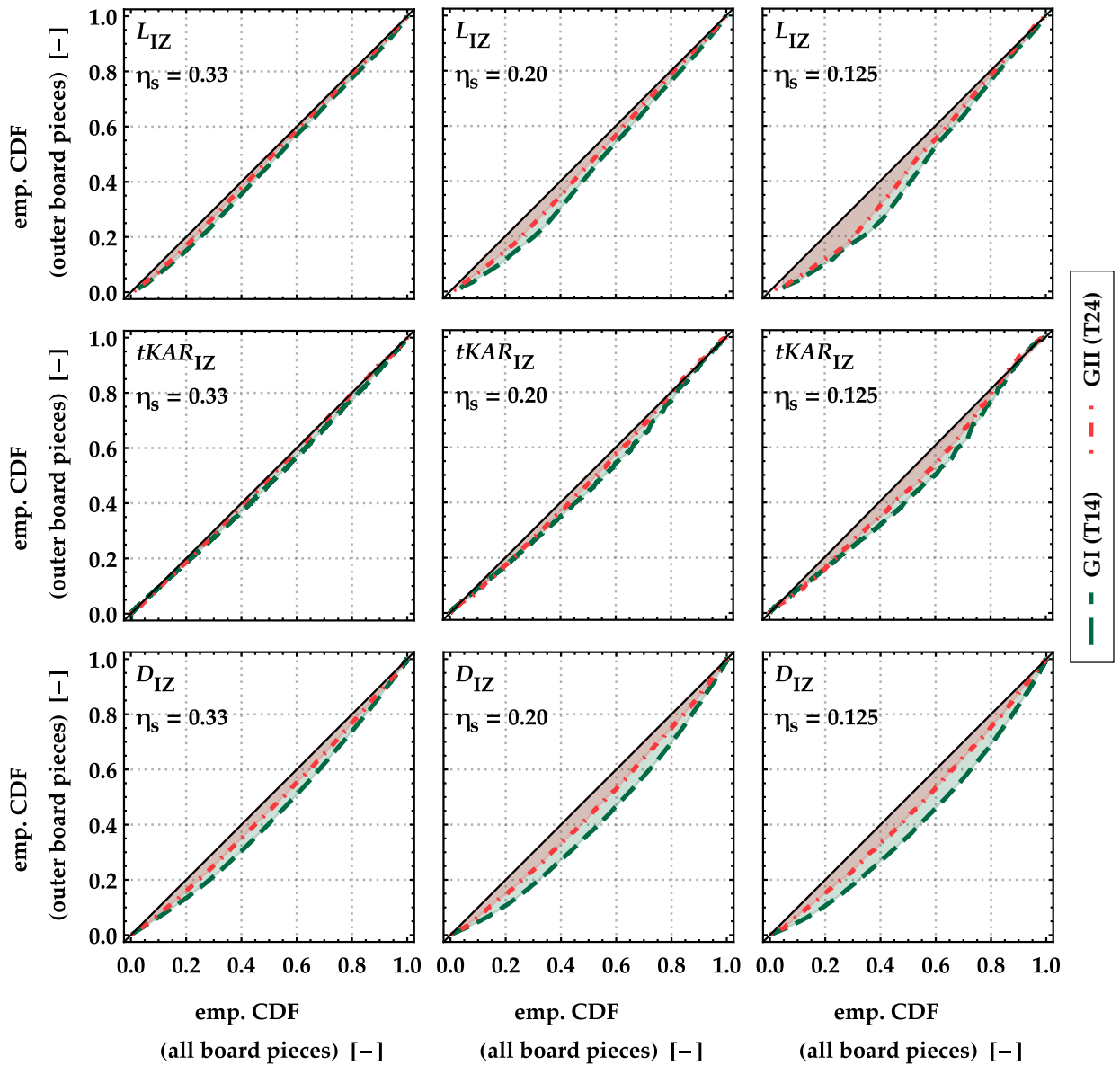


Figure 2-22: P-P plots of the empirical distributions of all residual board pieces versus that of the outer residual board pieces for the geometric parameters $\{L_{IZ}; tKAR_{IZ}; D_{IZ}\}$ and the separation ratios of $\eta_s = \{0.33; 0.20; 0.125\}$ allocated to groups GI (T14) and GII (T24).

Based on the comparison of the empirical distributions in **Figure 2-21** and **Figure 2-22** and the previously drawn conclusions, the derived statistics are approximately applicable for both cases.

2-4.4 Distributions of the Geometric Parameters

Apart from the statistics of investigated geometric parameters, which were found to depend on board width and separation ratio, for their thorough probabilistic characterisation also knowledge on their statistical distributions is required. In selecting representative statistical distribution models, the restriction of the geometric parameters to the positive domain and other underlying physical phenomena on hand were considered. For comparison, the

representativeness of several distribution models, explicitly lognormal (LND), Weibull (WD), gamma (GD) and beta distribution (BD), were analysed for each parameter. The parameters of the distribution models were calibrated directly on the test data and compared with models from literature.

Figure 2-23 shows histograms and density functions calibrated to the length of the weak and the intermediate zones of boards featuring a width of $w_b = 150$ mm, for group GI (T14) and different separation ratios. The peak for L_{IZ} within the class of $15 \div 20$ mm, which corresponds to single small knots with a diameter of $5 \div 7$ mm, might be explained by inaccuracies in the manually measured data. Please note: knots with a diameter below 5 mm were usually not recorded. The default size of the circle used to mark knots in the software **KnotLogger** [24] is set to 5 mm. Therefore, it is possible that some knots slightly below 5 mm diameter were also recorded with 5 mm. The best representation of the empirical data of the lengths of weak and the intermediate zones can be achieved with a lognormal distribution. The same distribution model was used by **Isaksson** [11] and **Brandner** [12] to model the length of the weak zone. Other probabilistic board models assume a fixed length of the weak zone with $L_{WZ} = 150$ mm (**Fink** [3], **Frese** [4], **Blaß et al.** [5]) or $L_{WZ} = 100$ mm (**Tapia** [6]). For the length of intermediate zones **Brandner** [12] also used a lognormal distribution. Besides this model no other models are known to the author which deals with the length of smaller intermediate knot sections.

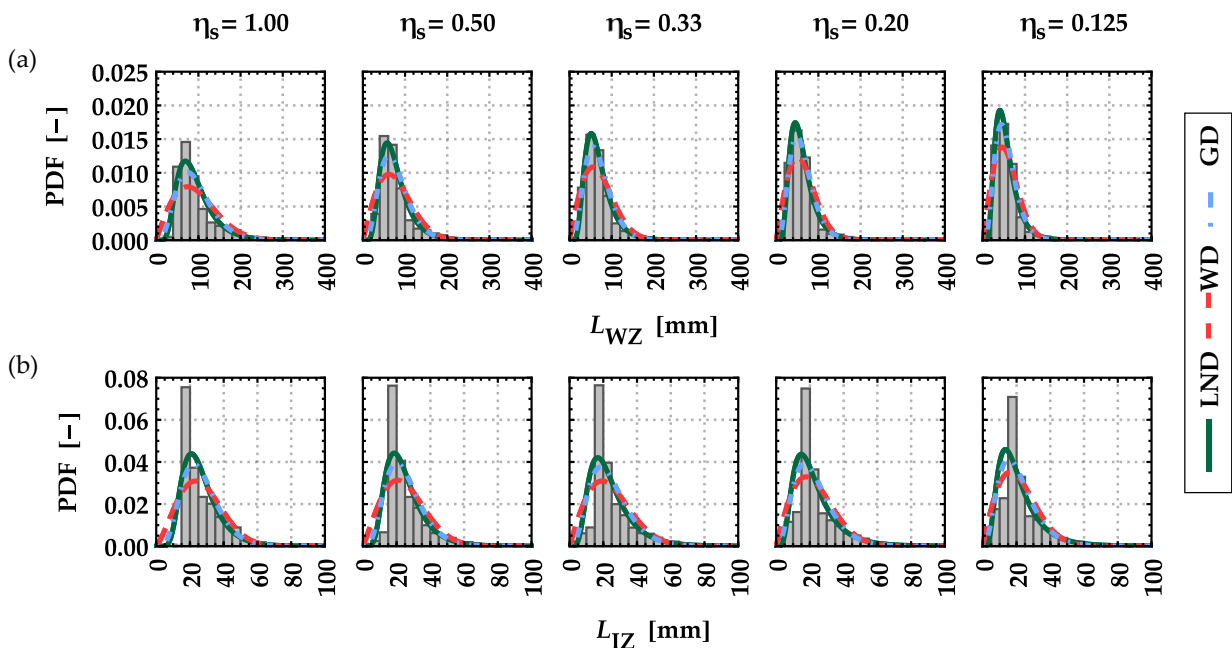


Figure 2-23: Histograms and density functions {LND; WD; GD} calibrated to the length of (a) the weak zones L_{WZ} and (b) of the intermediate zones L_{IZ} of boards featuring a width of $w_b = 150$ mm, for group GI (T14) and separation ratios of $\eta_s = \{1.00; 0.50; 0.33; 0.20; 0.125\}$.

Figure 2-24 shows histograms and density functions calibrated to the $tKAR$ -values of the weak and intermediate zones of boards featuring a width of $w_b = 150$ mm, group GI (T14) and different separation ratios. For $tKAR_{WZ}$ the best representation is achieved by a lognormal

distribution model. Models in **Fink [3]**, **Brandner [12]**, **Ehlbeck & Colling [25]** also describe the $tKAR$ -value of the weak zone via the lognormal distribution. By means of this distribution model theoretically values of $tKAR_{WZ} > 1.0$ are possible but physically not. The basic beta distribution, on the other hand, is only defined in the domain $[0;1]$, which corresponds to the physically possible domain of the $tKAR$ -value of weak zones. The beta distribution is also able to represent the data in a satisfactory manner and no additional truncation of the probability density function to restrict the domain to a physically plausible range is necessary. The $tKAR$ -values of the intermediate zones are best represented by the beta distribution model. The only probabilistic board model so far which considers intermediate zones in **Brandner [12]** describes $tKAR_{IZ}$ via a lognormal distribution.

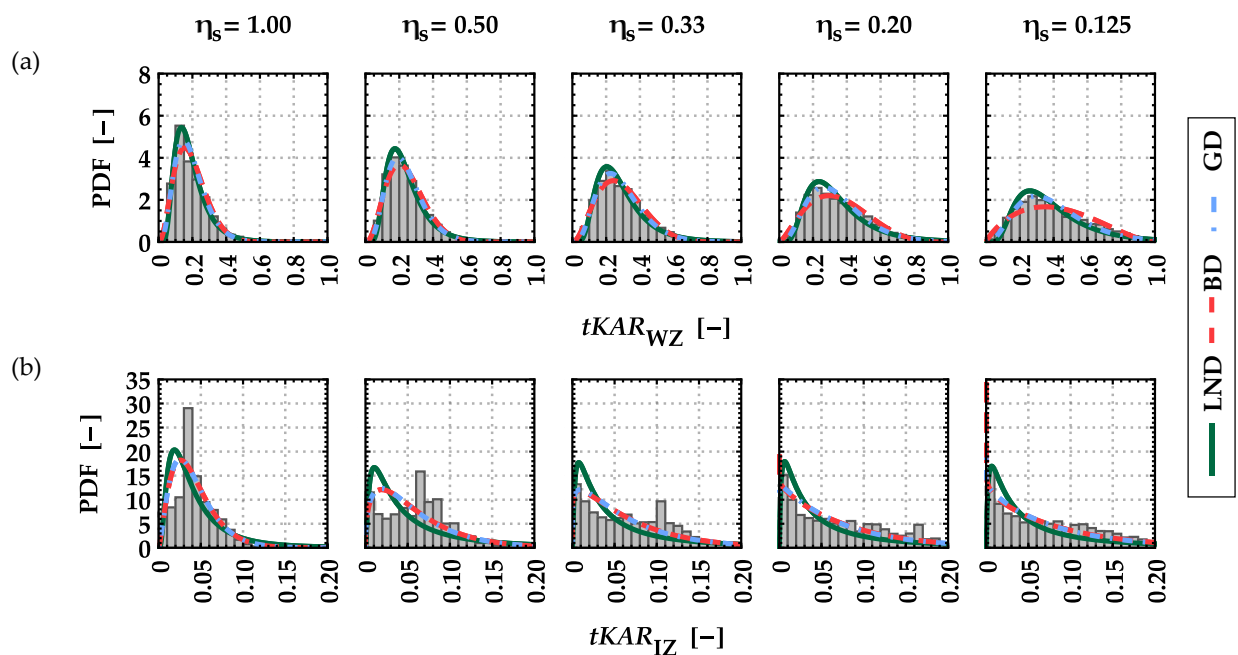


Figure 2-24: Histograms and density functions {LND; BD; GD} calibrated to the $tKAR$ -value of (a) the weak zones $tKAR_{WZ}$ and (b) of the intermediate zones $tKAR_{IZ}$ of boards featuring a width of $w_b = 150$ mm, for group GI (T14) and separation ratios of $\eta_s = \{1.00; 0.50; 0.33; 0.20; 0.125\}$.

Figure 2-25 shows histograms and density functions calibrated to the distance of the weak and the intermediate zones of boards featuring a width of $w_b = 150$ mm, for group GI (T14) and for different separation ratios. The best representation of the empirical data of the distance of the weak zone and the intermediate zone can be achieved with a gamma distribution model. The same distribution was used by **Fink [3]**, **Isaksson [11]**, **Ehlbeck & Colling [25]**. The gamma distribution represents also the time or distance to a specific number of events in the Poisson process. **Brandner [12]**, on the other hand, used a lognormal distribution also for the description of the distances.

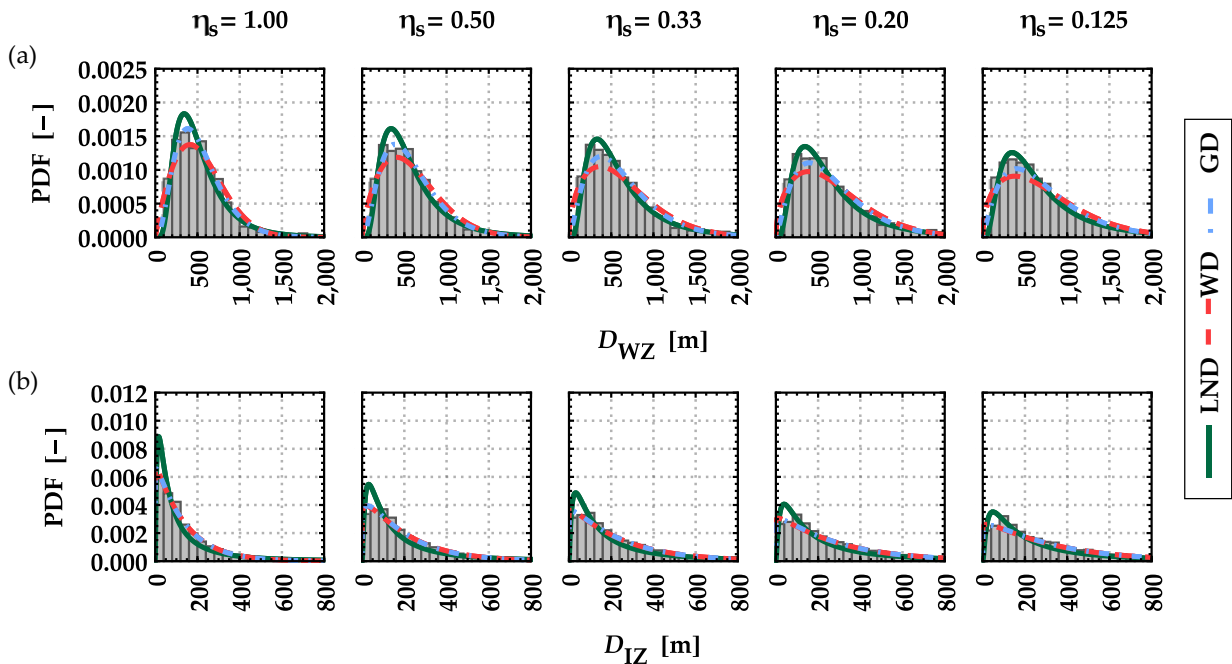


Figure 2-25: Histograms and density functions {LND; WD; GD} calibrated to the distance between (a) weak zones D_{WZ} and (b) intermediate zones D_{IZ} of boards featuring a width of $w_b = 150$ mm, for group GI (T14) and separation ratios of $\eta_s = \{1.00; 0.50; 0.33; 0.20; 0.125\}$.

2-4.5 Comparison of Selected Model Parameters with the Literature

As already mentioned in [Section 2-1](#), in the literature numerous models for the properties of boards along the longitudinal direction are found; see [\[3, 11, 25\]](#). All these models try to depict the occurrence and magnitude of knots in timber boards realistically. Within this section the focus is set on Norway spruce boards. Please note: the results of the model developed in [Brandner \[12\]](#) is not mentioned explicitly as the majority of the boards used to derive the model parameters originate from the same database.

In most other probabilistic board models the length of the weak zone is assumed with a fixed length; e.g. $L_{WZ} = 150$ mm in [\[3–5, 25\]](#). The length of weak sections in boards was also analysed by [Isaksson \[11\]](#). He applied a different definition of the weak zone; see [Figure 2-26](#). Hereby, the length of the weak zone is as long as the $tKAR$ -value is above a certain threshold. [Isaksson \[11\]](#) set this threshold to 40 % and 50 % of the maximum $tKAR$ -value of each board. The resulting lengths of the weak zones are summarised in [Table 2-6](#). Due to the different definitions of the length of the weak zones a direct comparison is difficult. Nonetheless, the expected values of the lengths $\{L_{WZ,0.4}; L_{WZ,0.5}\}$ are approximately 35 ÷ 50 mm larger than the values of L_{WZ} within the new probabilistic board model. A similar discrepancy is seen in the example illustrated in [Figure 2-26](#). The coefficients of variation of the length of the weak zone is in a similar range in both investigations. Regarding the distribution of the length of the weak zones [Isaksson \[11\]](#) stated the best representation could be achieved by a lognormal distribution. Additionally, the length of the weak zone seems not to be influenced by the origin of the boards, as similar results are achieved for boards from Austria & Switzerland and Sweden.

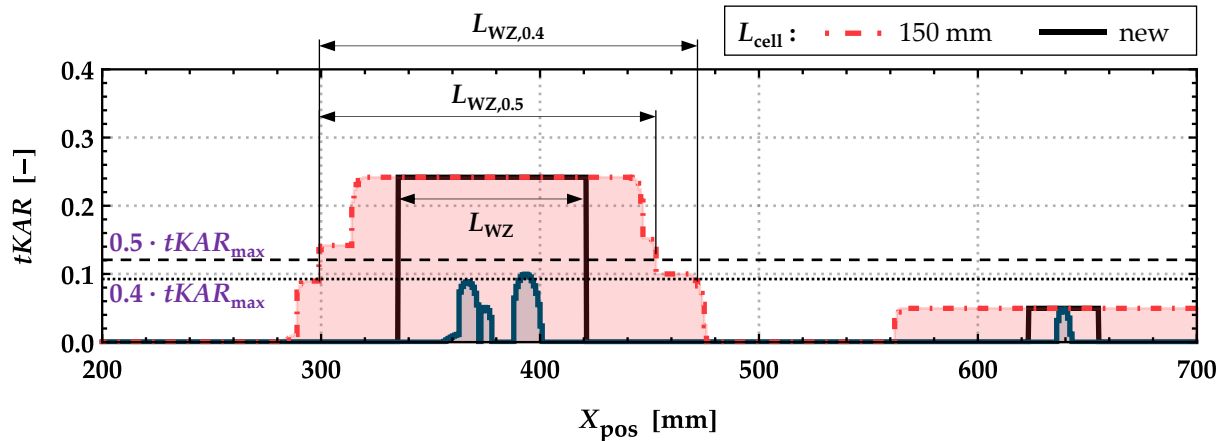


Figure 2-26: Definition of the length of the weak zone L_{Wz} according to the new probabilistic board model compared to the approach in Isaksson [11] ($L_{Wz,0.4}$; $L_{Wz,0.5}$).

Table 2-6: Comparison of the length of the weak zones for GI (T14) & GII (T24) with investigations in the literature; see [11].

	GI (T14)	GII (T24)	Isaksson [11] $L_{Wz,0.4}$	Isaksson [11] $L_{Wz,0.5}$
$E(L_{Wz})$ [mm]	98.5	82.6	134.5	121.9
$COV(L_{Wz})$ [%]	54.8	45.6	38.4	40.9
$Q_{equi}(L_{Wz})$ [-]	0.10	0.16	–	–
w_b [mm]	150		140	
Strength class ¹	~ T14 (C24)	~ T24 (C35)	~ T22 (C30)	~ T22 (C30)
Distribution model	LND		LND	
Provenance	AT/CH		SE	

¹... assumed strength class with similar properties

Most board models define the $tKAR$ -value of the weak zone with a fixed length of $L_{Wz} = 150$ mm as the knot area projected onto the cross-section area (overlapping knot areas are counted only once); see [1, 3–5, 26]. As already discussed in Section 2-2.1, in the new probabilistic board model the influence of the variable length of the weak zone on the $tKAR$ -value is neglectable. In Table 2-7 $tKAR$ -values of the weak zones for GI (T14) and GII (T24) are compared with investigations in the literature [3, 26]. Hereby, group GI (T14), L25 in Fink [3] and GII in Colling & Dinort [26] have similar mechanical properties. The same is true for group GII (T24), L40 in Fink [3] and GI in Colling & Dinort [26]. The mean value of $tKAR_{wz}$ ranges from $0.21 \div 0.24$ for the lower strength classes and from $0.16 \div 0.19$ for the higher strength classes, respectively. As already mentioned, the variation can be further separated into a variation within a single board and between boards. The ratio between the variation of the board mean and the total variation is expressed by the equi-correlation; see Section 2-5.1 for further details. The coefficient of variation is slightly lower in Fink [3], but the tendency of a lower COV for the higher strength class is similar to the trend between GI (T14) and GII (T24). The equi-correlation, on the other hand, is slightly higher in Fink [3] than for GI (T14) and GII (T24). Overall, the results are

within a comparable range with the new approach and the origin of the boards seems not to be influencing the $tKAR$ -values of weak zones.

Table 2-7: Comparison of the $tKAR$ -value of the weak zones for GI (T14) & GII (T24) with investigations in the literature; see [3, 26].

	GI (T14)	GI (T14)	Fink [3] (L25)	Fink [3] (L40)	Colling & Dinort [26] GII	Colling & Dinort [26] GI
$E(tKAR_{wz}) [-]$	0.21	0.16	0.24	0.19	0.22	0.17
$COV(tKAR_{wz}) [%]$	52.2	41.7	39.6	33.3	–	–
$q_{equi}(tKAR_{wz}) [-]$	0.14	0.17	0.22	0.26	–	–
w_b [mm]	150		126		170	
Strength class¹	~ T14 (C24)	~ T24 (C35)	~ T14 (C24)	~ T26 (C40)	~ T14 (C24)	~ T22 (C30)
Distribution model	BD		LND		LND	
Provenance	AT/CH		DE		SK/DE/AT	

¹assumed strength class with similar properties

Most board models define the distance between weak zones D_{wz} as the distance between their centres; see [1, 3, 11, 26]. Therefore, it is not influenced by the length of the weak zone, but dependent on the definition whether a single knot or knot cluster is treated as such. Nonetheless, the results of the different investigations regarding the distance between weak zones should be comparable as most board models identify the weak zones in a similar manner. **Table 2-8** shows a comparison of the distances between weak zones for GI (T14) and GII (T24) with investigations in the literature [3, 11, 26].

The mean value of D_{wz} ranges from 440 ÷ 607 mm and the coefficient of variation from 38.5 ÷ 64.2 %. The mean value for GI (T14) is within this range, whereas the mean value of D_{wz} for GII (T24) is slightly higher. This influence of the strength class was not found in other investigations; see [3, 26]. The “Karlsruher Rechenmodell” treats the distance between knots by the probability whether or not knots are present in neighbouring board elements; see [1, 4, 5]. On the mean level every third element contains knots, which equals to $E(D_{wz}) \approx 450$ mm, considering the fixed element length of 150 mm. The results from **Isaksson [11]** show how the classification of weak zones can influence the distance of the WZs, as the mean value changes from 440 mm to 494 mm, respectively, by changing the limit of $tKAR_{max}$ from 40 % to 50 %; see **Figure 2-26**. Overall, the results achieved with the new probabilistic board model are within a comparable range than previous investigations. Additionally, no influence regarding the origin of the boards was observed, a circumstance which clearly extends the range of application and allows more general conclusions.

Table 2-8: Comparison of the distance of the weak zones for GI (T14) & GII (T24) with investigations in the literature; see [3, 11, 26].

	GI (T14)	GI (T14)	GII (T24)	Fink [3] (L25 & L40)	Isaksson [11] $L_{WZ,0.4}$	Isaksson [11] $L_{WZ,0.5}$	Colling & Dinort [26] GI & GII
$E(D_{WZ})$ [mm]	498	607	607	529	440	494	483
$COV(D_{WZ})$ [%]	54.2	52.2	52.2	46.5	61.3	64.2	38.5
$q_{equi}(D_{WZ})$ [-]	0.20	0.10	0.10	–	–	–	–
w_b [mm]	150		150	126	140		170
Strength class ¹	~ T14 (C24)	~ T24 (C35)	~ T24 (C35)	~ T14 (C24) & T26 (C40)	~ T22 (C30)		~ T14 (C24) & T22 (C30)
Distribution model	GD		GD	GD	GD		LND
Provenance	AT/CH		AT/CH	DE	SE		SK/DE/AT

¹assumed strength class with similar properties

A comparison of the statistics of the intermediate zones with data from the literature is not possible, as most models neglect knots below a certain threshold. Any literature regarding the influence of lengthwise splitting on the statistics of the weak zones as well as on the intermediate zones is not known to the author.

2-4.6 Correlation between Geometric Parameters

Beside the statistical distribution model and corresponding distribution parameters of each individual geometric parameter also the correlation between them needs to be known. Although it is not the best choice for every pair of parameters the Pearson correlation coefficient, as a linear correlation measure, was calculated for all board widths and groups GI (T14) and GII (T24) separately. Due to the random number of weak zones and intermediate zones within each board, the mean values of the parameters of each board were used for this analysis. Only minor differences were found regarding the influence of the board width and groups. Therefore, no distinction between the board widths and strength classes was made in the following. The resulting correlations (Pearson) between the geometric parameters are listed in **Table 2-9** and illustrated in **Figure 2-27** for a separation ratio of $\eta_s = 1.00$ and in **Figure 2-28** for $\eta_s = 0.125$ (other separation ratios are shown in **Annex C-1.4**). The plots show non-linear dependencies between individual geometric parameters. The Pearson correlation coefficient is intended to describe linear dependencies. Nonetheless, it is used here as a rough estimate in order to show the influences on the correlation. It is apparent that the correlation between certain parameters changes with the separation ratio η_s . This needs to be implemented within the probabilistic board model, especially for the geometric parameter combinations with notable correlations $|\rho| \geq 0.20$.

Table 2-9: Estimated Pearson correlation coefficients between the global (mean) board parameters $\{L_{wz}; tKAR_{wz}; D_{wz}; L_{iz}; tKAR_{iz}; D_{iz}\}$ of all boards within the database for different separation ratios $\eta_s = \{1.00; 0.50; 0.33; 0.20; 0.125\}$.

separation ratio η_s [-]	correlation ρ [-]				
	1.00	0.50	0.33	0.20	0.125
$L_{wz} - tKAR_{wz}$	0.64	0.61	0.49	0.42	0.39
$L_{wz} - D_{wz}$	0.03	-0.07	-0.03	0.00	0.02
$L_{wz} - L_{iz}$	0.01	-0.05	-0.01	0.03	0.07
$L_{wz} - tKAR_{iz}$	-0.23	-0.18	-0.13	-0.07	-0.03
$L_{wz} - D_{iz}$	-0.27	-0.24	-0.18	-0.10	-0.01
$tKAR_{wz} - D_{wz}$	-0.13	-0.11	0.01	0.06	0.05
$tKAR_{wz} - L_{iz}$	-0.12	-0.02	0.10	0.14	0.15
$tKAR_{wz} - tKAR_{iz}$	-0.04	0.08	0.12	0.15	0.10
$tKAR_{wz} - D_{iz}$	-0.30	-0.14	0.03	0.18	0.24
$D_{wz} - L_{iz}$	0.23	0.15	0.14	0.13	0.12
$D_{wz} - tKAR_{iz}$	0.10	0.09	0.06	0.04	0.04
$D_{wz} - D_{iz}$	0.47	0.44	0.46	0.44	0.45
$L_{iz} - tKAR_{iz}$	0.51	0.29	0.11	0.05	0.03
$L_{iz} - D_{iz}$	0.50	0.49	0.42	0.39	0.38
$tKAR_{iz} - D_{iz}$	0.43	0.35	0.23	0.13	0.10

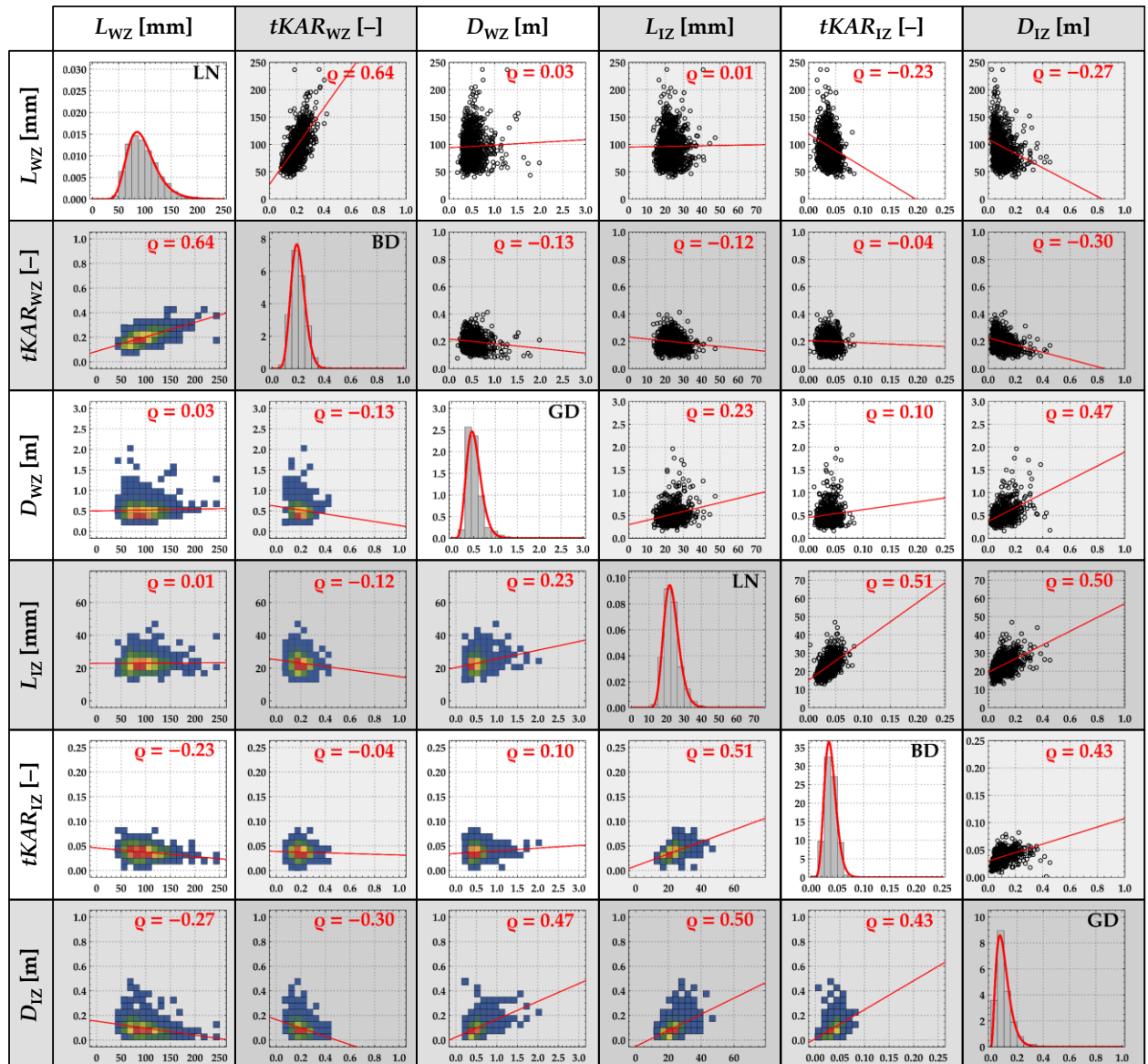


Figure 2-27: Correlations and linear trendlines together with histograms and calibrated density functions of global (mean) board properties of $\{L_{Wz}; tKAR_{Wz}; D_{Wz}; L_{Iz}; tKAR_{Iz}; D_{Iz}\}$ of all boards in the databases given a separation ratio of $\eta_s = 1.00$.

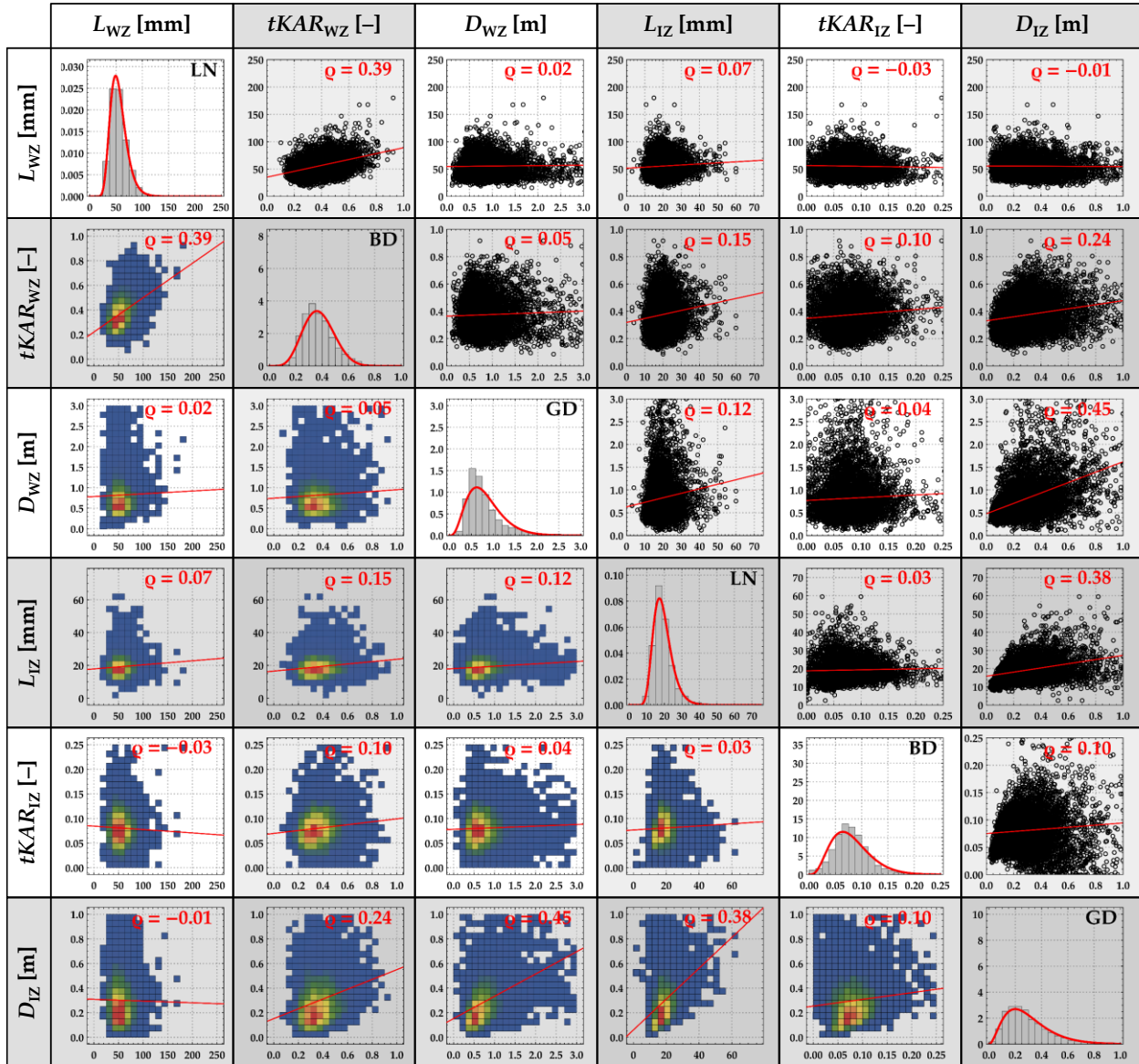


Figure 2-28: Correlations and linear trendlines together with histograms and calibrated density functions of global (mean) board properties of $\{L_{WZ}; tKAR_{WZ}; D_{WZ}; L_{IZ}; tKAR_{IZ}; D_{IZ}\}$ of all boards in the databases given a separation ratio of $\eta_s = 0.125$.

2-5 Probabilistic Representation of Timber Boards

2-5.1 Concept of the Probabilistic Board Model

The aim of the probabilistic board model is to generate pseudo random numbers as artificial realisations of identified random variables, e.g. the geometric parameters as analysed in [Section 2-4](#), which are consistent with the corresponding marginal distributions and correlations. This is accomplished with a Gaussian copula. The basic principles are shown exemplarily for the variables L_{WZ} and $tKAR_{WZ}$ in [Figure 2-29](#). First, correlated pseudo random numbers are drawn from two uniform distributions and afterwards transformed via their respective inverse distribution functions. Based on the correlation and the marginal distributions of the random variables a bi-variate probability density function is created; see [Figure 2-29 \(c\)](#). This principal was extended to all six random variables $X = \{L_{WZ}; tKAR_{WZ}; D_{WZ}; L_{IZ}; tKAR_{IZ}; D_{IZ}\}$ to generate a six-dimensional multi-variate probability distribution.

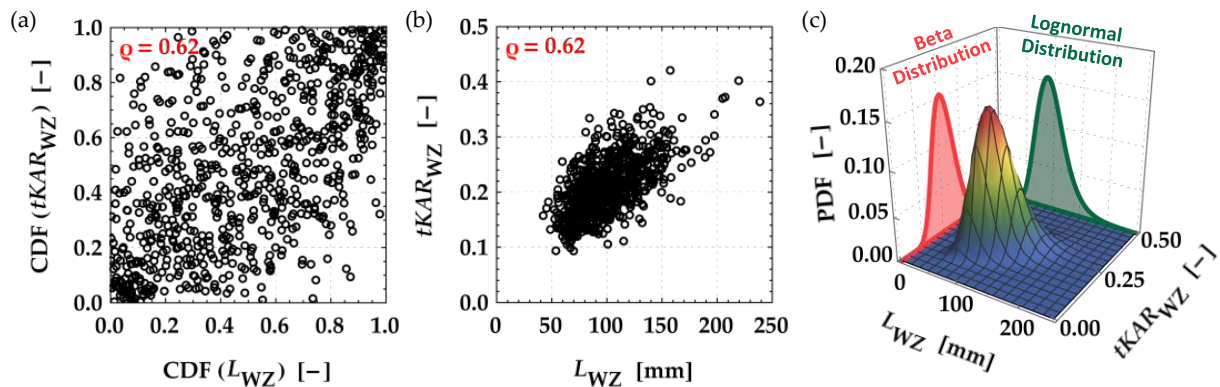


Figure 2-29: Basic principle of a Gaussian copula: (a) scatter-plot of two correlated uniformly distributed pseudo-random numbers as realisations of a bi-variate cumulative distribution (CDF) of two transformed correlated random variables; (b) scatter-plot of artificial realisations of the correlated random variables L_{WZ} and $tKAR_{WZ}$; (c) bi-variate probability density function of the correlated random variables L_{WZ} and $tKAR_{WZ}$ and their corresponding marginal distributions.

Furthermore, with focus on the hierarchical material structure of timber, in particular on boards, the variation in properties can be separated into variation (i) between boards (variation of average properties) and (ii) within boards (variation of local properties). This separation can be represented by a so-called two-level hierarchical model. This class of models has already been successfully used for similar applications in previous investigations; see [\[3–6, 12, 27–29\]](#). For the separation of the variation the spatial correlation of the properties within a board needs to be known. In the literature therefore in principle two approaches are applied to model the properties of timber boards in frame of a stochastic process, namely auto- and equi-correlation. The equi-correlation is the simplest approach for characterising the spatial correlation structure of random variables as it is independent of the lag-distance, i.e. the correlation between local properties within a specific board is not depending on the distance between them. Despite its simplicity it is well suited to model the spatial correlation within timber boards, as successfully demonstrated

by e.g. Fink [3], Isaksson [11], Brandner [12], Ditlevsen & Källsner [28]. Figure 2-30 (a) shows the principle of the employed two-level probabilistic hierarchical model as well as the definition of the corresponding equi-correlation. The hierarchical model describes the local properties represented by the random variable Z_{ij} of a specific board segment i in board j as sum from the average value of the same property Y_j of board j and the local deviation from this average value represented by Ψ_{ij} . The model can be directly inferred from the hierarchical material structure of timber as natural raw material. It allows to separate the total variation σ_z^2 in (i) the variation between the individual boards, σ_y^2 , and (ii) the variation within a single board, σ_ψ^2 , as discussed before.

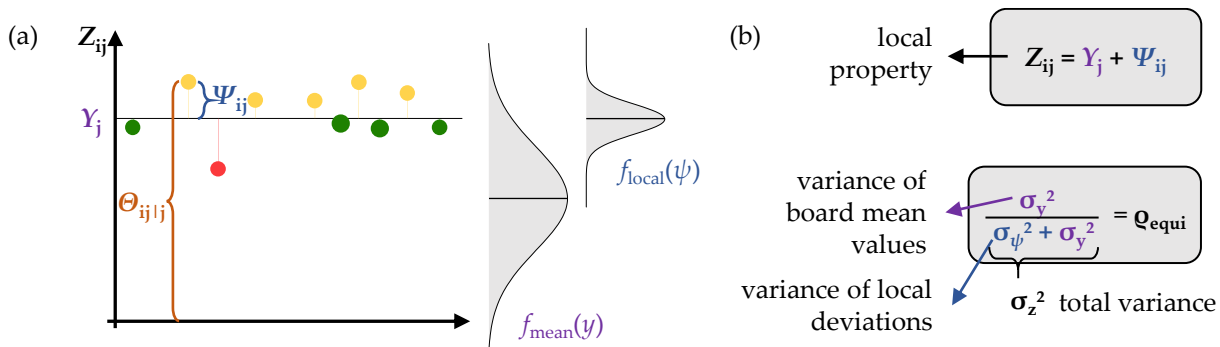


Figure 2-30: Two-level probabilistic hierarchical model (a) as well as the definition of its components (b).

Within the literature the hierarchical model is implemented via an additive approach and assuming an expected value of the local deviation $E(\Psi) = 0$; see Equation (2.4). This is only applicable for probability density functions which allow such an expected value. To circumvent this limitation and to allow a wider scope of probability functions, the formulation was rearranged as seen in Equation (2.5). Hereby, the local deviation is calculated via a statistical distribution function with the board mean value as expected value and the variance of the local deviation of the random variable X within a specific board j .

$$Y_j | X \sim F(y|E X ; \sigma_y^2(X)) = F(y|E X ; \sigma_z^2(X) \cdot \rho_{\text{equi}}(X)) \quad (2.3)$$

$$\Psi_{ij} | X \sim F(\psi|0 ; \sigma_\psi^2(X)) = F(\psi|0 ; \sigma_z^2(X) \cdot (1 - \rho_{\text{equi}}(X))) \quad (2.4)$$

$$\theta_{ij|j} | X \sim F(\theta|Y_j | X ; \sigma_\psi^2(X)) \quad (2.5)$$

with

F statistical distribution function of the random variable X

X random variables; $X = \{LWZ; tKARWZ; DWZ; LIZ; tKARIZ; DIV\}$

$Y_j | X$ mean value of X within the board j

$\theta_{ij|j} | X$ local deviations of X of segment i within board j with board mean $Y_j(X)$

$E X$ expected value of the random variable X

$\sigma_z^2(X)$ variance of the random variable X

$\sigma_y^2(X)$ variance of board mean values of the random variable X

$\sigma_\psi^2(X)$ variance of local deviations of the random variable X within a specific board j

With the previously described probabilistic board model, the six-dimensional multi-variate probability distribution, respectively two six-dimensional multi-variate probability distributions when the two-level probabilistic hierarchical model is taken into account, is used to pseudo randomly generate the geometric setting of artificial timber boards. In a next step the mechanical properties $\{E_{t,0,ij}; f_{t,0,ij}\}$ are allocated to each individual board section based on the $tKAR$ -value and the dynamic modulus of elasticity based on eigen-frequency. The latter serves as indicator for the global (mean) board potential and is one of the most commonly used indicators for mechanical strength grading of timber boards. The local deviations from the average strength of each individual board are dependent on the $tKAR$ -values of each individual board section. The regression models needed for the local allocation of the tensile parallel to grain properties are taken from **Fink [3]**.

In the following sections each part of the probabilistic board model is described in detail. The schematic generation process of the timber boards is illustrated in **Section 2-6**.

2-5.2 Model for the Geometric Parameters

2-5.2.1 Distributions and Hierarchical Models

According to **Section 2-4.6**, the following distributions were used to generate the random variables: The length of the weak zones L_{WZ} and the intermediate knot zones L_{IZ} can be adequately described by the lognormal distribution. For the $tKAR$ -value of the weak zone $tKAR_{WZ}$ and the intermediate zone $tKAR_{IZ}$ a beta distribution is used. The distances between the weak zones D_{WZ} and the intermediate zones D_{IZ} are represented by a gamma distribution. For all random variables the hierarchical model was implemented as described in **Equations (2.6)** and **(2.7)**. A detailed description of the hierarchical model for the individual distributions is given in **Annex B-1**.

$$Y_j | X \sim F(Y|E(X); COV^2(X) \cdot \rho_{equi}(X)) \quad (2.6)$$

$$\theta_{ij|j} | X \sim F(\theta|Y_j; COV^2(X) \cdot (1 - \rho_{equi}(X))) \quad (2.7)$$

with

F statistical distribution function of the random variable X in dependency on the expected value $E(X)$, the coefficient of variation $COV(X)$ and the equi-correlation coefficient $\rho_{equi}(X)$

X random variable; $X = \{L_{WZ}; tKAR_{WZ}; D_{WZ}; L_{IZ}; tKAR_{IZ}; D_{IZ}\}$

$Y_j | X$ mean value of the random variable X within board j

$\theta_{ij|j} | X$ local deviation i within board j with a specific board mean Y_j

$E(X)$ expected value of the random variable X

$COV(X)$... coefficient of variation of the random variable X [%]

$\rho_{equi}(X)$ equi-correlation of the random variable X [-]

2-5.2.2 Moments and Equi-correlation

The moments and the equi-correlation $\{E(X); COV(X); \rho_{\text{equi}}(X)\}$ of the random variables $X = \{L_{WZ}; tKAR_{WZ}; D_{WZ}; L_{IZ}; tKAR_{IZ}; D_{IZ}\}$ were estimated by means of a Bayesian approach; this was done for all board widths $w_b = \{110; 150; 170; 230\}$ mm and separately for each separation ratio $\eta_s = \{1.00; 0.50; 0.33; 0.20; 0.125\}$. Therefore, the hierarchical models in **Section 2-5.2.1** were implemented in the software application **Stan [30]**. Within **Stan [30]** the Hamiltonian Monte Carlo (HMC) algorithm is used with $n = 3,000$ samples in total, where the first 500 are discarded. The preparation of the data and postprocessing was done with **Mathematica [22]**. Thereby not only point estimates but also confidence intervals (95 %) are determined which are illustrated in **Figure 2-31** and **Figure 2-32**. To enable the estimation of the moments and equi-correlation in dependency of the board width, by the board width ratio factor $\eta_w = w_b/150$, and the separation ratio factor $\eta_s = w_{b,res}/w_b$ a regression analysis was carried out in **Stan [30]**. As a non-informative prior was used in the Bayesian analysis the point estimates for the regression coefficients are the same as according to the frequentist approach. Because of its simplicity the latter is implemented; nevertheless, the uncertainties in the estimated variables and coefficients are submerged in the error term. **Equation (2.8)** shows the principle regression model for the expected value, the coefficient of variation and the equi-correlation. The form of the regression model was chosen by visual inspection of data. The analysis of the fitted residuals showed no trends and were overall normal distributed. **Table 2-10** summarises the regression coefficients, the standard deviation of the error term and the reference values of the regression models for all random variables X , as well as the coefficients of determination. Please note: In previous publications **[31, 32]** similar tables are presented, unfortunately with some errors which got updated now in **Table 2-10** which summarises those values which were implemented in the model.

$$Y(X) = (\beta_{00} + \beta_{10} \cdot (\eta_w)^{\beta_{11}} + \beta_{20} \cdot (\eta_s)^{\beta_{21}} + \varepsilon) \cdot \text{Ref}_{\text{GI/GII}}(X) \quad (2.8)$$

with

- Y..... regression model for
 $Y = \{E\dots\text{expected value}; COV\dots\text{coefficient of variation}; \rho_{\text{equi}}\dots\text{equi-correlation}\}$
- X random variable $X = \{L_{WZ}; tKAR_{WZ}; D_{WZ}; L_{IZ}; tKAR_{IZ}; D_{IZ}\}$
- β_{ij} coefficients of the regression model [-]; see **Table 2-10**
- η_w board width ratio factor [-]; $\eta_w = \{\eta_w; 1 - \eta_w\}$, with $\eta_w = w_b/150$; see **Table 2-10**
- η_s separation ratio factor [-]; $\eta_s = \{\eta_s; 1 - \eta_s\}$, with $\eta_s = w_{b,res}/w_b$; see **Table 2-10**
- w_b board width [mm]
- $w_{b,res}$ residual board width [mm]
- ε error term; $\varepsilon \sim \text{ND}(0; \sigma_\varepsilon^2)$ [-]; see **Table 2-10**
- $\text{Ref}_{\text{GI/GII}}$... reference value [mm; %; -] for $\eta_w = 1$ $w_b = 150$ mm and $\eta_s = 1$; see **Table 2-10**

Table 2-10: Regression coefficients β_{ij} , standard deviations σ_ε of the error term, reference values of the regression models and coefficients of determination R^2 for the description of the expected values, coefficients of variation, and equi-correlation coefficients for all model parameters of GI (T14) and GII (T24).

		β_{00}	β_{10}	β_{11}	β_{20}	β_{21}	σ_ε	η_w	η_s	Ref _{GI}	Ref _{GI}	R^2
<i>L_{wz}</i>	E(X)	0.00	0.40	0.60	0.60	0.60	0.036	η_w	η_s	100	80	0.97
	COV(X)	1.00	0.00	0.00	0.00	0.00	0.053		50%	40%	0.00	
	$Q_{\text{equi}}(X)$	1.00	0.00	0.00	0.00	0.00	0.468 ¹		0.10	0.16	-0.01	
<i>tKAR_{wz}</i>	E(X)	0.00	1.00	-0.35	1.60	2.90	0.165		0.21	0.16	0.96	
	COV(X)	1.00	0.00	0.00	0.00	0.00	0.075		50%	40%	-0.02	
	$Q_{\text{equi}}(X)$	1.00	0.00	0.00	0.00	0.00	0.284 ¹		0.14	0.17	0.00	
<i>D_{wz}</i>	E(X)	0.95	0.00	0.00	0.60	2.10	0.115		500	600	0.72	
	COV(X)	1.00	0.00	0.00	0.40	1.70	0.048		50%	50%	0.78	
	$Q_{\text{equi}}(X)$	1.00	0.00	0.00	0.00 ¹	0.00 ¹	0.142 ¹		0.20	0.10	-0.13	
<i>L_{iz}</i>	E(X)	1.00	0.00	0.00	0.15	1.00	0.106		$1 - \eta_s$	25	-0.09	
	COV(X)	0.95	0.00	0.00	0.35	1.00	0.114			45 %	0.52	
	$Q_{\text{equi}}(X)$	0.95	0.00	0.00	0.00 ¹	0.00 ¹	0.212			0.09	0.00	
<i>tKAR_{iz}</i>	E(X)	1.00	0.00	0.00	1.30	1.90	0.156	0.04		0.77		
	COV(X)	1.00	0.00	0.00	0.50	1.00	0.069	65 %		0.54		
	$Q_{\text{equi}}(X)$	1.00	0.00	0.00	0.85 ¹	1.00	0.192 ¹	0.10		0.69		
<i>D_{iz}</i>	E(X)	1.05	0.00	0.00	2.35	2.05	0.507	100		135	0.73	
	COV(X)	0.95	0.00	0.00	0.00	0.00	0.046	95 %		95 %	-0.12	
	$Q_{\text{equi}}(X)$	1.00	0.00	0.00	0.00	0.00	0.289 ¹	0.17		0.17	0.00	

¹....updated values

Figure 2-31 shows the normalised plots of the regression models for the moments and equi-correlation coefficient in dependence on the board width ratio η_w and the separation ratio η_s for the model parameters of the weak zones $\{L_{wz}; tKAR_{wz}; D_{wz}\}$. The model achieves an overall good representation of the expected values. For the coefficients of variation and the equi-correlation no clear trend was observed in most cases due to the large uncertainties within the data. In these cases $\{COV(L_{wz}); COV(tKAR_{wz}); Q_{\text{equi}}(L_{wz}); Q_{\text{equi}}(tKAR_{wz}); Q_{\text{equi}}(D_{wz})\}$ the parameters were estimated via a global mean value ($R^2 \approx 0$).

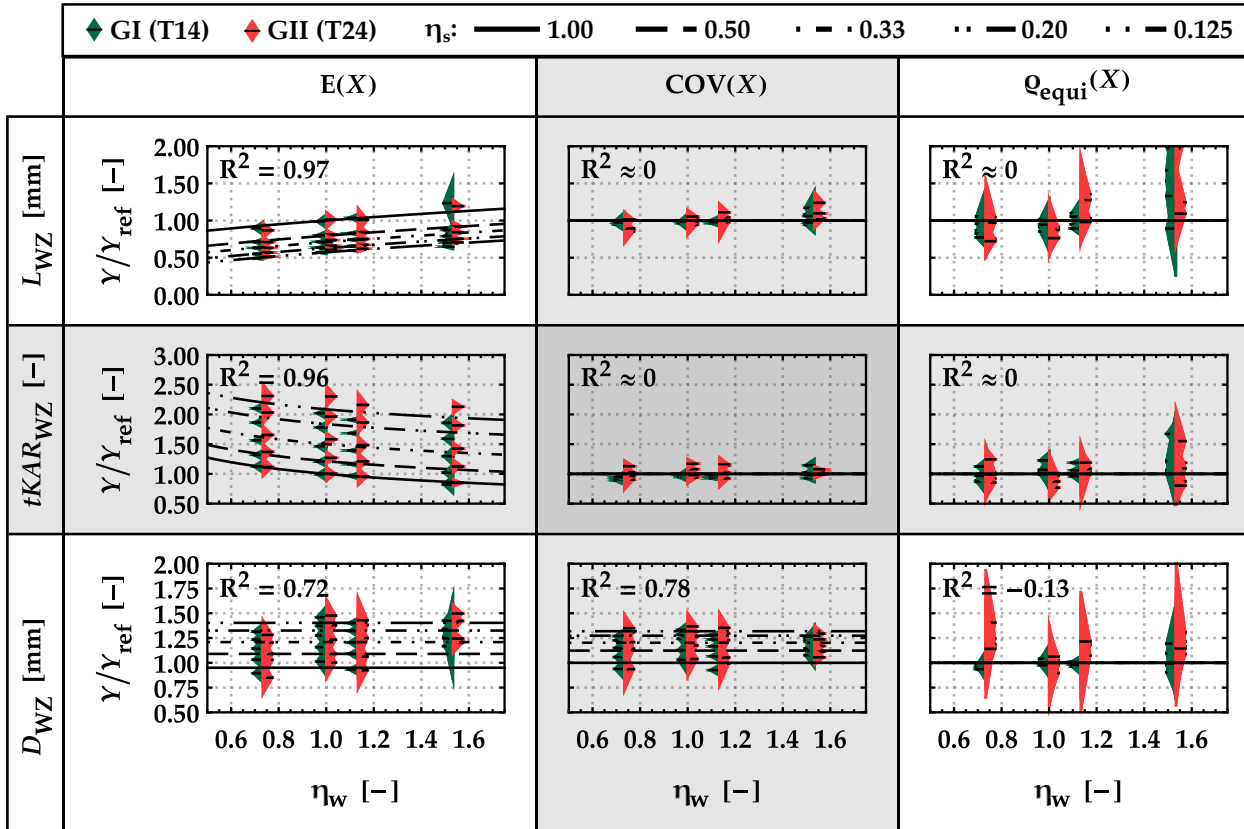


Figure 2-31: Normalised plots of the regression models for the moments and the equi-correlation coefficient $\{E(X); COV(X); \rho_{\text{equi}}(X)\}$ in dependence on the board width ratio η_w and the separation ratio η_s for the random variables of the weak zone $\{L_{\text{WZ}}; tKAR_{\text{WZ}}; D_{\text{WZ}}\}$ including a CI of 95 % for group GI (T14) and group GII (T24) and overall coefficients of determination.

Figure 2-32 shows the normalised plots of the regression models for the moments and the equi-correlation coefficient in dependence on the board width ratio η_w and the separation ratio η_s for the model parameters of the intermediate zones $\{L_{\text{IZ}}; tKAR_{\text{IZ}}; D_{\text{IZ}}\}$. As a simplification and due to the overall lesser influence of the intermediate zone the dependency on the board width is further neglected. Based on these simplifications the coefficients of determination are not as high as for the weak zones. As before, in some cases no clear trend was observed due to the large uncertainties within the data. In these cases $\{COV(D_{\text{IZ}}); \rho_{\text{equi}}(L_{\text{IZ}}); \rho_{\text{equi}}(D_{\text{IZ}})\}$ the parameters were estimated via a global mean value ($R^2 \approx 0$).

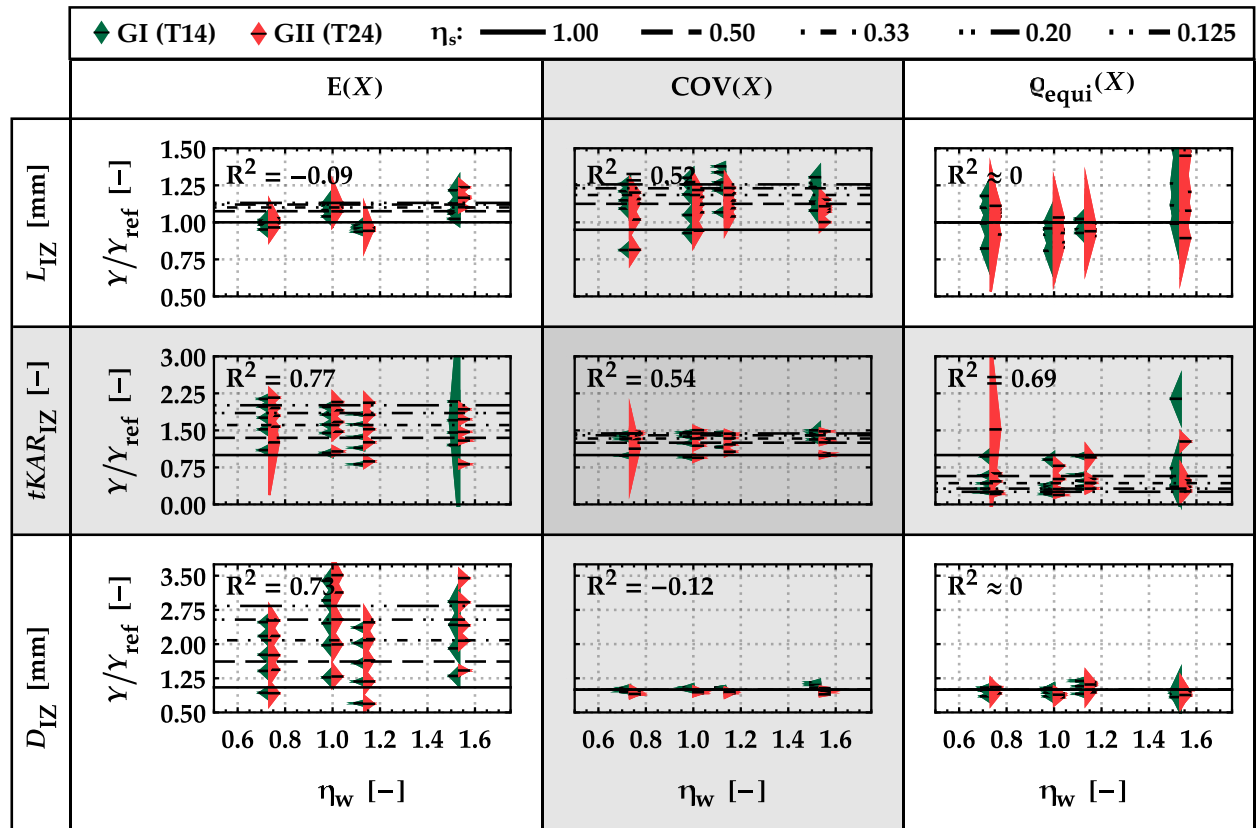


Figure 2-32: Normalised plots of the regression models for the moments and the equi-correlation coefficient $\{E(X); COV(X); Q_{equi}(X)\}$ in dependence on the board width ratio η_w and the separation ratio η_s for the random variables of the intermediate zone $\{L_{Iz}; tKAR_{Iz}; D_{Iz}\}$ including a CI of 95 % for group GI (T14) and group GII (T24) and overall coefficients of determination.

As already mentioned, the moments and equi-correlation coefficient $\{E(X); COV(X); Q_{equi}(X)\}$ were estimated in Stan [30] with a HMC algorithm. Based on the resulting samples the Pearson correlation coefficient between the input parameters were calculated; these are summarised in Table 2-11. The found correlations are overall weak and are probably be caused by the deviations of the empirical data from the assumed distributions. Nonetheless, this information is used to generate correlated error terms for the moments and equi-correlation coefficient $\{E(X); COV(X); Q_{equi}(X)\}$ via a Gaussian copula.

Table 2-11: Correlations between the moments and equi-correlation coefficient $\{E(X); COV(X); Q_{equi}(X)\}$ used to generate error terms.

	L_{wz}	$tKAR_{wz}$	D_{wz}	L_{Iz}	$tKAR_{Iz}$	D_{Iz}
$E(X) - COV(X)$	0.25	-0.10	0.15	0.25	0.00	0.15
$E(X) - Q_{equi}(X)$	0.05	0.00	0.30	0.05	0.25	0.25
$COV(X) - Q_{equi}(X)$	0.25	0.35	0.35	0.25	0.25	0.55

2-5.2.3 Correlations between Model Parameters

In total 15 pairwise combinations are required to fully describe all correlations between the six random variables $\{L_{wz}; tKAR_{wz}; D_{wz}; L_{iz}; tKAR_{iz}; D_{iz}\}$. To also gain information on the variability of the correlation coefficients, 1,000 pseudo random samples $\{E(X); COV(X); \rho_{\text{equi}}(X)\}$ for each random variable were generated; see [Section 2-5.2.1](#) and [Section 2-5.2.2](#). The corresponding cumulative probability distribution of the board mean values were used to transform the empirical data of the board mean values. The Pearson correlation of the transformed coefficients were determined for all possible combinations of the model parameters as well as for each board width $w_b = \{110; 150; 170; 230\}$ mm and separation ratio $\eta_s = \{1.00; 0.50; 0.33; 0.20; 0.125\}$. Based on these results the confidence intervals of the correlation coefficients were estimated; see [Figure 2-33](#). As already stated in [Section 2-4.6](#), a differentiation between groups GI (T14) and GII (T24) was not necessary.

The principle regression model for the correlation between the model parameters is given in [Equation \(2.9\)](#). The regression coefficients, the standard deviation of the error term and the reference values of the regression models for all model parameters, as well as the coefficients of determination, are listed in [Table 2-12](#). For some parameters almost no correlation is observed. Nonetheless, the regression model is used to model all correlation coefficients. The calculation of each entry of the correlation matrix separately may lead to a non-positive semidefinite matrix which would make it invalid. In these cases, the matrix is adjusted to the “nearest” positive semidefinite matrix using the approach as described in [Rebonato & Jaeckel \[33\]](#).

$$Y(X) = (\beta_{00} + \beta_{10} \cdot (\eta_w)^{\beta_{11}} + \beta_{20} \cdot (\eta_s)^{\beta_{21}} + \varepsilon) \cdot \text{Ref}_{\text{GI/GII}} \quad (2.9)$$

with

- Y..... regression model for the correlation coefficient ρ
- X combination of two random variables $X = \{L_{wz}; tKAR_{wz}; D_{wz}; L_{iz}; tKAR_{iz}; D_{iz}\}$
- β_{ij} coefficients of the regression model [-]; see [Table 2-12](#)
- η_w board width ratio factor [-]; $\eta_w = \{\eta_w; 1 - \eta_w\}$, with $\eta_w = w_b/150$; see [Table 2-12](#)
- η_s separation ratio factor [-]; $\eta_s = \{\eta_s; 1 - \eta_s\}$, with $\eta_s = w_{b,\text{res}}/w_b$; see [Table 2-12](#)
- w_b board width [mm]
- $w_{b,\text{res}}$ residual board width [mm]
- ε error term; $\varepsilon \sim \text{ND}(0; \sigma_\varepsilon^2)$ [-]; see [Table 2-12](#)
- $\text{Ref}_{\text{GI/GII}}$... reference value [-] for $\eta_w = 1$ $w_b = 150$ mm and $\eta_s = 1$; see [Table 2-12](#)

Table 2-12: Regression coefficients β_{ij} , standard deviations of the error term σ_ε , reference values of the regression models and coefficients of determination R^2 for the correlation coefficient between model parameters of GI(T14) and GII(T24).

	β_{00}	β_{10}	β_{11}	β_{20}	β_{21}	σ_ε	η_w	η_s	Ref _{GI/GII}	R^2
$L_{WZ} - tKAR_{WZ}$	1.00	0.00	0.00	-0.50	2.00	0.128	$1 - \eta_w$	$1 - \eta_s$	0.65	0.36
$L_{WZ} - D_{WZ}$	0.90	0.00	0.00	0.00	0.00	1.329			0.04	0.00
$L_{WZ} - L_{IZ}$	1.00	-2.80	1.00	0.00	0.00	2.445			0.05	0.15
$L_{WZ} - tKAR_{IZ}$	0.25	0.00	0.00	0.00	0.00	4.064			-0.03	0.00
$L_{WZ} - D_{IZ}$	1.00	0.00	0.00	-1.00	4.00	0.485			-0.20	0.04
$tKAR_{WZ} - D_{WZ}$	0.85	2.80	1.00	0.00	0.00	3.536			0.03	0.12
$tKAR_{WZ} - L_{IZ}$	1.00	0.00	0.00	0.00	0.00	2.646			0.04	0.00
$tKAR_{WZ} - tKAR_{IZ}$	1.00	0.00	0.00	0.00	0.00	11.97			0.01	0.00
$tKAR_{WZ} - D_{IZ}$	1.00	0.00	0.00	-1.25	1.00	0.170			-0.20	0.33
$D_{WZ} - L_{IZ}$	1.00	0.00	0.00	0.00	0.00	2.080			0.04	0.00
$D_{WZ} - tKAR_{IZ}$	1.00	0.00	0.00	0.00	0.00	1.991			0.06	0.00
$D_{WZ} - D_{IZ}$	1.00	0.00	0.00	0.00	0.00	0.239			0.40	0.00
$L_{IZ} - tKAR_{IZ}$	1.00	0.00	0.00	-1.10	1.00	0.197			0.45	0.58
$L_{IZ} - D_{IZ}$	1.00	0.00	0.00	0.00	0.00	0.382			0.25	0.00
$tKAR_{IZ} - D_{IZ}$	1.00	0.00	0.00	-0.80	1.00	0.307			0.30	0.25

Figure 2-33 shows plots of the correlation coefficient in dependence on the board width ratio η_w and the separation ratio η_s for all 15 pairwise combinations of the model parameters $X = \{L_{WZ}; tKAR_{WZ}; D_{WZ}; L_{IZ}; tKAR_{IZ}; D_{IZ}\}$. For the parameter combinations with a higher correlation and/or clear tendencies, e.g. $\{L_{WZ} - tKAR_{WZ}; L_{IZ} - tKAR_{IZ}; D_{WZ} - D_{IZ}\}$, models were calibrated to the data. Parameter combinations with no linear correlation $\rho \approx 0$ and visually without clear relationship are further represented via a global mean value which consequence $R^2 \approx 0$.

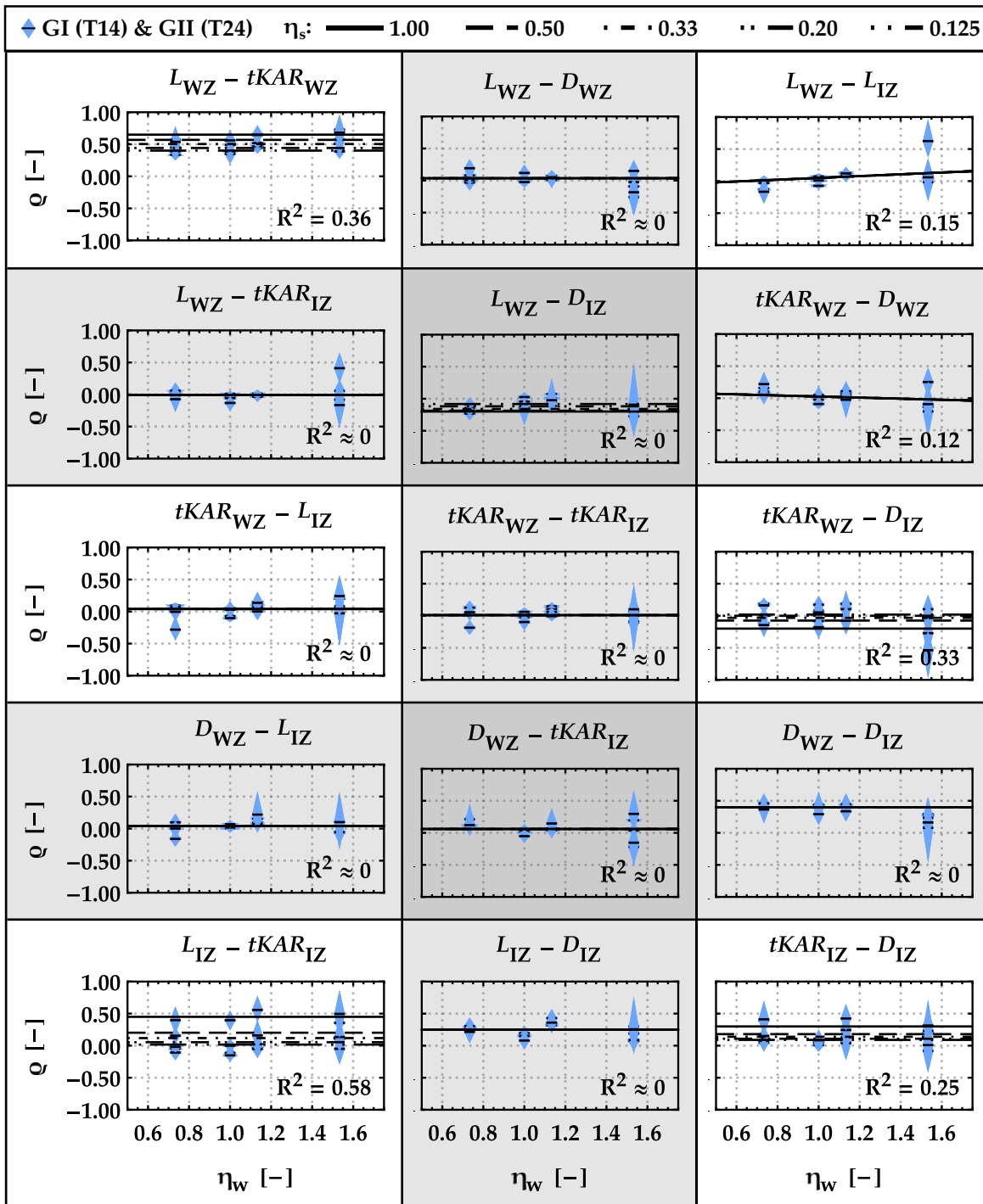


Figure 2-33: Plots of the correlation coefficients between pairs of model parameters $X = \{L_{WZ}; tKAR_{WZ}; D_{WZ}; L_{IZ}; tKAR_{IZ}; D_{IZ}\}$ in dependence on the board width ratio η_w and the separation ratio of η_s including CI of 95 % for group GI (T14) and group GII (T24) and overall coefficient of determination of the model.

2-5.3 Dynamic Modulus of Elasticity

Within the board model, the dynamic modulus of elasticity is randomly assigned to the boards based on a lognormal distribution, as done in **Fink [3]**. The mentioned procedure has to be adapted and extended to incorporate the influence of lengthwise splitting of the boards. This is accomplished by modifying the parameters of the used lognormal distribution model. The modifications are shown in **Equations (2.10) to (2.13)** and the corresponding reference values in **Table 2-13**.

$$E_{DYN,b} \sim \text{LND}(\mu_{E,DYN}; \sigma_{E,DYN}^2) \quad (2.10)$$

$$\mu_{E,DYN} = \ln \left(\frac{E(E_{DYN,ref})}{\sqrt{1 + \text{COV}^2 E_{DYN}}} \right) \quad (2.11)$$

$$\sigma_{E,DYN} = \sqrt{\ln(1 + \text{COV}^2 E_{DYN})} \quad (2.12)$$

$$\text{COV } E_{DYN} = (\eta_s^{-1/4}) \cdot \text{COV}(E_{DYN,ref}) \quad (2.13)$$

with

- $E_{DYN,b}$ dynamic modulus of elasticity of the board [MPa]
- $\mu_{E,DYN}$ location parameter of the dynamic modulus of elasticity
- $\sigma_{E,DYN}$ dispersion parameter of the dynamic modulus of elasticity
- $E(E_{DYN,ref})$ reference mean value of the dynamic modulus of elasticity [MPa]; see **Table 2-13**
- $\text{COV}(E_{DYN,ref})$... reference COV of the dynamic modulus of elasticity [MPa]; see **Table 2-13**
- η_s separation ratio [-]; with $\eta_s = w_{b,res}/w_b$
- w_b board width [mm]
- $w_{b,res}$ residual board width [mm]

Table 2-13: Reference values for the dynamic modulus of elasticity $E_{DYN,ref}$ of boards allocated to groups GI (T14) & GII (T24).

	GI (T14)	GI (T14)
$E(E_{DYN,ref})$ [MPa]	11,500	14,000
$\text{COV}(E_{DYN,ref})$ [%]	13.0	13.0

The models for the main statistics were derived from test data taken from **Kastner et al. [15]** and from own investigations (see also **Scherfler [34]**). Within both investigations the dynamic modulus of elasticity based on the eigen-frequency $E_{DYN,F}$ was measured before and after the lengthwise splitting of the boards. The results are summarised in **Table 2-14**. **Figure 2-34** illustrates the change of the main statistics $\{E(X); \text{COV}(X); \chi_{05,LN}\}$ due to the splitting process relative to the full cross-section properties. The mean value remains almost constant, whereas the coefficient of variation is increasing with a decreasing separation ratio η_s .

Table 2-14: Statistics of the dynamic modulus of elasticity based on eigen-frequency $E_{DYN,F}$ of boards in unsplit and lengthwise split conditions from **Kastner et al. [15]** and own investigations (see also **Scherfler [34]** for further details).

separation ratio η_s [-]	Kastner et al. [15]		own investigations ¹		
	1.00	0.50	1.00	0.66	0.33
#	279	558	54	54	54
mean [MPa]	12,057	11,848	14,341	14,182	14,086
COV [%]	7.5	9.1	15.2	16.7	20.0
$\chi_{05,LN}$ [MPa]	10,623	10,168	10,647	9,830	8,847

¹for further details see also **Scherfler [34]**

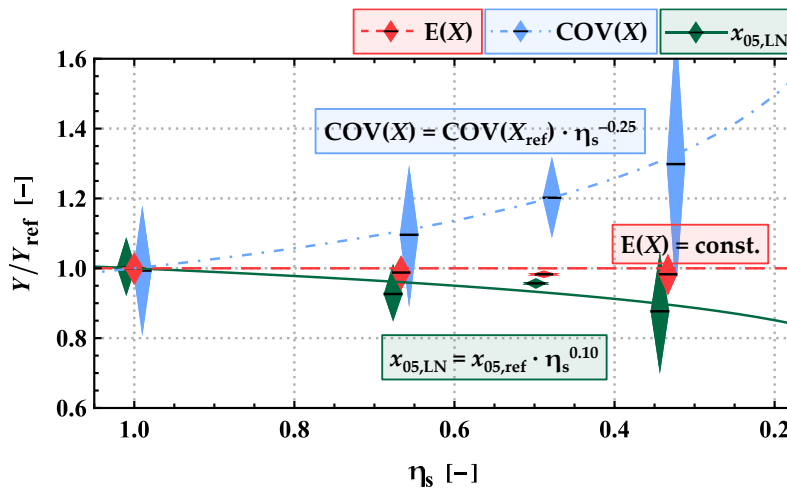


Figure 2-34: Influence of the lengthwise splitting on the main statistics $Y = \{E(X); COV(X); \chi_{05,LN}\}$ of the dynamic modulus of elasticity of boards ($X = E_{DYN,F}$) relative to the statistics at full cross-section with 95 % CI (data taken from **Kastner et al. [15]** and own investigations).

2-5.4 Allocation of Material Properties

The allocation of the mechanical properties is achieved via regression models based on the dynamic modulus of elasticity and the $tKAR$ -value. The model in **Equation (2.14)** is taken from **Fink [3]**. The corresponding regression coefficients are summarised in **Table 2-15**. This approach was chosen as the dynamic modulus of elasticity in combination with the $tKAR$ -value is a good predictor for the tensile parallel to grain properties. The “Karlsruher Rechenmodell” is using regression models based on the oven-dry density as proposed by **Ehlbeck et al. [10]** in 1985. Nowadays machine strength grading of timber relies mostly on the dynamic modulus of elasticity. Therefore, it seems reasonable to use a regression model with the same basis.

$$\ln Y = \beta_0 + \beta_1 \cdot E_{DYN,b,j} + \beta_2 \cdot tKAR_{ij} + \varepsilon \quad (2.14)$$

with

- Y local board properties $\{f_{t,0,ij}; E_{t,0,ij}\}$ [MPa]
- β_i coefficients of regression model [-]
- $E_{DYN,b,j}$ dynamic modulus of elasticity of board j [MPa]
- $tKAR_{ij}$ $tKAR$ -value of board section i of board j [-]
- ε error term; $\varepsilon \sim ND(0; \sigma_\varepsilon^2)$ [-]

Table 2-15: Regression coefficients and standard deviation of the error term for the regression model in **Equation (2.14)** for $Y = \{f_{t,0,ij}; E_{t,0,ij}\}$; taken from **Fink et al. [35]**.

	β_0	β_1	β_2	σ_ϵ
$f_{t,0,ij}$ [MPa]	2.96	$8.50 \cdot 10^{-5}$	-2.22	0.20
$E_{t,0,ij}$ [MPa]	8.41	$7.69 \cdot 10^{-5}$	$-9.02 \cdot 10^{-1}$	0.10

For the error terms of the strength and the modulus of elasticity a correlation of $\rho = 0.8$, as in **Fink et al. [35]**, was applied. Similar to the two-level hierarchical model approach and in line with the findings in **Colling [2]** the error terms are further separated into two parts: one describing the variation between a global (mean) board potential and the regression model and the second the variation within one board. **Colling [2]** states that approximately 70 % of the total standard deviation is due to the global (mean) board deviation. This ratio corresponds to an equi-correlation of $\rho_{\text{equi}} = 0.49$. In **Fink et al. [35]** the ratio was set with ~ 66 %, which results in an equi-correlation of $\rho_{\text{equi}} = 0.44$. These values always refer to the weak zones in the respective board models. For the clear wood sections, only the deviation for the global (mean) value is applied, i.e. no variation along the board length in the clear wood section is implemented.

Within the current probabilistic board model the separation of the error term is considered in the same manner with an equi-correlation of $\rho_{\text{equi,WZ}} = 0.45$, based on the finding in **[2, 3]**. In contrast to the previous mentioned model approaches, also for the clear wood sections a variation along the board length is introduced. The longitudinal variation within one board in the properties of the clear wood sections is rather small compared to that of the weak sections. The equi-correlation for the CW section was estimated with $\rho_{\text{equi,CW}} = 0.90$. From a logical point of view the lengthwise variability of the properties of the intermediate knot zones within a single board should be somewhere in between the WZ and CW sections. Therefore, an equi-correlation of $\rho_{\text{equi,IZ}} = 0.70$ was chosen for the intermediate knot zones. With this approach the different homogeneities of the board section classes {WZ; IZ; CW} are taken into account. Although **Brandner [12]** stated slightly higher equi-correlation coefficients for the weak zones with respect to the modulus of elasticity than for the tensile strength parallel to the grain, no differentiation has been made here for the sake of simplification.

2-6 Board Generation Process and Properties

Within this section the board generation process, as illustrated in **Figure 2-35 (a)**, is described in detail. At first, the main statistics $\{E(X); \text{COV}(X); \rho_{\text{equi}}(X)\}$ and the marginal distributions of all six random variables $X = \{L_{WZ}; tKAR_{WZ}; D_{WZ}; L_{IZ}; tKAR_{IZ}; D_{IZ}\}$ are generated based on the input parameters $\{w_b; \eta_s; \text{GI/GII}\}$. Additionally, the pairwise correlations of the variables are generated. With the correlation matrix and the marginal distributions, the six-dimensional Gaussian copula is formulated and a random vector Y_i , containing the global (mean) board properties, is sampled. In the next step, the local values $X_{ij} = \{L_{WZ,ij}; tKAR_{WZ,ij}; D_{WZ,ij}\}$ based on the mean board properties are generated by means of the first alternating renewal process (ARN 1). Within the distance to the next weak zone, the intermediate knot zones are generated

by means of a second alternating renewal process (ARN 2). These last two steps are repeated until a board of predefined length is fully characterised. Due to this procedure all boards would start with a weak zone. To ensure a random start of each virtual board, the boards are generated with an overlength and the first four meters are discarded. These two interlaced alternating renewal processes used to generate the geometry of the boards were already successfully applied in **Brandner [36]**.

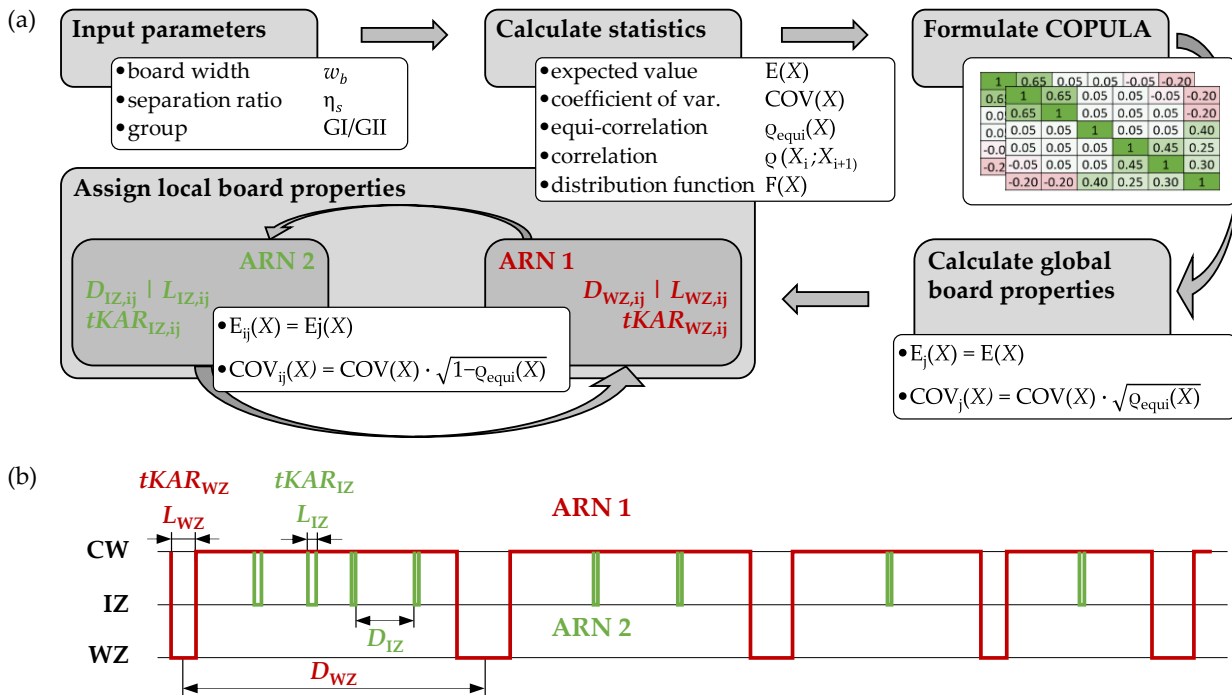


Figure 2-35: Board generation process (a) and scheme of the two interlaced alternating renewal (ARN) processes responsible for the assignment of local board properties (b).

The overall generation of the geometry of the virtual boards is quite time consuming. To reduce the computational effort datasets containing the geometry for different board widths and separation ratios were precalculated. Each dataset contains 1,000 boards with a length of 16 m (first 4 m already discarded) for each group GI & GII, the full board width w_b and lengthwise split boards with the residual board width of $w_{b,res} = \{w_b - 5; w_b - 10; \dots; 5\}$ mm.

When a virtual board with a specific set of properties $\{w_b; w_{b,res}; \text{group}\}$ is needed, it is arbitrarily picked from the dataset and the length-profile of the virtual board with its length of l_b is randomly taken from the pre-processed 16 m long boards. **Figure 2-36 (a)&(b)** show exemplarily the alternating renewal processes (ARN) and the $tKAR$ -values along the length-axis of three virtually generated boards from group GI (T14). The weak zones of the boards are highlighted in the corresponding colours.

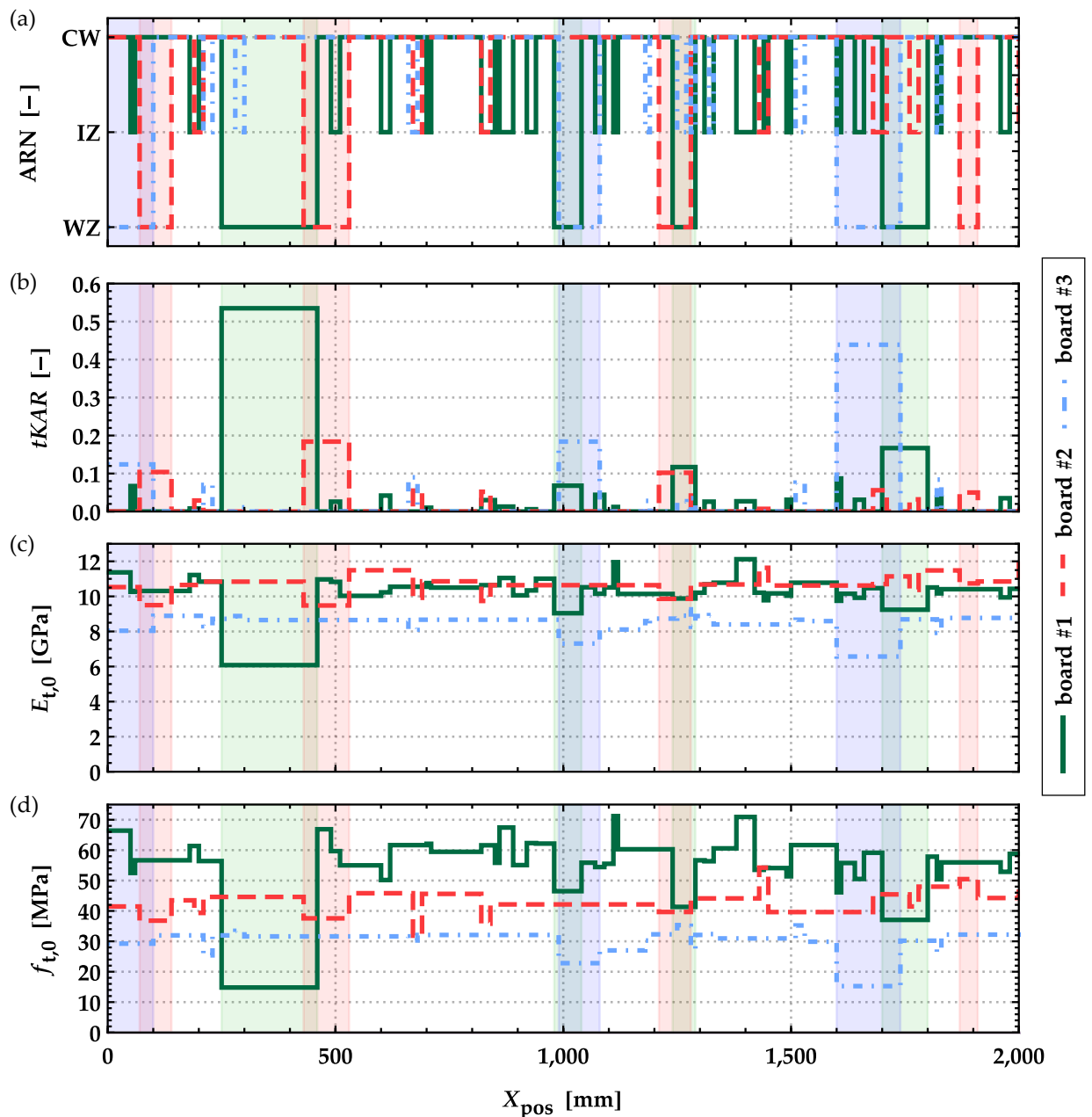


Figure 2-36: Properties along the length-axis (X_{pos}) of three generated boards from group GI for (a) the alternating renewal processes ARN 1 & 2; (b) the $tKAR$ -value; (c) the modulus of elasticity parallel to the grain in tension $E_{t,0}$ and (d) the tensile strength parallel to the grain $f_{t,0}$; the weak zones are highlighted in all plots.

In the next step, a dynamic modulus of elasticity $E_{\text{DYN},b}$ is randomly assigned to each board and based on $E_{\text{DYN},b}$ and the $tKAR$ -profile of the board the mechanical properties are calculated for each board segment. The profiles of the modulus of elasticity and the tensile strength parallel to the grain are shown in **Figure 2-36 (c)&(d)**. Besides the properties along the length-axis, also the global board properties are of interest. Hereby, the tensile strength of the board is defined as the minimal tensile strength of all board-segments and the modulus of elasticity is calculated as a series of springs; see **Equations (2.15)** and **(2.16)**.

$$f_{t,0,b,j} = \min(f_{t,0,ij}) \quad (2.15)$$

$$E_{t,0,b,j} = l_{b,j} \cdot \left(\sum \left(\frac{l_{b,ij}}{E_{t,0,ij}} \right) \right)^{-1} \quad (2.16)$$

with

- $f_{t,0,b,j}$ tensile strength parallel to the grain of board j [MPa]
- $f_{t,0,ij}$ tensile strength parallel to the grain of board-segment i in board j [MPa]
- $E_{t,0,b,j}$ modulus of elasticity parallel to the grain of board j [MPa]
- $E_{t,0,ij}$ modulus of elasticity parallel to the grain of board-segment i in board j [MPa]
- $l_{b,j}$ length of the board j [mm]
- $l_{b,ij}$ length of the board-segment i in board j [mm]

2-7 Application & Validation of the Probabilistic Board Model

2-7.1 Boards in Full Width

The aim of this section is to demonstrate at first the applicability of the probabilistic board model by quantifying influences of the geometric parameters, like board width w_b and length l_b , on the main statistics of the tensile properties parallel to the grain. The results of the applied probabilistic board model are compared and validated with experimental and numerical/simulation data from the literature.

In timber engineering so-called size effects are often modelled by means of the Weibull's weakest link theory and consequently power regression models are used to describe the influences of the volume on the strength; [16, 37, 38]. For timber perfect brittle behaviour as well as other boundary conditions of the Weibull theory are generally not applicable. **Brandner [12]** showed that also for other material behaviour, including plasticity and load redistribution, power regression models can be used to describe size effects in timber, which are independent of the Weibull theory; see **Equation (2.17)**.

$$Y = Y_{\text{ref}} \cdot (\eta_{w|l})^k \quad (2.17)$$

with

- Y main statistics $\{E(X); \text{COV}(X); \chi_{05, \text{LN}}\}$ [MPa; %; MPa]
- Y_{ref} reference value $\{E(X_{\text{ref}}); \text{COV}(X_{\text{ref}}); \chi_{05, \text{LN, ref}}\}$ at reference dimensions $\{w_{b, \text{ref}}; l_{b, \text{ref}}\}$ [MPa; %]
- $\eta_{w|l}$ board dimensions $\{w_b; l_b\}$ relative to reference dimensions $\{w_{b, \text{ref}}; l_{b, \text{ref}}\}$ [-];
with $\{\eta_w = w_b/w_{b, \text{ref}}; \eta_l = l_b/l_{b, \text{ref}}\}$
- k power coefficient [-]

2-7.1.1 Influence of the Board Width w_b at Reference Board Length of $l_{b,ref} = 9 \cdot w_b$

To analyse the influence of the board width on the main statistics of the tensile properties, $1.5 \cdot 10^4$ timber boards were generated. The boards from both groups GI (T14) and GII (T24) feature a width of $w_b = \{100; 150; 200; 250\}$ mm and a length of $l_b = 9 \cdot w_b$, which corresponds with the reference length of $l_{b,ref} \geq 9 \cdot w_b$ for tensile tests according to EN 408 [39]. The results of the tensile strength and modulus of elasticity in tension parallel to the grain are summarised in Table 2-16; more detailed results are given in Table Annex D-7.

The average modulus of elasticity in tension is approximately 500 MPa lower than the value assigned to the strength classes T14 (GI) and T24 (GII) in EN 338 [8]. Similar results are reported in Fink [3], whose regression models were applied to allocate the mechanical properties to each board segments. According to Fink [3], the used regression model underestimates the modulus of elasticity of the clear wood section by approximately $\sim 3\%$. An influence of the board width w_b on the modulus of elasticity is not observed for the mean values nor for the coefficients of variation.

Table 2-16: Main statistics of the tensile strength parallel to the grain $f_{t,0,b}$ and the modulus of elasticity parallel to the grain in tension $E_{t,0,b}$ calculated from $1.5 \cdot 10^4$ virtually generated boards (for each combination) separated in respect to width, group and test length of $l_b = 9 \cdot w_b$ according to EN 408 [39].

Width w_b [mm]		GI (T14)				GII (T24)			
		100	150	200	250	100	150	200	250
$f_{t,0,b}$	mean [MPa]	27.8	27.4	27.7	27.6	40.4	40.2	40.4	40.1
	COV [%]	34.8	31.6	30.0	29.3	30.1	28.1	27.0	26.6
	$x_{05,LN}$ [MPa]	14.4	15.3	15.9	16.0	23.6	24.4	25.1	25.2
	$x_{05,LN}/x_{05,LN,ref}^1$ [-]	0.94	1.00	1.04	1.05	0.97	1.00	1.03	1.03
$E_{t,0,b}$	mean [MPa]	10,454	10,442	10,485	10,486	12,988	13,008	13,062	12,992
	COV [%]	15.3	14.9	14.9	14.8	17.2	17.3	17.1	17.2

¹ $x_{05,LN,ref}$ with $w_{b,ref} = 150$ mm and $l_{b,ref} = 9 \cdot w_{b,ref}$

Figure 2-37 shows the influence of the board width on the main statistics $\{E(X); COV(X); x_{05,LN}\}$ of the tensile strength parallel to the grain. The mean values remain almost constant whereas the coefficient of variation and the 5 %-quantile values decrease and increase, respectively, with increasing board width. For the width effect on the tensile strength at the reference length $l_{b,ref} = 9 \cdot w_b$ power coefficients of $k_{w,9b,05,GI} = 0.10$ for GI (T14) and $k_{w,9b,05,GII} = 0.06$ for GII (T24) are found; see Equation (2.17). Burger [23] found similar coefficients for the visual grading classes S10 and S13 according to DIN 4074-1 [9] with $k_{w,05,S10} = 0.14$ and $k_{w,05,S13} = 0.07$. Based on EN 1912 [40] the grading classes S10 and S13 can be assigned to the strength classes C24 (T14) and C30 (T22) according to EN 338 [8]. In the results here, as well as in Burger [23], the width effect is more pronounced within the lower strength class. The observed trends regarding the influence of the board width on the tensile strength are in direct contradiction to the frequently applied Weibull's weakest link theory, whereby the strength is declining with an

increasing stressed volume. The higher tensile strength for wider boards is partially caused by the sorting/grading process and also by the morphology of timber. Branches or knots in trees have a certain diameter and their relative share reduces as the boards get wider. This is also visible in the declining $tKAR$ -values for wider boards in [Section 2-4.2.2](#).

Nonetheless, the observed deviations of the simulated tensile strength at different board widths are within a small range $\pm 5\%$ for GI (T14) and $\pm 3\%$ for GII (T24) for the 5 %-quantile values. As the reference length $l_{b,ref} = 9 \cdot w_b$ (acc. to [EN 408 \[39\]](#)) is directly coupled with the board width w_b , the previously stated width effect also includes a length effect to a certain extent. This circumstance is analysed further in the next [Section 2-7.1.2](#).

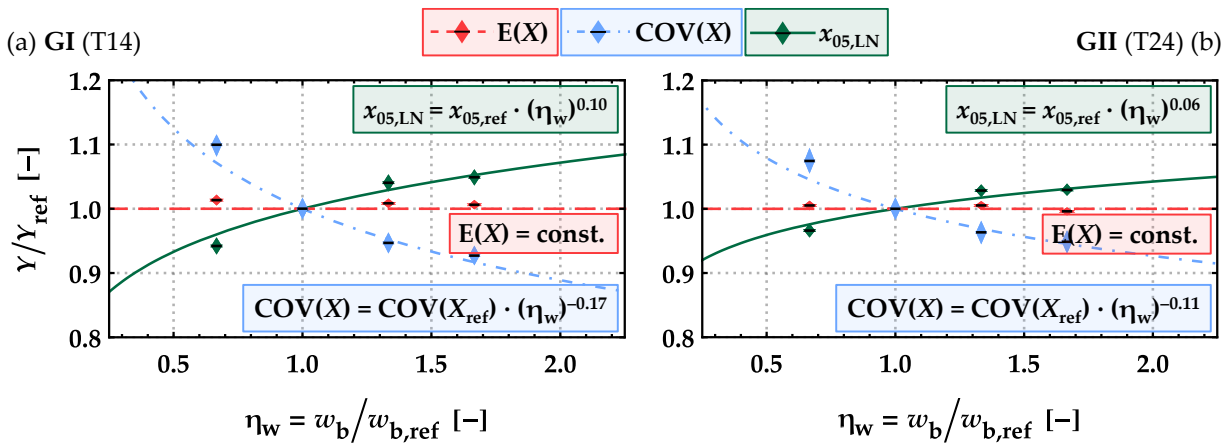


Figure 2-37: Influence of the width w_b on the main statistics $Y = \{E(X); COV(X); x_{05,LN}\}$ of the tensile strength parallel to the grain of boards ($X = f_{t,0,b}$) featuring a length $l_b = 9 \cdot w_b$ relative to the statistics at reference width $w_{b,ref} = 150$ mm and length $l_{b,ref} = 9 \cdot w_{b,ref}$; analysis based on virtually generated boards for GI (a) and GII (b).

2-7.1.2 Influence of the Board Width w_b at fixed Board Lengths

For a more isolated view on the width effect on the main statistics of the tensile properties parallel to the grain, the length of the boards was fixed with $l_b = \{2.0; 4.0\}$ m. In the former glulam standard [EN 1194 \[37\]](#) $l_b = 2$ m was also as the reference length for the tensile strength and $l_b = 4$ m is a board length commonly produced in Austria. For each length, group GI (T14) and GII (T24) and board width $w_b = \{100; 150; 200; 250\}$ mm, $1.5 \cdot 10^4$ timber boards were generated. The results for the tensile strength and modulus of elasticity in tension parallel to the grain are summarised in [Table 2-17](#); more detailed results are given in [Table Annex D-8](#).

As expected for the modulus of elasticity in tension parallel to the grain the same results are observed as for the reference length $l_{b,ref} = 9 \cdot w_b$; the mean values and coefficients of variation show no influence from the board width.

Table 2-17: Main statistics of the tensile strength parallel to the grain $f_{t,0,b}$ and the modulus of elasticity parallel to the grain in tension $E_{t,0,b}$ calculated from $1.5 \cdot 10^4$ virtually generated boards (for each combination) separated in respect to width, group and test length $l_b = \{2.0; 4.0\}$ m.

Width w_b [mm]		GI (T14)				GII (T24)				
		100	150	200	250	100	150	200	250	
$l_b = 2.0$ m	$f_{t,0,b}$	mean [MPa]	23.4	25.6	27.3	28.0	35.8	38.2	39.7	40.4
		COV [%]	33.7	31.6	30.0	29.7	28.6	28.0	26.8	26.3
		$x_{05,LN}$ [MPa]	12.5	14.3	15.7	16.2	21.5	23.4	24.8	25.5
		$x_{05,LN}/x_{05,LN,ref}^1$ [-]	0.87	1.00	1.10	1.13	0.92	1.00	1.06	1.09
	$E_{t,0,b}$	mean [MPa]	10,429	10,454	10,495	10,487	12,991	13,014	13,025	13,003
	COV [%]	15.2	15.1	15.1	15.0	17.0	17.5	17.1	17.0	
$l_b = 4.0$ m	$f_{t,0,b}$	mean [MPa]	20.3	22.8	24.3	25.3	32.5	35.2	36.8	37.7
		COV [%]	32.8	31.2	29.6	28.9	27.4	27.4	26.3	26.6
		$x_{05,LN}$ [MPa]	11.1	12.8	14.1	14.8	19.9	21.8	23.2	23.6
		$x_{05,LN}/x_{05,LN,ref}^1$ [-]	0.86	1.00	1.09	1.15	0.92	1.00	1.07	1.09
	$E_{t,0,b}$	mean [MPa]	10,419	10,456	10,463	10,477	12,947	13,014	13,018	13,051
	COV [%]	14.9	15.0	14.9	14.9	16.8	17.2	17.0	17.3	

¹... $x_{05,LN,ref}$ with $w_{b,ref} = 150$ mm and $l_b = \{2.0; 4.0\}$ m

Figure 2-38 shows the influence of the board width on the main statistics $\{E(X); COV(X); x_{05,LN}\}$ of the tensile strength parallel to the grain at constant board lengths of $l_{b,ref} = \{2.0; 4.0\}$ m. Given a constant reference length, the power coefficients (see **Equation (2.17)**) for adjusting the 5 %-quantile of the tensile strength parallel to the grain to the reference width result in $k_{w,2|4m,05,GI} = 0.25$ and $k_{w,2|4m,05,GII} = 0.20$, respectively, for GI and GII.

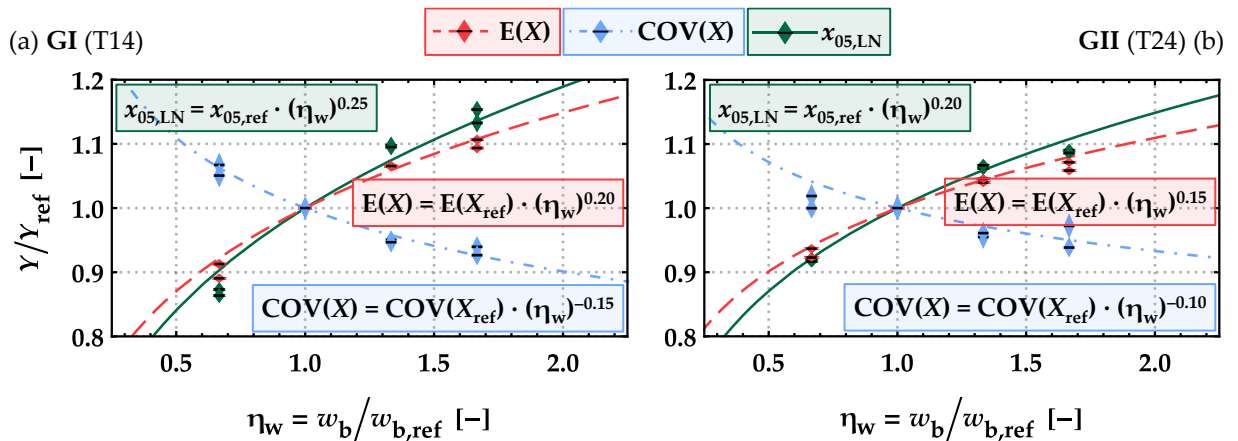


Figure 2-38: Influence of the width w_b on the main statistics $Y = \{E(X); COV(X); x_{05,LN}\}$ of the tensile strength parallel to the grain of boards ($X = f_{t,0,b}$) featuring a fixed length $l_b = \{2.0; 4.0\}$ m relative to the statistics at reference width $w_{b,ref} = 150$ mm and length $l_{b,ref} = \{2.0; 4.0\}$ m; analysis based on virtually generated boards for GI (a) and GII (b).

The underlying reference length for the boards in the original grading process used to derive the stochastic board model is $l_{b,ref} = 9 \cdot w_b$. Therefore, with the fixed reference length of $l_{b,ref} = \{2.0; 4.0\}$ m a certain length effect is contained within this analysis. By connecting this length bias with the found influences in **Section 2-7.1.3** the power coefficients reduce to $k_{w,2|4m,05,GI} = 0.10$

and $k_{w,214m,05,GII} = 0.09$ for the board width, which is of similar magnitude as the results from **Section 2-7.1.1**. As already mentioned in the previous section, the effect of the board width is also influenced by the sorting/grading process itself. Additionally, it includes a certain length effect, as the current test standard **EN 408 [39]** specifies for tensile tests a test length of $l_{b,ref} \geq 9 \cdot w_b$.

2-7.1.3 Influence of the Board Length

The board length is an additional factor which also influences the tensile properties of timber boards. This was also seen in the previous sections. To analyse this influence, again $1.5 \cdot 10^4$ timber boards for both groups with a width of $w_b = \{100; 150; 200; 250\}$ mm and length of $l_b = \{0.90; 1.35; 2.00; 2.25; 4.00\}$ m were generated. The results of the tensile strength and modulus of elasticity in tension parallel to the grain are summarised in **Table 2-18** for a width of $w_b = 150$ mm and in **Table Annex D-9** for all board widths $w_b = \{100; 150; 200; 250\}$ mm.

No changes are observed for the mean value and the coefficient of variation of the modulus of elasticity parallel to the grain in tension $E_{t,0}$ due to the board length.

Table 2-18: Main statistics of the tensile strength parallel to the grain $f_{t,0,b}$ and the modulus of elasticity parallel to the grain in tension $E_{t,0,b}$ calculated from $1.5 \cdot 10^4$ virtually generated boards (for each combination) separated in respect to group and length $l_b = \{0.90; 1.35; 2.00; 2.25; 4.00\}$ m featuring a board width of $w_b = 150$ mm.

Length l_b [m]		GI (T14)					GII (T24)					
		0.90	1.35	2.00	2.25	4.00	0.90	1.35	2.00	2.25	4.00	
$w_b = 150$ mm	$f_{t,0,b}$	mean [MPa]	29.7	27.4	25.6	25.1	22.8	42.5	40.2	38.2	37.6	35.2
		COV [%]	32.3	31.6	31.6	31.3	31.2	28.1	28.1	28.0	27.7	27.4
		$\chi_{05,LN}$ [MPa]	16.3	15.3	14.3	14.0	12.8	25.8	24.4	23.4	23.0	21.8
		$\chi_{05,LN}/\chi_{05,LN,ref}^1$ [-]	1.06	1.00	0.93	0.91	0.84	1.05	1.00	0.96	0.94	0.89
	$E_{t,0,b}$	mean [MPa]	10,477	10,442	10,454	10,446	10,456	13,009	13,008	13,014	12,994	13,014
		COV [%]	15.3	14.9	15.1	15.0	15.0	17.2	17.3	17.5	17.0	17.2

¹ ... $\chi_{05,LN,ref}$ with $l_{b,ref} = 9 \cdot w_b$

The influence of the board length l_b on the main statistics of the tensile strength parallel to the grain of boards featuring widths of $w_b = \{100; 150; 200; 250\}$ mm relative to their corresponding reference length of $l_{b,ref} = 9 \cdot w_b$ is shown in **Figure 2-39**.

By means of power regression models calibrated to the 5 %-quantile tensile strength values for group GI and GII, respectively, power coefficients $k_{1,9b,05,GI} = -0.15$ and $k_{1,9b,05,GII} = -0.11$ are found. **Fink [3]** reports a comparable decreasing tensile strength parallel to the grain with increasing board lengths with $k_{1,9b,05,L25} = -0.15$ for L25 and $k_{1,9b,05,L40} = -0.10$ for L40. **Brandner & Schickhofer [41]** calculated power coefficients for length effects in dependence on the variation of the tensile strength of the boards. They proposed $k_{1,05,COV25} = -0.13$ and $k_{1,05,COV35} = -0.21$, respectively, for boards with coefficients of variation for the tensile strength parallel to the grain in the range of $COV(f_{t,0,b}) = 25 \pm 5 \%$ and $COV(f_{t,0,b}) = 35 \pm 5 \%$. In contrast to the results here, they and **Brandner [12]** report a less pronounced length effect with respect to the

mean values of the tensile strength parallel to the grain. A similar trend was observed within test result presented in **Burger [23]**. A possible explanation for the differences is the different modelling approach used in **Brandner [12]**. There the equi-correlation for the tensile strength was directly used to model the boards with $\rho_{\text{equi}}(f_{t,0,ij}) \approx 0.40 \div 0.50$, whereas in the probabilistic board model used here only the equi-correlation of the $tKAR$ -value is defined with $\rho_{\text{equi}}(tKAR_{wz}) \approx 0.10 \div 0.16$. Nonetheless, the length effect at the 5 %-quantile level is in a similar range as found in the literature.

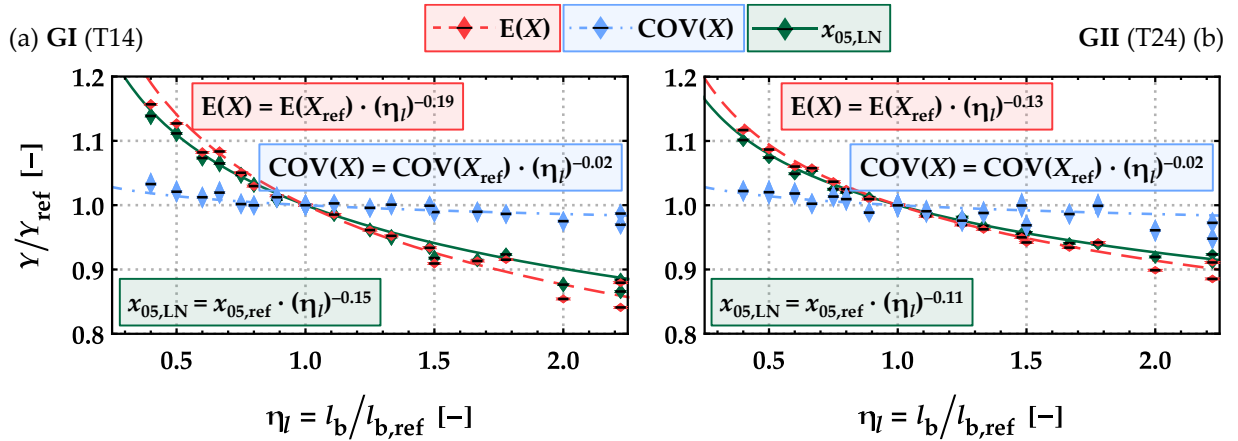


Figure 2-39: Influence of the length l_b on the main statistics $Y = \{E(X); COV(X); x_{05,LN}\}$ of the tensile strength parallel to the grain of boards ($X = f_{t,0,b}$) featuring a width of $w_b = \{100; 150; 200; 250\}$ mm relative to the statistics at reference length $l_{b,ref} = 9 \cdot w_b$; analysis based on virtually generated boards for GI (a) and GII (b).

2-7.1.4 Influence of the Reference Board Length

As demonstrated in previous sections, the tensile strength parallel to the grain of timber boards is dependent on the board length. With increasing board length, the probability for larger knots and knot clusters (weak zones) increases. Therefore, the reference length for the tensile tests is of utmost importance to characterise the tensile strength correctly. The current test standard **EN 408 [39]** imposes a reference (test) length of at least $l_{b,ref} \geq 9 \cdot w_b$ and the former glulam standard **EN 1194 [37]** states a fixed reference length of $l_{b,ref} = 2.0$ m. **Figure 2-42** shows the number of weak zones n_{wz} for board widths $w_b = \{100; 150; 200; 250\}$ mm featuring a board length $l_{b,ref} = \{9 \cdot w_b; 2.0\}$ m. As the distance of weak zones is almost constant for all board widths the number of weak zones increases with the variable reference length $l_{b,ref} = 9 \cdot w_b$ currently anchored in **EN 408 [39]**, whereas the number of weak zones is constant for the fixed reference length $l_{b,ref} = 2.0$ m; see **EN 1194 [37]**.

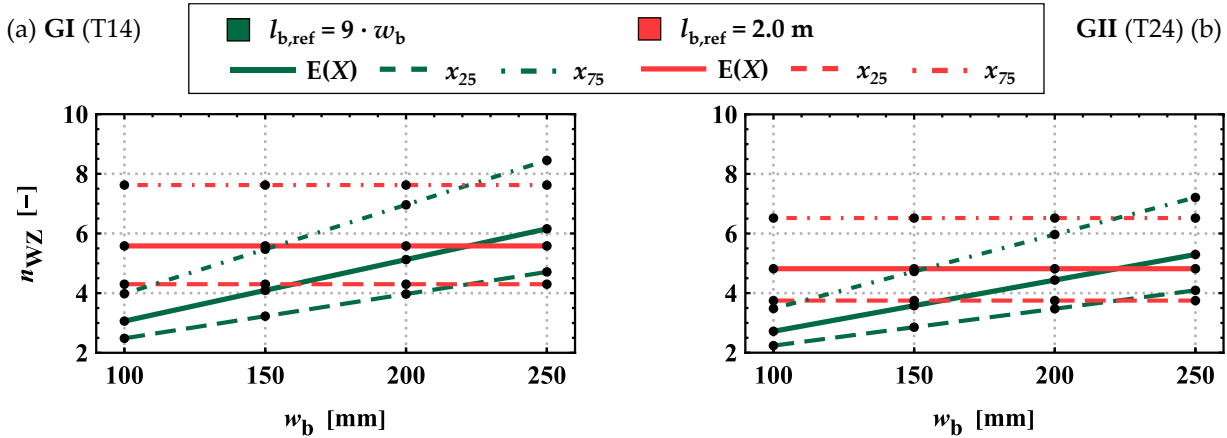


Figure 2-40: Mean, 25 %- and 75 %-quantile values of the number of weak zones n_{WZ} in dependence of the board width w_b featuring a reference board lengths $l_{b,ref} = \{9 \cdot w_b; 2.0 \text{ m}\}$ for (a) group GI (T14) and (b) group GII (T24).

With the number of weak zones within the reference length, the probability of a weak zone with a higher $tKAR$ -value increases. **Figure 4-21** shows the probability of a $tKAR$ -value larger than $tKAR_{max}$ within the reference length of $l_{b,ref} = 9 \cdot w_b$ featuring different board widths $w_b = \{100; 150; 200; 250\}$ mm relative to the probability within a reference length of $l_{b,ref} = 2.0 \text{ m}$. Thereby, a fixed distance between the weak zone of $D_{WZ} = D_{WZ,50}$ is assumed. For the board widths $w_b = \{200; 250\}$ mm the relative probability stays almost constant as the reference length of $l_{b,ref} = 9 \cdot w_b$ is approximately 2.0 m. For the smaller board widths the probability ratio gets significantly lower for both groups GII (T14) and GII (T24). For example, the relative probability of a $tKAR$ -value larger than $tKAR \geq 0.40$ for GI (T14) is $P(tKAR_{max,9wb}) / P(tKAR_{max,2m}) = \{0.62; 0.76; 0.92; 1.09\}$ for a board width of $w_b = \{100; 150; 200; 250\}$ mm respectively. In order to achieve a similar number of weak zones within the test length, as well as a similar magnitude of the weak zones ($tKAR$ -value), a fixed reference length for determining the tensile strength parallel to the grain of timber boards independent of the board width is necessary. Hereby, a length of $l_{b,ref} = 2.0 \text{ m}$ is recommended, which is in line with a proposal already made by **Burger [23]**.

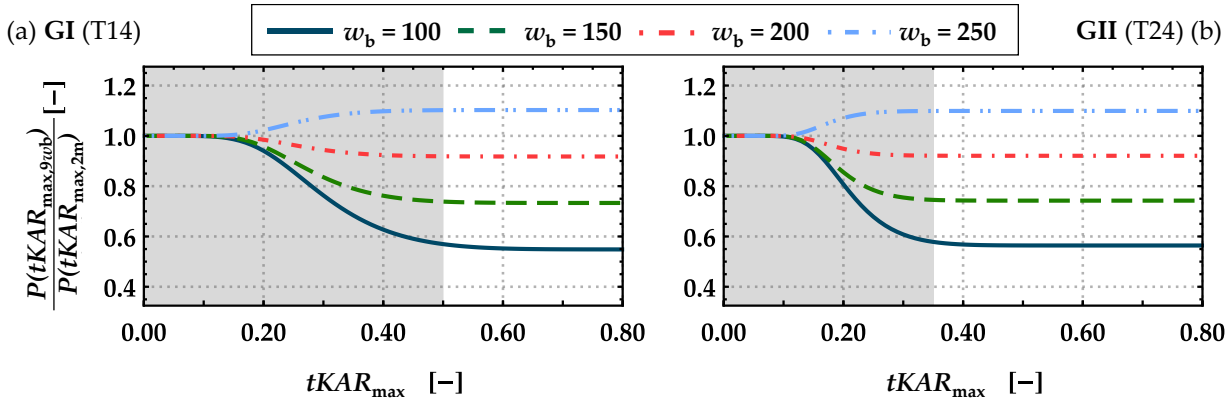


Figure 2-41: Probability of a $tKAR$ -value larger than $tKAR_{max}$ within the reference length $l_{b,ref} = 9 \cdot w_b$ featuring different board widths $w_b = \{100; 150; 200; 250\}$ mm considering a fixed distance between weak zones of $D_{WZ} = D_{WZ,50}$ relative to the probability at a reference length $l_{b,ref} = 2.0 \text{ m}$ for GI (a) and GII (b).

2-7.2 Boards in Split Condition

The probabilistic board model is also capable of describing the changes of tensile properties due to the lengthwise splitting of boards after they had been strength graded in full cross-section width. For validation of the new probabilistic board model a comparison is made between simulated data and test data from the literature as well as from additionally conducted own test series.

2-7.2.1 Influence of Lengthwise Splitting of Boards

To analyse the influence of lengthwise splitting of boards on the tensile properties, multiple sets of boards (each with $1.5 \cdot 10^4$ realisations) were generated. The sets of boards contain all possible combinations of the original board widths $w_b = \{100; 150; 200; 250\}$ mm, the board lengths of $l_b = \{2.0; 4.0\}$ m and the separation ratios $\eta_s = \{1.00; 0.67; 0.50; 0.33; 0.25; 0.13\}$. The results of the tensile strength and modulus of elasticity in tension parallel to the grain are summarised in **Table 2-19** for a width of $w_b = 150$ mm and a length of $l_b = 2.0$ m. The results for all combinations are summarised in **Table Annex D-10** and **Table Annex D-11**.

With respect to the modulus of elasticity in tension parallel to the grain, constant mean values together with increasing coefficients of variation with decreasing separation ratios η_s are observed.

Table 2-19: Main statistics of the tensile strength parallel to the grain $f_{t,0,b}$ and the modulus of elasticity parallel to the grain in tension $E_{t,0,b}$ calculated from $1.5 \cdot 10^4$ virtually generated boards (for each combination) separated in respect to groups and separation ratios $\eta_s = \{1.00; 0.67; 0.50; 0.33; 0.25; 0.13\}$ featuring a width of $w_b = 150$ mm and a length of $l_b = 2.0$ m.

Length $l_b = 2.0$ m			GI (T14)						GII (T24)					
Separation ratio η_s [-]			1.00	0.67	0.50	0.33	0.25	0.13	1.00	0.67	0.50	0.33	0.25	0.13
$w_b = 150$ mm	$f_{t,0,b}$	mean [MPa]	25.6	24.9	22.9	20.2	18.4	15.3	38.2	37.7	36.1	32.8	31.0	28.1
		COV [%]	31.6	33.0	36.8	42.2	46.1	56.3	28.0	29.1	31.7	35.3	38.5	46.3
		$\chi_{05,LN}$ [MPa]	14.3	13.5	11.5	9.2	7.9	5.6	23.4	22.5	20.6	17.4	15.7	12.4
		$\chi_{05,LN}/\chi_{05,LN,ref}^1$ [-]	1.00	0.94	0.81	0.65	0.56	0.39	1.00	0.96	0.88	0.74	0.67	0.53
	$E_{t,0,b}$	mean [GPa]	10.5	10.5	10.5	10.5	10.5	10.5	13.0	13.1	13.1	13.1	13.2	13.3
		COV [%]	15.1	16.1	17.1	18.7	19.7	22.7	17.5	18.5	19.8	19.8	21.5	27.2
		COV/COV _{ref} ¹ [-]	1.00	1.09	1.15	1.22	1.31	1.61	1.00	1.10	1.17	1.17	1.24	1.68

¹.....{COV_{ref}; $\chi_{05,LN,ref}$ } with $\eta_{s,ref} = 1.00$

Figure 2-42 shows the influence of lengthwise splitting on the tensile strength parallel to the grain relative to that of boards with full cross-section ($\eta_s = 1.00$) and for $w_b = \{100; 150; 200; 250\}$ mm. The slight variation in placing the individual datapoints along the x-axis (η_s) is caused by the applied fixed resolution of 5 mm in the residual width $w_{b,res}$ of the pre-generated boards; see **Section 2-5.4**. For example, a board featuring a width of $w_b = 100$ mm and a separation ratio of $\eta_s = 0.33$ results in a residual width of $w_{b,res} = 33$ mm. Due to the resolution of 5 mm, the nearest pre-generated board features a residual width of $w_{b,res} = 35$ mm and a separation ratio of $\eta_s = 0.35$.

Overall, with decreasing separation ratio η_s (or residual width $w_{b,res}$) the coefficient of variation of the tensile strength is increasing while the mean and the 5 %-quantile values are decreasing. These tendencies are more pronounced within the lower strength class GI (T14), which also features a higher mean level and variation of the $tKAR$ -value of the weak zone $tKAR_{wz}$ in boards in full cross-section. **Viguier et al. [42]** investigated the influence of lengthwise splitting of boards on the edgewise bending strength. They virtually split boards into two and three equally wide pieces ($\eta_s = \{0.50; 0.33\}$) and conducted virtual bending tests. Information on the orientation of boards and the coefficient of variation of the bending strength is not explicitly provided. For the 5 %-quantiles of the bending strength a reduction to 78 % and 57 % of the full cross-section bending strength was found for boards originally assigned to strength class C24 (acc. to **EN 338 [8]**). For boards from strength class C40 reductions to 83 % and 75 % were reported for $\eta_s = \{0.50; 0.33\}$. In the current investigation similar reductions are observed for the tensile strength parallel to the grain; see **Table 2-19**.

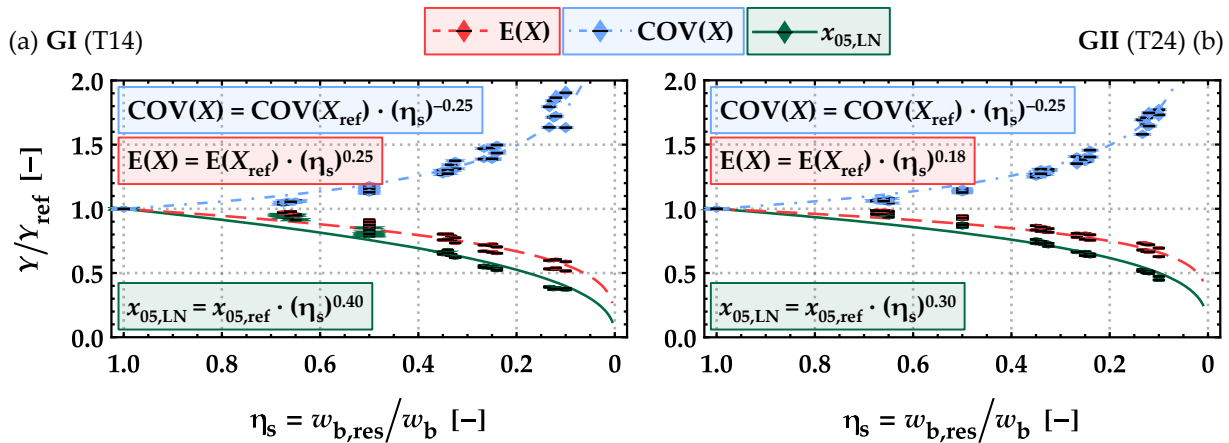


Figure 2-42: Influence of lengthwise splitting on the main statistics $Y = \{E(X); COV(X); x_{05,LN}\}$ of the tensile strength parallel to the grain of boards ($X = f_{t,0,b}$) featuring a width of $w_b = \{100; 150; 200; 250\}$ mm and board length of $l_b = \{2.0; 4.0\}$ m relative to the statistics of full cross-section properties; analysis based on virtually generated boards for GI (a) and GII (b).

2-7.2.2 Validation of the Influence of Lengthwise Splitting of Boards

To validate the model for the tensile strength, test data from the literature (**Kastner et al. [15]**) was used and complemented by additional own investigations (see also **Scherfler [34]** for further details).

The result of the tensile tests in **Kastner et al. [15]** are summarised in **Table 2-20**. They conducted tests on unsplit boards ($\eta_s = 1.00$), which were assigned to the strength class T14.5 according to **EN 338 [8]**, and lengthwise centrally split boards ($\eta_s = 0.50$). The modulus of elasticity $E_{t,0,b}$ and the density $\rho_{12,b}$ of the two series in **Kastner et al. [15]** have similar mean values and coefficients of variations. The tensile strength $f_{t,0,b,05}$ of the boards in full cross-section width are on a similar level, whereas the mean values and the coefficient of variation are approximately ~ 5 % higher in GI (T14).

Figure 2-43 illustrates and compares the relative loss in tensile strength due to the lengthwise splitting to the results of the probabilistic board model for GI (T14) in **Section 2-7.2.1**. Overall, the same tendencies are observed within the tests and the model predictions. The mean and the 5 %-quantile values of the tensile strength are decreasing and the coefficient of variation is increasing after the boards got split. The model predicts slightly higher losses in the tensile strength compared to the test results in **Kastner et al. [15]**. One reason for this is seen in the higher coefficient of variation of the tensile strength observed within GI (T14).

Table 2-20: Results from the tensile tests parallel to the grain on boards with separation ratios $\eta_s = \{1.00; 0.50\}$; from **Kastner et al. [15]**.

Separation ratio η_s [-]		1.00	0.50
$f_{t,0,b}$	# [-]	49	196
	mean [MPa]	23.8	22.1
	mean/mean _{ref} ¹ [-]	1.00	0.93
	COV [%]	25.5	28.4
	COV/COV _{ref} ¹ [-]	1.00	1.11
	$x_{05,LN}$ [MPa]	15.4	13.1
	$x_{05,LN}/x_{05,LN,ref}$ ¹ [-]	1.00	0.85
$E_{t,0,b}$	mean [GPa]	11.2	10.9
	COV [%]	8.8	9.1
$\rho_{12,b}$	mean [kg/m ³]	433	431
	COV [%]	7.5	8.1

¹ ... {mean_{ref}; COV_{ref}; $x_{05,LN,ref}$ } with $\eta_{s,ref} = 1.00$

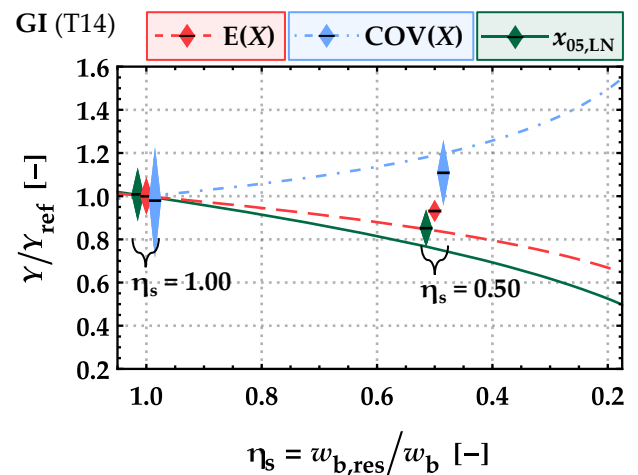


Figure 2-43: Model predictions versus the main statistics $Y = \{E(X); COV(X); x_{05,LN}\}$ from test results ($X = f_{t,0,b}$) relative to the properties of boards at full width from **Kastner et al. [15]** with 95 % CIs assuming $X \sim LN$.

Additional tests were carried out on boards with nominal strength class T14 according to **EN 338 [8]**. Half of the boards were tested with full cross-section ($\eta_s = 1.00$) and the other half of the boards were lengthwise split into two unequally-wide pieces to generate specimen with separation ratios $\eta_s = \{0.67; 0.33\}$, and tested afterwards. For further details regarding the test configuration and board dimensions see **Scherfler [34]** and **Sieder & Brandner [32]**.

The test results of the tensile tests with the separation ratios of $\eta_s = \{1.00; 0.67; 0.33\}$ are summarised in **Table 2-21**. The density $\rho_{12,b}$ of the three series have similar mean values and coefficients of variations. The mean value and the coefficient of variation of the local modulus of elasticity $E_{t,0,b}$ is slightly decreasing with decreasing separation ratios. Hereby, the three series are more comparable to the boards used for GII (T24). The tensile strength $f_{t,0,b,05}$ of the boards in full cross-section is closer to GI (T14). Please note: although T14 according to **EN 338 [8]** was ordered, the delivered material contains obviously also a high share of boards of higher strength classes. This fact is visible in the high mean tensile strength for the declared strength class T14 according to **EN 338 [8]** and in the unexpectedly high coefficient of variation $COV(f_{t,0,b}) \cong 40$ %.

Figure 2-44 illustrates the relative loss in the tensile strength due to the lengthwise splitting as observed from tests and compares those to the results of the probabilistic board model for GI (T14) in **Section 2-7.2.1**. Again, the same tendencies in test data and model prediction are found: With decreasing separation ratios the mean and the 5 %-quantiles values of the tensile strength are decreasing and the coefficient of variation is increasing. The probabilistic board model predicts less reductions for the 5 %-quantiles of the tensile strength. The observed differences between the model for GI (T14) and the test results in this case might be due to the lower, but more common, variation of $\text{COV}(f_{t,0,b}) \cong 30\%$ in the model; see also the recommendations in the probabilistic model code of the **JCSS-3.05** [43].

An increased variation of the modulus of elasticity, was also observed within the simulated boards. The reduction of the mean modulus of elasticity as found in these tests, was neither detected in **Kastner et al. [15]** nor in the simulated boards.

Table 2-21: Results from the tensile tests parallel to the grain on boards with separation ratios $\eta_s = \{1.00; 0.67; 0.33\}$; from own investigations (see also **Scherfler [34]** for further details)

Separation ratio η_s [-]		1.00	0.67	0.33
$f_{t,0,b}$	# [-]	54	54	54
	mean [MPa]	41.5	37.4	34.2
	mean/mean _{ref} ¹ [-]	1.00	0.90	0.82
	COV [%]	40.6	46.5	52.8
	COV/COV _{ref} ¹ [-]	1.00	1.15	1.30
	$\chi_{05,LN}$ [MPa]	18.7	12.5	9.2
	$\chi_{05,LN}/\chi_{05,LN,ref}$ ¹ [-]	1.00	0.67	0.49
$E_{t,0,b}$	mean [GPa]	14.0	13.1	12.6
	COV [%]	18.6	16.8	11.9
$Q_{12,b}$	mean [kg/m ³]	458	451	453
	COV [%]	8.7	8.2	11.9

¹.... {mean_{ref}; COV_{ref}; $\chi_{05,LN,ref}$ } with $\eta_{s,ref} = 1.00$

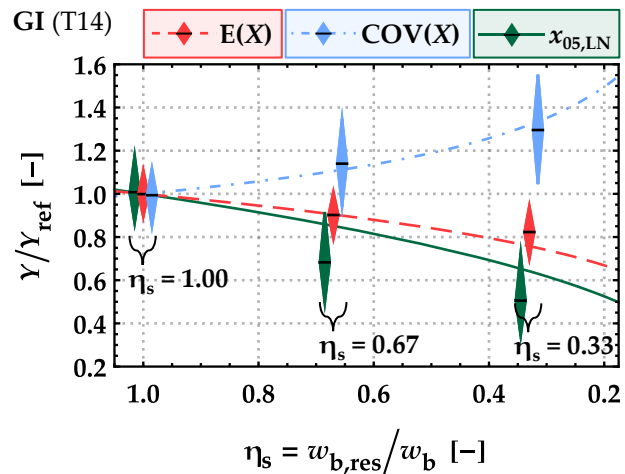


Figure 2-44: Model predictions versus the main statistics $Y = \{E(X); \text{COV}(X); \chi_{05,LN}\}$ from test results ($X = f_{t,0,b}$) relative to properties of boards at full width from own investigations (see also **Scherfler [34]** for further details) with 95 % CIs assuming $X \sim \text{LN}$.

The presented probabilistic board model which is also formulated to predict the influence of lengthwise splitting of timber boards gives predictions which are mostly well in line with the compared test results. By means of the formulated regression models to predict the tensile strength of unsplit and lengthwise split boards it is also possible to characterise the properties of boards which were graded in full width but got arbitrary reduced in their width to an extent larger than currently permitted in **EN 14081-1** [7].

2-8 Characterisation of Finger Joints

For engineered timber products the available board lengths are usually not sufficient. Therefore, finger joints are necessary to joint boards and board segments lengthwise. The resulting endless lamellas are then cut into pieces of required length. The finger joints in engineered timber products can be characterised by two parts: First, the tensile strength of the finger joints and secondly the distribution of finger joints along the board (segments), for example by statistics on the length of boards (segments) lengthwise joined via finger joints to endless lamellas.

2-8.1 Tensile Properties of Finger Joints

The tensile properties parallel to the grain of the finger joints are governed by the mechanical properties of the two joined boards. In addition, the execution conditions, the machinery and other production process-related parameters also influence the mechanical properties. These latter influences are assumed to be sufficiently controlled and are not given further consideration.

Due to their geometry, finger joints reduce the effective cross-section of the board, resulting in a decreased load-bearing capacity compared to solid, unjointed timber. To circumvent this loss, finger joints have to be placed in zones without knots and in sufficient distance from these to avoid negative influences from local grain deviations. These necessities are also part of the regulations in e.g. **EN 14080 [16]**. In addition, the minimal requirement regarding the mechanical properties of the finger joints are set in the product standards (e.g. **EN 14080 [16]**); see **Equation (2.18) to (2.20)**.

$$1.4 \cdot f_{t,0,b,k} \leq f_{m,FJ,k} \leq 1.4 \cdot f_{t,0,b,k} + 12 \quad (2.18)$$

$$f_{m,FJ,k} = 1.4 \cdot f_{t,FJ,k} \quad (2.19)$$

$$f_{t,0,b,k} \leq f_{t,FJ,k} \leq f_{t,0,b,k} + 8.5 \quad (2.20)$$

with

$f_{t,0,b,k}$ char. tensile strength parallel to the grain of boards [MPa]

$f_{m,FJ,k}$ char. bending strength of the finger joints flatwise [MPa]

$f_{t,FJ,k}$ char. tensile strength of the finger joints [MPa]

For the assignment of the mechanical properties to the finger joints the approach in **Fink [3]** was employed. Hereby, a specific $tKAR$ -value in combination with the model to predict the properties of the knot zones is used to model the finger joints. This approach was already used in previous strength models of finger joints; see **Colling [2]**. **Fink [3]** proposed a value of $tKAR_{FJ} = 0.20$, which was calibrated with test data and models taken from **Blaß et al. [5]**; see **Fink & Kohler [44]**. Following this procedure, the tensile strength of the finger joint is calculated from the minimum strength ($f_{t,FJ,(i+1)}$) of the two joined boards at the specific position; see

Equation (2.21). The modulus of elasticity parallel to the grain is approximated as the average of the module of elasticity of the clear wood zones from both boards; see **Equation (2.22)**.

$$f_{t,FJ} = \text{Min} [f_{t,FJ,i} ; f_{t,FJ,i+1}] \quad (2.21)$$

$$E_{t,FJ} = \text{Mean} [E_{t,CW,i} ; E_{t,CW,i+1}] \quad (2.22)$$

with

- $f_{t,FJ}$ tensile strength parallel to the grain of the finger joints [MPa]
- $f_{t,FJ,(i; i+1)}$ tensile strength parallel to the grain of board sections $\{i; i + 1\}$ [MPa],
calculated with $tKAR_{FJ} = 0.20$
- $E_{t,FJ}$ modulus of elasticity parallel to the grain in tension of the finger joint [MPa]
- $E_{t,CW,(i; i+1)}$ modulus of elasticity parallel to the grain in tension of
board clear wood sections $\{i; i + 1\}$ [MPa]

The main statistics of the tensile strength of the finger joints and boards featuring a width of $w_b = 150$ mm and a length of $l_b = 2.0$ m are summarised in **Table 2-22**. **Figure 2-45** shows histograms of the finger joint strength in tension together with calibrated lognormal density functions. The strength requirements according to **Equation (2.20)** are fulfilled by both groups. The ratio between the strength of the finger joints and the boards $f_{t,FJ,05,LN} / f_{t,0,b,05,LN}$ is 1.46 for GI (T14) and 1.07 for GII (T24). The modelled finger joint strengths are within the range found in the literature; see [45, 46]. Due to the used modelling strategy the strength of the finger joint is independent of the board width, which seems reasonable for the assumed flatwise oriented finger joints. Furthermore, these strength ratios are also influenced by the board length and depend on the chosen “reference” length $l_{b,ref}$. When referring to a board length of $l_b = 4.0$ m, the strength ratios calculate to 1.63 for GI (T14) and 1.15 for GII (T24).

Table 2-22: Main statistics of the tensile strength of $1.5 \cdot 10^4$ simulated finger joints ($f_{t,FJ}$) and the tensile strength of $1.5 \cdot 10^4$ simulated boards ($f_{t,0,b}$) featuring $w_b = 150$ mm and $l_b = 2.0$ m.

		GI (T14)	GII (T24)
$f_{t,FJ}$	mean [MPa]	29.3	36.1
	COV [%]	19.5	20.9
	$\chi_{05,LN}$ [MPa]	20.9	25.1
$f_{t,0,b}^1$	mean [MPa]	25.6	38.2
	COV [%]	31.6	28.0
	$\chi_{05,LN}$ [MPa]	14.3	23.4
$f_{t,FJ,05,LN} / f_{t,0,b,05,LN}$		1.46	1.07

¹.... with $w_b = 150$ mm and $l_b = 2.0$ m

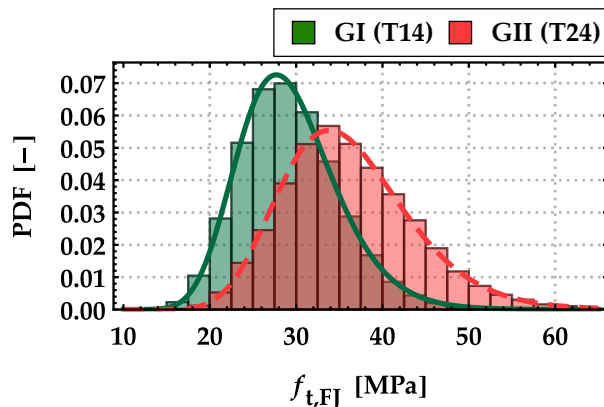


Figure 2-45: Histograms of the finger joint tensile strength parallel to the grain $f_{t,FJ}$ in [MPa] together with calibrated lognormal density functions for groups GI (T14) and GII (T24).

The 5 %-quantile values of the tensile strength of $1.5 \cdot 10^4$ virtually generated finger joints at different separation ratios $\eta_s = \{1.00; 0.67; 0.50; 0.33; 0.25; 0.125\}$ are summarised in **Table 2-23**. The tensile strength values decrease with decreasing separation ratio η_s . For a separation ratio of $\eta_s = 0.125$ a reduction of appr. 10 % is observed. This reduction in strength is due to the lower observed dynamic modulus of elasticity $E_{DYN,b}$ for smaller separation ratios η_s . A possible physical explanation for this is, that with very small residual board width $w_{b,res}$ the influence of local grain deviations (which is implicitly covered by the larger deviations of the dynamic modulus of elasticity), incomplete single finger (milling error) or alignment errors (e.g. two finger in one groove) is stronger and therefore a reduced tensile strength is observed, but no experimental investigations regarding this topic are known to the author. Overall, the results seem plausible and are of minor importance compared to the reduction of appr. 50 % of the tensile strength of the lengthwise split boards at the same separation ratio.

Table 2-23: 5 %-quantile values of the tensile strength parallel to the grain of $1.5 \cdot 10^4$ virtually generated finger joints $f_{t,FJ}$ featuring separation ratios of $\eta_s = \{1.00; 0.67; 0.50; 0.33; 0.25; 0.125\}$.

Separation ratio η_s [-]		1.00	0.67	0.50	0.33	0.25	0.125
GI (T14)	$f_{t,FJ,05,LN}$ [MPa]	20.9	20.8	20.4	20.0	19.9	19.2
	$\chi_{05,LN}/\chi_{05,LN,ref}^1$ [-]	1.00	1.00	0.98	0.96	0.95	0.92
GII (T24)	$f_{t,FJ,05,LN}$ [MPa]	25.1	24.7	24.3	24.0	23.3	22.4
	$\chi_{05,LN}/\chi_{05,LN,ref}^1$ [-]	1.00	0.98	0.97	0.96	0.93	0.89

¹.... $\chi_{05,LN,ref}$ with $\eta_s = 1.00$

2-8.2 Positioning of Finger Joints

Within the probabilistic model the positioning of the finger joints also plays an essential role. In previous investigations ([3, 5]), the length of the board segments or distance between finger joints was kept random and represented by a normal distribution. The input data for the normal distribution was gained by measuring the length of board segments in industrially produced glulam beams. Fink [3] used a normal distribution for the board length with the parameters $ND(4.30; 0.71^2)$ and the finger joints are placed at least 100 mm from the outmost weak zones. How the predetermined board length is achieved with respect to the variable distances of the weak zone is not clearly stated. A similar approach was used in Blaß et al. [5] with the parameters $ND(4.50; 0.70^2)$ for the board length. Due to the coarse mesh of $l_{FE} = 150$ mm in those investigations a minimal distance between the finger joints and knot sections is defined indirectly.

According to EN 14080 [16] finger joints should be placed at least three times the knot diameter d_{knot} away from the closest knot and knots below a diameter of $d_{knot} = 6$ mm can be disregarded. The approach within the present investigation is based on these regulations and the current production process. Hereby, a board is generated with a fixed board length and the finger joints are placed within a knot-free zone (CW) as close as possible to the board ends; see

Figure 2-46. Thereby, knot zones with $tKAR$ -values below $tKAR = 0.025$ are disregarded. The finger joints with a length of 20 mm are placed in the middle of a knot-free zone with a length of $L_{CW,FJ} = 90 \text{ mm} \leq L_{CW}$. According to the definition of the length of the knot zones $\{L_{WZ}; L_{LZ}\}$ in **Section 2-2**, by means of this procedure the distance between finger joints and a knot within the knot zone is 1.0 times the relevant knot diameter plus the additional length of $L_{CW,FJ} / 2 = 45 \text{ mm}$. **Brandner [12]** analysed knot diameters within the boards of the here used databases and stated a mean knot diameter of $d_{\text{knot,mean}} = 10 \text{ mm}$ and a 95 %-quantile of $d_{\text{knot,95}} = 25 \text{ mm}$. Therefore, the distance between a knot and the finger joint results in a worst-case scenario to $2.8 \cdot d_{\text{knot,95}}$. This approximation seems to be an adequate solution to implement the regulations anchored in **EN 14080 [16]**.

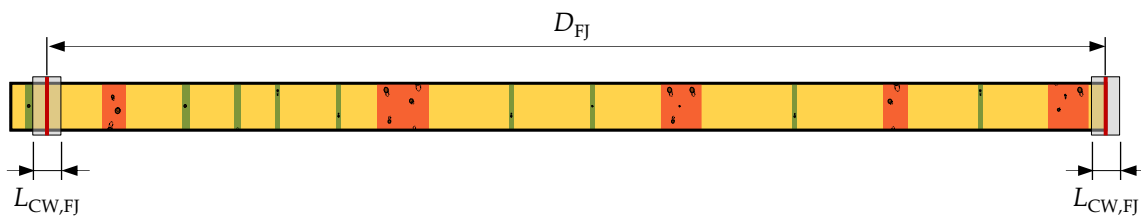


Figure 2-46: Board with positioned finger joints and distance of finger joints D_{FJ} .

The main statistics of the distance between finger joints D_{FJ} are summarised in **Table 2-24**. Additionally, the distributions of D_{FJ} for different separation ratios $\eta_s = \{1.00; 0.50; 0.33; 0.125\}$ are shown in **Figure 2-47**. Hereby, the board length was assumed with $l_b = 4.0 \text{ m}$, a board length commonly used in Austria.

Table 2-24: Main statistics of the distance between finger joints D_{FJ} of each $1.5 \cdot 10^4$ virtually generated boards (for each combination) featuring separation ratios of $\eta_s = \{1.00; 0.67; 0.50; 0.33; 0.25; 0.125\}$.

Separation ratio η_s [-]		1.00	0.67	0.50	0.33	0.25	0.125
GI (T14)	mean [m]	3.82	3.85	3.87	3.89	3.90	3.91
	COV [%]	4.26	3.16	2.51	2.05	1.93	1.69
GII (T24)	mean [m]	3.87	3.88	3.90	3.91	3.91	3.92
	COV [%]	2.69	2.28	1.83	1.56	1.45	1.28

The mean distance of the finger joints D_{FJ} is slightly increasing and the coefficient of variation is decreasing with lower separation ratios η_s . In a real production line, the boards would be finger jointed to endless lamellas and lengthwise split afterwards. Thus, there is no plausible reason for any change in statistics of D_{FJ} . Within the presented model the boards are generated in split condition and must be joined afterwards. The observed deviations at the mean level of approximately 2.5 % due to the positioning of the finger joints in the already split board seem negligible.

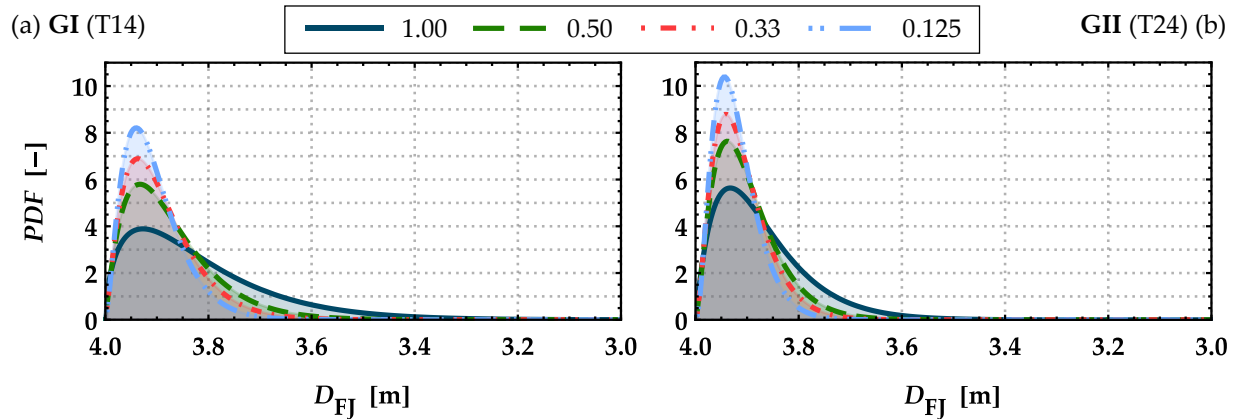


Figure 2-47: Calibrated beta density functions $\{0; 4\}$ for representing the distance between finger joints D_{FJ} placed in boards as well as lengthwise split boards featuring separation ratios of $\eta_s = \{1.00; 0.50; 0.33; 0.125\}$, assuming a reference board length of $l_b = 4.0$ m for the base material (a) GI (T14) and (b) GII (T24); $1.5 \cdot 10^4$ simulations for each combination.

In most production lines of GLT or CLT the boards have a specific length and are already strength graded. Therefore, only finger joints need to be placed in knot-free zones as close to the board ends as possible. In contrast to previous models, the new approach delivers plausible and realistic board lengths/distances between finger joints D_{FJ} within endless lamellas. Additionally, the new method is not dependent on measurements in production facilities and is easily adaptable to various board lengths.

2-9 Bending Strength of Simulated Boards

For certain engineered timber products in which boards are loaded edgewise, the bending strength may also significantly influence the load-bearing behaviour. Therefore, virtual bending tests on boards were carried out. This was accomplished with the same stochastic-numerical beam model which is used later for modelling the bending strength of engineered timber products; see [Section 3-3.1](#). With the mentioned assumptions regarding the mesh size for the edgewise load case, the bending strength of these boards assuming a test configuration according to [EN 408 \[39\]](#) with a span of $l_{span} = 18 \cdot w_b$ was calculated. The main statistics of the bending strength $f_{m,b}$ and the modulus of elasticity $E_{m,b}$ are summarised in [Table 2-25](#).

Table 2-25: Main statistics of the bending strength $f_{m,b}$ and modulus of elasticity $E_{m,b}$ calculated from 10^3 virtually tested boards (for each combination) from both groups GI (T14) and GII (T24) featuring a test span of $l_{span} = 18 \cdot w_b$ and board widths of $w_b = \{100; 150; 200\}$ mm.

Width w_b [mm]		GI (T14)			GII (T24)		
		100	150	200	100	150	200
$f_{m,b}$	mean [MPa]	37.8	35.3	33.2	55.5	51.5	48.2
	COV [%]	35.6	31.1	30.6	30.0	27.8	26.9
	$\chi_{05,LN}$ [MPa]	19.2	19.7	19.1	32.4	31.5	30.3
$E_{m,b}$	mean [MPa]	10,492	10,497	10,472	12,988	12,951	13,050
	COV [%]	16.0	15.1	15.3	17.8	17.1	18.0

The statistics of the bending strength are within a plausible range of the stated bending strength in **EN 338 [8]** with 20,5 MPa for T14 and 33.0 MPa for T24. The coefficients of variation with $\text{COV}(f_{m,b}) \approx 30 \div 35 \%$ for GI (T14) and $\text{COV}(f_{m,b}) \approx 27 \div 30 \%$ for GII (T24) are quite high compared to the 25 % stated in **JCSS-3.05 [43]**. Possible reasons for this are, that the boards are graded/sorted based on their tensile properties and the position of knots within the cross-sections is not known within the present model. Knots in marginal areas of the board have larger influence on the bending strength. Consequently, considering only knots in the marginal (outer) areas of the boards, would decrease the magnitude of knots and their occurrence, which would lead to an overall smaller coefficient of variation of the bending strength. For the modulus of elasticity similar results are achieved as within the virtual tensile tests. Nonetheless, the results of the bending strength with the assumed mesh size are within a plausible range for GI (T14) and GII (T24) despite the rather simplified approach and rough assumptions.

2-10 Intermediate Conclusions

The presented probabilistic board model is capable of predicting the tensile strength parallel to the grain of boards. Size effects with respect to the board width and length are within a plausible range as found in experimental investigations in the literature (e.g. **[3, 23, 41]**). The size effects are partially dependent on the different testing lengths of $l_{b,\text{ref}} = 9 \cdot w_b$ (see **EN 408 [39]**) and their dependence on the board width, i.e. partly combined length and width effects are given. For clear reference conditions, reference cross-sections as well as fixed reference lengths for testing the properties of the base material boards and thereof built up engineered timber products are recommended. For the base material such an approach was given in the former European glulam standard **EN 1194 [37]**. **EN 1194 [37]** stated a reference length of $l_{b,\text{ref}} = 2.0$ m and a reference width of $w_{b,\text{ref}} = 150$ mm. Deviating board dimensions could be corrected to the reference dimension via power functions using power coefficients of $k_{w,\text{EN1194}} = 0.05$ and $k_{l,\text{EN1194}} = 0.10$, respectively, for the width and the length. Such regulations are missing in the current product standard **EN 14080 [16]** for GLT. As already mentioned, the influence of the board width is neglectable or partly excluded due to knot parameters that take the width into account e.g. the *tKAR*-value. A fixed testing length for the tensile strength independent of the board cross-section is recommended which is in line with a proposal already made by **Burger [23]**.

The modelling approach for the finger joints delivers plausible tensile properties and residual board lengths found in current production facilities. Additionally, it can be adapted to different base board lengths. The stochastic board model is also capable of predicting the edgewise bending strength of the boards for GI (T14) and GII (T24) in a satisfactory manner. Nonetheless, a better approximation would be achieved by taking into account the position of the knots within the cross-section.

Besides the characterisation of the mechanical properties of timber boards in their full cross-section width, the herein presented probabilistic board model is also capable to quantify the impact of lengthwise splitting on the tensile properties parallel to the grain. With the presented regression models it is also possible to characterise the properties of boards graded in full cross-section width before they got arbitrary reduced in their width to an extent larger than currently permitted in [EN 14081-1 \[7\]](#).

Based on the insights regarding the coupled length and/or width effect on the tensile strength due to the regulations in [EN 408 \[39\]](#) and in line with the former glulam standard [EN 1194 \[37\]](#), a fixed reference length of $l_{b,ref} = 2.0$ m is used within the stochastic-numerical load-bearing models.

Chapter 3:

Stochastic-Numerical Beam Model

In this chapter the stochastic-numerical beam model is presented. First, the virtual production process is outlined. Afterwards, the beam generation procedure and its implementation in the software applications are demonstrated. At the end of the chapter the implementation in virtual bending tests is illustrated.

3-1 Introduction and Overview

For a safe and economic design of timber structures, the appropriate description of the mechanical properties of all structural parts is essential. Engineered timber products, as one of those parts, are not only characterised by their components, e.g. boards and finger joints, but in the sense of systems are more than the number of its individual components. The interaction of these components leads to a complex system behaviour. As a consequence, any model trying to depict the strength and stiffness of engineered timber products has to take into account the serial and sub-parallel structure given by the interacting boards, finger joints and various laminations/layers. In the following, the mechanical part of this interaction is covered with finite element models. The finite element method (FEM) was successfully applied in numerous past investigations, for GLT beams, e.g. by [Ehlbeck et al. \[1\]](#), [Fink \[3\]](#), [Tapia \[6\]](#), [Blaß & Frese \[47\]](#), [Vida et al. \[48\]](#), [Kandler et al. \[49\]](#).

To account also for the uncertainty, these beam models are implemented in Monte Carlo simulations (MCs) which vary material properties of boards and the positioning of finger joints and their properties by means of probabilistic models with the aim to derive the mechanical properties of engineered timber products including also their variabilities and uncertainties. The combination of FEM and MC is also classified as “stochastic finite element method” (SFEM). Such models can be used to determine the properties and behaviour of system products such as glulam given a predefined set of input parameters, for example to characterise the tensile properties along boards and that of finger joints, as well as to analyse the impact of varied input parameters on the output of such complex systems, e.g. size and system effects as consequence of varying dimensions and number of sub-parallel acting components within the product. Therefore, certain system and size effects of beam elements can be derived and quantified better than in experimental investigation provided that the probabilistic-mechanical models represent reality sufficiently accurate. Such SFEM are thus of high relevance for sensitivity analyses in various ways as the effects of certain controlled parameter variations can be easily quantified. This circumstance is also of utmost importance for the present thesis with focus on the analyses of the influence of arbitrary positioned lengthwise split lamellas within the cross-section of engineered timber products.

Models from the literature differ in certain aspects, like mesh-size, implemented non-linearities and failure criteria. Concerning the latter, three different types of failure criteria {load drop; stiffness drop; fracture of the lowest lamella} can be identified. The first criterion is mostly used in newer investigations and is implemented by means of fracture mechanics (e.g. [\[6, 48, 49\]](#)). These non-linear approaches would add an additional time penalty on top of the already high computation times and seems improper for the investigations intended in this thesis. The stiffness criterion is similar to the load drop criterion, but with the advantage that it can be implemented also in a linear FE-problem. The last criterion, “fracture of the lowest lamella”, is in principle only applicable in a sensible manner in case of GLT, where only one board/lamination

is present at the outermost bottom of the beam. By considering all the advantageous and disadvantageous of all these failure criteria it has to be noted that all of them are usually calibrated on experimental tests which to some extent counteract possible influences from the made model assumptions.

All models in the literature were developed for common GLT which is the reason why these models are reduced to a two-dimensional (2D) FE-problem. To characterize the mechanical properties of the beams investigated in this thesis, as illustrated in **Figure 1-1**, it is essential to consider the parallel-acting boards, which may occur in both split and unsplit conditions. Therefore, the afterwards presented stochastic-numerical beam model is one of the first three-dimensional (3D) beam models and the first one capable of depicting parallel system effects. In the following, the virtual production process and the implementation into a stochastic-numerical beam model is described in detail.

3-2 Virtual Production Process

3-2.1 Multi-Layered Panels (MLP)

The first steps in the virtual production process of the beam elements are illustrated in **Figure 3-1**. At first, the boards are joined to an endless lamella via finger jointing. Thereby, the initial board length $l_{b,s}$ is chosen randomly with $0 < l_{b,s} \leq l_{b,i}$ whereas the following board segments have a length of $l_{b,i} = D_{FJ,i} \leq l_b$; see **Section 2-8.2**. Secondly, the endless lamella is trimmed according to the length of the beam l_g and edge-bonded to a single-layered solid wood panel (SWP) with the thickness $t_{lay} = t_b$. In a third step the SWP is cut to the required width w_{lay} . Hereby, the width of the first board $w_{b,s}$ is chosen randomly with $0 < w_{b,s} \leq w_b$. Afterwards, a predefined number of SWPs are face bonded unidirectionally and/or orthogonally to multi-layered panels (MLPs) and in the final step the beam elements in requested dimensions and geometry are cut out from the MLPs.

The overlap of the board edges between neighbouring layers, Δ_{edge} , is dependent on the width of the used boards w_b , the width of the multi-layered panels w_{MLP} and the width of the tool used for cutting single-layered wood panels $w_{cut,SWP}$. The overlap can be calculated and adjusted based on **Equation (3.1)**, assuming a constant board width w_b . In the following investigations, the tool (e.g. saw blade) width to cut the SWP is fixed with $w_{cut,SWP} = 5$ mm. Three different cases with $\Delta_{edge} = \{0; 1/3; 1/2\} \cdot w_b$ are illustrated in **Figure 3-2**. For MLPs with orthogonal layers two virtual production processes are used: One for the SWP of the longitudinal and a second for the cross layers. Hence, the overlap of the board edges Δ_{edge} for orthogonal multi-layered panels is measured between neighbouring layers with the same orientation.

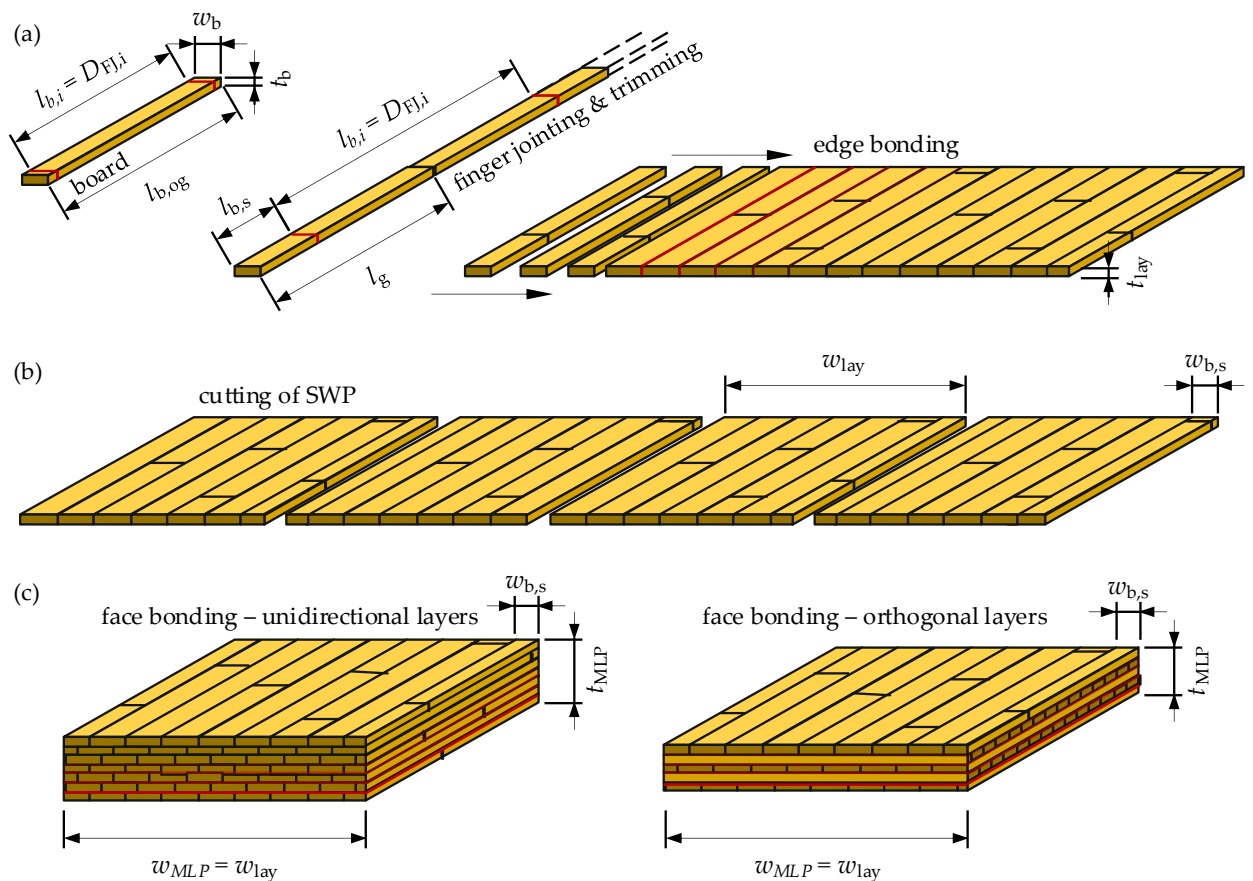


Figure 3-1: Steps of the virtual production of flex_GLT-CLT beams: (a) finger jointing of board segments to lamella, cutting of lamellas to length and edge bonding to endless single-layered solid wood panel (SWP); (b) cutting of SWP to width; (c) face bonding of SWP to multi-layered panels (MLPs) with unidirectional and/or orthogonal layers.

$$\Delta_{edge} = \min \begin{cases} w_b - w_{MLP} \bmod w_b - w_{cut,SWP} \\ w_{MLP} \bmod w_b + w_{cut,SWP} \end{cases} \quad (3.1)$$

with

Δ_{edge} overlap of the board edges of neighbouring layers (with same orientation) [mm]

w_b board width [mm]

w_{MLP} width of the multi-layered panel [mm]

$w_{cut,SWP}$ width of the cutting tool for the SWP [mm]; here assumed with $w_{cut,SWP} = 5$ mm

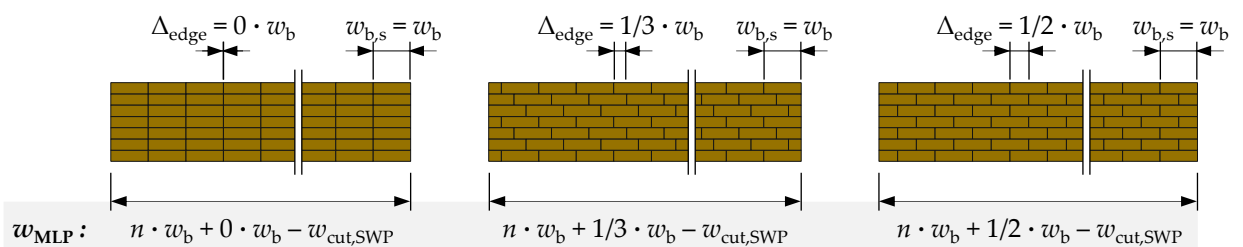


Figure 3-2: Influence of the width of the multi-layered panel w_{MLP} on the overlap of the board edges between neighbouring layers Δ_{edge} .

3-2.2 Beam Elements

In the last virtual production step, the multi-layered panels are cut into beam elements. Depending on the orientation or main load direction (bending moment) the beams can be distinguished into flex_GLT type A and type B; see **Figure 3-3**.

For flex_GLT type A beams the boards are primary loaded edgewise, the thickness of the MLP t_{MLP} is equal to the beam width $w_{g,A}$ and the beam depth $h_{g,A}$ is flexible and depends on the placement of the cuts. Within flex_GLT type B beams the boards are primary loaded flatwise like in conventional GLT. Hereby, the panel thickness t_{MLP} is equal to the beam depth $h_{g,B}$ whereas the width $w_{g,B}$ is flexible.

Figure 3-3 shows also possible cross-section patterns (positioning of boards and lengthwise split boards within beams), which are arbitrary due to the first board width $w_{b,s}$ which is chosen randomly. In a next step one beam is taken randomly from the multi-layered panel and afterwards a new MLP is generated and the process repeated. An analysis of the first board width of the beams $w_{b,s}$ between this sampling strategy and the “real” production process (considering all beams from the MLP) showed deviations of $\pm 0.5\%$ on the mean level and for the coefficient of variation. Therefore, the previously mentioned sampling method generates comparable beams and is simpler to implement and parallelise in software packages.

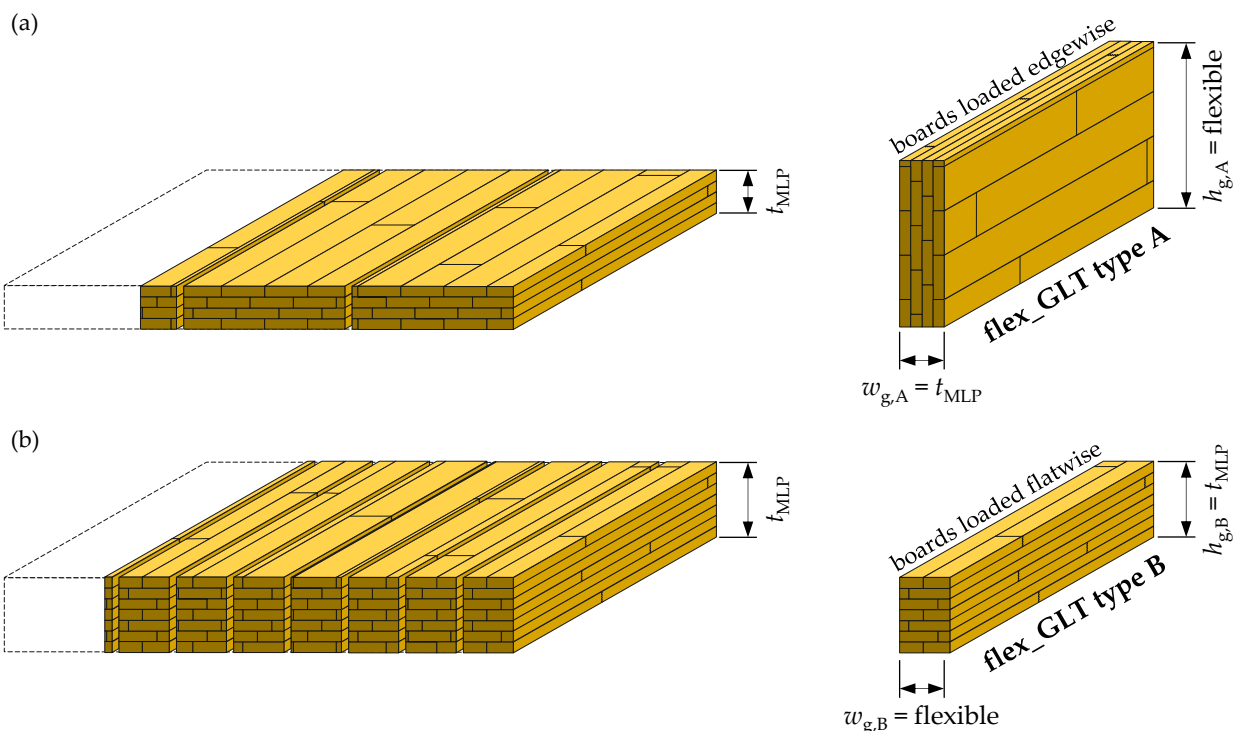


Figure 3-3: Beam types cut from unidirectional MLPs: (a) flex_GLT type A and (b) flex_GLT type B.

Analog to the unidirectionally laminated multi-layered panels, orthogonally laminated MLPs can be distinguished depending on the orientation or load direction (bending moment) into flex_CLT beams and flex_CLT slabs, see **Figure 3-4**.

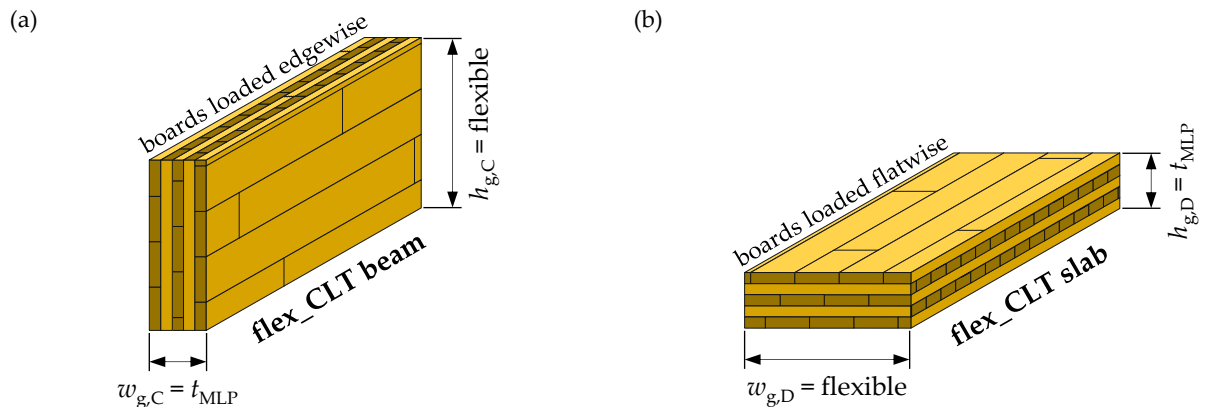


Figure 3-4: Beam types cut from orthogonal MLPs: (a) CLT as beam and (b) CLT as slab.

3-2.3 Special Cases

By setting specific input parameters special cases, i.e. beam cross-sections, can be analysed with the presented virtual production process. One special case is conventional GLT, as illustrated in **Figure 3-5 (a)**. This is accomplished when the board width w_b is equal to the beam width w_g , all board edges are aligned and the beams are cut exactly along the board edges from the MLP. A second special case also occurs when the beam width w_g is a fraction $\{1/2; 1/3\}$ of the board width w_b with the precondition, as before, that all board edges in neighbouring layers stay aligned. Such beams are known as resawn glulam. **Figure 3-5 (b)** shows resawn glulam beams with one cut ($w_g = 1/2 \cdot w_b$). To reliably create such special cases the random starting width $w_{b,s}$ of the SWP is deactivated.

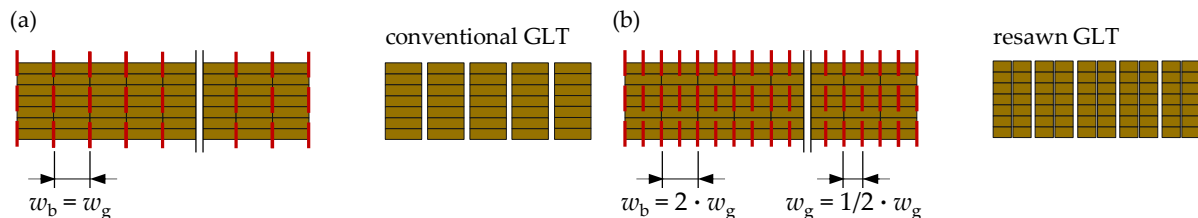


Figure 3-5: Special cases of the virtual production process: (a) conventional GLT and (b) resawn GLT.

3-3 Stochastic-Numerical Beam Model

3-3.1 Basic Principles

The basics principles and the simulation process of the numerical beam model are shown in **Figure 3-6**. After the virtual production process and the simulation of the board properties within **Mathematica [22]**, the FE-model is generated within the software package **Ansys [50]** and the mechanical properties are passed to each element. In the next step, a fixed load is applied and the model is solved. Based on the mean tensile stress parallel to the grain in each element the utilisation in tension parallel to the grain is calculated. The maximum load of the step is calculated based on the magnitude of the applied load and the maximum utilisation in tension parallel to

the grain. The modulus of elasticity of the board section (zone) {WZ; IZ; CW; FJ} containing the element with the highest degree of utilisation is set to $E_{t,0,ij} = 0$. Then, the load is reapplied and the FE-model is solved again. This loop is repeated until the reduction of the global stiffness always related to the initial cross-section is greater than 20 % of its initial value. The maximum load of each iteration is recorded and used to calculate the strength of the beam; further details in [Section 3-3.2](#).

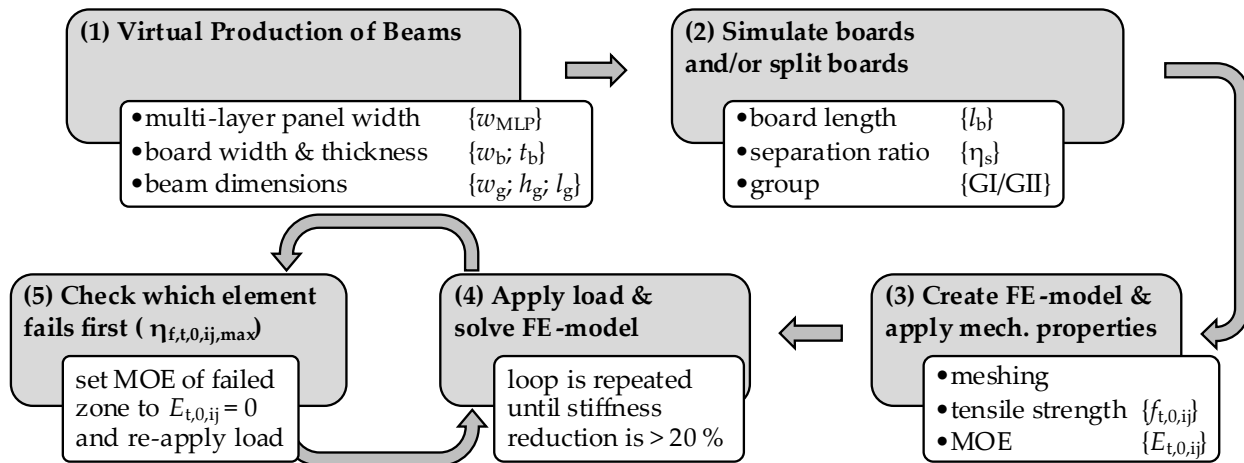


Figure 3-6: Flow-chart of beam generation and simulation process.

For illustration of the implementation within the stochastic-numerical FE-model a part of a flex_GLT-beam type B is shown in [Figure 3-7](#) highlighting the distribution of knot zones and finger joints as well as the distribution of $tKAR_{ij}$ and the tensile properties $f_{t,0,ij}$ and $E_{t,0,ij}$. For the board segments and finger joints 8-noded elements of type SOLID185 were used to model the orthotropic behaviour. The modulus of elasticity along the boards was modelled based on the probabilistic board model with $E_x = E_{t,0,ij}$. The other material constants were assumed as fix values with $\{E_y = E_z = 300 \text{ MPa}; G_{xy} = G_{xz} = G_0 = 650 \text{ MPa}\}$ according to [EN 14080 \[16\]](#) and the rolling shear modulus with $G_{yz} = G_{zy} = G_{90} = 100 \text{ MPa}$ ($w_b/t_b \geq 4$) in alignment with [Brandner et al. \[51\]](#). In the “Karlsruher Rechenmodell” different regression models are used for representation of the tension and compression zones in glulam beams loaded in bending; see [Ehlbeck et al. \[10\]](#). Nonetheless, the mean modulus of elasticity in tension and compression of the boards used to derive these regression models are almost identical and have a similar coefficient of variation. Based on the observations and similar to [Fink \[3\]](#), [Tapia \[6\]](#), no differentiation between tensile and compressive material properties was made $\{E_{c,0,ij} = E_{t,0,ij}\}$. In contrast to other stochastic-numerical models (e.g. [\[4–6, 48\]](#)) a failure or yielding within the bending-compression zone is not considered. Failures in the virtually produced and tested beams can only occur in tension parallel to the grain within the beam. This mirrors also experiences from real testing at least for the lower and medium glulam strength classes. Nevertheless, glulam beams of higher strength class or general glulam beams featuring high resistance in the bending-tension zone may yield in the bending-compression zone prior ultimate failure in the bending-tension zone. Neglecting such

phenomena in the stochastic-numerical models used in this thesis, however, enables a significant reduction in the calculation time as only a linear elastic model needs to be solved.

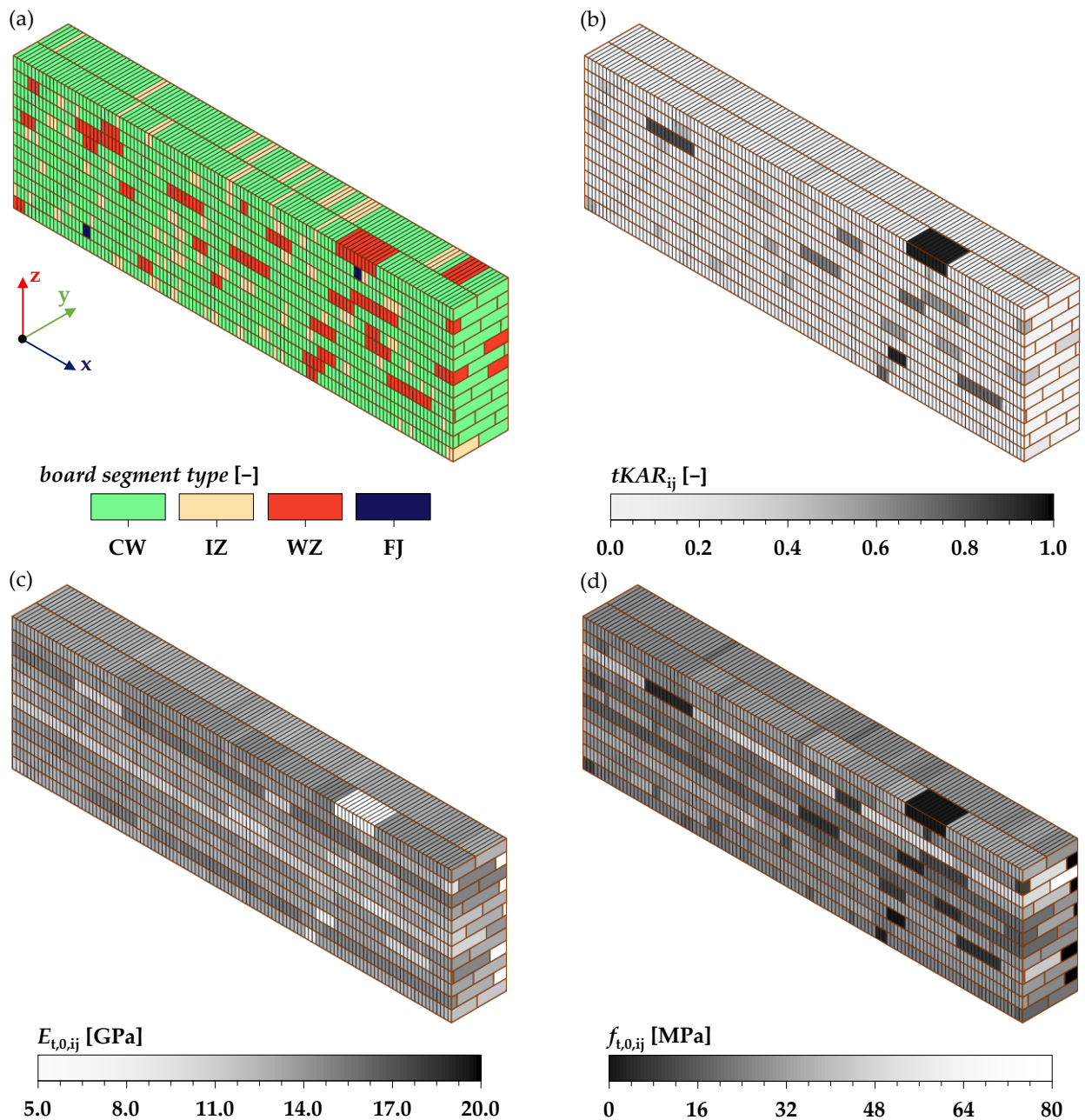


Figure 3-7: Exemplary representation of one part of a flex_GLT-beam type B as implemented in the stochastic-numerical beam model: (a) board segment type {CW; IZ; WZ; FJ}; (b) $tKAR$ -value; (c) distribution of the modulus of elasticity parallel to the grain (x-axis) $E_{t,0,ij}$; (d) distribution of the tensile strength parallel to the grain (x-axis) $f_{t,0,ij}$.

The contact between the boards at their edges and faces, representing structural adhesive bonds, was modelled rigid via surface contact elements TARGET170 and CONTA174. For the load introduction and support plates in steel the quadratic elements SOLID186 with isotropic material behaviour with $E_s = 10^{10}$ MPa were used. Hereby, a rigid contact perpendicular to the contact surface was assumed. The tangential stiffness of the contact surface was modelled with a

very small stiffness to prevent an influence of the stiff plates on the load-bearing behaviour of the beam elements.

Figure 3-8 shows the FE-mesh of a board loaded flatwise and edgewise in bending. Thereby, the element size in x -direction is set to $l_{e,x} = 10$ mm. This rather small value was chosen to realistically depict the morphology of the knot zones in the probabilistic board model. In the direction of the board thickness one element per lamination is used ($l_{e,t} = t_b$). The element size in width direction $l_{e,w}$ is dependent on the load case. If boards are loaded flatwise one element in width direction is used ($l_{e,w,f} = w_b$; see **Figure 3-8 (a)**). In case of edgewise loading the number of elements in width direction was chosen such, that the maximum element size is $l_{e,w,e} \leq 30$ mm; see **Figure 3-8 (b)**. The exact models and configurations used for the virtual bending tests are described in **Section 3-3.2**.

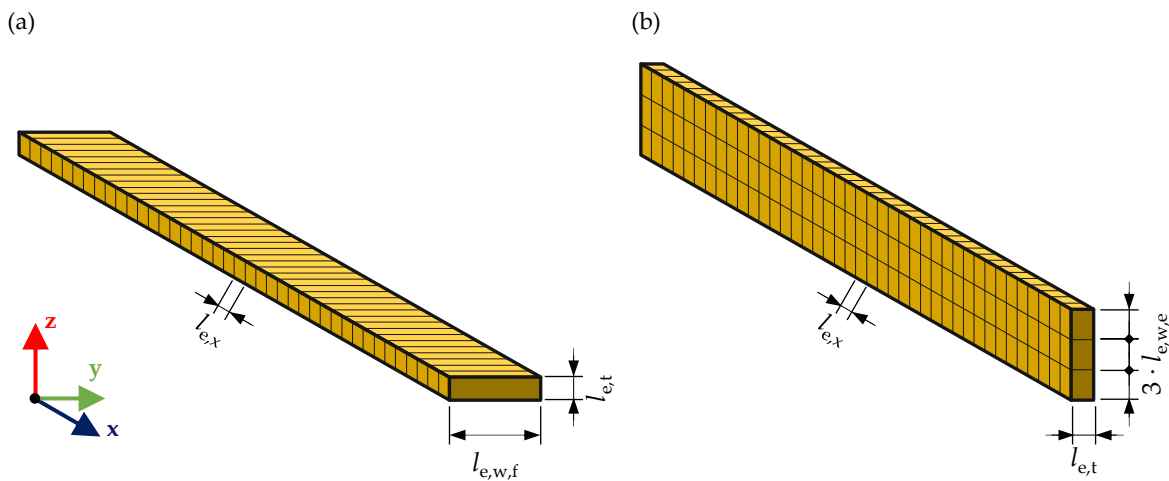


Figure 3-8: Examples of FE-meshes for a single board loaded (a) flatwise and (b) edgewise in bending.

3-3.2 Stochastic-Numerical Model for the Bending Strength

In order to determine the bending strength $f_{m,g}$ of virtually generated beams, virtual four-point-bending tests in accordance with prescriptions for real bending tests in **EN 408 [39]** were carried out. The test setup within the FE-software application **Ansys [50]** is shown in **Figure 3-9**. Predetermined loads $F_{test} / 2$ are applied in the third points of the test span and the simulation process in **Figure 3-6** is started. As the stiffness abort criteria the global modulus of elasticity $E_{glob,k}$ is used. For each iteration k and based on the maximum degree of utilisation of each element in tension parallel to the grain the maximal load is calculated. The exact calculation procedures are shown in **Equations (3.4) to (3.7)** and in **Annex B-2**.

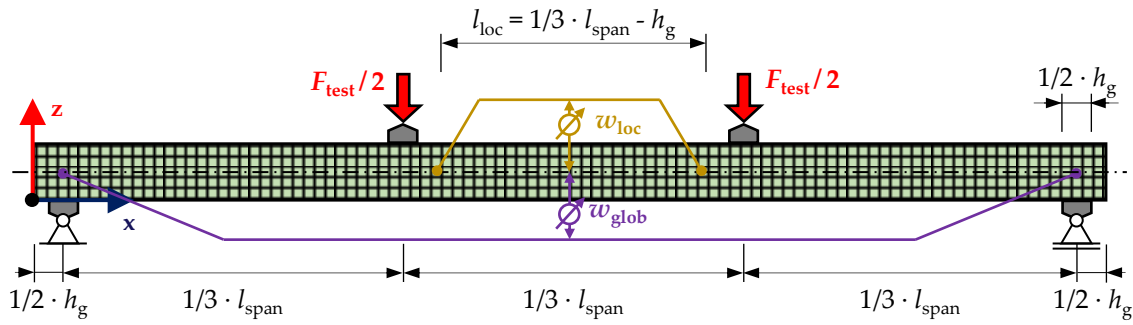


Figure 3-9: Four-point-bending test setup as implemented in the FE-software application **Ansys [50]** in accordance with **EN 408 [39]**.

$$E_{loc} = \frac{l_{span} \cdot l_{loc}^2 \cdot F_{test}}{48 \cdot I_{eff} \cdot w_{loc,1}} \quad (3.2)$$

$$E_{glob,k} = \frac{23 \cdot F_{test} \cdot l_{span}^3}{27 \cdot I_{eff} \cdot \left(48 \cdot GA_{eff} \cdot \frac{w_{glob,k}}{F_{test}} - 8 \cdot l_{span} \right)} \quad (3.3)$$

$$F_{max,k} = \frac{F_{test}}{\max(\eta_{f_{t,0,ij,k}})} \quad (3.4)$$

$$F_{ult} = \max(F_{max,k}) \quad (3.5)$$

$$M_{ult} = \frac{F_{ult}}{2} \cdot \frac{l_{span}}{3} \quad (3.6)$$

$$f_{m,g} = \frac{M_{ult}}{W_{eff}} \quad (3.7)$$

with

- E_{loc} local modulus of elasticity of the beam in bending [MPa]
- l_{span} span of four-point-bending test [mm]
- l_{loc} reference length for determination of the local of modulus of elasticity [mm];
with $l_{loc} = 1/3 \cdot l_{span} - h_g$
- F_{test} load applied in FE-model [N]
- I_{eff} effective moment of inertia of the beam [mm⁴]; see **Annex B-2**
- $w_{loc,1}$ local deflection at the first iteration [mm]
- $E_{glob,k}$ global modulus of elasticity of the beam at iteration k [MPa]
- GA_{eff} effective shear stiffness of the beam [N]; see **Annex B-2**
- $w_{glob,k}$ global deflection at iteration k [mm]
- $F_{max,k}$ maximum load at iteration k [N]
- $\eta_{f_{t,0,ij,k}}$ degree of utilisation in tension parallel to the grain of elements at iteration k [-]
- F_{ult} ultimate load carrying capacity of the beam [N]
- M_{ult} ultimate moment carrying capacity of the beam [Nmm]
- $f_{m,g}$ bending strength of the beam [MPa]
- W_{eff} effective section modulus of the beam [mm³]; see **Annex B-2**

Figure 3-10 illustrates load-deflection curves of five virtual glulam bending tests. In these simulations, failure was defined as a 20% reduction in the initial stiffness (global modulus of elasticity), allowing for a certain degree of load redistribution within the glulam or flex beam. The ultimate load in each virtual bending test is identified as the point immediately preceding a significant load drop in the load–deflection curve. Using this approach, the predictions obtained with the presented method are comparable to those based on a pure load-drop criterion, while avoiding the need to employ fracture mechanics (see [52–54]). However, comparing different stochastic beam models and failure criteria is challenging, as each model varies in certain aspects, such as the computational program, input parameters, mesh size, and/or failure criteria. Consequently, benchmarking the stochastic model against empirical test data is of critical importance. For this reason, the presented stochastic-numerical model is validated and compared with both accompanying experimental tests and results from literature in the following sections.

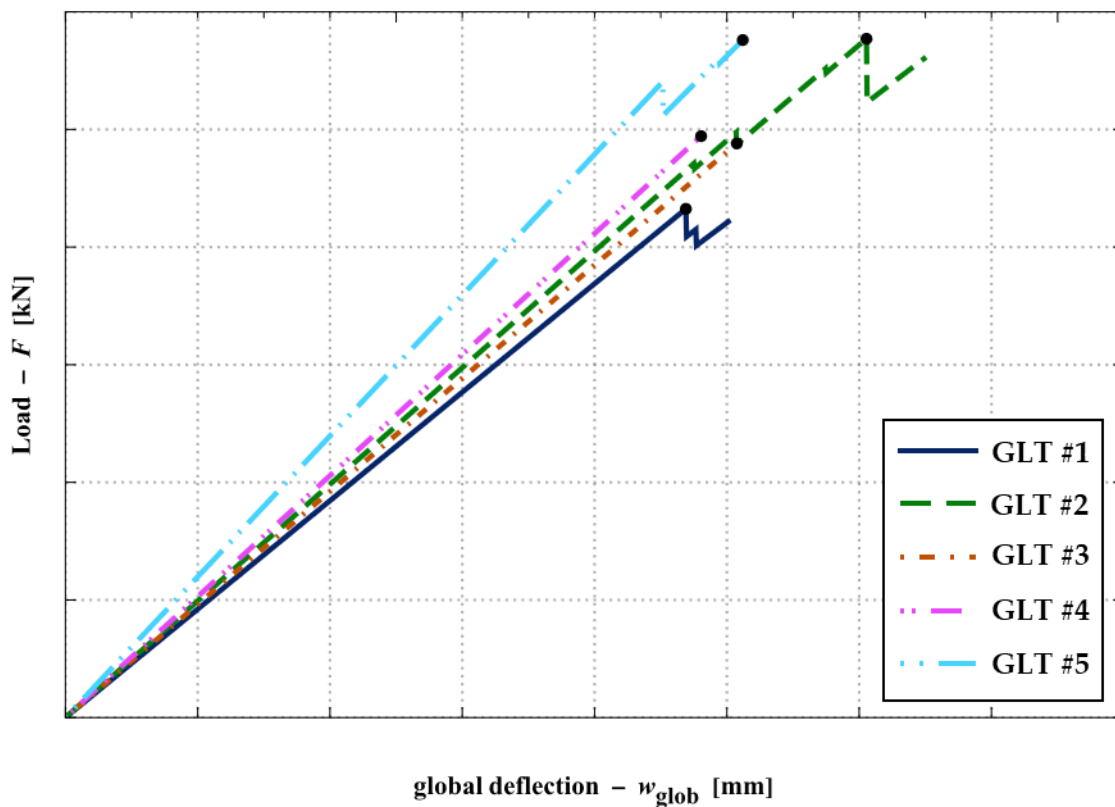


Figure 3-10: Load-deflection curves of five virtual GLT bending test on beams.

Chapter 4:

Unidirectionally Laminated Engineered Timber Products

In this Chapter the results of the stochastic-numerical beam model for unidirectionally laminated engineered timber products are presented. First, conventional GLT beams are analysed. The results are used for validation of the stochastic-numerical beam model and serve as benchmark for the influence of split lamellas in flex_GLT-CLT beams. Afterwards, the new stochastic-numerical beam model is used to advance the knowledge on resawing glulam beams. Finally, system and size effects are analysed for the newly developed flex_GLT beams.

4-1 Overview

In the following the results from virtual bending tests conducted on unidirectionally laminated engineered timber products are presented and discussed. In all cases 10^3 virtual tests were carried out for each combination of parameters. The length of the boards was fixed with $l_b = 4$ m, which is a common dimension in Austria. The finger joints were placed according to the procedure presented in [Section 2-8](#). As the strength of the boards is dependent on the board length (see [Section 2-7.1.3](#)), a fixed reference length of $l_{b,ref} = 2.0$ m was used within the presented load-bearing models. This reference length was also anchored in the former glulam standard [EN 1194 \[37\]](#). Similar to the tensile strength also the bending strength assuming a constant bending moment over the reference length $l_{b,ref} = 2.0$ m is introduced. The used input parameters as required for load-bearing models, the tensile strength of the boards $f_{t,0,b,ref}$ and finger joints $f_{t,FJ,ref}$ as well as the bending strength $f_{m,b,ref}$, are summarised in [Annex D-2](#).

4-2 Glulam

Within this Section the mechanical properties of glulam are analysed via the stochastic-numerical beam model. The results are compared and validated with investigations in the literature. [Figure 4-1](#) illustrates loading situations or use cases of glulam exposed to bending moments. At first, the main use case of glulam, where the lamellas are loaded flatwise, is investigated. Afterwards, the edgewise loading of glulam lamellas and the special use case of resawn glulam are examined. The board thickness was fixed with $t_b = 40$ mm for all glulam investigations. This board thickness corresponds to the reference thickness of European glulam beams.

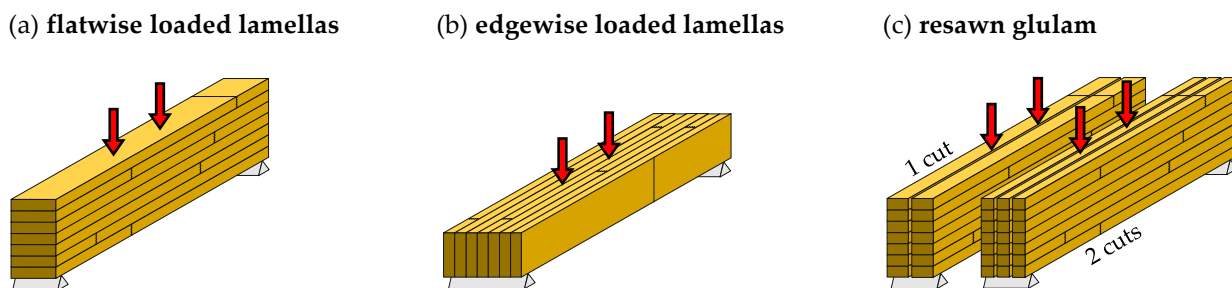


Figure 4-1: Loading situations of glulam and sub-product categories exposed to bending moments: (a) glulam with flatwise loaded lamellas, (b) glulam with edgewise loaded lamellas and (c) resawn glulam beams with one and two cuts.

4-2.1 Glulam – Flatwise Loaded Lamellas

4-2.1.1 Bending Properties of Glulam

To validate the stochastic-numerical beam model glulam beams with a width of $w_g = 150$ mm and depth of $h_g = \{280; 600; 920\}$ mm were simulated (each combination with 10^3 realizations). The results for the bending properties $\{f_{m,g}; E_{m,g}\}$ of the virtually tested beams are

summarised in **Table 4-1**. In accordance with the glulam standard **EN 14080 [16]** a reference depth $h_{g,ref} = 600$ mm was used in this analysis. The strength $f_{m,g}$ is decreasing on the mean as well as the 5 %-quantile level with increasing beam depth whereas the mean value of the modulus of elasticity $E_{m,g}$ remains constant, i.e. unaffected by the varied beam depth.

Table 4-1: Main statistics of the bending strength $f_{m,g}$ and the modulus of elasticity $E_{m,g}$ calculated from 10^3 virtually tested glulam beams (for each combination) featuring a depth of $h_g = \{280; 600; 920\}$ mm, a width of $w_g = 150$ mm and a test span of $l_{span} = 18 \cdot h_g$, built up from boards of group GI (T14) and GII (T24).

Depth h_g [mm]		GI (T14)			GII (T24)		
		280	600	920	280	600	920
$f_{m,g}$	mean [MPa]	32.0	26.5	24.5	44.9	37.1	34.3
	COV [%]	18.7	13.0	11.0	17.4	12.6	10.0
	$\chi_{05,LN}$ [MPa]	23.0	21.2	20.2	33.3	29.9	28.9
	$\chi_{05,LN}/\chi_{05,LN,ref}^1$ [-]	1.08	1.00	0.96	1.11	1.00	0.97
	$k_{ch} = (600/h_g)^{0.10}$ [16]	1.08	1.00	0.96	1.08	1.00	0.96
	k_{ch} [55]	1.09	1.00	0.93	1.09	1.00	0.93
$E_{m,g}$	mean [MPa]	10,459	10,438	10,469	12,953	12,950	12,981
	COV [%]	7.0	4.6	3.6	7.9	5.3	4.1

¹... $\chi_{05,LN,ref}$ with $h_{g,ref} = 600$ mm

²... $k_{ch} = 1.19 - 3.73 \cdot 10^{-4} \cdot h_g + 1.04 \cdot 10^{-7} \cdot h_g^2$ for $300 \leq h_g \leq 1,800$ mm

Figure 4-2 shows histograms of the bending strength of beams with a depth of $h_g = \{280; 600; 920\}$ mm together with calibrated lognormal density functions. The lognormal distribution represents the data in a satisfactory manner. This is in line with the assumption for the bending strength of glulam and timber in the probabilistic model code for timber **JCSS-3.05 [43]**.

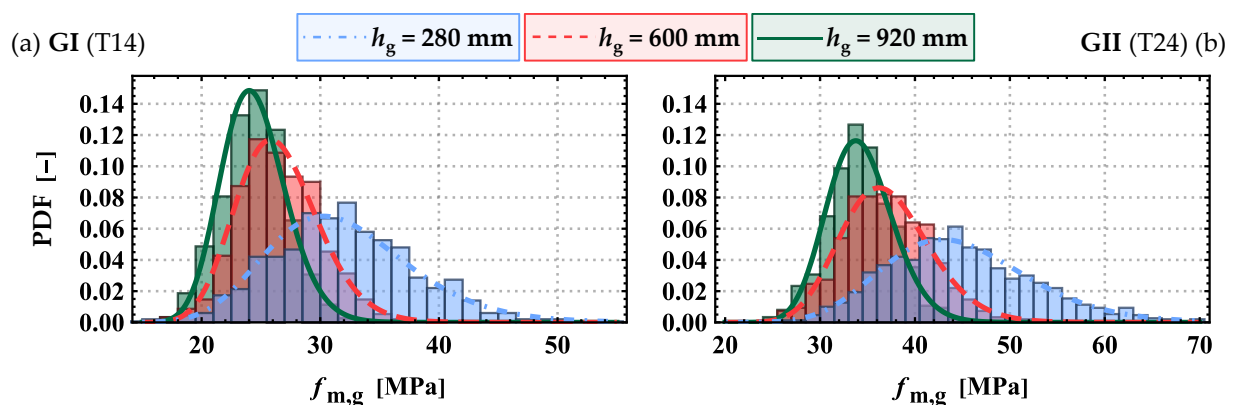


Figure 4-2: Histograms of the bending strength $f_{m,g}$ based on simulated glulam beams with a width of $w_g = 150$ mm and different depths $h_g = \{280; 600; 920\}$ mm built up from base material (a) GI (T14) and (b) GII (T24) together with calibrated lognormal density functions; 10^3 simulations for each combination.

A summary of failure types at the ultimate load are illustrated in **Figure 4-3**. The share of finger joint failures is overall larger in the glulam beams from strength class GII (T24). This is in line with investigations in **Schickhofer [56]**, where a share of $5 \div 9$ % is stated for MS10 (\approx GI)

and $24 \div 39\%$ for MS17 (\approx GII). Based on his stochastic-numerical beam model [Fink et al. \[35\]](#) found a share of finger joint failures within beams with non-shortened boards of 14% for class GL24h (\approx GI) and 26% for class GL36h (\approx GII).

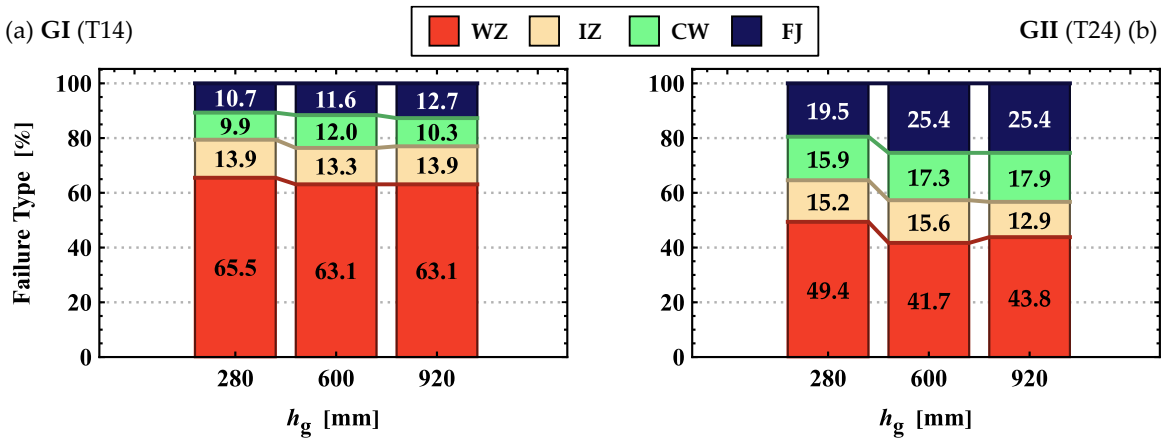


Figure 4-3: Relative share of failure types as observed in virtually tested glulam beams at ultimate load classified according to the types of board segments in {WZ—Weak zone; IZ—Intermediate knot zone; CW—Clear wood; FJ—Finger joint} at different depths $h_g = \{280; 600; 920\}$ mm built up from base material (a) GI (T14) and (b) GII (T24).

Figure 4-4 shows the ratio between the 5 %-quantile values of the bending strength at different beam depths $h_g = \{280; 600; 920\}$ mm and that at the reference beam depth $h_{g,ref} = 600$ mm vs. the beam depth. The decrease of this ratio with increasing beam depth is in good agreement with size (depth) effect models, e.g. $k_h = (h_g/600)^{0.10}$ as anchored in [EN 14080 \[16\]](#) and the model proposed in [Frese & Blaß \[55\]](#). Hereby, the power law model better fits the simulation data and is easier to use than the quadratic model from [Frese & Blaß \[55\]](#). The observed depth effect also incorporates a certain length effect as the test configuration or span in [EN 408 \[39\]](#) is regulated in dependency on the specimen depth.

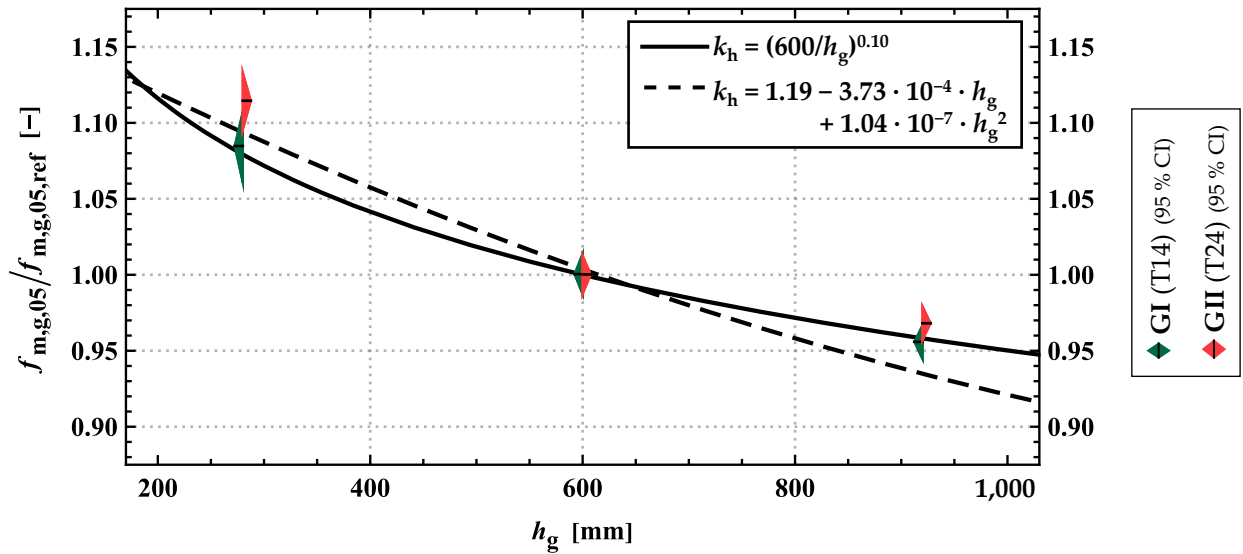


Figure 4-4: 5 %-quantile value of the bending strength of glulam at different depths $h_g = \{280; 600; 920\}$ mm built up from base material GI (T14) and GII (T24) relative to the bending strength at reference depth $h_{g,ref} = 600$ mm together with size effect models according to [EN 14080 \[16\]](#) and [Frese & Blaß \[55\]](#).

Besides the bending strength, the current European glulam product standard [EN 14080 \[16\]](#) also regulates the modulus of elasticity parallel to the grain of glulam beams. The definition is based on the properties of the board material in tension parallel to the grain with a 5 % higher mean value; see [Equation \(4.1\)](#).

$$E_{0,g,mean} = 1.05 \cdot E_{t,0,b,mean} \quad (4.1)$$

with

$E_{0,g,mean}$... mean modulus of elasticity parallel to the grain of glulam beams [MPa]

$E_{t,0,b,mean}$... mean modulus of elasticity in tension parallel to the grain of the base material [MPa]

[Figure 4-5](#) shows boxplots of the modulus of elasticity in tension of the boards and in bending of glulam beams.

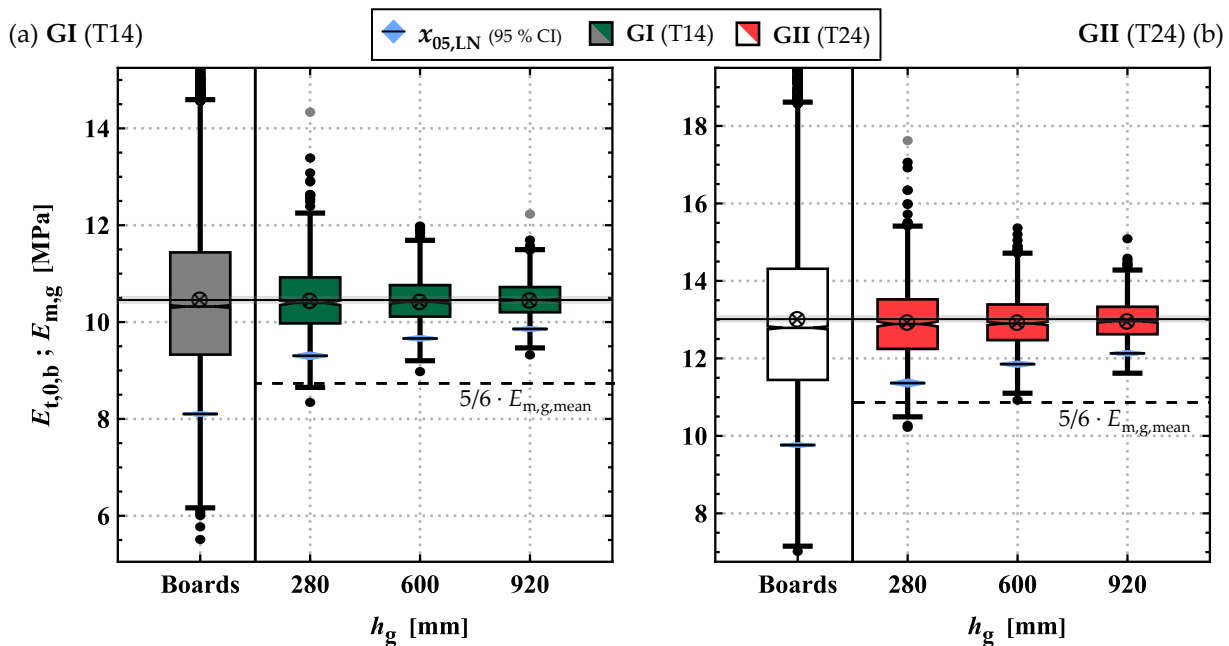


Figure 4-5: Boxplots of the modulus of elasticity in tension of boards $E_{t,0,b}$ and in bending of glulam beams $E_{m,g}$ at different beam depths $h_g = \{280; 600; 920\}$ mm built up from base material (a) GI (T14) and (b) GII (T24).

It can be clearly seen, that the 5 % higher mean value is not present in the current investigation where the mean value remains constant and independent of the beam depth. Results in [Fink \[3\]](#), [Frese \[4\]](#), [Blaß et al. \[5\]](#), [Brandner & Schickhofer \[57\]](#) give the same conclusion. On the other hand, the coefficient of variation decreases with increasing beam depth. [Fink \[3\]](#) stated similar values of $COV(E_{m,g}) = 4\%$ for beams with a depth of $h_g = 600$ mm and also observed the same tendencies regarding the beam depth. Constant mean values together with decreasing coefficients of variation lead to increasing 5 %-quantiles with increasing beam depth. [EN 14080 \[16\]](#) states a fixed value of $E_{m,g,05} = 5/6 \cdot E_{m,g,mean}$ as the 5 %-quantile, which implicitly refers to the reference cross-section of glulam featuring a depth of $h_{g,ref} = 600$ mm, a lamella thickness of $t_{b,ref} = 40$ mm and therefore 15 laminations in total. Looking at the results in [Figure 4-5](#) and to previous investigations ([\[3–5, 57\]](#)) it is obvious, that the ratio $E_{m,g,05}/E_{0,g,mean}$ depends on the number of lamellas composing the glulam beam, i.e. the more lamellas the higher the ratio, and that the ratio in all simulated beam depths and lamella qualities is higher than regulated. Nevertheless, it has to be remarked that [EN 14080 \[16\]](#) defined glulam already for ≥ 2 laminations. The 5 %-quantiles of the modulus of elasticity is used in the design of timber structures for stability verifications of timber members. As a higher stiffness is better for the stability this approximation with $E_{m,g,05} = 5/6 \cdot E_{m,g,mean}$ seems to be on the conservative side.

4-2.1.2 Load-Bearing Models for the Bending Strength of Glulam Beams

Load-bearing models are used to predict the characteristic (5 %-quantile) bending strength of glulam beams based on the tensile properties of the boards $f_{t,0,b,05}$ and that of the finger joints $f_{t,FJ,05}$. Over the last decades numerous of such models were developed. The model of the

current product standard **EN 14080 [16]** is shown in **Equation (4.4)**. The equation actually describes the characteristic value of the bending strength. However, it was derived from the 5 %-quantile of the lognormal distribution of both simulations and test results. Consequently, these values are considered equivalent within this context. A second load-bearing model proposed by **Brandner & Schickhofer [58]** is described in **Equation (4.5)**. The factor ζ describes the relationship between the tensile strength of the boards and the finger joints, for which tabulated values for a fixed coefficient of variation of the finger joints of $\text{COV}(f_{t,\text{FJ}}) = 15\%$ are provided in **Brandner & Schickhofer [58]**. The exact derivation is explained in **Brandner [12]** and described in **Equation (4.2)**. For the ease of use, an approximation of the strength relationship factor ζ is shown in **Equation (4.3)**.

$$\zeta_{05} = e^{-k_{05}\sqrt{\ln(1+\text{COV}(f_{t,0,b})^2)}} \cdot e^{k_{05}\sqrt{\ln(1+\text{COV}(f_{t,\text{FJ}})^2)}} \quad (4.2)$$

$$\zeta_{\text{new}} \approx e^{1.55 \cdot \text{COV}(f_{t,0,b}) - 1.60 \cdot \text{COV}(f_{t,\text{FJ}})} \quad (4.3)$$

with

$\text{COV}(f_{t,0,b})$... coefficient of variation of the tensile strength parallel to the grain of the boards [-]

$\text{COV}(f_{t,\text{FJ}})$... coefficient of variation of the tensile strength of the finger joints [-]

Additionally, a new model **Equation (4.6)** was derived by calibrating multiplication factors (underlined figures) to the simulation results; see **Table Annex D-16**. For the new model a similar approach as in **Brandner & Schickhofer [58]** was chosen to correctly capture the influence of the uncertainty within the base material properties, here represented by the coefficient of variation of the tensile strength, even beyond the simulated board properties.

Figure 4-6 illustrates the bending strength of all simulated glulam beams (see also **Table Annex D-16**) versus the model predictions on the level of 5 %-quantiles, which were corrected to a reference depth of $h_g = 600$ mm with a power coefficient of $k_{h,05} = 0.10$ according to **EN 14080 [16]**.

$$f_{m,g,05,EN14080} = -2.2 + 2.5 \cdot f_{t,0,b,05}^{0.75} + 1.5 \cdot (f_{t,FJ,05} - f_{t,0,b,05} + 6)^{0.65} \quad (4.4)$$

$$f_{m,g,05,Brandner} = 1.88 \cdot e^{1.14 \cdot COV(f_{t,0,b})} \cdot \text{Min} \left[f_{t,0,b,05} ; \frac{f_{t,FJ,05}}{\zeta_{Brandner}} \right]^{0.80} \quad (4.5)$$

$$\text{with } \zeta_{Brandner} \approx 0.65 + 2.15 \cdot COV(f_{t,0,b})$$

$$f_{m,g,05,new} = 1.80 \cdot e^{1.15 \cdot COV(f_{t,0,b})} \cdot \text{Min} \left[f_{t,0,b,05} ; \frac{f_{t,FJ,05}}{\zeta_{new}} \right]^{0.80} \quad (4.6)$$

$$\text{with } \zeta_{new} = e^{1.55 \cdot COV(f_{t,0,b}) - 1.60 \cdot COV(f_{t,FJ})}$$

with

$f_{m,g,05}$ characteristic (5 %-quantile) bending strength of glulam beams at
 $h_g = h_{g,ref} = 600 \text{ mm}$ [MPa]

$f_{t,0,b,05}$ characteristic (5 %-quantile) tensile strength of boards at a length of $l_{ref} = 2.0 \text{ m}$ [MPa]

$f_{t,FJ,05}$ characteristic (5 %-quantile) tensile strength of the finger joints [MPa]

$COV(f_{t,0,b})$.. coefficient of variation of the tensile strength parallel to the grain of the boards [-]

$COV(f_{t,FJ})$... coefficient of variation of the tensile strength of the finger joints [-]

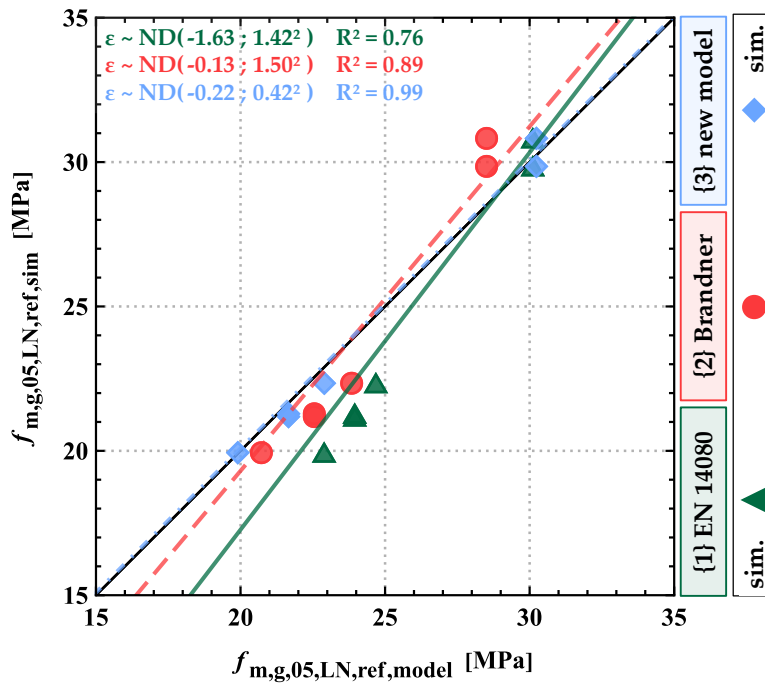


Figure 4-6: Results of simulated bending test (5 %-quantiles) of glulam beams adjusted to $h_{g,ref} = 600 \text{ mm}$ vs. model predictions of {1} EN 14080 [16], {2} Brandner & Schickhofer [58] and {3} the new model in Equation (4.6).

The model {2} Brandner & Schickhofer [58] slightly overestimates the characteristic bending strength for glulam beams of lower strength class whereas the strength of glulam beams of higher strength class are slightly underestimated. Based on the data presented in Section 2-8.1, the coefficient of variation of the finger joint strength is above the assumed 15 % in the model, which may be one reason for the deviations of the model. The model {1} EN 14080 [16] overestimates the characteristic bending strength significantly at lower strength classes. The

model is partially based on results presented in **Blaß et al. [5]**, **Frese & Blaß [55]**, where a clear distinction between visually and machine graded timber was made. Model {1} assumes boards with a higher coefficient of variation of the tensile strength parallel to the grain $COV(f_{t,0,b}) \approx 40\%$ for lower strength classes. Therefore, the lower coefficient of variation $COV(f_{t,0,b}) \approx 30\%$ within the current investigations explains the deviations of the model. The overall mean residue of the model prediction, also known as bias, is $\varepsilon_{\text{mean}} = -1.63$ MPa combined with a coefficient of determination of $R^2 = 0.76$. The other two models consider the coefficient of variation of the used boards of $COV(f_{t,0,b}) \approx 30\%$ and therefore are capable of correctly depicting the simulation data. This is also visible within the mean residue close to $\varepsilon_{\text{mean}} \approx 0$ MPa, i.e. roughly no bias, and the higher coefficient of determination R^2 . The new model is based on the model {2} and is slightly adapted to better represent the simulation data.

4-2.2 Glulam – Edgewise Loaded Lamellas

Apart from the major load case of glulam beams with flatwise loaded lamellas, glulam beams might also be loaded perpendicular in bending, i.e. with lamellas loaded edgewise. Typical examples are glulam beams exposed to bending stresses in primary and secondary direction as well as glulam beams used as floor elements or as bridge deck, just to name a few. **Table 4-2** summarises the results of virtual bending tests on glulam beams with edgewise loaded lamellas ($w_b = 150$ mm) with a depth of $h_g = 150$ mm at different widths $w_g = \{40; 80; 120; 280; 600\}$ mm, which corresponds to $n_{\text{par}} = \{1; 2; 3; 7; 15\}$ sub-parallel acting lamellas with $h_b = 40$ mm, for groups GI (T14) and GII (T24). Hereby, for the simulation with $n_{\text{par}} = 1$ also finger joints are present, which is the reason for the deviating values compared to **Table 2-25**.

Table 4-2: Main statistics of the bending strength $f_{m,g}$ and modulus of elasticity $E_{m,g}$ calculated from 10^3 virtually tested beams (for each combination) featuring a width of $w_g = \{40; 80; 120; 280; 600\}$ mm, a depth of $h_g = 150$ mm and a test span of $l_{\text{span}} = 18 \cdot h_g$, built up from boards of group GI (T14) and GII (T24).

Width w_g [mm]		GI (T14)					GII (T24)				
		40	80	120	280	600	40	80	120	280	600
# lamellas n_{par} [-]		1	2	3	7	15	1	2	3	7	15
$f_{m,g}$	mean [MPa]	33.4	31.5	31.6	30.2	29.1	48.6	45.1	44.8	42.3	40.9
	COV [%]	30.5	21.4	18.2	13.4	9.3	26.7	20.5	17.5	12.3	9.1
	$\chi_{05,LN}$ [MPa]	18.8	21.5	22.8	23.9	24.8	30.2	31.8	33.1	34.4	35.0
	$k_{\text{sys},05} = \chi_{05,LN}/\chi_{05,LN,\text{ref}}^1$ [-]	1.00	1.14	1.21	1.27	1.32	1.00	1.05	1.09	1.14	1.16
$E_{m,g}$	mean [GPa]	10.4	10.4	10.6	10.5	10.5	12.9	12.9	13.0	13.0	13.0
	COV [%]	14.8	10.2	8.4	5.6	3.8	17.0	12.1	9.9	6.3	4.5
	$\chi_{05,LN}$ [GPa]	8.1	8.8	9.2	9.6	9.8	9.7	10.6	11.0	11.7	12.0

¹... $\chi_{05,LN,\text{ref}}$ with $w_{g,\text{ref}} = 40$ mm

The mean value slightly decreases with increasing number of parallel acting lamellas n_{par} . The coefficient of variation is decreasing significantly and therefore the 5 %-quantile values of the bending strength are increasing with increasing n_{par} . This increase in bending strength is more distinctive for the lower strength class. These tendencies are a combination of two effects:

One, with a larger number of lamellas the probability of knots and finger joints in the bending tension zone increases, which lowers the bending strength. Second, with a higher number of boards acting parallel, the influence of knots within a single board decreases. A further analysis of the bending strength via the system factor is presented later in **Figure 4-8**.

Figure 4-7 shows the summary of failure types at the ultimate load in dependence on the number of parallel acting lamellas. The share of finger joint failures stays at an almost constant level, whereas the share of failures within clear wood section jumps with $n_{\text{par}} = 2$. Both observations reflect the possibility to share loads from a weak section or finger joint to a neighbouring defect free board section.

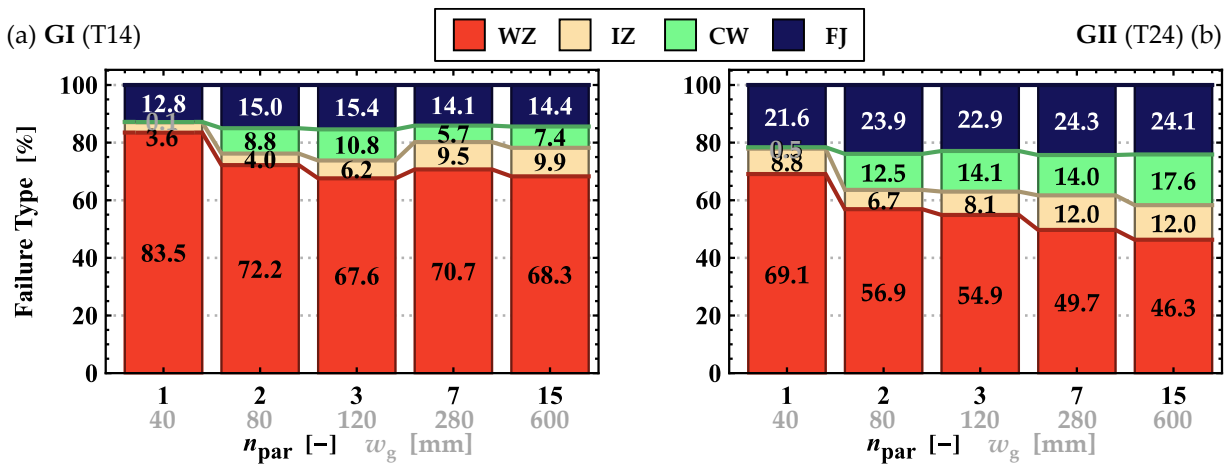


Figure 4-7: Relative share of failure types of beams at ultimate load classified according to the types of board segments in {WZ—Weak zone; IZ—Intermediate knot zone; CW—Clear wood; FJ—Finger joint} for glulam at different widths $w_g = \{40; 80; 120; 280; 600\}$ mm and depth $h_g = 150$ mm built up from base material (a) GI (T14) and (b) GII (T24).

With increasing number of parallel acting lamellas more and more system effects are activated, which leads to increasing 5 %-quantile values of the bending strength. Such system effects are, for example, considered as system factors k_{sys} in **ON EN 1995-1-1 [59]**. Herein, k_{sys} is regulated as bi-linear function with $k_{\text{sys}} = 1.00$ for $n_{\text{par}} = 1$ steadily increasing until $n_{\text{par}} = 8$ and $k_{\text{sys}} = 1.20$ for $n_{\text{par}} \geq 8$. The Australian standard **AS 1720.1 [60]** regulates the system effect via a non-linear function and allows an up to 33 % higher bending strength for $n \geq 10$. Compared to the simulation results in **Figure 4-8** the model in **AS 1720.1 [60]** represents the upper limit regarding the system effects. The model in **ON EN 1995-1-1 [59]** is suitable as a lower bound limit for GI (T14), but overestimates the system effect observed for the higher strength class GII (T24). **Brandner & Schickhofer [61]** analysed test results of edgewise loaded glulam beams with different number of parallel acting lamellas $n_{\text{par}} = \{1; 2; 4; 8\}$ and stated a system factor of up to $k_{\text{sys}} = \{1.12; 1.33; 1.51\}$ for $n_{\text{par}} = \{2; 4; 8\}$, respectively. The corresponding reference series with $n_{\text{par}} = 1$ featured a similar 5 %-quantile value of the bending strength with $f_{m,b,05} = 20.8$ MPa and coefficient of variation $\text{COV}(f_{m,b}) = 36.7$ % as GI (T14).

The results indicate, that the system factor is dependent on the properties of the base material, that of boards and finger joints, i.e. it is higher for wood products composed of base material of lower strength class and/or higher variation. This can be argued by the circumstance that the difference between weak zones and clear wood zones in neighboring lamellas is usually higher in lower strength classes than in boards classified to higher strength classes. Therefore, the benefit of the parallel acting member is lower and theoretically would be zero in an ideal homogeneous material. This circumstance is expressed by the model in **Equation (4.7)**. This model with three regression coefficients approaches asymptotically the value of $k_{\text{sys,max}}$ so that regulations for limiting the maximum number of parallel acting members can be omitted. **Equation (4.7)**, as shown in **Figure 4-8**, is capable of depicting the system effect for both strength classes in a satisfactory manner. The value $k_{\text{sys,max}}$ is fitted to the here simulated data. How differently sorted boards or other ratios between board and finger joint strength influence $k_{\text{sys,max}}$ cannot be extrapolated from the simulations.

$$k_{\text{sys},05,\text{new}} = 1 + k_{\text{sys},\text{max}} \cdot \left(\frac{n_{\text{par}} - 1}{n_{\text{par}}} \right) \tag{4.7}$$

$$k_{\text{sys},\text{max}} = 0.22 \cdot \left(\frac{f_{\text{m,b},05,n=1}}{24} \right)^{-1.55}$$

with

- $k_{\text{sys},05,\text{new}}$ system factor of the bending strength of glulam with edgewise loaded lamellas [-]
- $f_{\text{m,b},05,n=1}$ characteristic (5 %-quantile) edgewise bending strength of a single lamella [MPa]
- $k_{\text{sys},\text{max}}$ maximal achievable system factor [-]
- n_{par} number of parallel acting boards / lamellas [-]

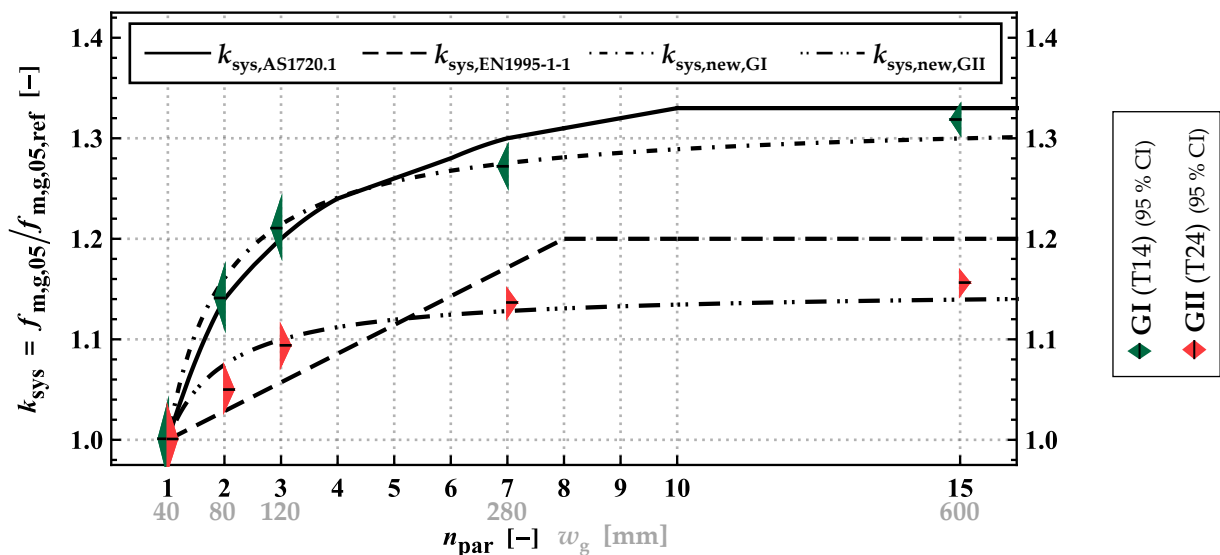


Figure 4-8: System effect k_{sys} as ratio between strength of glulam beams with a width of $w_b = 150$ mm loaded edgewise and number of layers relative to $n_{\text{par}} = 1$, built up from base material GI (T14) and GII (T24), together with system effect models from **AS 1720.1** [60], **ON EN 1995-1-1** [59] and an own model acc. to **Equation (4.7)**.

Figure 4-9 shows boxplots of the modulus of elasticity in tension parallel to the grain of boards and of edgewise in bending loaded glulam beams. The mean values remain almost constant, so the 5 % higher values for glulam as regulated in EN 14080 [16] cannot be confirmed. Similar to the bending strength also the 5 %-quantile of the modulus of elasticity is increasing with increasing number of parallel acting lamellas n_{par} . This effect is governed by the decreasing coefficient of variation with increasing n_{par} ; see Figure 4-10. The results are in an almost perfect agreement with the theoretical background for parallel system effects, where the COV is decreasing with $(n_{par})^{-0.50}$. Already at $n_{par} \geq 2$ the ratio $E_{m,g,05} / E_{m,g,mean}$ is higher than 5/6 as stated for glulam in general in EN 14080 [16]. As already mentioned before the 5 %-quantile of the modulus of elasticity is essential for the verification of the stability of timber members, i.e. buckling along the minor cross-section axis or lateral torsional buckling. Consequently, the stability of timber members with this approximation seems to be on the conservative side.

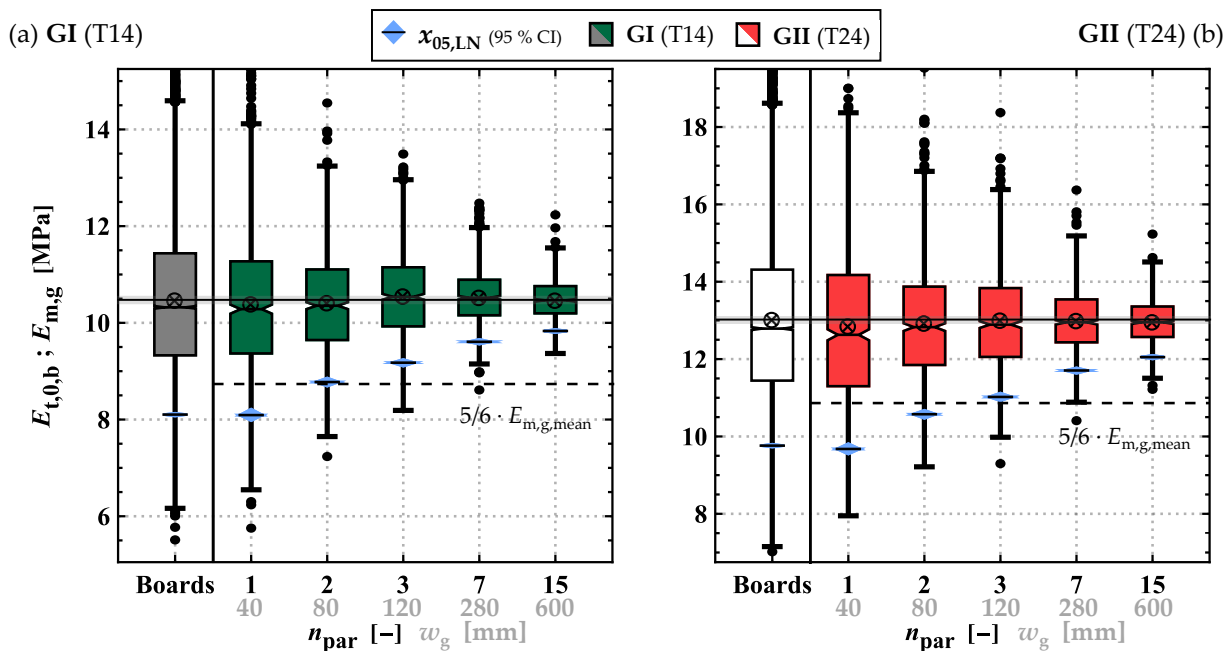


Figure 4-9: Boxplots of the modulus of elasticity in tension of the boards $E_{t,0,b}$ and in bending of glulam beams with edgewise loaded lamellas $E_{m,g}$ with a depth of $h_g = 150$ mm and different widths $w_g = \{40; 80; 120; 280; 600\}$ mm built up from base material (a) GI (T14) and (b) GII (T24).

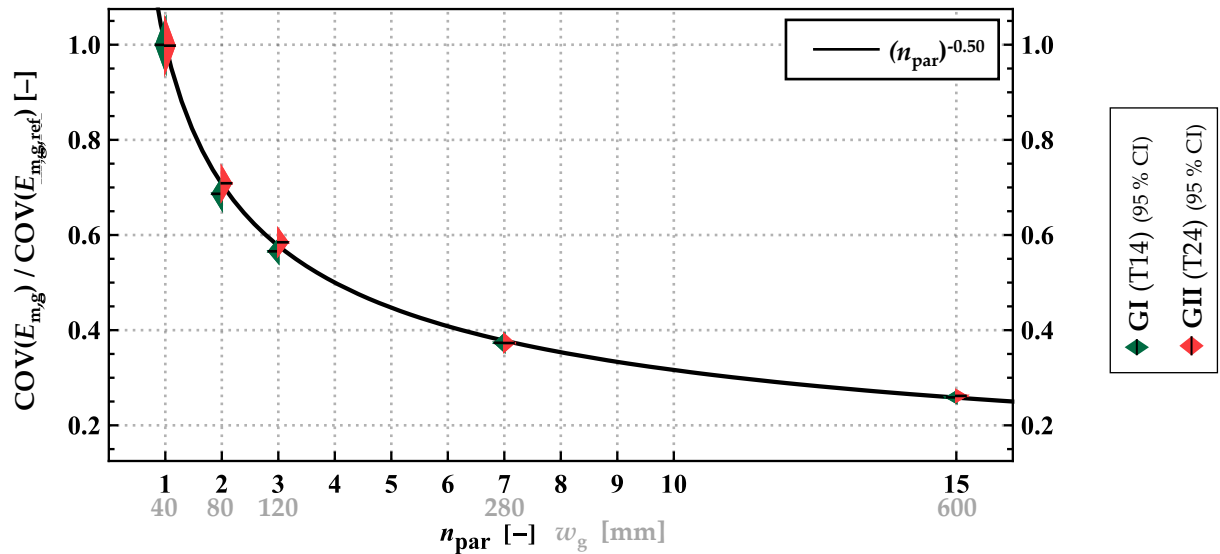


Figure 4-10: Relative coefficient of variation of the modulus of elasticity of glulam beams with a width of $w_b = 150$ mm loaded edgewise and number of layers relative to $n_{par} = 1$; built up from base material GI (T14) and GII (T24); together with function of a perfect parallel system effect.

4-2.3 Glulam – Flatwise vs. Edgewise Loaded Lamellas

The bending strength of glulam refers to beams of a specific depth h_g and the corresponding test length of $l_{span} = 18 \cdot h_g$ usually associated with a constant moment over the central third part of the beam ($6 \cdot h_g$) acc. to **EN 408 [39]**. This regulation leads to discrepancies between the bending properties of edgewise and flatwise loaded glulam beams, i.e., whereas a change in depth by constant width in case of glulam beams with flatwise loaded lamellas is associated with a combined depth and length effect, after the beams are rotated by 90° so that the lamellas are now loaded edgewise the bending properties are only affected by a width effect, i.e. a parallel system effect. In the current standard of glulam **EN 14080 [16]** no differentiation is made between the bending strength of glulam beams loaded flatwise $f_{m,g,05,flat}$ or edgewise $f_{m,g,05,edge}$ (see **Figure 4-11**) and the strength for both cases is determined via h_g . Whereas for example the properties of laminated veneer lumber (LVL) or glulam made out of hardwood are separately defined for these loading cases; see **EN 14374 [62]**, **EAD 130320-00-0304 [63]**.

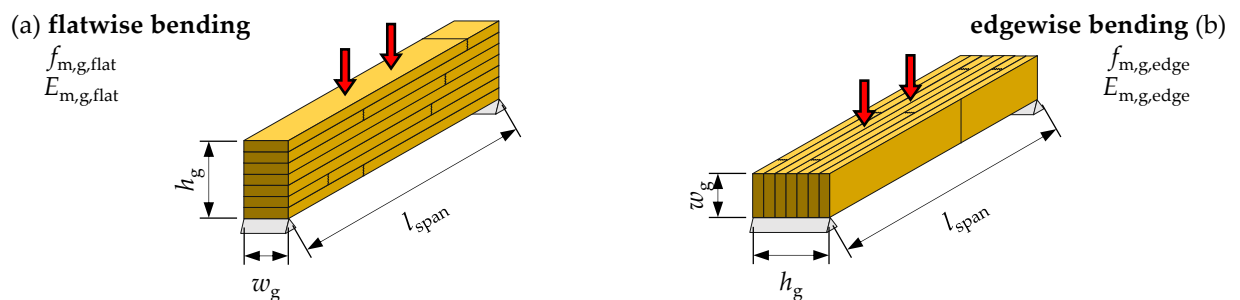


Figure 4-11: Glulam beam in bending with (a) flatwise and (b) edgewise loaded lamellas.

To analyse whether these regulations are applicable, bending tests with edgewise loaded lamellas were simulated on glulam beams featuring the same test span of $l_{span} = 18 \cdot h_g$, with $h_g = \{280; 600\}$ mm, as the beams with lamellas loaded flatwise. The results of these simulations are illustrated in **Figure 4-12**. The bending strength edgewise at the 5 %-quantile level is about the same for the beam dimension 150×280 mm² and about 10 % higher for dimensions of 150×600 mm² compared to the same beam geometry in flatwise bending. For the 5 %-quantile values of the modulus of elasticity, the observed difference of ~4 % is neglectable. Based on these results it seems to be safe to use the flatwise properties also for edgewise loading situations for glulam of both groups GI (T14) and GII (T24). This additionally supports the ease of use for engineers but neglects part of the mechanical potential.

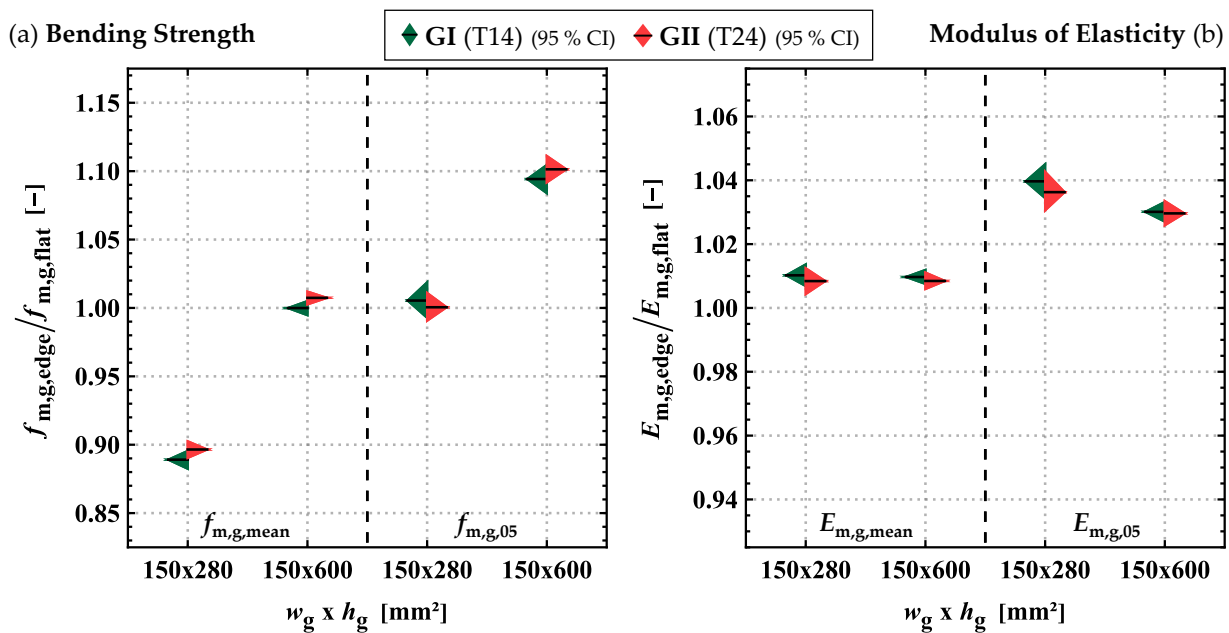


Figure 4-12: Properties of glulam beams with lamellas loaded edgewise relative to the properties of beams with flatwise loaded lamellas considering the same test span of $l_{span} = 18 \cdot h_g$, with depth $h_g = \{280; 600\}$ mm and both groups GI (T14) and GII (T24) for (a) the bending strength $f_{m,g}$ and (b) for the modulus of elasticity $E_{m,g}$.

4-2.4 Resawn Glulam

4-2.4.1 Glulam in Split Condition

Through the lengthwise splitting of boards their tensile properties change. This is also true for the bending properties of resawn glulam beams. To analyse the influence of splitting glulam beams, virtual bending tests were carried out on unsplit and resawn glulam beams. The results of the bending strength $f_{m,g}$ are summarised in **Table 4-3**. The relative bending strength of resawn glulam is, apart from the strength class of the base material, also dependent on the beam width and depth. This influence is of relatively minor significance compared to the influence of the number of cuts, i.e. the separation ratio η_s . The 5 %-quantile and mean values of the bending strength of the beams also vary with the beam width w_g . These are consequences from the different testing lengths of boards in tension parallel to the grain, as anchored in **EN 408 [39]** and already discussed in **Section 2-7.1.3**.

Table 4-3: Main statistics of the bending strength $f_{m,g}$ from 10^3 virtually tested glulam beams (for each combination) featuring a width of $w_g = \{100; 150; 200\}$ mm and a depth of $h_g = \{280; 600\}$ mm, built up from boards of group GI (T14) and GII (T24).

Full Dim. $w_g \times h_g$ [mm ²]		GI (T14)				GII (T24)	
		100x280	150x280	200x280	150x600	150x280	150x600
$f_{m,g,mean}$ [MPa]	Full	30.4	32.0	33.3	26.5	44.9	37.1
	1-Cut	29.4 (0.97) ¹	30.5 (0.95) ¹	31.5 (0.95) ¹	24.9 (0.94) ¹	43.8 (0.97) ¹	36.2 (0.98) ¹
	2-Cuts	–	29.3 (0.91) ¹	30.1 (0.90) ¹	23.3 (0.88) ¹	41.8 (0.93) ¹	34.5 (0.93) ¹
COV($f_{m,g}$) [%]	Full	19.5	18.7	18.5	13.0	17.4	12.6
	1-Cut	22.1 (1.13) ¹	20.9 (1.12) ¹	19.8 (1.07) ¹	14.2 (1.09) ¹	18.3 (1.05) ¹	13.1 (1.04) ¹
	2-Cuts	–	24.1 (1.29) ¹	22.4 (1.21) ¹	15.2 (1.17) ¹	21.3 (1.22) ¹	13.5 (1.07) ¹
$f_{m,g,05}$ [MPa]	Full	21.5	23.0	24.1	21.2	33.3	29.9
	1-Cut	19.5 (0.91) ¹	20.9 (0.91) ¹	22.1 (0.92) ¹	19.5 (0.92) ¹	32.0 (0.96) ¹	28.9 (0.97) ¹
	2-Cuts	–	18.5 (0.80) ¹	20.2 (0.84) ¹	17.8 (0.84) ¹	28.9 (0.87) ¹	27.4 (0.92) ¹

¹.....relative to the properties at full cross-section, i.e., to the properties of glulam beams before splitting

The influence of resawing glulam beams on the main statistics of the bending strength relative to that of glulam beams with full cross-section ($\eta_s = 1$) is shown in **Figure 4-13**. With an increasing number of cuts, the mean and 5 %-quantile values relative to the statistics at full cross-section are decreasing and the coefficient of variation is increasing. These effects are more distinctive for glulam beams of lower strength class. One reason for this is seen in the higher coefficient of variation in the physical properties of the boards, in particular in their tensile strength parallel to the grain, and another the higher share of knots.

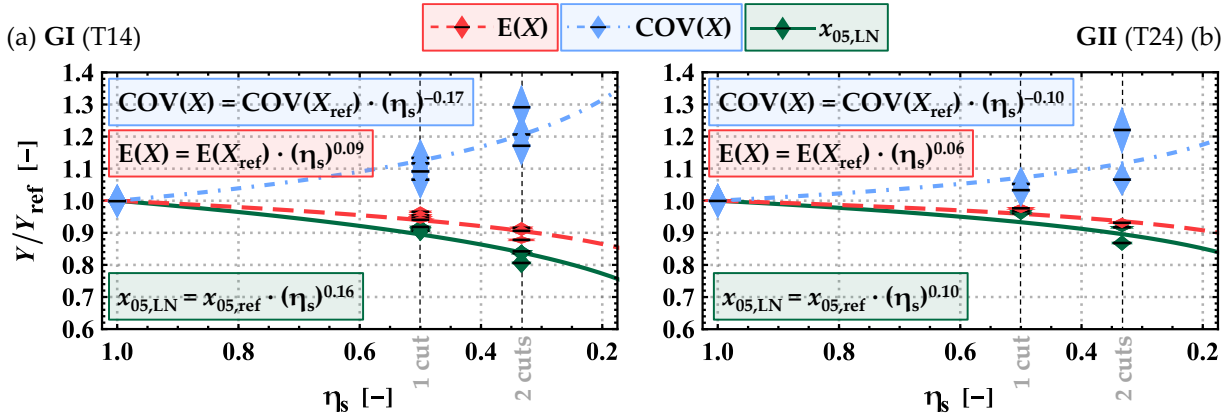


Figure 4-13: Influence of lengthwise splitting on the main statistics $Y = \{E(X); COV(X); x_{05,LN}\}$ of the bending strength ($X = f_{m,g}$) of resawn glulam beams relative to the statistics of the bending strength of glulam beams with full cross-section; analysis based on virtually tested glulam beams built up from boards of (a) GI (T14) and (b) GII (T24).

The results of the modulus of elasticity $E_{m,g}$ are summarised in **Table 4-4** and the relative changes are illustrated in **Figure 4-14**. With the number of cuts the coefficient of variation is increasing and the 5 %-quantile values are slightly decreasing. The mean modulus of elasticity remains almost constant.

Table 4-4: Main statistics of the modulus of elasticity $E_{m,g}$ from 10^3 virtually tested glulam beams (for each combination) featuring a width of $w_g = \{100; 150; 200\}$ mm and a depth of $h_g = \{280; 600\}$ mm, built up from boards of group GI (T14) and GII (T24).

Full Dim. $w_g \times h_g$ [mm ²]		GI (T14)				GII (T24)	
		100x280	150x280	200x280	150x600	150x280	150x600
$E_{m,g,mean}$ [GPa]	Full	10.4	10.5	10.5	10.4	13.0	12.9
	1-Cut	10.4 (1.00) ¹	10.4 (0.99) ¹	10.5 (1.00) ¹	10.5 (1.01) ¹	13.0 (1.00) ¹	13.1 (1.01) ¹
	2-Cuts	–	10.5 (1.00) ¹	10.5 (1.00) ¹	10.6 (1.02) ¹	13.0 (1.00) ¹	13.1 (1.01) ¹
COV($E_{m,g}$) [%]	Full	7.4	7.0	7.3	4.6	7.9	5.3
	1-Cut	8.2 (1.10) ¹	7.9 (1.13) ¹	7.9 (1.08) ¹	5.3 (1.14) ¹	9.5 (1.20) ¹	6.1 (1.14) ¹
	2-Cuts	–	8.7 (1.25) ¹	8.9 (1.22) ¹	5.8 (1.26) ¹	10.1 (1.28) ¹	6.5 (1.23) ¹
$E_{m,g,05}$ [GPa]	Full	9.2	9.3	9.3	9.7	11.4	11.9
	1-Cut	9.1 (0.99) ¹	9.1 (0.98) ¹	9.2 (0.99) ¹	9.6 (0.99) ¹	11.1 (0.97) ¹	11.8 (0.99) ¹
	2-Cuts	–	9.1 (0.98) ¹	9.1 (0.98) ¹	9.6 (0.99) ¹	11.0 (0.96) ¹	11.7 (0.98) ¹

¹relative to the properties at full cross-section, i.e., to the properties of glulam beams before splitting

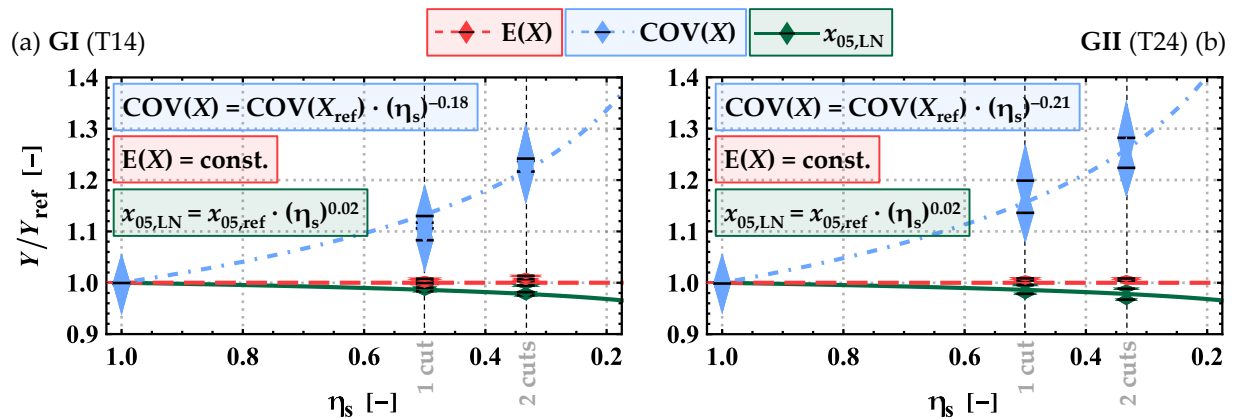


Figure 4-14: Influence of lengthwise splitting on the main statistics $Y = \{E(X); COV(X); x_{05,LN}\}$ of the modulus of elasticity in bending ($X = E_{m,g}$) of resawn glulam beams relative to the statistics of the modulus of elasticity in bending of glulam beams with full cross-section; analysis based on virtually tested glulam beams built up from boards of (a) GI (T14) and (b) GII (T24).

Beside the changes in mechanical properties, also the failure mechanism of glulam and resawn glulam were analysed. **Figure 4-15** shows the average relative shares of failure types as recorded at ultimate load of glulam and resawn glulam beams with one and two cuts. As already mentioned, the share of failures in finger joints is higher for GII (T24) than for the lower strength class GI (T14). The lengthwise splitting of the lamellas should have no effect on the strength of the finger joints, as they are already placed in a clear wood sections of the boards. Thus, the share of finger joint failures should be lower for resawn glulam. This is also visible in the results of the simulations. The share of finger joint failures for beams from GI (T14) is reducing from 11.0 % (full) to 9.4 % for one cut and to 6.9 % for two cuts and for GII (T24) from 22.5 % (full) to 17.8 % and 13.1 % for one and two cuts, respectively.

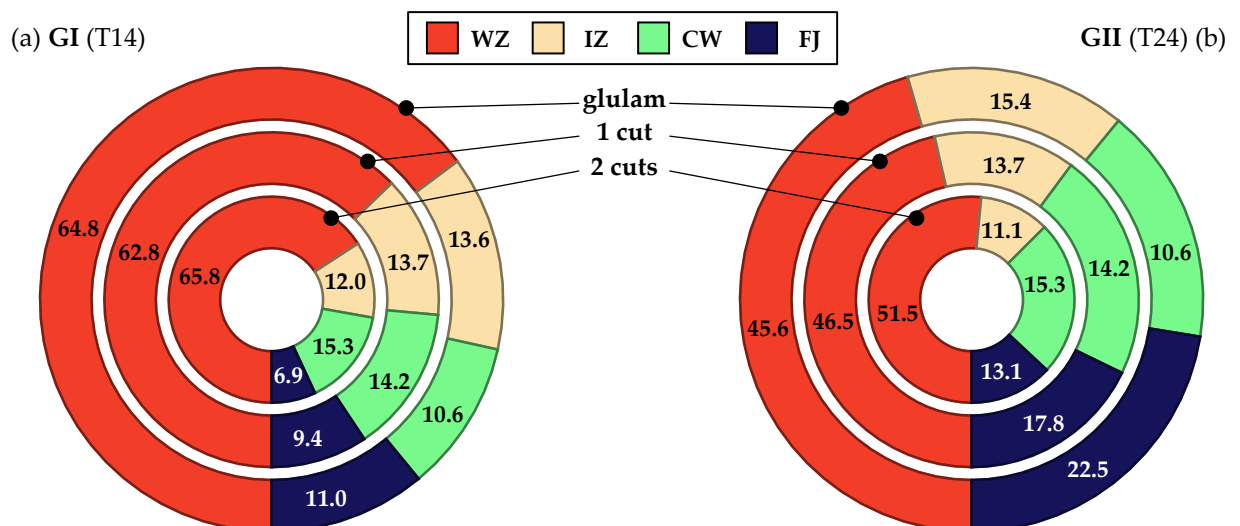


Figure 4-15: Mean relative shares of failure types of beams at ultimate load classified according to the types of board segments in {WZ—Weak zone; IZ—Intermediate knot zone; CW—Clear wood; FJ—Finger joint} for glulam and resawn glulam with one and two cuts built up from base material (a) GI (T14) and (b) GII (T24).

4-2.4.2 Comparison with Previous Investigations

Regarding resawn glulam beams only a few experimental investigations are known to the author. **Figure 4-16** summarises the results from various investigations (**Kastner et al. [15]**, **Viguiet et al. [42]**, **Crocetti [64]**, **Cleason [65]**) and compares them to the model predictions from **Section 4-2.4.1**. These investigations are mostly limited to a small number of specimen ($n \leq 20$; apart from [15]) and number of cuts, which leads to rather large uncertainties within the test data. These uncertainties may be one reason for the partially inconclusive results.

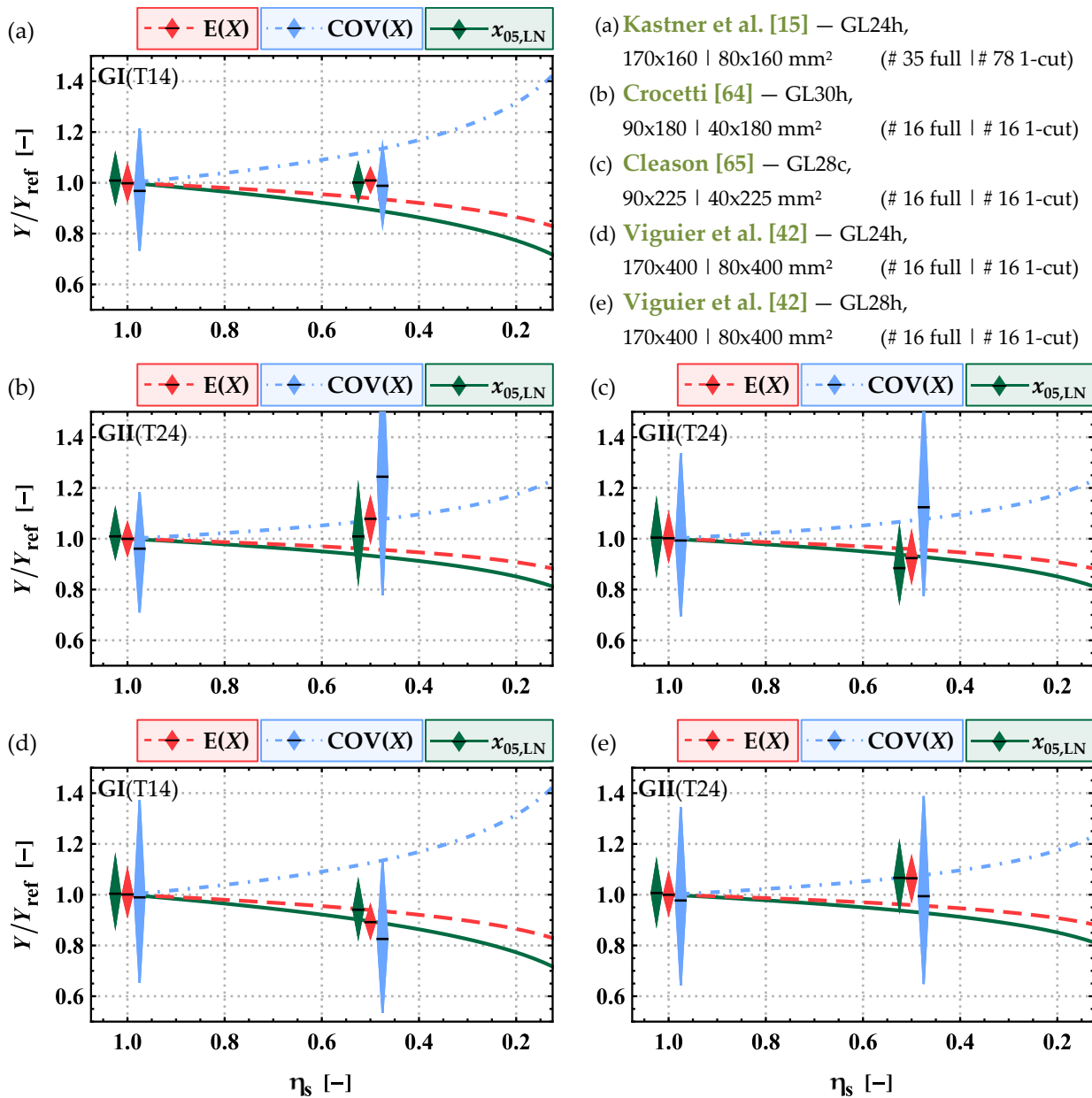


Figure 4-16: Main statistics $Y = \{E(X); COV(X); x_{05,LN}\}$ of the bending strength from split glulam beams relative to unsplit glulam beams ($X = f_{m,g}$) based on model predictions (dashed lines; GI or GII) and from test results taken from the literature together with 95 % CI assuming $X \sim LN$.

The comparison in **Figure 4-16** is made based on relative values with reference to unsplit glulam beams. The main model results, decreasing mean and 5 %-quantile values as well as an increasing coefficient of variation with increasing number of cuts, can be also found within the majority of the experimental investigations. Even though, the model only considers two strength classes GI (T14) and GII (T24). However, results from **Kastner et al. [15]** and that of GL28h in **Viguiet et al. [42]** conclude no influence of the resawing on the bending strength at all. Experimental investigations on resawn glulam with two cuts ($\eta_s = 1/3$) are not known to the authors. Nevertheless, there are regulations for resawn glulam beams with two cuts in the current glulam product standard **EN 14080 [16]**.

4-2.4.3 Load-Bearing Models for the Bending Strength of Resawn Glulam Beams

Models Based on the Tensile Strength of the Boards

One possible model approach for estimating the bending strength of resawn glulam is to use the load-bearing model for conventional glulam but with adapted tensile properties to account for the lengthwise splitting of boards. Hereby, the formulas for the tensile strength of lengthwise split boards from **Section 2-7.2.1; Figure 2-42** were used. **Figure 4-17 (a)** shows the results of the simulated glulam and resawn glulam beams from **Table 4-3** versus the model predictions of {1} **EN 14080 [16]**, {2} **Brandner [58]** and {3} the new model in **Equation (4.6)**.

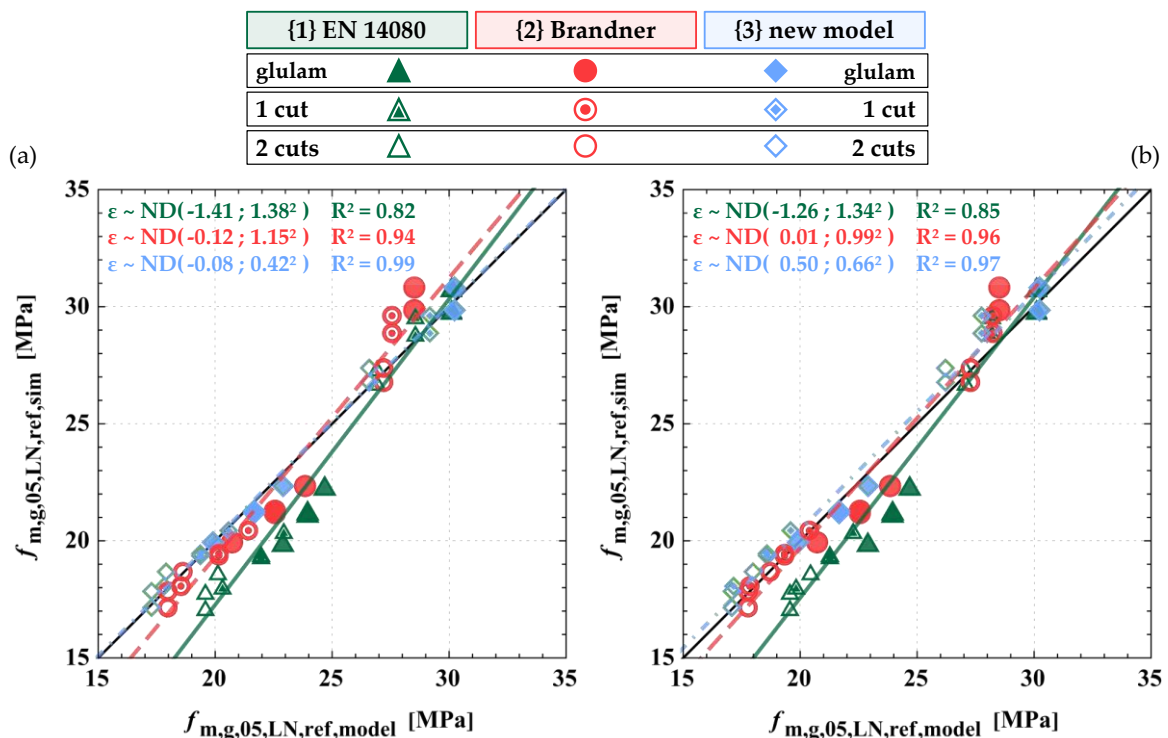


Figure 4-17: Results of simulated bending tests (5 %-quantiles) of glulam and resawn glulam beams with one and two cuts adjusted to $h_{g,ref} = 600$ mm vs. predictions of model {1} **EN 14080 [16]**, {2} **Brandner [58]** and {3} the new model acc. to **Equation (4.6)** based on (a) the simulation data for the tensile properties of unsplit and split boards and (b) the simulation data for unsplit boards and approximated tensile properties via functions in **Section 2-7.2.1** for the split boards.

The simulation results are corrected to a reference depth of $h_{g,ref} = 600$ mm according to **EN 14080 [16]**. The model {1} significantly overestimates the bending strength of resawn glulam beams built up from the lower strength class GI (T14). The overall mean residue of the model prediction is $\varepsilon_{mean} = -1.41$ MPa combined with a coefficient of determination of $R^2 = 0.82$. By contrast, models {2} and {3} give overall good approximations of the bending strength of resawn glulam ($\varepsilon_{mean} \approx 0$ MPa; $R^2 > 0.90$). Apart from these general observations, one major disadvantage of this approach is that the tensile properties of lengthwise split boards have to be known. These tensile properties are usually not available, so unknown. The models presented in **Section 2-7.2.1** allow to estimate the properties of lengthwise split boards on the basis of the unsplit boards at least for the two analysed board strength classes, GI (T14) and GII (T24). The results are illustrated in **Figure 4-17 (b)**. The model predictions are slightly lower than according to the first approach. The models {2} and {3} are still superior compared to the currently anchored model {1} **EN 14080 [16]**.

Models Based on the Bending Strength of Glulam Beams and the Tensile Strength of the Boards

Another possibility to characterise the bending properties of resawn glulam beams is via the properties of the unsplit glulam beams and the unsplit boards. This approach is currently anchored in **EN 14080 [16]**; see **Equation (4.8)**. An adapted version of this model calibrated to the simulation results is shown in **Equation (4.9)**.

$$f_{m,s,05,EN14080} = f_{m,g,05} - \frac{96}{f_{t,0,b,05} - 6} + \begin{cases} 4 & \text{for 1 cut} \\ 0 & \text{for 2 cuts} \end{cases} \quad (4.8)$$

$$f_{m,s,05,new} = f_{m,g,05} - \frac{40}{f_{t,0,b,05} + 6} - \begin{cases} 1 & \text{for 1 cut} \\ 3 & \text{for 2 cuts} \end{cases} \quad (4.9)$$

with

- $f_{m,s,05}$ characteristic (5 %-quantile) bending strength of resawn glulam [MPa]
- $f_{m,g,05}$ characteristic (5 %-quantile) bending strength of glulam before splitting [MPa]
- $f_{t,0,b,05}$ characteristic (5 %-quantile) tensile strength parallel to the grain of boards before splitting [MPa]

The results of the simulated bending tests on resawn glulam versus the predictions from models in **Equation (4.8)** and **(4.9)** are illustrated in **Figure 4-18**. The model {1} from **EN 14080 [16]** was originally derived from tests on resawn glulam beams of higher strength classes (see [64, 65]) and is restricted to glulam beams built up from boards with a tensile strength of at least $f_{t,0,k} = 18$ MPa. If the model {1} is applied to resawn glulam beams of lower strength class the characteristic (5 %-quantile) bending strength gets significantly underestimated. The overall mean residue of the model prediction is $\varepsilon_{mean} = 4.72$ MPa combined with a coefficient of determination of $R^2 = 0.15$. The new adapted model {2} also predicts the characteristic (5 %-quantile) bending strength of resawn glulam beams from lower strength classes in a satisfactory manner with a coefficient of determination of $R^2 = 0.93$ even by accepting a constant bias of

approximately 1 MPa which was deliberately set to deliver conservative estimates, which could be easily corrected just by adding +1 to the estimates (0 instead 1 for one cut and 2 instead of 3 for two cuts).

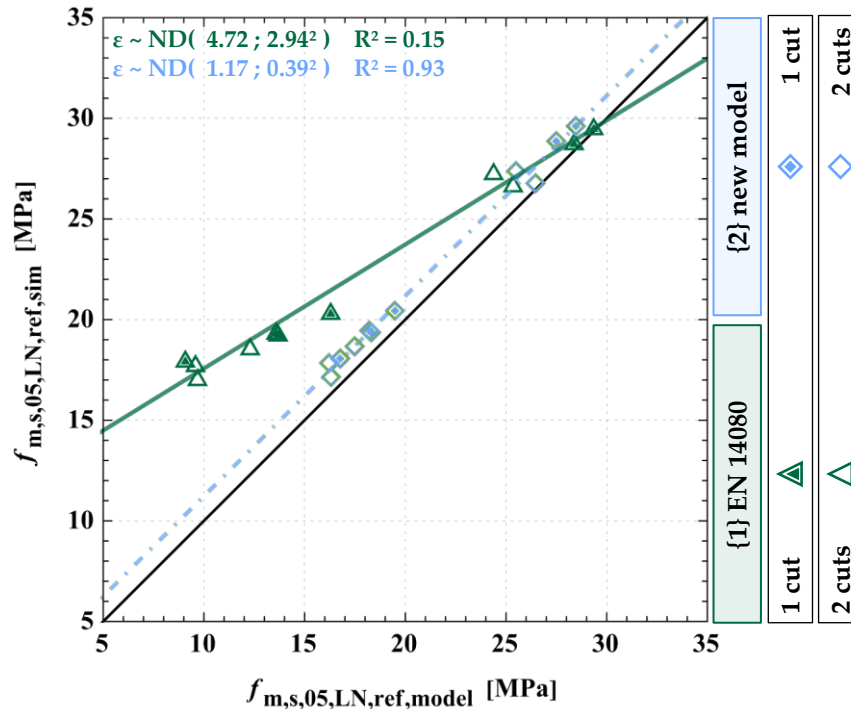


Figure 4-18: Results of simulated bending tests (5 %-quantiles) of resawn glulam beams with one and two cuts adjusted to $h_{g,ref} = 600$ mm vs. predictions of model {1} EN 14080 [16] and {2}, the new model in Equation (4.9).

The predicted characteristic (5 %-quantile) bending strengths of resawn glulam according to both models are summarised in Table 4-5 for common homogenous glulam strength classes. The predictions for GL32h are quite similar whereas rather large deviations are observed for GL24h. In contrast to the current regulation, the new model is applicable also for lower strength classes and allows a more economical use of resawn glulam beams.

Table 4-5: Comparison of the 5 %-quantiles of the bending strength $f_{m,s,k}$ in [MPa] of resawn glulam beams according to the current regulations in EN 14080 [16] and the new model in Equation (4.9).

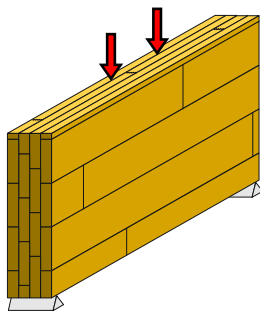
Glulam strength class	Board strength class	EN 14080 [16]		new model Equation (4.9)	
		1 Cut	2 Cuts	1 Cut	2 Cuts
GL24h	T14	16.0 ¹	12.0 ¹	21.0 (+31.3 %)	19.0 (+58.3 %)
GL28h	T18	24.0	20.0	25.3 (+5.4 %)	23.3 (+16.5 %)
GL32h	T24	30.7	26.7	29.7 (-3.3 %)	27.7 (+3.7 %)

¹... not allowed according to EN 14080 [16]

4-3 flex_GLT

In the following the mechanical properties of flex_GLT are analysed based on simulation results from the stochastic-numerical beam model. **Figure 4-19** illustrates loading situations or use cases of flex_GLT, namely type A, where the lamellas are loaded edgewise and type B with flatwise loaded lamellas. The detailed production process of flex_GLT is described and illustrated in **Section 3-2**. The main difference to conventional glulam is the random arrangement on lamellas within the cross-section. Additionally, size and system effects occur due to the parallel acting boards/lamellas. The results are compared and validated with experimental investigations carried out within the FFG BRIDGE research project “flex_GLT-CLT-beams” (No. 877111), which are in particular described in detail in the test and research report **Sieder & Brandner [66]**. Within the experimental campaign the board thickness was fixed with $t_b = 30$ mm for all flex_GLT investigations.

(a) **Type A** – edgewise loaded lamellas



Type B – flatwise loaded lamellas (b)

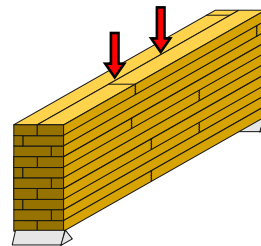


Figure 4-19: Loading situations of flex_GLT (a) type A with edgewise loaded lamellas and (b) type B with flatwise loaded lamellas.

4-3.1 Type A – Edgewise Loaded Lamellas

4-3.1.1 Bending Properties of flex_GLT type A

The bending properties of flex_GLT type A are influenced by various layup, system and/or size effects, as illustrated in **Figure 4-20**.

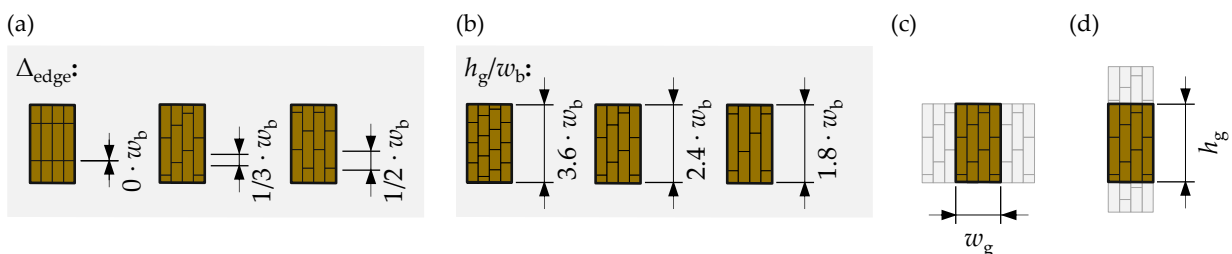


Figure 4-20: Possible influences on the bending strength of flex_GLT type A beams: (a) the overlap of the board edges of neighbouring layers, (b) the number of boards over the beam depth, (c) the number of boards within the bending-tension zone (width effect) and (d) the depth of the beam.

The first possible influence on the bending properties comes from the overlap of the board edges between neighbouring layers within the cross-section; see **Figure 4-20 (a)**. The second possible impact on the bending properties is due to the number of boards over the beam depth which is directly a function of the board/lamella width; see **Figure 4-20 (b)**. The third effect in **Figure 4-20 (c)** accounts for different flex_GLT widths, as long as the board/lamella thickness is constant, or more generally, the number of boards/lamellas in the bending-tension zone activating parallel system effects. The last influence in **Figure 4-20 (d)** addresses the depth effect, similar to conventional glulam. These mentioned potential influences on the bending properties of flex_GLT type A beams are presented and discussed in the following.

Overlap of Board Edges of Neighbouring Layers – flex_GLT type A

In order to analyse the influence of the overlap of the board edges on the bending strength of flex_GLT type A, three sets of beams with different overlaps $\Delta_{\text{edge}} = \{0; 33; 50\}$ mm were simulated. The beams feature a width of $w_g = 120$ mm, a depth of $h_g = 360$ mm and are built up from boards of group GI (T14) featuring a width of $w_b = 100$ mm. The results for the bending properties $\{f_{m,g}; E_{m,g}\}$ of the virtually tested beams are summarised in **Table 4-6** and illustrated in **Figure 4-21**. Based on them no significant influence of the overlap on the modulus of elasticity $E_{m,g}$ was observed, neither on the mean nor on the coefficient of variation. The mean and 5 %-quantile values of the bending strength $f_{m,g}$, on the other hand, are approximately 4 % higher in case of no overlap, i.e. $\Delta_{\text{edge}} = 0$ mm. In the subsequent simulations, all flex_GLT type A beams are modelled with an offset of $\Delta_{\text{edge}} = 33$ mm to achieve a somewhat conservative approximation and a more universal model for the bending strength of flex_GLT beams.

Table 4-6: Main statistics of the bending strength $f_{m,g}$ and modulus of elasticity $E_{m,g}$ calculated from 10^3 virtually tested flex_GLT type A beams (for each combination) at different overlaps of board edges of neighbouring layers $\Delta_{\text{edge}} = \{0; 33; 50\}$ mm featuring a width of $w_g = 120$ mm and a depth of $h_g = 360$ mm, built up from boards of group GI (T14) with dimensions of $w_b = 100$ mm and $t_b = 30$ mm.

Overlap Δ_{edge} [mm]		GI (T14)		
		0 ($0 \cdot w_b$)	33 ($1/3 \cdot w_b$)	50 ($1/2 \cdot w_b$)
$f_{m,g}$	mean [MPa]	24.4	23.7	23.7
	COV [%]	12.4	13.1	12.9
	$\chi_{05,LN}$ [MPa]	19.7	18.9	18.9
$E_{m,g}$	mean [MPa]	10,499	10,487	10,498
	COV [%]	4.3	4.3	4.1

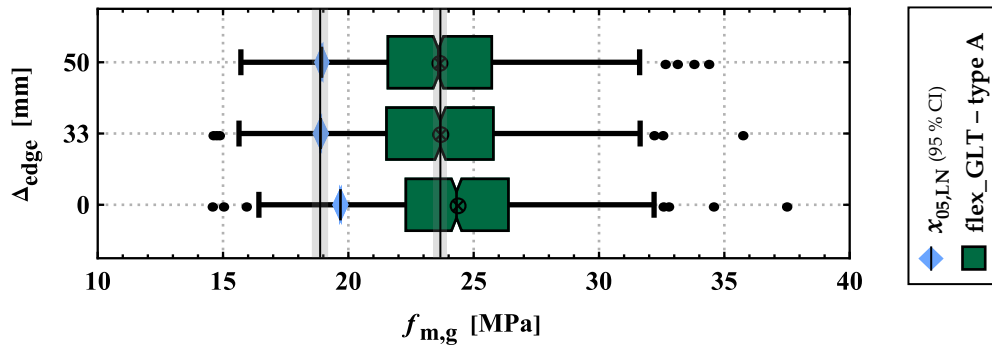


Figure 4-21: Boxplots of the bending strength $f_{m,g}$ of flex_GLT type A beams at different overlaps of board edges of neighbouring layers $\Delta_{edge} = \{0; 33; 50\}$ mm featuring a width of $w_g = 120$ mm and a depth of $h_g = 360$ mm, built up from boards of group GI (T14) with a width of $w_b = 100$ mm.

Number of Boards over the Beam Depth – flex GLT type A

For flex_GLT type A the number of boards over the beam depth might have an influence on the bending properties. In order to analyse this possible influence three sets of beams with different board widths $w_b = \{100; 150; 200\}$ mm by keeping the beam depth constant at $h_g = 360$ mm, resulting in a ratio of $h_g/w_b = \{3.6; 2.4; 1.8\}$, were simulated. The beams feature a width of $w_g = 150$ mm and are built up from boards of group GI (T14). The results for the bending properties $\{f_{m,g}; E_{m,g}\}$ of the virtually tested beams are summarised in **Table 4-7** and illustrated in **Figure 4-22**. The mean value as well as the coefficient of variation of the bending strength increase slightly with decreasing ratio of w_g/w_b , i.e. with decreasing number of boards over the beam depth. A possible explanation is with the number of boards over the beam depth, the ratio between tensile to bending stresses of the single boards changes and therefore the governing failure mode of the boards changes as well. Due to this, the 5 %-quantile values of the bending strength remain almost constant for all analysed ratios w_g/w_b . The mean modulus of elasticity $E_{m,g,mean}$ is not influenced by the number of boards over the beam depth but the coefficient of variation is decreasing with increasing ratio w_g/w_b .

Table 4-7: Main statistics of the bending strength $f_{m,g}$ and modulus of elasticity $E_{m,g}$ calculated from 10^3 virtually tested flex_GLT type A beams (for each combination) with different number of boards over the beam depth $h_g/w_b = \{3.6; 2.4; 1.8\}$ caused by different board widths $w_b = \{100; 150; 200\}$ mm featuring a constant width of $w_g = 150$ mm and a constant depth of $h_g = 360$ mm, built up from boards of group GI (T14) with dimensions of $w_b = 100$ mm and $t_b = 30$ mm.

Board Width w_b [mm]		GI (T14)		
		100	150	200
h_g/w_b [-]		3.6	2.4	1.8
$f_{m,g}$	mean [MPa]	24.1	24.5	24.8
	COV [%]	11.7	12.1	13.0
	$x_{05,LN}$ [MPa]	19.7	19.8	19.8
$E_{m,g}$	mean [MPa]	10,502	10,545	10,506
	COV [%]	3.9	4.2	4.6

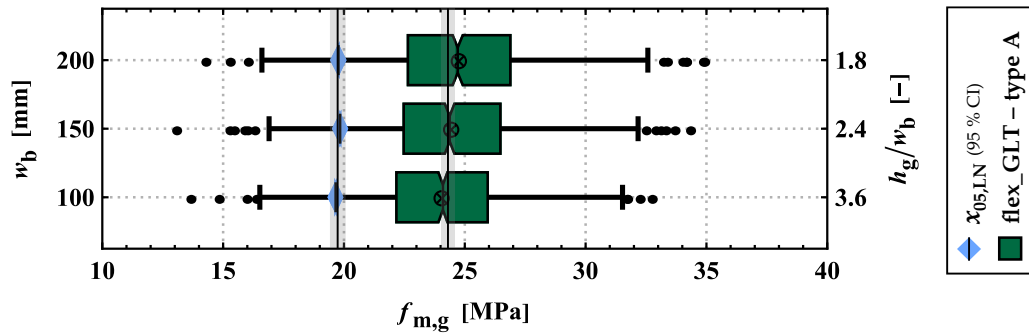


Figure 4-22: Boxplots of the bending strength $f_{m,g}$ of flex_GLT type A beams with different number of boards over the beam depth $h_g/w_b = \{3.6; 2.4; 1.8\}$ caused by different board widths $w_b = \{100; 150; 200\}$ mm featuring a constant width of $w_g = 150$ mm and a constant depth of $h_g = 360$ mm, built up from boards of group GI (T14).

Beam Width – flex_GLT type A

Within flex_GLT type A beams a multiple number of lamellas $n_{lay,par}$ can occur in the bending-tension zone. The number is dependent on the width of the beam w_g and the thickness of the boards t_b , with $n_{lay,par} = w_g/t_b$. The number of boards acting within a parallel system enables both load sharing and load redistribution following the occurrence of partial failure(s). The results of randomly built up flex_GLT type A beams featuring a depth of $h_g = 360$ mm and a width of $w_g = \{90; 120; 150; 270\}$ mm, which corresponds to $n_{lay,par} = \{3; 4; 5; 9\}$, are summarised in **Table 4-8**. All beams are built up from boards from group GI (T14) featuring a width of $w_b = 100$ mm. Additional to the ratio w_g/t_b the number of parallel acting layers $n_{lay,par}$ is stated.

The mean modulus of elasticity $E_{m,g,mean}$ appears to be unaffected by the beam width and is on the same level as found for conventional glulam. The coefficient of variation, on the other hand, is decreasing with increasing beam width. The mean bending strength is almost at a constant level whereas the coefficient of variation is decreasing with increasing beam width, and therefore, the 5 %-quantile values of the bending strength $f_{m,g,05,LN}$ increase.

Table 4-8: Main statistics of the bending strength $f_{m,g}$ and modulus of elasticity $E_{m,g}$ calculated from 10³ virtually tested flex_GLT type A beams (for each combination) at different widths $w_g = \{90; 120; 150; 270\}$ mm featuring a depth of $h_g = 360$ mm, built up from boards of group GI (T14) with dimensions of $w_b = 100$ mm and $t_b = 30$ mm.

		GI (T14)			
Width w_g [mm]		90	120	150	270
$n_{lay,par} = w_g/t_b$ [-]		3.0	4.0	5.0	9.0
$f_{m,g}$	mean [MPa]	23.9	23.7	24.1	23.8
	COV [%]	13.9	13.1	11.7	9.0
	$x_{05,LN}$ [MPa]	18.7	18.9	19.7	20.5
	$x_{05,LN}/x_{05,LN,ref}^1$ [-]	0.99	1.00	1.04	1.08
$E_{m,g}$	mean [MPa]	10,471	10,487	10,502	10,499
	COV [%]	4.8	4.3	3.9	2.6

¹.... $x_{05,LN,ref}$ with $w_g = 120$ mm

Figure 4-23 shows boxplots of the bending strength $f_{m,g}$ in dependence of the beam width of flex_GLT type A. The relationship between the 5 %-quantile of the bending strength and $n_{lay,par}$ can be described via a power law function with a power coefficient of $k_{w,flexA,05} = 0.06$. The general observations made regarding the width effect (i.e. $n_{lay,par}$) for flex_GLT type A, the widely constant mean values and the decreasing coefficients of variation with increasing number of parallel acting boards/lamellas, are consistent with the theoretical statistical background as the coefficient of variation decreases with the ratio of $n_{par}^{-0.5}$; see Brandner [36].

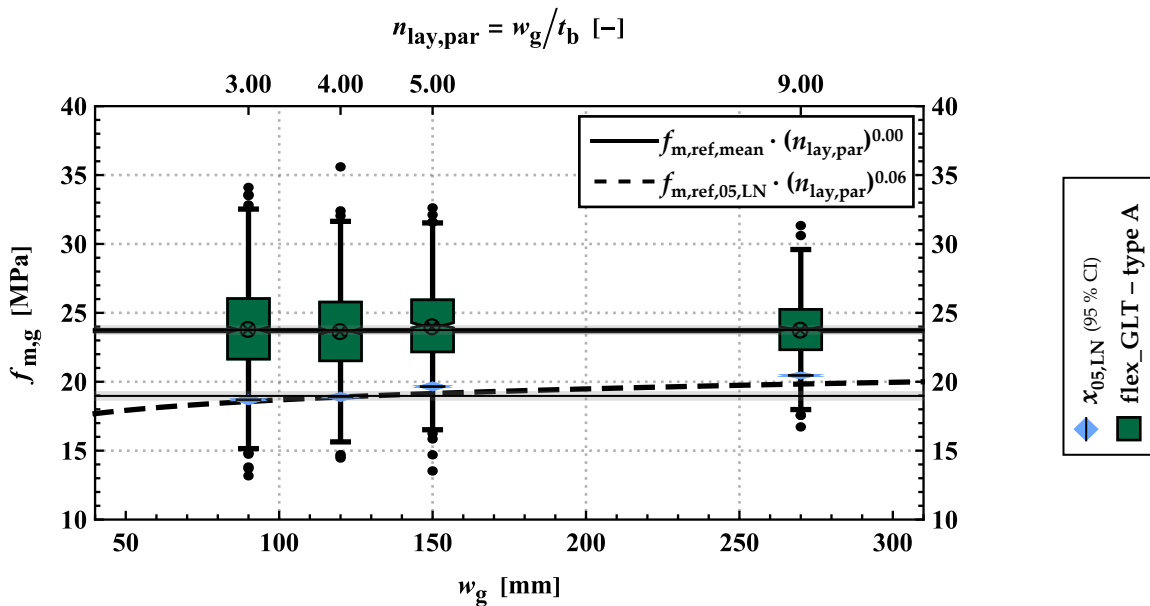


Figure 4-23: Boxplots of the bending strength $f_{m,g}$ of virtually tested flex_GLT type A beams featuring different widths $w_g = \{90; 120; 150; 270\}$ mm featuring a depth of $h_g = 360$ mm, built up from boards of group GI (T14) with dimensions $w_b = 100$ mm and $t_b = 30$ mm.

Beam Depth – flex GLT type A

The influence of the beam depth on the bending strength is known from timber and engineered timber products like glulam (see [2, 4, 5, 28, 31, 67] and also Section 4-2.1). To quantify the influence of the depth on the bending properties of flex_GLT type A beams various depths of $h_g = \{150; 360; 600\}$ mm of them were simulated all featuring a width of $w_b = 120$ mm, built up from boards of both groups but with constant width $w_b = 100$ mm. The results are summarised in Table 4-12. As expected, the mean and 5 %-quantile values of the bending strength are decreasing with increasing beam depth. The mean values of the modulus of elasticity $E_{m,g,mean}$ remain unaffected by the beam depth and are similar to conventional glulam. The coefficient of variation, however, is decreasing with increasing beam depth.

Figure 4-30 shows boxplots of the bending strength $f_{m,g}$ in dependence of the depth of flex_GLT type A beams. For the bending strength a power coefficient of $k_{h,mean} = 0.22$ for the mean and $k_{h,flexA,05} = 0.14$ for the 5 %-quantile values were found. The depth effect is the same for both groups GI (T14) and GII (T24). Furthermore, the magnitude of the power coefficient for the 5 %-

quantile values is within the same range as found in the literature for glulam, with $k_{h,0.05} = 0.10 \div 0.20$; see [2, 5, 16, 58, 68].

Table 4-9: Main statistics of the bending strength $f_{m,g}$ and modulus of elasticity $E_{m,g}$ calculated from 10^3 virtually tested flex_GLT type A beams (for each combination) at different depths $h_g = \{150; 360; 600\}$ mm featuring a width of $w_g = 120$ mm, built up from boards of both groups with dimensions of $w_b = 100$ mm and $t_b = 30$ mm.

Depth h_g [mm]		GI (T14)			GII (T24)		
		150	360	600	150	360	600
$f_{m,g}$	mean [MPa]	29.7	23.7	21.6	41.8	33.5	31.1
	COV [%]	15.7	13.1	11.6	14.0	11.8	10.3
	$\chi_{05,LN}$ [MPa]	22.5	18.9	17.7	32.8	27.4	26.1
	$\chi_{05,LN}/\chi_{05,LN,ref}^1$ [-]	1.27	1.07	1.00	1.26	1.05	1.00
$E_{m,g}$	mean [MPa]	10,526	10,487	10,485	13,026	12,996	12,980
	COV [%]	5.6	4.3	3.3	6.2	4.9	4.0

¹.... $\chi_{05,LN,ref}$ with $h_g = 600$ mm

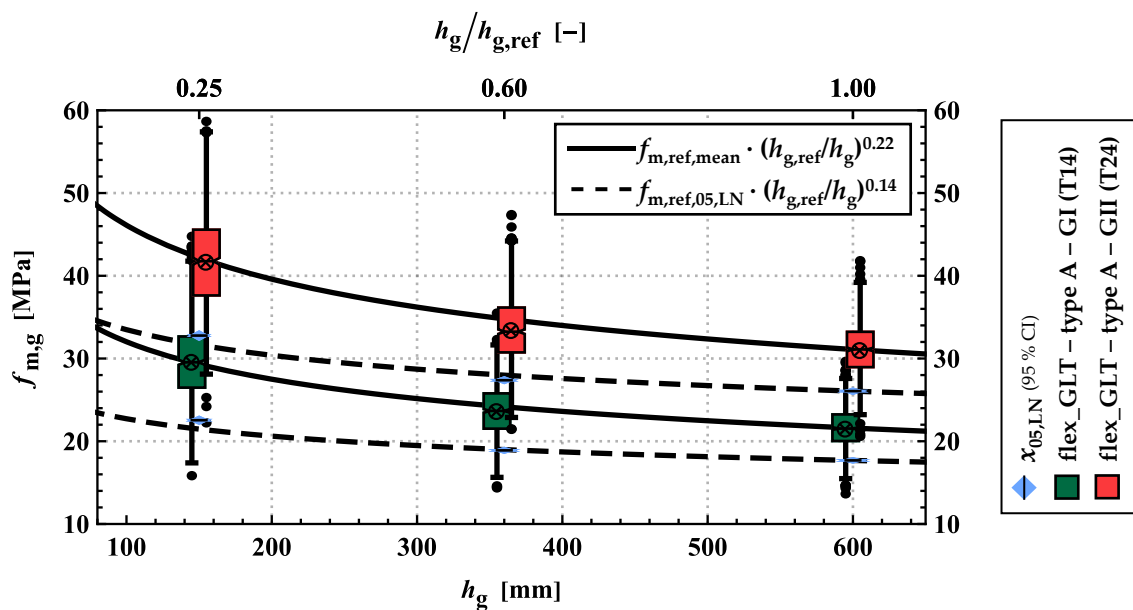


Figure 4-24: Boxplots of the bending strength $f_{m,g}$ of flex_GLT type A beams at different depths $h_g = \{150; 360; 600\}$ mm featuring a width of $w_g = 120$ mm, built up from boards of both groups.

4-3.1.2 Load-Bearing Models for the Bending Strength of flex_GLT type A Beams

Similar to glulam, the characteristic (5 %-quantile) bending strength of flex_GLT type A can be predicted based on the tensile properties of the boards $f_{t,b,0.05}$ and that of the finger joints $f_{t,FJ,0.05}$. **Figure 4-25** shows the bending strength of all simulated flex_GLT type A beams and experimental results from **Sieder & Brandner [66]** (see also **Table Annex D-17** to **Table Annex D-21**), which were adjusted to a reference depth of $h_g = 600$ mm with a power coefficient of $k_{h,0.05} = 0.14$. Additionally, the expected value of the experimental results $E(\text{test})$ is shown. In contrast to conventional glulam the boards are loaded edgewise, therefore the bending strength of the boards $f_{m,b,0.05}$ can also become a relevant contributing factor to the load-bearing

model of flex_GLT type A, in particular for beams with low ratios h_g / w_b . The boards used within the experimental campaign were visually graded according to **DIN 4074-1 [9]** and assigned to the strength class C24 according to **EN 338 [8]**. The bending strength of the boards was estimated with the given relationship in **EN 338 [8]** (see **Equation (4.10)**) and the coefficient of variation of the bending strength was assumed via **Equation (4.11)** based on **JCSS-3.05 [43]**.

$$f_{m,b,05,test} = \frac{f_{m,b,05,C24}}{f_{t,0,b,05,C24}} \cdot f_{t,0,b,05,test} = \frac{24}{14.5} \cdot 14.9 = 24.7 \quad (4.10)$$

$$COV(f_{m,b,test}) = \frac{COV(f_{t,0,b,test})}{1.2} = \frac{43.2}{1.2} = 36.0 \quad (4.11)$$

with

- $f_{m,b,05}$ characteristic (5 %-quantile) bending strength of boards [MPa]
- $f_{t,0,b,05}$ characteristic (5 %-quantile) tensile strength of boards [MPa]
- $COV(X)$ coefficient of variation [%]

The basis of all load-bearing models for the characteristic (5 %-quantile) bending strength is the adapted model from **Brandner & Schickhofer [58]** for glulam in **Equation (4.5)**. All three different modelling approaches were derived by calibrating multiplication factors (underlined figures) to the simulation results; see **Equations (4.12)** to **(4.14)**. The system effect of parallel acting boards is taken into account with $k_{sys,flexA} = n_{lay,par}^{0.06}$; see **Section 4-3.1.1**.

$$f_{m,g,05,(1)} = \underline{1.47} \cdot n_{lay,par}^{0.06} \cdot e^{1.15 \cdot COV(f_{t,0,b})} \cdot \text{Min} \left[f_{t,0,b,05} ; \frac{f_{t,FJ,05}}{\zeta_{new}} \right]^{0.80} \quad (4.12)$$

$$\text{with } \zeta_{new} = e^{1.55 \cdot COV(f_{t,0,b}) - 1.60 \cdot COV(f_{t,FJ})}$$

$$f_{m,g,05,(2)} = \underline{1.57} \cdot n_{lay,par}^{0.06} \cdot e^{1.15 \cdot (1.20 \cdot COV(f_{m,b}))} \cdot \text{Min} \left[f_{m,b,05} \cdot 0.65 ; \frac{f_{t,FJ,05}}{\zeta_{new,fm}} \right]^{0.80} \quad (4.13)$$

$$\text{with } \zeta_{new,fm} = e^{1.55 \cdot (1.20 \cdot COV(f_{m,b})) - 1.60 \cdot COV(f_{t,FJ})}$$

$$f_{m,g,05,(3)} = \underline{1.20} \cdot n_{lay,par}^{0.06} \cdot \left(\frac{f_{m,b,05}}{f_{t,0,b,05}} \right)^{0.80} \cdot e^{1.15 \cdot COV(f_{t,0,b})} \cdot \text{Min} \left[f_{t,0,b,05} ; \frac{f_{t,FJ,05}}{\zeta_{new}} \right]^{0.80} \quad (4.14)$$

$$\text{with } \zeta_{new} = e^{1.55 \cdot COV(f_{t,0,b}) - 1.60 \cdot COV(f_{t,FJ})}$$

with

- $f_{m,g,05}$ characteristic (5 %-quantile) bending strength of flex_GLT type A at $h_g = h_{g,ref} = 600$ mm [MPa]
- $f_{t,0,b,05}$ characteristic (5 %-quantile) tensile of boards at a length of $l_{ref} = 2.0$ m [MPa]
- $f_{m,b,05}$ characteristic (5 %-quantile) edgewise bending strength of the boards [MPa]
- $f_{t,FJ,05}$ characteristic (5 %-quantile) tensile strength of the finger joints [MPa]
- $COV(X)$ coefficient of variation [-]
- $n_{lay,par}$ number of layers acting parallel in the bending tension zone (w_g/t_b) [-]
- w_g width of the flex_GLT type A beam [mm]
- t_b thickness of boards [mm]

Model {1} is based on the tensile properties parallel to the grain of the boards and finger joints $\{f_{t,0,b,05}; \text{COV}(f_{t,0,b}); f_{t,FJ,05}\}$ acc. to **Equation (4.12)**. Model {2} is based on the bending properties of the boards $\{f_{m,b,05}; \text{COV}(f_{m,b}); f_{t,FJ,05}\}$ acc. to **Equation (4.13)** and model {3} is based on a combination of the tensile and the bending properties of the boards $\{f_{t,0,b,05}; \text{COV}(f_{t,0,b}); f_{m,b,05}; f_{t,FJ,05}\}$ acc. to **Equation (4.14)**.

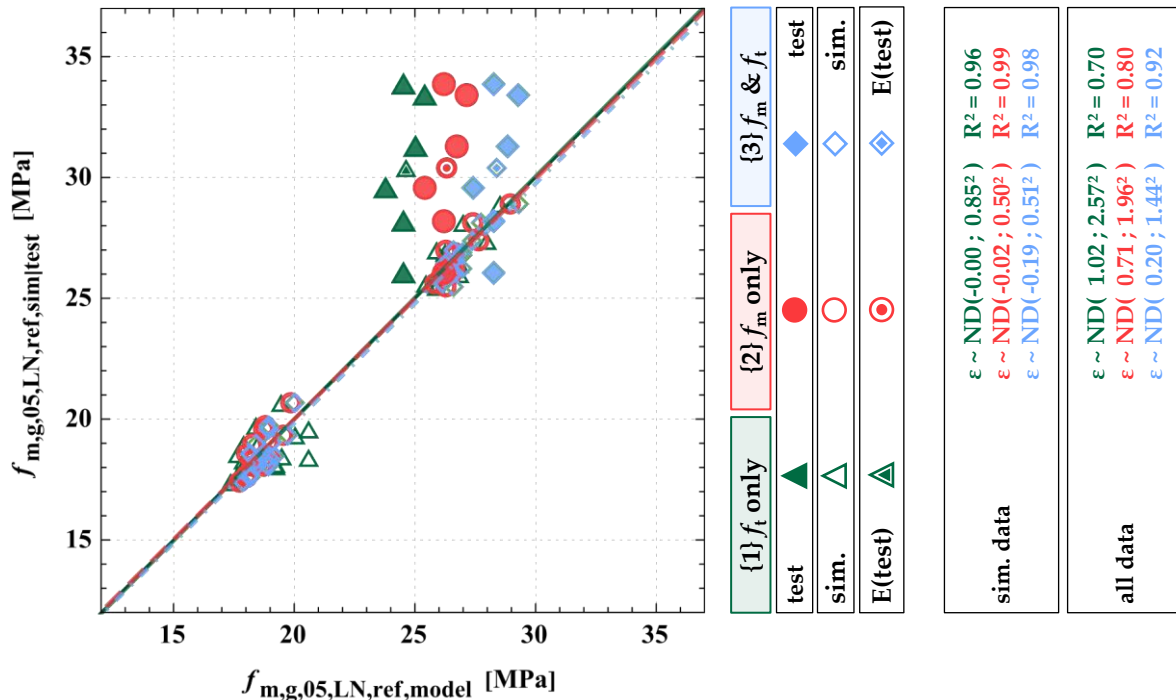


Figure 4-25: Results of bending tests and simulations (5 %-quantiles) of flex_GLT type A adjusted to $h_{g,ref} = 600$ mm (with $k_{th,05} = 0.14$) vs. model predictions based on {1} only tensile strength of the boards (f_t only; see **Equation (4.12)**), {2} only the bending strength of the boards (f_m only; see **Equation (4.13)**) and {3} the bending and the tensile strength of the boards (f_m & f_t ; see **Equation (4.14)**).

All models for flex_GLT type A are capable of predicting the bending strength of the simulated beams in a satisfactory manner ($\epsilon_{mean} \approx 0$ MPa; $R^2 > 0.95$). The best results are achieved with model {2} considering the edgewise bending properties of the boards. The bending strength of the experimental series are significantly underestimated by model {1} and {2} ($R^2 < 0.80$). One possible reason for these deviations is within the grading of the boards. The simulated boards can be assigned to the strength class T14 for group GI and T24 for GII. For T-classes acc. to **EN 338 [8]** the ratio between the tensile strength and the bending strength is $f_{t,0,b,k}/f_{m,b,k} \approx 0.70$ and for C-classes acc. to **EN 338 [8]** the ratio is $f_{t,0,b,k}/f_{m,b,k} \approx 0.62$. This difference seems to influence the bending strength of flex_GLT type A beams. Given this circumstance, the strength ratio was adjusted in model {3}. The mean residue of the prediction of model {3} for the simulation and test results together is $\epsilon_{mean} \approx 0$ MPa and the coefficient of determination is $R^2 = 0.92$. The characteristic bending strength of flex_GLT type A beams can be predicted by the load-bearing model in a satisfactory manner, which is true in particular for the simulations but less for the test outcomes. One possible reason for these deviations is that the board model is based on the tensile properties,

whereas for flex_CLT beams the edgewise bending properties may play a more important role on the load-bearing capacity. Nonetheless, a conservative prediction of the heterogeneous test results in the experimental campaign in [Sieder & Brandner \[66\]](#) is possible.

4-3.2 Type B – Flatwise Loaded Lamellas

4-3.2.1 Bending Properties of flex_GLT type B

The bending properties of flex_GLT type B are influenced by various geometric, system and/or size effects, like illustrated in [Figure 4-26](#). The first possible influence on the bending strength comes from the overlap of the board edges between neighbouring layers within the cross-section; see [Figure 4-26 \(a\)](#). The second effect in [Figure 4-26 \(b\)](#) accounts for the flex_GLT width as indicator for the number of boards/lamellas in the bending-tension zone activating parallel system effects. The last influence in [Figure 4-26 \(c\)](#) addresses the number of layers within the cross-section, also well-known as the depth effect from conventional glulam. These mentioned influences on the bending strength of flex_GLT type B beams are presented and discussed in the following.

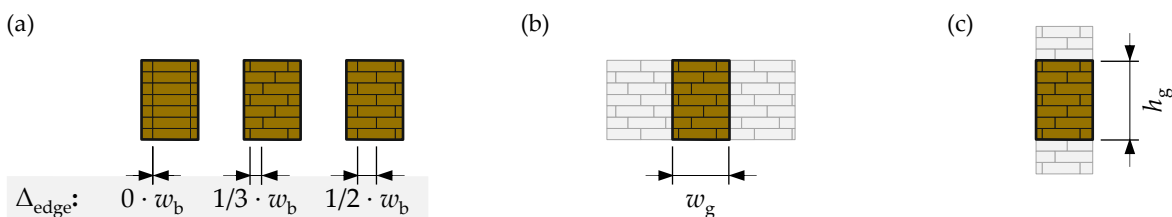


Figure 4-26: Possible influences on the bending strength of flex_GLT type B beams: (a) the overlap of the board edges of neighbouring layers, (b) the number of boards at the bending-tension zone (width effect) and (c) the number of layers (depth effect).

Overlap of Board Edges of Neighbouring Layers – flex_GLT type B

In order to analyse the influence of the overlap of the board edges on the bending strength of flex_GLT type B, three sets of beams with different overlaps $\Delta_{\text{edge}} = \{0; 33; 50\}$ mm were simulated. The beams feature a width of $w_g = 150$ mm, a depth of $h_g = 360$ mm and are built up from boards of group GI (T14) featuring a width of $w_b = 100$ mm. The results for the bending properties $\{f_{m,g}; E_{m,g}\}$ from virtually tested beams are summarised in [Table 4-10](#) and illustrated in [Figure 4-27](#). As the results indicate, no significant influence of the overlap on the bending strength $f_{m,g}$ was observed, neither on the mean nor on the 5 %-quantile level. The same conclusion can be drawn for the modulus of elasticity $E_{m,g}$.

Table 4-10: Main statistics of the bending strength $f_{m,g}$ and modulus of elasticity $E_{m,g}$ calculated from 10^3 virtually tested flex_GLT type B beams (for each combination) at different overlaps of board edges of neighbouring layers $\Delta_{edge} = \{0; 33; 50\}$ mm featuring a width of $w_g = 150$ mm and a depth of $h_g = 360$ mm, built up from boards of group GI (T14) with dimensions of $w_b = 100$ mm and $t_b = 30$ mm.

Overlap Δ_{edge} [mm]		GI (T14)		
		0 ($0 \cdot w_b$)	33 ($1/3 \cdot w_b$)	50 ($1/2 \cdot w_b$)
$f_{m,g}$	mean [MPa]	29.0	28.8	28.6
	COV [%]	12.3	11.7	12.1
	$\chi_{05,LN}$ [MPa]	23.5	23.5	23.2
$E_{m,g}$	mean [MPa]	10,495	10,514	10,489
	COV [%]	4.1	4.0	4.1

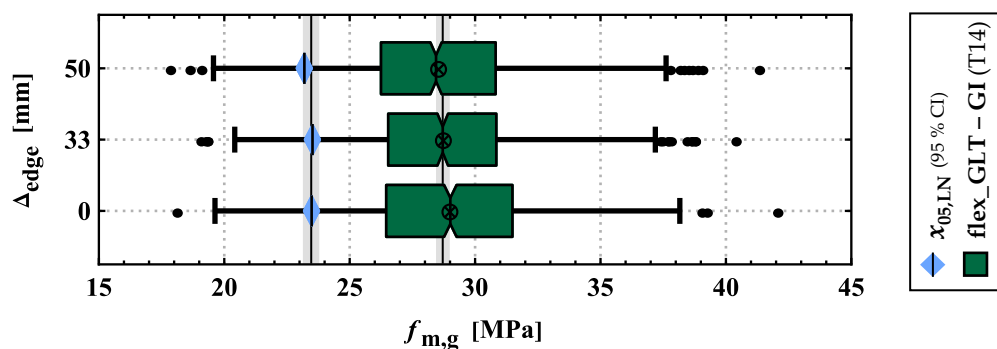


Figure 4-27: Boxplots of the bending strength $f_{m,g}$ of flex_GLT type B beams featuring different overlaps of board edges between neighbouring layers $\Delta_{edge} = \{0; 33; 50\}$ mm featuring a width of $w_g = 150$ mm and a depth of $h_g = 360$ mm, built up from boards of group GI (T14) with a width of $w_b = 100$ mm.

Beam Width – flex_GLT type B

In contrast to conventional glulam, within flex_GLT type B the number of lamellas in the bending-tension zone is dependent on the width of the beam w_g and the width of the boards w_b , i.e. $n_{par} = w_g/w_b$. The number of boards acting within a parallel system enables both load sharing and load redistribution following the occurrence of partial failure(s). The results of randomly built up flex_GLT type B beams featuring a depth of $h_g = 360$ mm and a width of $w_g = \{50; 100; 150; 250; 500\}$ mm are summarised in **Table 4-11**. All beams are built up from boards of group GI (T14) featuring a width of $w_b = 100$ mm. As a reference, a conventional glulam beam with similar dimensions and layup $\{w_g = w_b = 100$ mm; $t_b = 30$ mm} was simulated.

Given a width ratio of $w_g/w_b \geq 1.00$ the mean bending strength remains almost constant whereas the coefficient of variation is further decreasing with increasing width ratio, and therefore, the 5 %-quantile values of the bending strength $f_{m,g,05,LN}$ increase. At ratios below $w_g/w_b < 1.00$, the bending strength is significantly reduced at the mean level as well as on the 5 %-quantile level. This effect is of similar magnitude as observed within resawn glulam (see **Section 4-2.4**). This “change in system” or “kink” of the bending strength is also visible in the number of boards within the lowest layer of the randomly built up flex_GLT type B beams; (see

Figure 4-28). At a ratio of $w_g/w_b < 1.00$, the cross-section consists of only split boards, i.e. the mechanical properties of the base material are below the properties assigned during strength grading of boards in full cross-section. The mean modulus of elasticity $E_{m,g,mean}$ appears to be unaffected by the beam width and remains on the same level as for conventional glulam. The coefficient of variation, on the other hand, is decreasing with an increasing beam width.

Table 4-11: Main statistics of the bending strength $f_{m,g}$ and modulus of elasticity $E_{m,g}$ calculated from 10^3 virtually tested flex_GLT type B beams (for each combination) at different widths $w_g = \{50; 100; 150; 250; 500\}$ mm and from conventional glulam featuring a depth of $h_g = 360$ mm, built up from boards of group GI (T14) with dimensions $w_b = 100$ mm and $t_b = 30$ mm.

Width w_g [mm]		flex_GLT type B – GI (T14)					glulam
		50	100	150	250	500	100
$f_{m,g}$	mean [MPa]	27.1	28.7	28.9	28.6	28.1	27.9
	COV [%]	15.9	14.2	11.7	10.6	8.2	15.3
	$\chi_{05,LN}$ [MPa]	20.5	22.5	23.6	23.8	24.4	21.2
	$\chi_{05,LN}/\chi_{05,LN,ref}^1$ [-]	0.97	1.06	1.11	1.12	1.15	1.00
$E_{m,g}$	mean [MPa]	10,504	10,506	10,514	10,496	10,500	10,432
	COV [%]	5.7	4.8	4.0	3.3	2.4	5.6

¹ ... $\chi_{05,LN,ref}$ from conventional glulam with $w_g = w_b = 100$ mm, $t_b = 30$ mm and GI (T14)

Flex_GLT type B beams featuring the same ratio $w_g/w_b = 1.00$ as conventional glulam have a 6 % higher bending strength $f_{m,g,05,LN}$ than conventional glulam. Although flex_GLT beams type B comprise a certain share of lengthwise split boards, which have a lower tensile strength, the already present parallel system effects at this ratio (mean number of boards $n_{b,all} = 2$) counteract this reduction in bending strength.

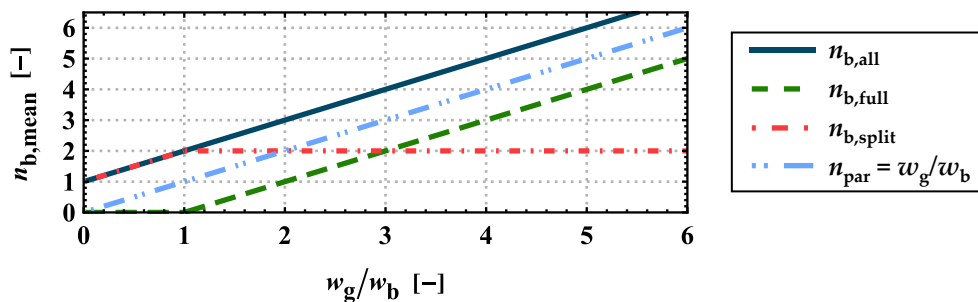


Figure 4-28: Mean number of boards in the bending-tension zone of flex_GLT type B beams in dependence of the width ratio w_g/w_b {total number of boards $n_{b,all}$; number of boards with full cross-section $n_{b,full}$; number of split boards $n_{b,split}$; n_{par} number of boards acting parallel}.

Figure 4-29 shows boxplots of the bending strength $f_{m,g}$ in dependence of the width of flex_GLT type B beams. Additional to the width ratio w_g/w_b , the mean number of parallel acting boards ($n_{b,all}$) and the mean number of boards with a full cross-section ($n_{b,full}$) are stated. For a width ratio of $w_g/w_b \geq 1.00$ the 5 %-quantile of the bending strength can be described via a power law function with a power coefficient of $k_{w,flexB,05} = 0.06$. The observations made generally regarding the width effect for flex_GLT type B, of approximately constant mean values and the decreasing coefficient of variation with increasing number of parallel acting boards/lamellas, are

consistent with some of the theoretical statistical background as the coefficient of variation decreases with the ratio of $n_{\text{par}}^{-0.5}$; see **Brandner [36]**.

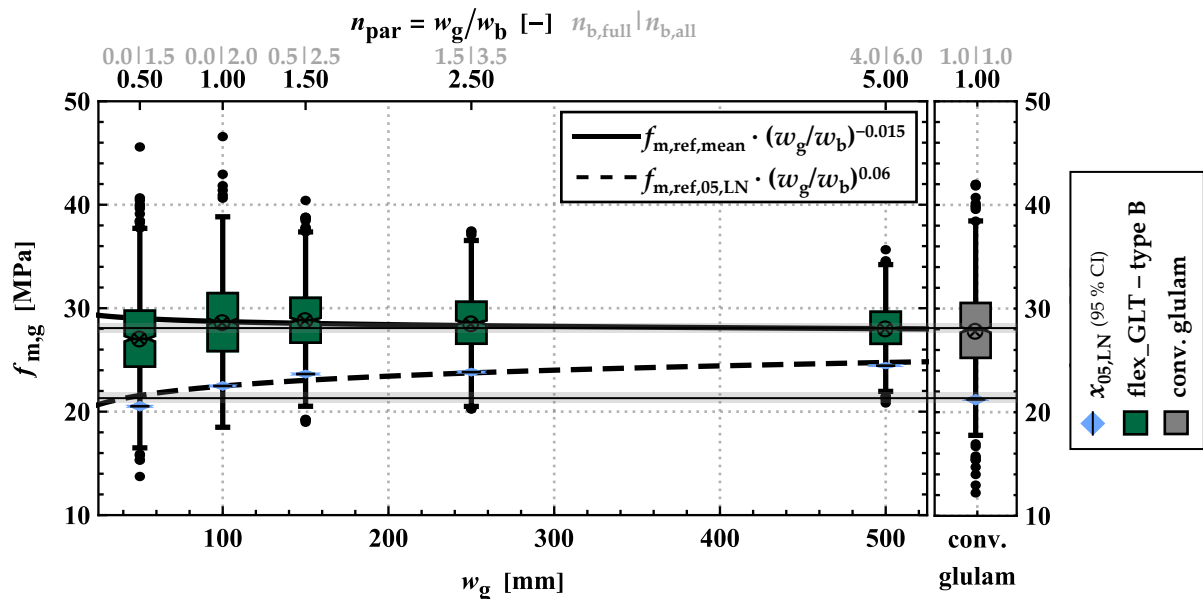


Figure 4-29: Boxplots of the bending strength $f_{m,g}$ from virtually tested flex_GLT type B beams with different widths $w_g = \{50; 100; 150; 250; 500\}$ mm in comparison to conventional glulam featuring a depth of $h_g = 360$ mm, built up from boards of group GI (T14) with dimensions $w_b = 100$ mm and $t_b = 30$ mm.

Beam Depth – flex_GLT type B

The influence of the beam depth on the bending strength is well known for timber and engineered timber products like glulam (see [2, 4, 5, 28, 31, 67] and **Section 4-2.1**). To quantify the influence of the depth on the bending strength, flex_GLT type B beams featuring a width of $w_b = 150$ mm and various depths of $h_g = \{210; 360; 600\}$ mm built up from boards of both groups and width $w_b = 100$ mm were simulated. The results are summarised in **Table 4-12**.

The mean and 5 %-quantile values of the bending strength are decreasing with increasing beam depth. The mean modulus of elasticity $E_{m,g,\text{mean}}$ remains unaffected by the beam depth and on the same level as for conventional glulam. The coefficient of variation, on the other hand, decreases with an increasing beam depth.

Figure 4-30 shows boxplots of the bending strength $f_{m,g}$ in dependence of the depth of flex_GLT type B beams. For the bending strength a power coefficient of $k_{h,\text{mean}} = 0.22$ for the mean value and $k_{h,\text{flexB},05} = 0.14$ for the 5 %-quantile value were found. This depth effect for the bending strength is the same for both groups GI (T14) and GII (T24). Similar values for the power coefficient for modelling the depth effect in conventional glulam in the range of $k_{h,05} = 0.10 \div 0.20$ are found in literature; see [2, 5, 16, 58, 68].

Table 4-12: Main statistics of the bending strength $f_{m,g}$ and modulus of elasticity $E_{m,g}$ calculated from 10^3 virtually tested flex_GLT type B beams (for each combination) with different depths $h_g = \{210; 360; 600\}$ mm featuring a width of $w_g = 150$ mm and built up from boards of both groups with dimensions of $w_b = 100$ mm and $t_b = 30$ mm.

Depth h_g [mm]		GI (T14)			GII (T24)		
		210	360	600	210	360	600
$f_{m,g}$	mean [MPa]	32.7	28.9	25.6	45.1	40.0	35.7
	COV [%]	14.4	11.7	9.4	14.3	11.6	9.7
	$\chi_{05,LN}$ [MPa]	25.5	23.6	21.8	35.3	32.8	30.2
	$\chi_{05,LN}/\chi_{05,LN,ref}^1$ [-]	1.17	1.08	1.00	1.17	1.08	1.00
$E_{m,g}$	mean [MPa]	10,509	10,514	10,495	12,972	13,008	13,000
	COV [%]	5.3	4.0	3.0	6.0	4.7	3.4

¹ ... $\chi_{05,LN,ref}$ with $h_g = 600$ mm

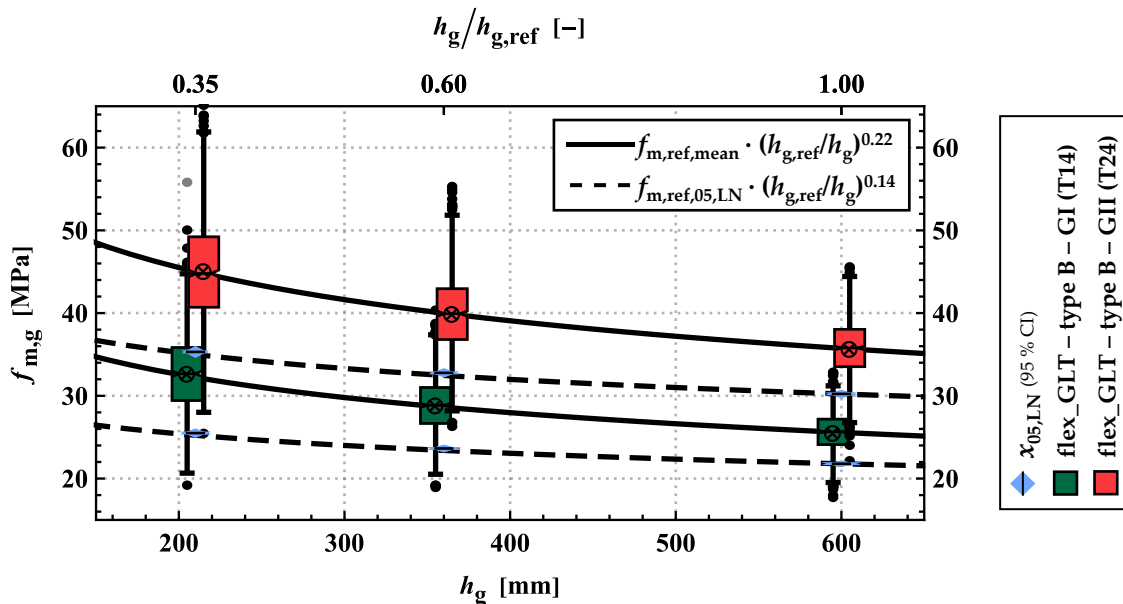


Figure 4-30: Boxplots of the bending strength $f_{m,g}$ of flex_GLT type B beams at different depth $h_g = \{210; 360; 600\}$ mm featuring a width of $w_g = 150$ mm, built up of boards from both groups.

4-3.2.2 Load-Bearing Models for the Bending Strength of flex_GLT type B Beams

The bending strength of flex_GLT type B beams can be predicted based on the tensile properties of the boards $f_{t,0,b,05}$ and of the finger joints $f_{t,FJ,05}$. Due to the similarity of flex_GLT type B beams with conventional glulam (flatwise loaded boards) the applicability of similar load-bearing models is expected. **Figure 4-31** shows the bending strength of all simulated flex_GLT beams and experimental results from **Sieder & Brandner [66]** (see also **Table Annex D-22** to **Table Annex D-24**), which were adjusted to a reference depth of $h_g = 600$ mm with a power coefficient of $k_{h,05} = 0.14$; see **Section 4-3.2.1**. In **Figure 4-31 (a)** the results are compared with the predictions according to the models {1} **EN 14080 [16]**, {2} **Brandner [58]** and {3}, the new model in **Equation (4.6)** derived for glulam. The models for glulam {1-3} are capable to roughly capturing ($R^2 \leq 0.78$) the characteristic (5 %-quantile) bending strength of the simulated and tested flex_GLT beams type B. These models are, however, not formulated to account for the influence

of beam width (w_g/w_b ratio), i.e. for product inherent system effects activated by parallel acting lamellas in the bending tension zone. By adapting the load-bearing models with a system factor $k_{\text{sys},w,\text{flexB}}$, which takes these effects into account (see Equation (4.15)), their accuracy can be increased significantly; see Section 4-3.2.1. Figure 4-31 (b) shows the predictions of the modified models. Model {1} EN 14080 [16] overestimates the bending strength of flex_GLT type B beams produced from lower strength classes in a similar manner as seen for conventional glulam; see Section 4-2.1.2. The other two models give an overall better approximation of the bending strength ($\epsilon_{\text{mean}} \approx 0$ MPa; $R^2 > 0.90$). The models are also successfully validated by experiments from Sieder & Brandner [66].

$$f_{m,g,05,\text{flexB}} = k_{\text{sys},\text{flexB}} \cdot f_{m,g,05,\text{glulam}} \quad (4.15)$$

with $k_{\text{sys},\text{flexB}} = 1.05 \cdot (n_{\text{par}})^{0.06}$

with

- $f_{m,g,05,\text{flexB}}$... characteristic (5 %-quantile) bending strength of flex_GLT type B beams at $h_g = h_{g,\text{ref}} = 600$ mm [MPa]
- $f_{m,g,05,\text{glulam}}$ characteristic (5 %-quantile) bending strength of glulam [MPa]
- n_{par} number of parallel acting boards (w_g/w_b) [-]
- w_g width of the flex_GLT type B beam [mm]
- w_b width of boards [mm]

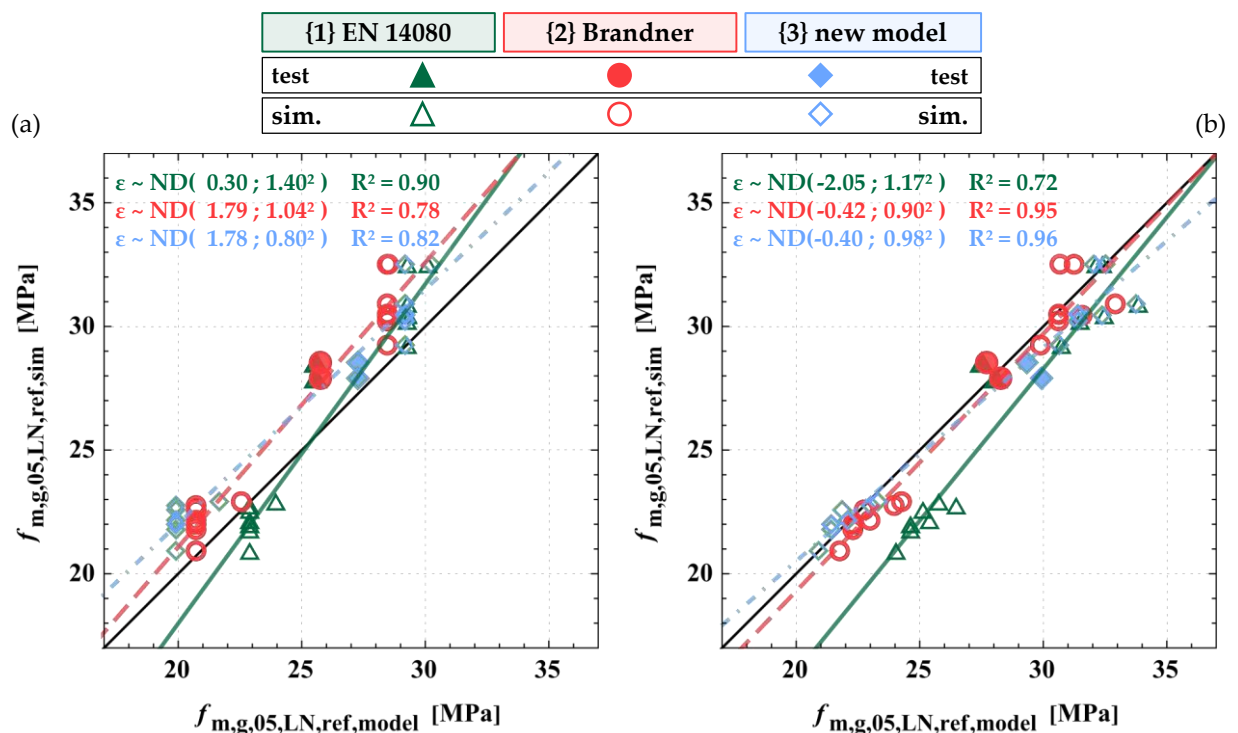


Figure 4-31: Results of bending tests and simulations (5 %-quantiles) on flex_GLT type B beams corrected to $h_{g,\text{ref}} = 600$ mm (with $k_{h,\text{flexB},05} = 0.14$) vs. model predictions for (a) glulam {1} EN 14080 [16], {2} Brandner [58] and {3} new model in Equation (4.6) and (b) predictions of the same models adapted by the width effect acc. to Equation (4.15).

4-4 Intermediate Conclusions

In this chapter the stochastic-numerical beam model presented in **Chapter 3** is applied to simulate the bending properties of unidirectionally laminated engineered timber products. In a first step and also as a benchmark of the stochastic-numerical beam model, glulam beams with different depths were simulated. The bending properties of the virtually conducted bending tests are well within a plausible range as found in the literature. Furthermore, a depth effect with a power coefficient of $k_h = 0.10$ was found for the characteristic (5 %-quantile) bending strength, which is well in line with the current product standard for glulam **EN 14080 [16]**. Current design rules for glulam give no reduction of the characteristic bending strength for beams with depths $h_g > 600$ mm; see **ON EN 1995-1-1 [59]**. Nonetheless, the presented simulation results outline a reduction of the characteristic (5 %-quantile) bending strength also for beams with a depth larger than $h_{g,ref} = 600$ mm. Similar reductions were observed by **Frese & Blaß [55]**. It has to be noted that this depth effect is rather a mixed depth and length effect, as the test span is a function of the beam depth; see **EN 408 [39]**. Based on these results it is necessary to consider the depth effect also for glulam beams with a depth higher than $h_g = 600$ mm. The **EN 14080 [16]** also states a mean modulus of elasticity of 1.05 times the modulus of elasticity in tension parallel to the grain of the boards, which was not observed within the simulation results. With respect to the simulation results and as suggestions in **Fink [3]**, **Frese [4]**, **Blaß et al. [5]**, **Brandner & Schickhofer [57]** this regulation should be revised, so that the mean modulus of elasticity of glulam should be equal to its base material.

Additionally, the bending strength of glulam beams with edgewise loaded lamellas was analysed. Within the current product standard **EN 14080 [16]** for glulam made out of coniferous wood no bending strength for glulam with edgewise loaded lamellas is defined. On the other hand, the European Assessment Document for glulam made out of hardwood **EAD 130320-00-0304 [63]** clearly states a bending strength for edgewise loaded lamellas. It is unclear if the bending strength with flatwise loaded lamellas should be used also for the case of edgewise loaded lamellas, or the edgewise bending strength of the lamellas including system effects (e.g. k_{sys} for parallel acting members) should be used. The analysis showed that the bending strength increases with increasing number of parallel acting lamellas in the bending-tension zone, which is consistent with system factor k_{sys} usually used for parallel acting members. **EAD 130320-00-0304 [63]** states that the edgewise bending strength may be calculated from the minimum of the edgewise bending strength of boards and finger joints by using k_{sys} taken from **ON EN 1995-1-1 [59]**. Simulation results indicate that this approach is a suitable prediction for the lower strength class GI (T14) but overestimates the edgewise bending strength of the higher strength class GII (T24). Furthermore, it was shown, that the bending strength with edgewise loaded lamellas (at least two lamellas parallel) is already higher than with flatwise loaded lamellas. Therefore, the flatwise bending strength seems safe to be used for edgewise bending as well, which enhances the ease of use for engineers in practise, but also neglects part of the mechanical potential.

The simulation results for glulam beams demonstrate the applicability of the stochastic-numerical beam model in deriving the bending properties of unidirectionally laminated engineered timber products. These results align well with experimental data and accurately capture depth effects of glulam as well as the system effect of parallel acting members within glulam.

The new stochastic-numerical beam model in combination with the probabilistic board models for lengthwise split boards is also able to depict the bending properties of resawn glulam. Hereby, functions accounting for the influence on the bending strength by resawing glulam beams were presented, which are well in line with experimental investigations in the literature. **EN 14080 [16]** allows resawing of glulam beams built up of boards of higher strength classes and provides formulas for the characteristic bending strength for residual cross-sections gained by one and two cuts. Regarding resawn glulam with two cuts no experimental investigations are known to the author. The results of herein conducted simulations are in line with the model in **EN 14080 [16]** for beams with higher strength classes. Nevertheless, the simulation results indicate also the possibility to resaw glulam beams built up of boards from lower strength classes and demonstrates conservative values for resawn glulam beams with two cuts when calculated according to **EN 14080 [16]**. An adapted model for the characteristic (5 %-quantile) bending strength of resawn glulam is presented, which also takes lower board strength classes into account. Besides the bending strength, for resawn glulam beams **EN 14080 [16]** also states a 500 MPa lower modulus of elasticity compared to the unsplit glulam beams. This reduction was not observed in the simulation results and lacks a physical explanation. As a consequence, it is proposed to revise the regulation regarding resawn glulam beams in the product standard **EN 14080 [16]**.

The main difference between conventional glulam and flex_GLT is the presence of one or more board cross-sections within the beam featuring arbitrarily reduced width(s). Due to the inherent differences in the layup of flex_GLT beams in contrast to conventional glulam different system and size effects occur. Such effects on the bending properties of flex_GLT beams were analysed separately for type A and B, i.e. flex-beams whose laminations are loaded edgewise and flatwise in bending, respectively. By doing so it was concluded that the overlap of board edges of neighbouring layers has only a minor influence on the bending strength of flex_GLT beams. The depth effect with a power coefficient of $k_{h,flexA,05} = k_{h,flexB,05} = 0.14$ for the characteristic (5 %-quantile) bending strength was found to be identical for both types A and B. The depth effect in flex_GLT is slightly higher than for conventional glulam. Possible reasons are different length effects of randomly lengthwise split lamellas, a higher probability of finger joints and their overall interaction in the bending tension zone. On the other hand and in contrast to conventional glulam (excluding brick & block glued glulam), within flex_GLT beams multiple boards in full cross-section and lengthwise split may act together with randomly lengthwise split lamellas, i.e. in parallel, in the bending tension zone. The resulting system effect increases the characteristic (5 %-quantile) bending strength of the flex_GLT beams. The kind of system effect or width effect is,

however, overall lower than found for glulam with edgewise in bending loaded lamellas; see **Section 4-2.2**. One possible reason is the unclear reference value, as for flex_GLT due to the arbitrary lengthwise splitting of lamellas no ideal reference cross-section with exactly one board ($n_{\text{par}} = 1$) in the bending tension zone is defined. Similar to the depth effect, for modelling the width (system) effect a power model was employed. A power coefficient of $k_{w,\text{flexA},05} = k_{w,\text{flexB},05} = 0.06$ was found for both flex_GLT beam types, whereby, type A is dependent on the number of parallel acting layers $n_{\text{lay,par}} = w_g/t_b$ and type B on the ratio between the beam and the board width $n_{\text{par}} = w_g/w_b$.

Based on the simulations, the mentioned effects as well as the experimental bending tests, and with the aim of also providing at least to some extent a safety margin in the regulation of the new product, minimal geometric requirements are proposed. These minimal requirements are illustrated in **Figure 4-32** for flex_GLT type A and B beams. Flex_GLT beams should be comprised of at least four layers in width and depth direction for flex_GLT type A and B, respectively. The minimum depth of flex_GLT type A beams should be at least 1.5 times the maximum board width used to build up the beam element. For flex_GLT type B the minimum width is defined as 1.5 times the board width. This regulation is a precautionary measure to make sure that at least one board in full cross-section is always present over the depth or width of the beam. Additionally, at least 66 % of all board edges should be offset by at least one times the greatest thickness of the adjacent layers. This is also a safety measure to ensure a secondary pathway for bending shear forces besides the glue line between the board edges. These regulations are incorporated in the European Assessment Document for flex_GLT **draft_EAD 130801-00-0304 [69]**, which is currently under development.

(a) Type A – edgewise loaded lamellas

Type B – flatwise loaded lamellas (b)

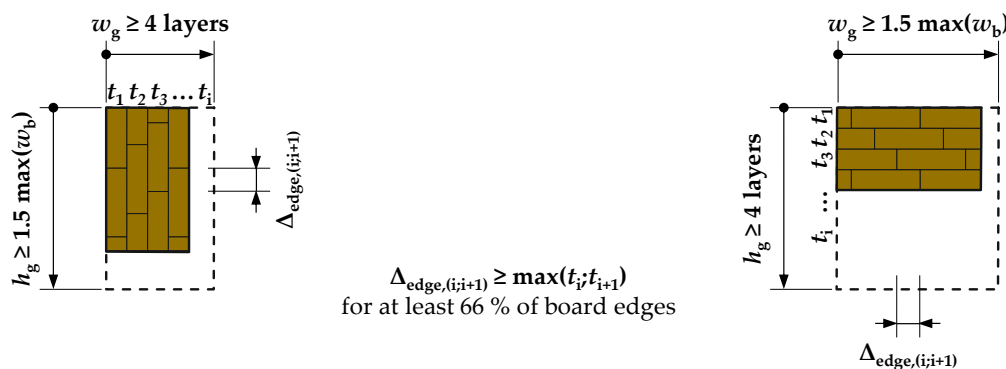


Figure 4-32: Proposed minimum requirements on the cross-section of flex_GLT beams (a) type A and (b) type B for a safe application in practise.

The presented stochastic-numerical beam model was successfully applied and validated to model the bending properties of unidirectionally laminated engineered timber products which may also include an arbitrary share of arbitrarily in width reduced boards/lamellas. Finally, based on simulation results load-bearing models for flex_GLT types A and B were developed and successfully validated by means of experimental investigations and results from literature.

Chapter 5: Orthogonally Laminated Engineered Timber Products

In this chapter the results of the stochastic-numerical beam model adapted for orthogonally laminated engineered timber products are presented. Hereby the focus is set on flex_CLT beams. System and size effects are analysed and discussed for the newly developed flex_CLT beams.

5-1 Overview

In the following, the results of the virtual bending tests conducted on orthogonally laminated engineered timber products are presented and discussed. For all cases 10^3 virtual tests were carried out for each combination of the investigated parameters. The length of the boards used was fixed with $l_b = 4$ m, which is a common dimension in Austria. The finger joints were placed according to the procedure presented in [Section 2-8](#). As the strength of the boards is dependent on the board length (see [Section 2-7.1.3](#)), a fixed reference length of $l_{b,ref} = 2.0$ m was used within the presented load-bearing models. This reference length was also anchored in the former glulam standard [EN 1194 \[37\]](#). Similar to the tensile strength also the bending strength is introduced assuming again a constant bending moment over the reference length $l_{b,ref} = 2.0$ m. The used input parameters for the load-bearing models are summarised in [Annex D-2](#), i.e. the tensile strength of the boards, $f_{t,0,b,ref}$, and of the finger joints, $f_{t,FJ,ref}$, as well as the bending strength $f_{m,b,ref}$.

5-2 flex_CLT

In this section the mechanical properties of flex_CLT are analysed by means of the stochastic-numerical beam model. [Figure 5-1](#) illustrates loading situations or use cases of flex_CLT, namely as beam, where the lamellas are loaded edgewise, and as slab, with flatwise loaded lamellas. The detailed production process of flex_CLT is described in [Section 3-2](#). The main difference to conventional cross laminated timber (CLT) is the structural edge-bonding of the boards. The random occurrence of lengthwise split lamellas is also a common fact in CLT elements as used nowadays; this circumstance is, however, usually neglected or if used as lintels or beams mechanical properties are subject to great uncertainties and still unknown. The results are compared and validated with investigations carried out within the FFG BRIDGE research project “flex_GLT-CLT-beams” (No. 877111), in particular it is referred to the test and research report [Sieder & Brandner \[66\]](#). Based on the layup of the experimental campaign the board thickness was fixed with $t_b = 30$ mm for all flex_CLT investigations.

(a) flex_CLT beams – edgewise loaded lamellas

flex_CLT slab – flatwise loaded lamellas (b)

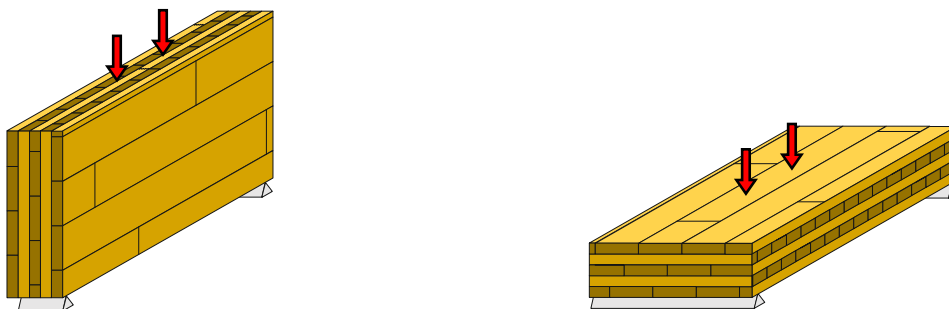


Figure 5-1: Loading situations of flex_CLT (a) beams with edgewise loaded lamellas and (b) slabs with flatwise loaded lamellas.

5-2.1 flex_CLT beams – Edgewise Loaded Lamellas

5-2.1.1 Bending Properties of flex_CLT beams

The bending properties of flex_CLT beams are influenced by various system and/or size effects, like illustrated in **Figure 5-2**.

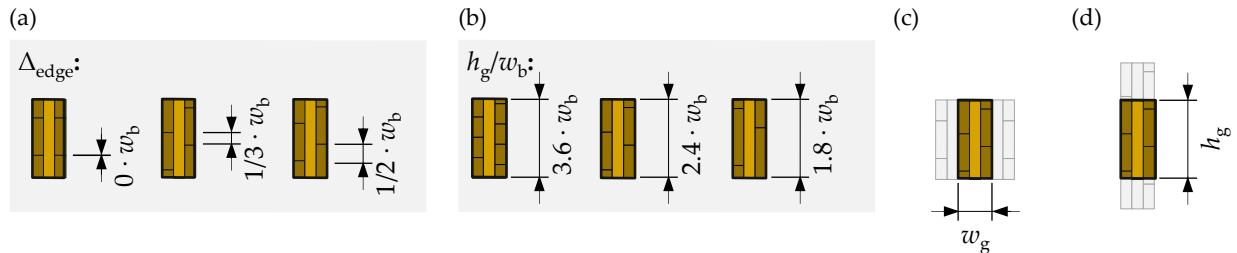


Figure 5-2: Possible influences on the bending properties of flex_CLT beams: (a) the overlap of the board edges of neighbouring longitudinal layers, (b) the number of boards over the beam depth, (b) the number of longitudinal layers (width effect) and (c) the depth of the beam (depth effect).

The first possible influence on the bending properties comes from the overlap of the board edges between neighbouring longitudinal layers within the cross-section; see **Figure 5-2 (a)**. The second possible impact on the bending properties is the number of boards/lamellas over the beam depth; see **Figure 5-2 (b)**. The third effect in **Figure 5-2 (c)** accounts for flex_CLT beam width and the number of longitudinal layers activating parallel system effects. The last influence in **Figure 5-2 (d)** addresses the depth effect, like known from conventional glulam. These mentioned influences on the bending properties of flex_CLT beams are presented and discussed in the following.

Overlap of Board Edges of Neighbouring Longitudinal Layers – flex CLT beams

In order to analyse the influence of the overlap of the board edges on the bending strength of flex_CLT beams, three sets of beams with different overlaps $\Delta_{\text{edge}} = \{0; 33; 50\}$ mm were simulated. The beams feature a width of $w_g = 90$ mm (three layers), a depth of $h_g = 360$ mm and are built up from boards of group GI (T14) featuring a width of $w_b = 100$ mm. The results for the bending properties $\{f_{m,g}; E_{m,g}\}$ of the virtually tested beams are summarised in **Table 5-1** and illustrated in **Figure 5-3**. As the results indicate, no significant influence of the overlap on the bending strength $f_{m,g}$ was observed, neither on the mean nor on the 5 %-quantile level. The same conclusion can be drawn for the modulus of elasticity $E_{m,g}$.

Table 5-1: Main statistics of the bending strength $f_{m,g}$ and modulus of elasticity $E_{m,g}$ calculated from 10^3 virtually tested flex_CLT beams (for each combination) at different overlaps of board edges of neighbouring longitudinal layers $\Delta_{edge} = \{0; 33; 50\}$ mm featuring a width of $w_g = 90$ mm (three layers) and a depth of $h_g = 360$ mm, built up from boards of group GI (T14) with dimensions of $w_b = 100$ mm and $t_b = 30$ mm.

Overlap Δ_{edge} [mm]		GI (T14)		
		0 ($0 \cdot w_b$)	33 ($1/3 \cdot w_b$)	50 ($1/2 \cdot w_b$)
$f_{m,g}$	mean [MPa]	25.9	26.1	26.0
	COV [%]	14.7	15.1	15.2
	$\chi_{05,LN}$ [MPa]	20.0	20.1	19.9
$E_{m,g}$	mean [MPa]	10,594	10,636	10,590
	COV [%]	6.1	5.7	6.0

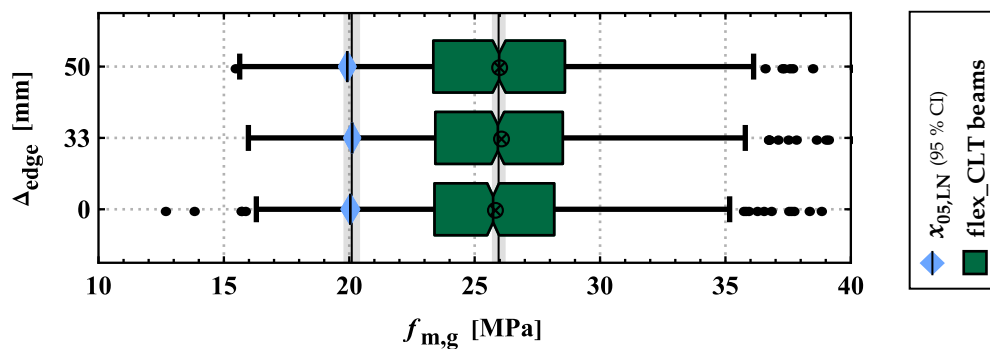


Figure 5-3: Boxplots of the bending strength $f_{m,g}$ of flex_CLT beams at different overlaps of board edges of neighbouring longitudinal layers $\Delta_{edge} = \{0; 33; 50\}$ mm featuring a width of $w_g = 90$ mm (three layers) and a depth of $h_g = 360$ mm, built up from boards of group GI (T14) with a width of $w_b = 100$ mm.

Number of Boards over the Beam Depth – flex CLT beams

For flex_CLT beams, the number of boards over the beam depth may influence the bending properties as well. In order to analyse this influence three sets of beams with different board widths $w_b = \{100; 150; 200\}$ mm but constant beam depth of $h_g = 360$ mm, resulting in ratios of $h_g/w_b = \{3.6; 2.4; 1.8\}$, were simulated. The beams featured a width of $w_g = 90$ mm (three layers) and are built up from boards of group GI (T14). The results for the bending properties $\{f_{m,g}; E_{m,g}\}$ of the virtually tested beams are summarised in **Table 5-2** and illustrated in **Figure 5-4**.

The mean value as well as the coefficient of variation of the bending strength are slightly increasing with decreasing ratio h_g/w_b , i.e. with decreasing number of boards over the beam depth. As a consequence, the 5 %-quantile value of the bending strength is almost constant (slightly decreasing) for all ratios. The mean value of the modulus of elasticity in bending $E_{m,g,mean}$ is not influenced by the number of boards over the beam depth, whereas, as expected, the coefficient of variation is decreasing with increasing ratio h_g/w_b .

Table 5-2: Main statistics of the bending strength $f_{m,g}$ and modulus of elasticity $E_{m,g}$ calculated from 10^3 virtually tested flex_CLT beams (for each combination) with different number of boards over the beam depth $w_g/w_b = \{3.6; 2.4; 1.8\}$ or the board width $w_b = \{100; 150; 200\}$ mm featuring a width of $w_g = 90$ mm (three layers) and a depth of $h_g = 360$ mm, built up from boards of group GI (T14) with a thickness of $t_b = 30$ mm.

Board Width w_b [mm]		GI (T14)		
		100 ($w_g/w_b = 3.6$)	150 ($w_g/w_b = 2.4$)	200 ($w_g/w_b = 1.8$)
$f_{m,g}$	mean [MPa]	26.1	26.3	26.5
	COV [%]	15.1	16.0	17.1
	$\chi_{05,LN}$ [MPa]	20.1	19.9	19.6
$E_{m,g}$	mean [MPa]	10,636	10,608	10,637
	COV [%]	5.7	6.6	6.9

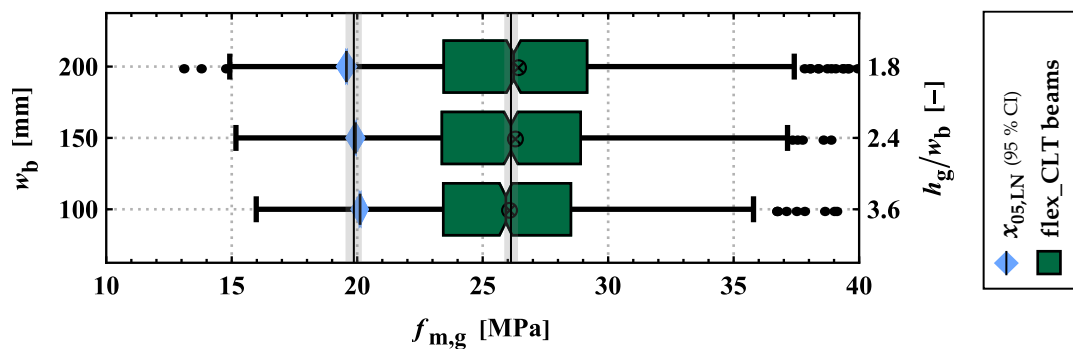


Figure 5-4: Boxplots of the bending strength $f_{m,g}$ of flex_CLT beams with different number of boards over the beam depth $h_g/w_b = \{3.6; 2.4; 1.8\}$ given different board widths $w_b = \{100; 150; 200\}$ mm featuring a width of $w_g = 90$ mm (three layers) and a depth of $h_g = 360$ mm, built up from boards of group GI (T14).

Beam Width – flex CLT beams

Within flex_CLT beams, a multiple number of lamellas are in the bending-tension zone. The number is dependent on the width of the beam w_g and the thickness of the boards/lamellas t_b which is equal to the thickness of the corresponding layer. The multiple boards acting in a parallel system enable load sharing and redistributions after partial failure(s). The results of randomly built up flex_CLT beams featuring a depth of $h_g = 360$ mm and a width of $w_g = \{90; 150; 270\}$ mm or $n_{lay} = \{3; 5; 9\}$ are summarised in **Table 5-3**. All beams are built up of boards from group GI (T14) featuring a width of $w_b = 100$ mm. Additionally, the number of longitudinal layers ($n_{lay,par}$) is stated.

The mean value of the modulus of elasticity $E_{m,g,mean}$ remains unaffected by variation of the beam width and is on the same level as for conventional glulam. The coefficient of variation, on the other hand, is decreasing with increasing beam width.

The mean value of the bending strength is increasing with increasing number of layers, whereas the coefficient of variation is decreasing. As a consequence, the 5 %-quantile value of the bending strength $f_{m,g,05,LN}$ is increasing with increasing number of layers. **Figure 5-5** shows boxplots of the bending strength $f_{m,g}$ in dependence of the beam width of flex_CLT beams. The

5 %-quantile values of the bending strength in dependency of the number of layers can be described via a power function with a power coefficient of $k_{w,flexCLT-beam,05} = 0.14$. Also, the mean value of the bending strength is rising with the number of parallel acting boards/layers. One reason may be the better load sharing and redistribution due to the layers perpendicular to the span direction. Flaig [70] found similar tendencies in his experimental investigations, i.e. slightly increasing mean and 5 %-quantile values. Based on his experimental results, a power coefficient of approximately $k_{w,Flaig,05} = 0.10$ can be calculated.

Table 5-3: Main statistics of the bending strength $f_{m,g}$ and modulus of elasticity $E_{m,g}$ calculated from 10^3 virtually tested flex_CLT beams (for each combination) featuring different widths $w_g = \{90; 150; 270\}$ mm which correspond to $n_{lay} = \{3; 5; 9\}$ or $n_{lay,par} = \{2; 3; 5\}$, built up from boards of group GI (T14) with dimensions $w_b = 100$ mm and $t_b = 30$ mm.

		GI (T14)		
Width w_g [mm]		90	150	270
$n_{lay,par}$ [-]		2.0	3.0	5.0
$f_{m,g}$	mean [MPa]	26.1	27.1	27.6
	COV [%]	15.1	11.5	9.3
	$x_{05,LN}$ [MPa]	20.1	22.2	23.6
$E_{m,g}$	mean [MPa]	10,636	10,696	10,745
	COV [%]	5.7	4.8	3.6

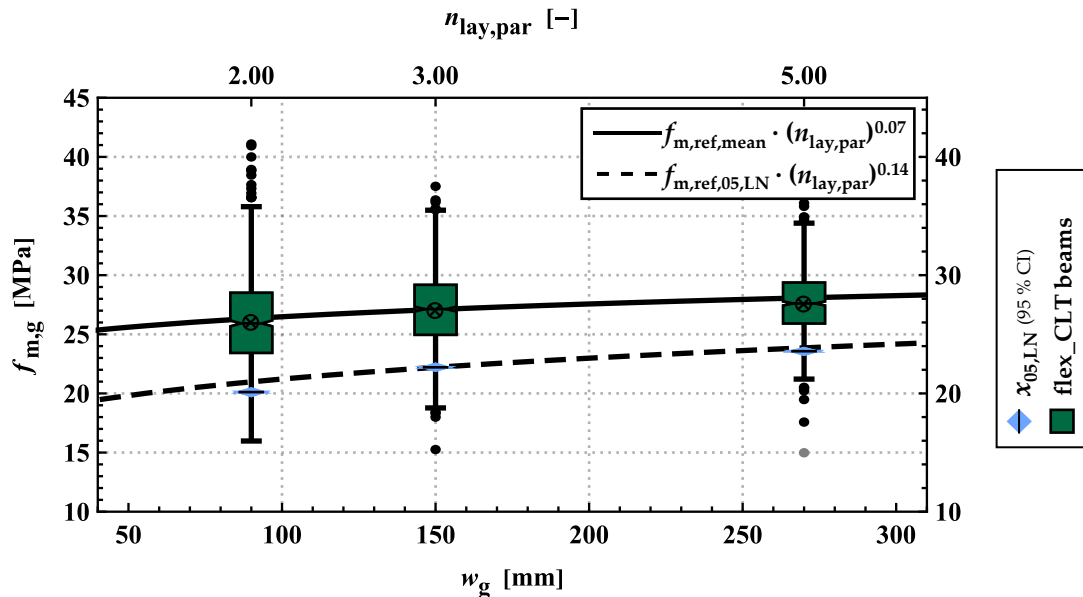


Figure 5-5: Boxplots of the bending strength $f_{m,g}$ of virtually tested flex_CLT beams featuring different widths $w_g = \{90; 150; 270\}$ mm which correspond to $n_{lay,par} = \{2; 3; 5\}$ built up from boards of group GI (T14) with dimensions $w_b = 100$ mm and $t_b = 30$ mm.

Beam Depth – flex_CLT beams

The influence of the beam depth on the bending strength is known from timber and engineered timber products like glulam (see [2, 4, 5, 28, 31, 67] and Section 4-2.1). To quantify the influence of the depth on the bending properties of flex_CLT beams, virtually bending tests on

such beams were conducted featuring a width of $w_b = 90$ mm (three layers) and depths of $h_g = \{150; 300; 360; 600\}$ mm built up from boards of both groups with a width $w_b = 100$ mm. The results are summarised in **Table 5-4**.

With increasing beam depth the bending strength is decreasing on the mean and stays almost constant at the 5 %-quantile level. The mean value of the modulus of elasticity $E_{m,g}$ is unaffected by the beam depth. The coefficient of variation, on the other hand, is decreasing with increasing beam depth.

Table 5-4: Main statistics of the bending strength $f_{m,g}$ and modulus of elasticity $E_{m,g}$ calculated from 10^3 virtually tested flex_CLT beams (for each combination) at different depths $h_g = \{150; 300; 360; 600\}$ mm featuring a width of $w_g = 90$ mm (three layers), built up from boards of both groups with dimensions of $w_b = 100$ mm and $t_b = 30$ mm.

Depth h_g [mm]		GI (T14)				GII (T24)			
		150	300	360	600	150	300	360	600
$f_{m,g}$	mean [MPa]	30.8	26.7	26.1	24.5	42.3	37.7	36.2	33.8
	COV [%]	22.1	16.4	15.1	11.2	19.3	14.5	12.8	10.1
	$x_{05,LN}$ [MPa]	20.6	19.9	20.1	20.2	29.4	29.4	29.1	28.5
	$x_{05,LN}/x_{05,LN,ref}^1$ [-]	1.02	0.99	1.00	1.00	1.06	1.03	1.02	1.00
$E_{m,g}$	mean [MPa]	10,641	10,627	10,636	10,618	13,195	13,128	13,136	13,164
	COV [%]	7.9	6.5	5.7	4.8	8.8	6.9	6.6	5.2

¹ $x_{05,LN,ref}$ with $h_g = 600$ mm

Figure 5-6 shows boxplots of the bending strength $f_{m,g}$ in dependence of the beam depth of flex_CLT beams. For the bending strength power coefficients of $k_{h,flexCLT-beam,mean} = 0.15$ for the mean values and $k_{h,flexCLT-beam,05} = 0.03$ for the 5 %-quantile values were found. **Flaig [70]** simulated bending tests on conventional CLT beams with different depths without edge bonding. He used boards from grading class S10 according to **DIN 4074-1 [9]** (\approx T14) and found almost no influence of the beam depth on the 5 %-quantile values of the bending strength. His results are well in line with the simulation results for GI (T14) and GII (T24). **Flaig [70]** argues that due to the multiple boards in the bending zone the beams are more homogeneous than glulam and therefore the depth effect is less pronounced. This should also be true for flex_GLT type A beams. There, however, a depth effect is present as shown in **Section 4-3.1.1**. The almost not existing depth effect for flex_CLT beams is probably or partly due to the existence of orthogonal layers which might ease load sharing and redistribution within flex_CLT and CLT beams.

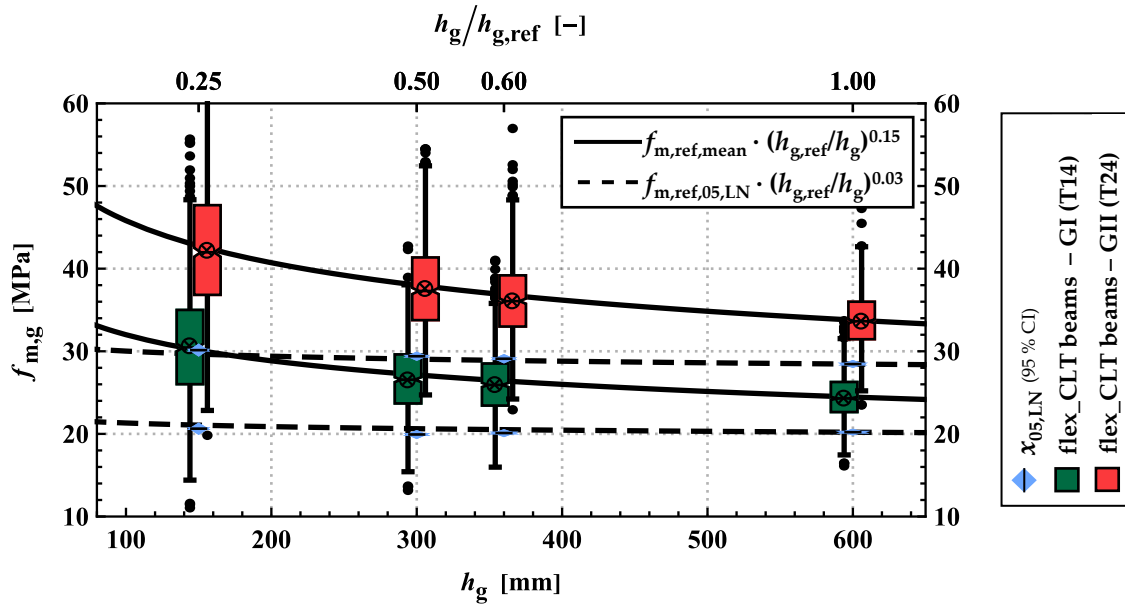


Figure 5-6: Boxplots of the bending strength $f_{m,g}$ of flex_CLT beams at different depths $h_g = \{150; 300; 360; 600\}$ mm featuring a width of $w_g = 90$ mm (three layers), built up from boards of both groups.

5-2.1.2 Load-Bearing Models for the Bending Strength of flex_CLT beams

Similar to glulam, it is aimed to predict the characteristic (5 %-quantile) bending strength of flex_CLT beams based on the tensile properties parallel to the grain of the boards $f_{t,0,b,05}$ and the finger joints $f_{t,FJ,05}$. In contrast to conventional glulam and similar to flex_GLT type A the boards/lamellas/layers are loaded edgewise, therefore the bending strength of the boards $f_{m,b,05}$ can also become a relevant parameter for the load-bearing model of flex_CLT beams, in particular for beams featuring a low ratio h_g / w_b . **Figure 5-7** shows the characteristic (5 %-quantile) bending strength of all simulated flex_CLT beams and of experimental results from **Sieder & Brandner [66]** (see also **Table Annex D-25** to **Table Annex D-28**), which were adjusted to a reference depth of $h_g = 600$ mm with a power coefficient of $k_{h,\text{flexCLT-beam},05} = 0.03$, which is almost negligible. Additionally, the expected value of the experimental results $E(\text{test})$ is shown. The boards used within the experimental campaign were visually graded and assigned to the strength class C24 acc. to **EN 338 [8]**. Regarding the bending strength of the boards the same assumptions were made as in **Section 4-3.1.2** for the load-bearing model of flex_GLT type A.

The basis of all load-bearing models for the characteristic (5 %-quantile) bending strength is the adapted model from **Brandner & Schickhofer [58]** for glulam in **Equation (4.5)**. All three different modelling approaches were derived by calibrating multiplication factors (underlined figures) to the simulation results; see **Equations (5.1) to (5.3)**. The system effect of parallel acting boards is taken into account with $k_{\text{sys},\text{flexCLT-beams}} = n_{\text{lay,par}}^{0.14}$; see **Section 5-2.1.1**. Again, three different models were calibrated to the simulation data based on {1} the tensile properties of the boards $\{f_{t,0,b,05}; \text{COV}(f_{t,0,b})\}$ in **Equation (5.1)**, {2} the bending properties of the boards $\{f_{m,b,05}; \text{COV}(f_{m,b})\}$ in **Equation (5.2)** and {3} a combination of the tensile and bending properties of the boards $\{f_{t,0,b,05}; \text{COV}(f_{t,0,b}); f_{m,b,05}\}$ in **Equation (5.3)**.

$$f_{m,g,05,(1)} = \underline{1.60} \cdot n_{lay,par}^{0.14} \cdot e^{1.15 \cdot COV(f_{t,0,b})} \cdot \text{Min} \left[f_{t,0,b,05} ; \frac{f_{t,FJ,05}}{\zeta_{new}} \right]^{0.80} \quad (5.1)$$

$$\text{with } \zeta_{new} = e^{1.55 \cdot COV(f_{t,0,b}) - 1.60 \cdot COV(f_{t,FJ})}$$

$$f_{m,g,05,(2)} = \underline{1.70} \cdot n_{lay,par}^{0.14} \cdot e^{1.15 \cdot (1.20 \cdot COV(f_{m,b}))} \cdot \text{Min} \left[f_{m,b,05} \cdot 0.65 ; \frac{f_{t,FJ,05}}{\zeta_{new,fm}} \right]^{0.80} \quad (5.2)$$

$$\text{with } \zeta_{new,fm} = e^{1.55 \cdot (1.20 \cdot COV(f_{m,b})) - 1.60 \cdot COV(f_{t,FJ})}$$

$$f_{m,g,05,(3)} = \underline{1.30} \cdot n_{lay,par}^{0.14} \cdot \left(\frac{f_{m,b,05}}{f_{t,0,b,05}} \right)^{0.80} \cdot e^{1.15 \cdot COV(f_{t,0,b})} \cdot \text{Min} \left[f_{t,0,b,05} ; \frac{f_{t,FJ,05}}{\zeta_{new}} \right]^{0.80} \quad (5.3)$$

$$\text{with } \zeta_{new} = e^{1.55 \cdot COV(f_{t,0,b}) - 1.60 \cdot COV(f_{t,FJ})}$$

with

$f_{m,g,05}$ characteristic (5 %-quantile) bending strength of flex_CLT beams
at $h_g = h_{g,ref} = 600$ mm [MPa]

$f_{t,0,b,05}$ characteristic (5 %-quantile) tensile strength of boards at a length of $l_{ref} = 2.0$ m [MPa]

$f_{m,b,05}$ characteristic (5 %-quantile) bending strength of the boards [MPa]

$f_{t,FJ,05}$ characteristic (5 %-quantile) tensile strength parallel to the grain of finger joints [MPa]

$COV(X)$ coefficient of variation [-]

$n_{lay,par}$ number of parallel acting (longitudinal) layers [-]

All load-bearing models for flex_CLT beams are capable of predicting the characteristic (5 %-quantile) bending strength of the simulated beams in a satisfactory manner ($\varepsilon_{mean} \approx 0$ MPa; $R^2 > 0.90$). The best results are achieved with model {3} considering the tensile properties parallel to the grain and the bending properties of the boards.

The bending strength values from the experimental investigations are significantly underestimated by model {1} and {2} ($R^2 < 0.75$). As before for flex_GLT type A beams a possible reason for this is given by the grading of the boards. The simulated boards can be assigned to strength class T14 for group GI and T24 for GII. For T-classes acc. to [EN 338 \[8\]](#) the ratio between the characteristic tensile strength and the characteristic bending strength is $f_{t,0,b,k}/f_{m,b,k} \approx 0.70$ and for C-classes acc. to [EN 338 \[8\]](#) the ratio is $f_{t,0,b,k}/f_{m,b,k} \approx 0.62$. This difference seems also to have an influence on the characteristic bending strength of flex_CLT beams and was implemented as strength ratio in model {3}. The mean residue of the prediction of model {3} is $\varepsilon_{mean} \approx 0$ MPa and the coefficient of determination is $R^2 = 0.88$. The overall characteristic bending strength of flex_CLT beams can be predicted by the load-bearing model in a satisfactory manner, which is true in particular for the simulations but less for the test outcomes. One possible reason for these deviations is that the board model is based on the tensile properties, whereas for flex_CLT beams the edgewise bending properties may play a more important role on the load-bearing capacity. Nonetheless, a conservative prediction of the heterogeneous test results in the experimental campaign in [Sieder & Brandner \[66\]](#) is possible.

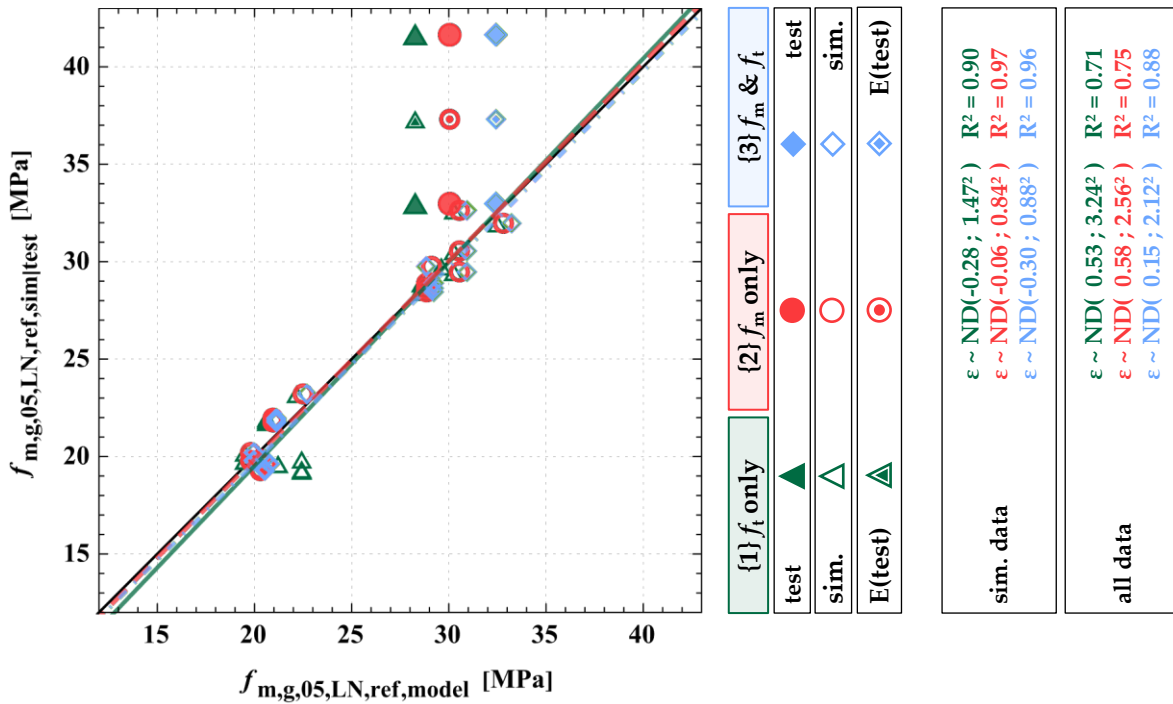


Figure 5-7: Results of bending test (5 %-quantiles) of flex_CLT beams adjusted to $h_{g,ref} = 600$ mm (with $k_{h,flexCLT-beam,05} = 0.03$) vs. prediction of models based on {1} only the tensile strength of the boards (f_t only; see Equation (5.1)), {2} only the bending strength of the boards (f_m only; see Equation (5.2)) and {3} the bending and the tensile strength of the boards (f_m & f_t ; see Equation (5.3)).

5-2.2 flex_CLT slabs – Flatwise Loaded Lamellas

5-2.2.1 Bending Properties of flex_CLT slabs

The bending properties of flex_CLT slabs are influenced by various geometric, system and/or size effects, as illustrated in Figure 5-8. The first possible impact on the bending strength is the alignment of boards within the slab, whether only boards in full cross-section are present or not; see Figure 5-8 (a). The second effect in Figure 5-8 (b) accounts for the width of flex_CLT slabs and thus for the number of longitudinal layers activating parallel system effects. The last influence in Figure 5-8 (c) addresses the depth effect, as known from conventional glulam. These mentioned influences on the bending strength of flex_CLT slabs are presented and discussed in the following.

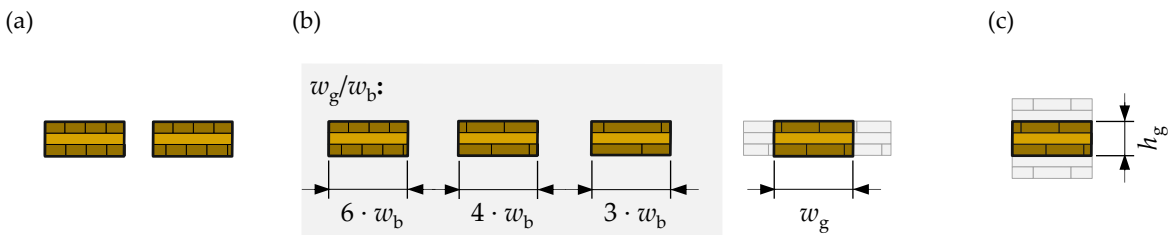


Figure 5-8: Possible influences on the bending strength of flex_CLT slabs: (a) alignment of the boards in equally oriented layers within the slab; (b) the number of boards at the bending-tension zone (width effect) and (c) the depth of the slabs, i.e. the number of layers within the layup.

Alignment of Board Edges within flex CLT slabs

In order to analyse the influence of the alignment of the board edges in equally oriented layers on the bending strength of flex_CLT slabs, two sets of slabs were simulated. The slabs featured a width of $w_g = 600$ mm, a depth of $h_g = 150$ mm, consisted of five layers ($n_{lay} = 5$) and were built up from boards of group GI (T14) with a width of $w_b = 150$ mm. This geometry reflects also the reference cross-section of conventional CLT; see [71–73]. In the first set the boards were aligned with the edge of the slab, meaning only boards with a full cross-section are present within the slab cross-section. In the second set the boards were randomly positioned in the slab, i.e. the board edges in equally oriented layers were shifted randomly. The results for the bending properties $\{f_{m,g}; E_{m,g}\}$ of the virtually tested slabs are summarised in **Table 5-5** and illustrated in **Figure 5-9**. No significant influence of the alignment of the boards within the cross-section on the bending strength $f_{m,g}$ was observed, neither on the mean nor on the 5 %-quantile level. The same conclusion can be drawn for the modulus of elasticity $E_{m,g}$.

Table 5-5: Main statistics of the bending strength $f_{m,g}$ and modulus of elasticity $E_{m,g}$ calculated from 10^3 virtually tested flex_CLT slabs (for each combination) featuring a width of $w_g = 600$ mm and a depth of $h_g = 150$ mm with different alignments of board edges, built up from boards of group GI (T14) with dimensions of $w_b = 150$ mm and $t_b = 30$ mm.

Alignment [-]		GI (T14)	
		random shift	only full boards
$f_{m,g}$	mean [MPa]	35.2	35.2
	COV [%]	14.2	14.4
	$x_{05,LN}$ [MPa]	27.4	27.3
$E_{m,g}$	mean [MPa]	10,526	10,522
	COV [%]	4.9	4.9

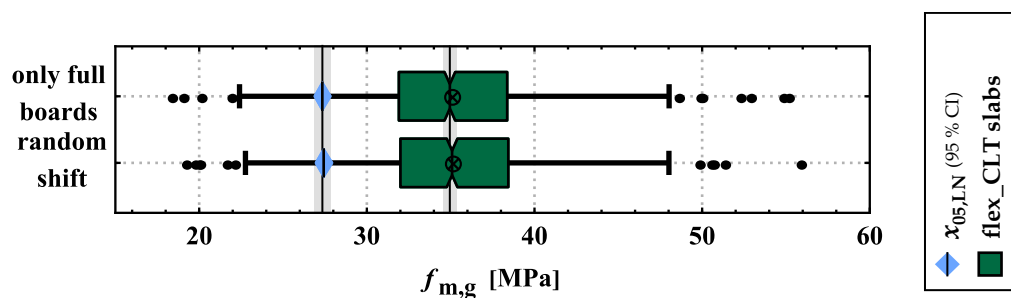


Figure 5-9: Boxplots of the bending strength $f_{m,g}$ of flex_CLT beams with different alignments of board edges featuring a width of $w_g = 600$ mm and a depth of $h_g = 150$ mm, built up from boards of group GI (T14) with a width $w_b = 150$ mm.

Beam Width – flex CLT slabs

Within flex_CLT slabs multiple number of lamellas are in the bending-tension zone. The number is dependent on the width of the beam w_g and the width of the boards w_b , i.e. $n_{par} = w_g / w_b$. The multiple boards acting in a parallel system enables load sharing and redistributions after partial failure(s). The results of randomly built up flex_CLT slabs featuring a depth of $h_g = 150$ mm consisting of five layers ($n_{lay} = 5$) and a width of $w_g = \{150; 300; 600; 1,200\}$ mm, i.e.

$n_{par} = \{1.0; 2.0; 4.0; 8.0\}$, are summarised in **Table 5-6**. All slabs are built up from boards from group GI (T14) with a width of $w_b = 150$ mm.

The mean modulus of elasticity $E_{m,g,mean}$ is unaffected by the beam width. The coefficient of variation, on the other hand, is decreasing with increasing beam width. The mean bending strength remains almost at a constant level and the coefficient of variation is decreasing with increasing width ratio w_g / w_b , and therefore, the 5 %-quantile value of the bending strength $f_{m,g,05,LN}$ increases.

Table 5-6: Main statistics of the bending strength $f_{m,g}$ and modulus of elasticity $E_{m,g}$ calculated from 10³ virtually tested flex_CLT slabs (for each combination) featuring different widths $w_g = \{150; 300; 600; 1,200\}$ mm, built up from boards of group GI (T14) with dimensions $w_b = 150$ mm and $t_b = 30$ mm.

Width w_g [mm]		GI (T14)			
		150	300	600	1,200
$f_{m,g}$	mean [MPa]	36.2	36.1	35.2	34.6
	COV [%]	24.7	19.1	14.2	10.1
	$\chi_{05,LN}$ [MPa]	23.0	25.8	27.4	29.1
	$\chi_{05,LN}/\chi_{05,LN,ref}^1$ [-]	0.84	0.94	1.00	1.06
$E_{m,g}$	mean [MPa]	10,519	10,532	10,526	10,569
	COV [%]	8.5	6.6	4.9	3.6

¹ ... $\chi_{05,LN,ref}$ with $w_g = 600$ mm

Figure 5-10 shows boxplots of the bending strength $f_{m,g}$ in dependence of the beam width of flex_CLT slabs. The relationships between statistics of the bending strength and the width of flex_CLT slabs or more precisely the ratio w_g / w_b can be described via a power function, for example with a power coefficient of $k_{w,flexCLT-slabs,05} = 0.10$ for the 5 %-quantile values.

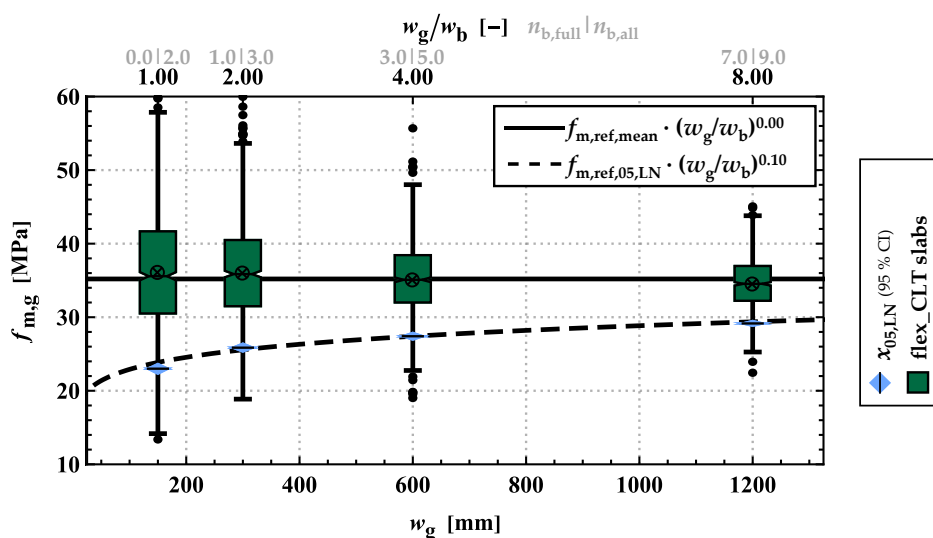


Figure 5-10: Boxplots of the bending strength $f_{m,g}$ of the virtually tested flex_CLT slabs at different widths $w_g = \{150; 300; 600; 1,200\}$ mm featuring a depth of $h_g = 150$ mm and $n_{lay} = 5$, built up from boards of group GI (T14) with dimensions $w_b = 150$ mm and $t_b = 30$ mm.

Figure 5-11 shows the boxplots of the bending strength $f_{m,g}$ relative to the 5 %-quantile values of the tensile strength $f_{t,0,b,05}$ in dependence of the width ratio w_g/w_b of flex_CLT slabs featuring a width of $w_g = \{200; 600; 1,200\}$ mm and built up with boards from GI (T14) and board widths of $w_b = \{100; 150; 200\}$ mm.

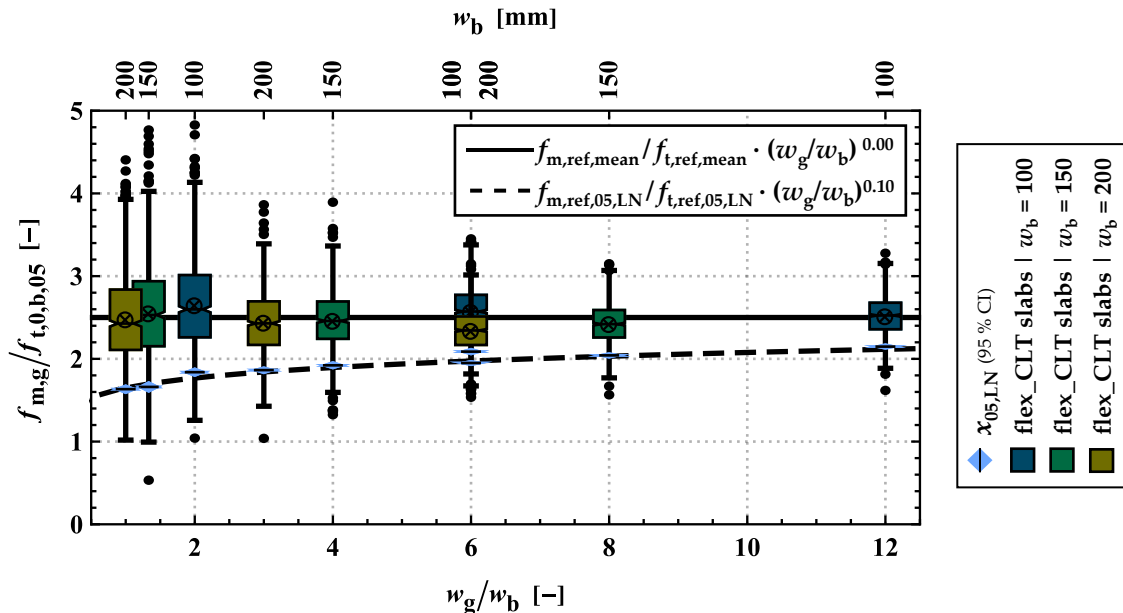


Figure 5-11: Boxplots of the relative bending strength $f_{m,g}/f_{t,0,b,05}$ of the virtually tested flex_CLT slabs at different widths $w_g = \{200; 600; 1,200\}$ mm featuring a depth of $h_g = 150$ mm and $n_{lay} = 5$, built up from boards of group GI (T14) with dimensions $w_b = \{100; 150; 200\}$ mm and $t_b = 30$ mm.

Also for different combinations of slab widths w_g and board widths w_b , the increase in the 5 %-quantile values of the bending strength can be described with a power coefficient of $k_{w,flexCLT-slabs,05} = 0.10$. The observations made generally regarding the width-effect for flex_CLT slabs, of approximately constant mean values and the decreasing coefficient of variation with increasing number of parallel acting boards/lamellas are, consistent with the theoretical statistical background as the coefficient of variation decreases with the ratio of $n_{par}^{-0.5}$; see **Brandner [36]**.

Beam Depth – flex CLT slabs

To quantify the influence of the depth on the bending properties of flex_CLT slabs with various depths of $h_g = \{90; 150; 210\}$ mm, i.e. various $n_{lay} = h_g / t_b = \{3; 5; 7\}$ featuring a width of $w_g = 600$ mm and built up from boards of both groups with dimensions $w_b = 150$ mm and $t_b = 30$ mm were simulated. The results are summarised in **Table 5-7**.

The bending strength is decreasing with increasing beam depth on the mean as well as the 5 %-quantile level; the same holds for the coefficient of variation. The mean modulus of elasticity $E_{m,g,mean}$ is widely unaffected by the beam depth and is on the same level as conventional glulam. The coefficient of variation, on the other hand, is decreasing with increasing beam depth.

Table 5-7: Main statistics of the bending strength $f_{m,g}$ and modulus of elasticity $E_{m,g}$ calculated from 10^3 virtually tested flex_CLT beams (for each combination) at different depth $h_g = \{90; 150; 210\}$ mm featuring a width of $w_g = 600$ mm, built up from boards of both groups with dimensions of $w_b = 150$ mm and $t_b = 30$ mm.

Depth h_g [mm]		GI (T14)			GII (T24)		
		90	150	210	90	150	210
$f_{m,g}$	mean [MPa]	41.6	35.2	34.4	58.8	48.7	46.6
	COV [%]	17.0	14.2	11.9	15.1	13.2	11.0
	$\chi_{05,LN}$ [MPa]	30.9	27.4	28.1	45.3	38.9	38.7
	$\chi_{05,LN}/\chi_{05,LN,ref}^1$ [-]	1.13	1.00	1.02	1.16	1.00	0.99
$E_{m,g}$	mean [MPa]	10,241	10,526	10,623	12,350	12,858	13,051
	COV [%]	8.4	4.9	4.5	8.9	5.4	5.1

¹ ... $\chi_{05,LN,ref}$ with $h_g = 150$ mm

Figure 5-12 shows boxplots of the bending strength $f_{m,g}$ in dependence of the beam depth of flex_CLT slabs. For the bending strength a power coefficient of $k_{h,flexCLT-slabs,mean} = 0.20$ for the mean value and $k_{h,flexCLT-slabs,05} = 0.10$ for the 5 %-quantile value were found. This value is well within the range $k_{h,05} = 0.10 \div 0.20$ found in the literature for glulam and conventional CLT (see [2, 5, 16, 58, 68, 71]).

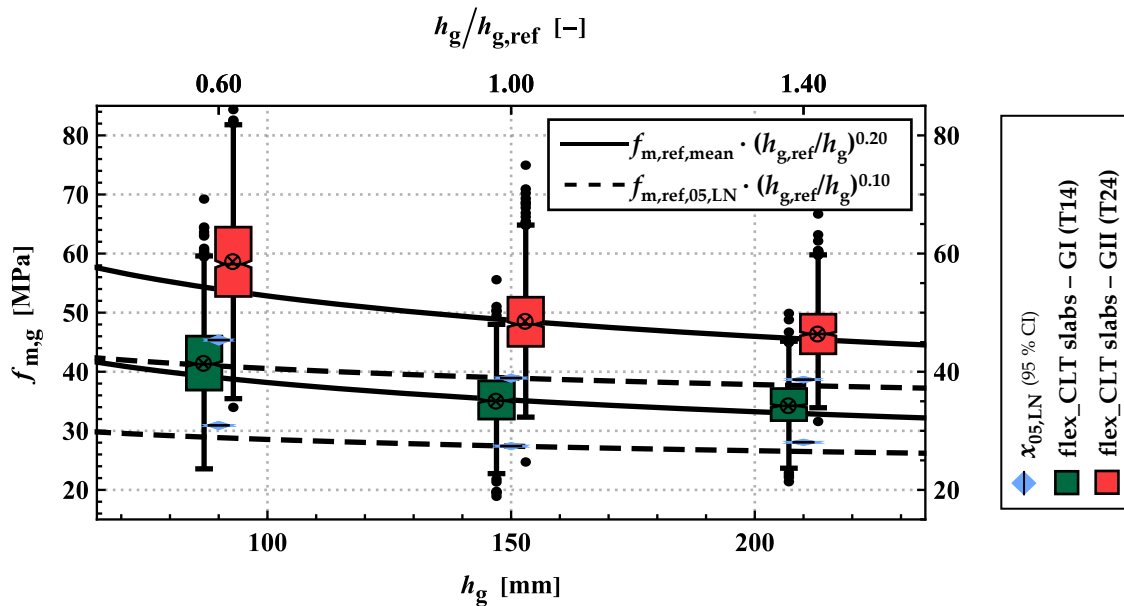


Figure 5-12: Boxplots of the bending strength $f_{m,g}$ of flex_CLT slabs at different depths of $h_g = \{90; 150; 210\}$ mm, i.e. $n_{lay} = \{3; 5; 7\}$ featuring a width of $w_g = 600$ mm, built up from boards of both groups with a width of $w_b = 150$ mm.

5-2.2.2 Load-Bearing Models for the Bending Strength of flex_CLT slabs

Similar to other board-based engineered timber products, it is aimed to predict the characteristic (5 %-quantile) bending strength of flex_CLT slabs based on the characteristic (5 %-quantile) tensile strengths parallel to the grain of the boards $f_{t,0,b,05}$ and the finger joints $f_{t,FJ,05}$. A model for conventional CLT as proposed by **Jöbstl et al. [72]** is shown in **Equation (5.4)**. **Equation (5.5)** gives a new model which is based on the herein generated simulation results; see

also **Table Annex D-29** to **Table Annex D-31**. For the new model a similar approach as in **Brandner & Schickhofer [58]** was chosen to correctly capture the influence of the coefficient of variation of the tensile strength parallel to the grain even beyond the simulated board properties and to incorporate the tensile strength of the finger joints. Additionally, a simplified model from **Brandner et al. [71]** is given in **Equation (5.6)**.

Figure 5-13 (a) shows the simulation results for flex_CLT slabs adjusted to a reference depth of $h_g = 150$ mm with a power coefficient of $k_{h,\text{flexCLT-slabs},05} = 0.10$ versus the predictions of the different models. The model {1} from **Jöbstl et al. [72]** (**Equation (5.4)**) is in good agreement for flex_CLT slabs despite the missing consideration of the finger joint strength. The new model {2} (**Equation (5.5)**) achieves comparable results. The simplified model {3} from **Brandner et al. [71]** (**Equation (5.6)**) underestimates the bending strength of flex_CLT slabs for the higher strength class GII (T24). This is due to the simplification of the model in combination with the coefficient of variation of the tensile strength parallel to the grain $\text{COV}(f_{t,0,b})$ slightly below 30 %. Nonetheless, it is capable of conservatively estimating the bending strength of flex_CLT slabs.

$$f_{m,g,05,\text{Jöbstl}} = \left(\begin{cases} 1.1 & n_{\text{par}} \geq 4 \\ 1.0 + \frac{(n_{\text{par}} - 1)}{30} & n_{\text{par}} < 4 \end{cases} \right) \cdot (1.61 - 4.6 \cdot \text{COV}(f_{t,0,b})) \cdot f_{t,0,b,05}^{0.80} \quad (5.4)$$

$$f_{m,g,05,\text{new}} = 1.95 \cdot n_{\text{par}}^{0.10} \cdot e^{1.15 \cdot \text{COV}(f_{t,0,b})} \cdot \text{Min} \left[f_{t,0,b,05} ; \frac{f_{t,\text{FJ},05}}{\zeta_{\text{new}}} \right]^{0.80} \quad (5.5)$$

with $\zeta_{\text{new}} = e^{1.55 \cdot \text{COV}(f_{t,0,b}) - 1.60 \cdot \text{COV}(f_{t,\text{FJ}})}$

$$f_{m,g,05,\text{Brandner}} = a_{05} \cdot \left(1.0 + 0.1 \cdot \frac{n_{\text{par}} - 1}{n_{\text{par}}} \right) \cdot \text{Min} \left[f_{t,0,b,05} ; \frac{f_{t,\text{FJ},05}}{\zeta_{05}} \right]^{0.80} \quad (5.6)$$

with $a_{05} = \begin{cases} 3.1 & \text{COV}(f_{t,0,b}) \geq 30\% \\ 2.7 & \text{COV}(f_{t,0,b}) < 30\% \end{cases}$
 $\zeta_{05} = \begin{cases} 1.4 & \text{COV}(f_{t,0,b}) \geq 30\% \\ 1.2 & \text{COV}(f_{t,0,b}) < 30\% \end{cases}$

with

$f_{m,g,05}$ characteristic (5 %-quantile) bending strength of flex_CLT slabs
at $h_g = h_{g,\text{ref}} = 150$ mm [MPa]

$f_{t,0,b,05}$ characteristic (5 %-quantile) tensile strength of boards at a length of $l_{\text{ref}} = 2.0$ m [MPa]

$f_{t,\text{FJ},05}$ characteristic (5 %-quantile) tensile strength of finger joints [MPa]

$\text{COV}(X)$ coefficient of variation [-]

n_{par} number of parallel acting boards (w_g/w_b) [-]

w_g width of slab [mm]

w_b width of board [mm]

Figure 5-13 (b) shows additionally to the simulations also test data of conventional CLT taken from **Brandner et al. [71]**, adjusted to a reference depth of $h_g = 150$ mm with a power coefficient of $k_{h,\text{flexCLT-slabs},05} = 0.10$ versus the predictions of the different models. Almost all CLT slabs within the test sample were produced without edge-bonding in contrast to the edge-bonded

flex_CLT slabs. Nevertheless, conventional CLT is capable of load sharing between lamellas in a similar manner as flex_CLT slabs and therefore the test data taken from [Brandner et al. \[71\]](#) is used as a benchmark for the developed load-bearing model of flex_CLT slabs. Model {1} overestimates three test series due to the missing consideration of the finger joint strength. The best prediction of the experimental data is achieved by the new model {2}, which is indicated by the lowest mean residue of $\varepsilon_{\text{mean}} \approx -0.86$ MPa and the highest coefficient of determination is $R^2 = 0.39$. Even though the simplified model {3} proposed by [Brandner et al. \[71\]](#) exhibits a lower coefficient of determination ($R^2 = 0.20$), it is still capable of providing a conservative estimate of the bending strength of flex_CLT and conventional CLT slabs, despite using fewer input parameter. The overall characteristic bending strength of flex_CLT slabs can be predicted by the load-bearing models {2} and {3} in a satisfactory manner.

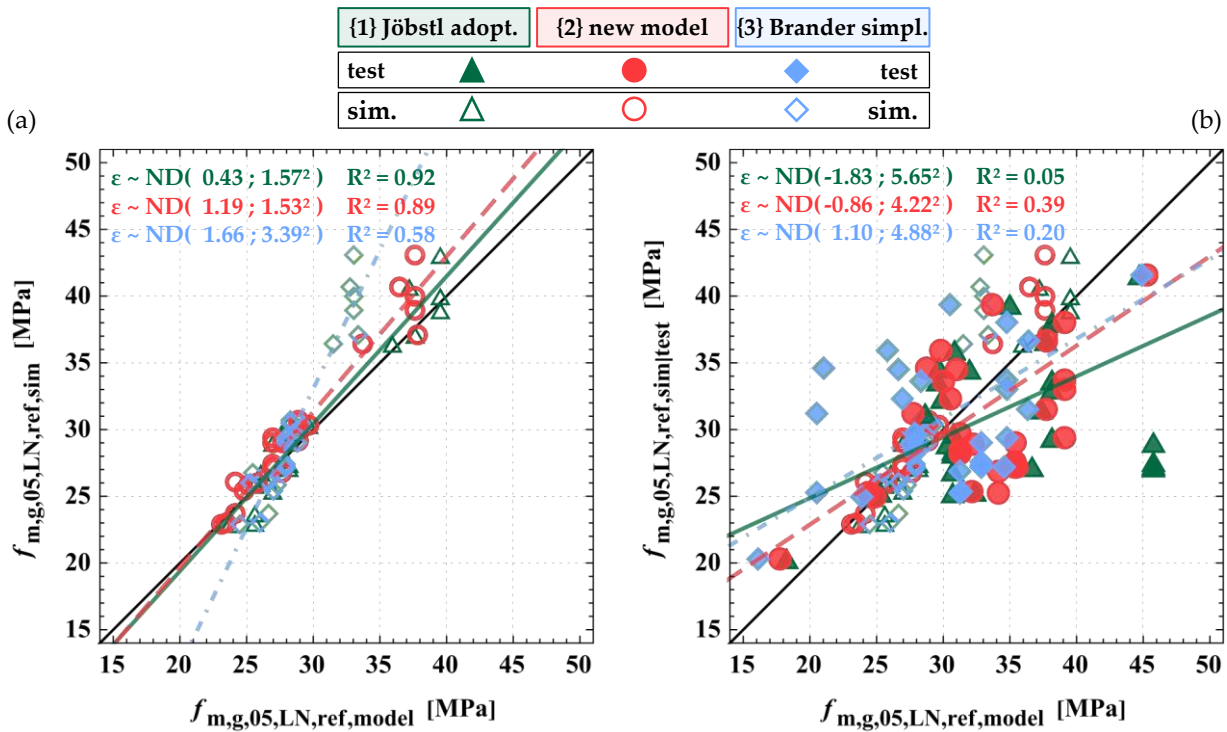


Figure 5-13: Results of (a) virtual bending tests (5 %-quantiles) conducted on flex_CLT slabs and (b) virtual and real test data of conventional CLT from [Brandner et al. \[71\]](#) adjusted to $h_{g,\text{ref}} = 150$ mm (with $k_{\text{th},\text{flexCLT-slabs},05} = 0.10$) vs. model predictions according to {1} the adapted model from [Jöbstl et al. \[72\]](#) (see [Equation \(5.4\)](#)), {2} the new model in [Equation \(5.5\)](#) and {3} the simplified model proposed in [Brandner et al. \[71\]](#) (see [Equation \(5.6\)](#)).

5-3 Intermediate Conclusions

In this chapter the stochastic-numerical beam model as introduced in [Chapter 3](#) is applied to simulate the bending properties of orthogonally laminated engineered timber products. Due to the orthogonal layout different system and size effects occur within flex_CLT in contrast to unidirectional engineered timber products, such as glulam or flex_GLT. The main difference being the cross layers with a rather low shear rigidity compared to shear parallel to the

grain. These influences on the bending strength were analysed for flex_CLT beams and slabs separately as they were found to be quite different.

For flex_CLT beams a depth effect with a power coefficient of $k_{h,\text{flexCLT-beam},05} = 0.03$ was observed, which is lower than found in conventional glulam or flex_GLT. A possible reason for this is the better load sharing and redistribution potential due to the orthogonal, flexible layers, a circumstance which can be also experienced by testing CLT beams. In contrast, the overlap of the board edges between equally oriented layers was found to have no influence on the load-bearing capacity in bending at all. Also the number of boards over the beam depth did not influence the bending strength significantly. On the other hand a higher characteristic (5 %-quantile) bending strength was found for beams with a higher number of longitudinal layers ($n_{\text{lay,par}}$) for flex_CLT beams, which could be described by means of a power model and a power coefficient of $k_{w,\text{flexCLT-beam},05} = 0.14$.

For flex_CLT slabs a depth effect with a power coefficient of $k_{h,\text{flexCLT-slab},05} = 0.10$ was observed, which is similar to conventional glulam. The alignment of the board edges between equally oriented layers within the cross-section was found to have no influence on the load-bearing capacity in bending at all. The characteristic (5 %-quantile) bending strength increased with the number of parallel acting boards ($n_{\text{par}} = w_g / w_b$) in the bending tension zone with a power coefficient of $k_{w,\text{flexCLT-slabs},05} = 0.10$.

Similar to flex_GLT also for the layup of flex_CLT some minimal geometric requirements are advised, for the sake of a safety margin in the mechanical properties and in respect to the applicability of the above stated load-bearing models. Based on the simulations, the mentioned influences as well as the experimental bending tests the minimal requirements are illustrated in **Figure 5-14**. According to this, flex_CLT shall consist of at least three orthogonally oriented layers, similar to conventional CLT; see **EN 16351 [17]**. The minimum depth of flex_CLT beams should be at least 1.5 times the maximum board width used to build up the longitudinal layers. For flex_CLT slabs the minimum width is defined as 1.5 times the board width of the longitudinal layers. Such a regulation regarding the minimum width are currently missing for conventional CLT. This regulation is a precautionary measure to make sure that at least one whole board is always present over the depth or width of the flex_CLT beams or slabs. In contrast to flex_GLT, no requirements for the minimal offset of board edges are given as the orthogonal layers act also as a reinforcement for bending shear forces.

(a) flex_CLT beams – edgewise loaded lamellas

flex_CLT slab – flatwise loaded lamellas (b)



Figure 5-14: Proposed minimum geometric requirements on the cross-section of flex_CLT (a) beams and (b) slabs for a safe application in practise.

The presented stochastic-numerical beam model was also successfully applied to model the bending strength of orthogonally laminated engineered timber products which may also include arbitrarily in width reduced boards. Finally, load-bearing models for flex_CLT used as beams or slabs were developed, presented and validated with experimental investigations and results from the literature.

Chapter 6: Summary, Conclusions and Outlook

6-1 Summary and Conclusions

This thesis deals with the influence of lengthwise split boards on the load-bearing capacity of unidirectionally and orthogonally laminated engineered timber products. To be able to depict the influence of a random share of randomly in width lengthwise split boards/lamellas on such products, at first a probabilistic board model was developed to characterise the mechanical properties of Norway spruce boards in their full cross-section and for two strength classes as well as after they got split lengthwise. The probabilistic board model is afterwards implemented in the framework of a new three-dimensional stochastic-numerical beam model, which is also capable of depicting parallel system effects, i.e. to account for the interaction of boards/lamellas in the bending-tension zone of beams exposed to bending moments. The stochastic-numerical beam model successfully allows to depict the bending properties (strength and modulus of elasticity) as well as size and system effects of unidirectionally and orthogonally laminated engineered timber products featuring boards/lamellas which might be either loaded flat- or edgewise. The following passages offer a brief summary of the individual chapters:

The new probabilistic board model for the tensile properties parallel to the grain, as a conglomerate of a large number of probabilistic sub-models, is presented in **Chapter 2**. This model is capable of representing the global and local growth characteristics and also their local and global properties in tension parallel to the grain in longitudinal direction not only for boards in full cross-section, but it also enables to quantify the impact of lengthwise splitting after grading on the residual cross-section properties. In doing so, knots serve as surrogates for the bulk of local growth characteristics which are implicitly taken into account by calibrating the model parameters on large data bases. The probabilistic board model was successfully validated with test data from the literature as well as from own investigations. Based on the simulation results, functions to describe the mechanical properties in tension parallel to the grain of lengthwise split boards were defined for two strength classes GI (T14) and GII (T24) according to **EN 338 [8]**. Via these functions it is possible to derive the tensile properties parallel to the grain of arbitrarily in width reduced boards based on the full cross-section properties. Additionally, the probabilistic board model is also able to depict the influence of the board length on the tensile strength parallel to the grain in a satisfactory manner. Based on the results it is suggested to revise the current test standard **EN 408 [39]** in respect to the test length $l_{b,ref} = 9 \cdot w_b$ and to regulate the tensile properties in reference to a fixed free test length of $l_{b,ref} = 2.0$ m. With this reference length it can be almost guaranteed, that a knot cluster is present within the free test span, as well as the same number of knot clusters, independent of the board width.

The probabilistic board model in combination with the probabilistic characterisation of the finger joints is the basis for the three-dimensional stochastic-numerical beam model presented in **Chapter 3**. This beam model is the first, capable of depicting size and system effects for unidirectionally as well as orthogonally laminated engineered timber products with and without a specific share of randomly by lengthwise splitting in width reduced boards/lamellas.

In **Chapter 4** the newly developed stochastic-numerical beam model was applied to derive the bending properties of conventional glulam beams. The overall results are well in line with results and load-bearing models in the literature. This clearly indicates the applicability of the model to correctly depict the load-bearing behaviour of unidirectionally laminated beams. Hereby, the magnitude of depth effect currently anchored in the product standard **EN 14080 [16]** was confirmed. Based on physics and model predictions it is highly recommended to apply this depth effect also for beam depths above the reference depth of $h_{g,ref} = 600$ mm in particular as glulam beams exceeding 2,000 mm in depth are frequently used in wide-spanned timber constructions.

In combination with the new probabilistic board model for lengthwise split boards, the bending properties for resawn glulam beams were modelled for the first time within a stochastic framework. The results indicate that it is also possible to manufacture resawn glulam beams from lower glulam strength classes, which is currently not allowed; see standard **EN 14080 [16]**. Additionally, a new model to derive the characteristic (5 %-quantile) bending strength of resawn glulam beams is presented.

For the new unidirectionally laminated engineered timber product, namely flex_GLT, size and system effects as well as the arbitrary positioning of lengthwise split boards are analysed in **Chapter 4**. In most cases the characteristic (5 %-quantile) bending strength of the beam elements is not influenced at all by the lengthwise split boards as parallel system effects within the product counteract the lower tensile strength parallel to the grain of them. The bending strength is positively influenced by the number of parallel acting members in the bending tension zone (beam width). The depth effect, a decreasing bending strength with increasing beam depths, is more pronounced than within conventional glulam. Besides the analysis of size and system effects also load-bearing models for flex_GLT beams type A and B are presented and validated by means of independently conducted experimental tests. Finally, minimal geometric requirements are stated for both flex_GLT products, type A and B.

The stochastic-numerical beam model is also used to derive the bending properties of orthogonally laminated engineered timber products; see **Chapter 5**. Here, the focus is set on flex_CLT used as beams or slabs. Similar to flex_GLT, also for flex_CLT the arbitrary positioned and lengthwise split boards/lamellas have only a minor influence, if one at all, on the bending strength of these products. The same parallel system effects are observed as for flex_GLT beams. In contrast to conventional glulam and flex_GLT the depth effect is almost not present for flex_CLT beams. Based on the simulation results load-bearing models for flex_CLT beams and slabs are presented and validated with experimental tests and data taken from the literature. Additionally, minimal geometric requirements are defined for flex_CLT beams and slabs.

6-2 Outlook

Within the presented thesis system and size effects on the bending strength are presented and discussed for various engineered timber products, including the new products flex_GLT and flex_CLT. In the following, possible future investigations are proposed:

- (i) The probabilistic board model, as input for the stochastic-numerical beam model, is currently developed for the wood species Norway spruce and two strength classes. Extending the model to predict the bending strength, by incorporating additional strength classes and other wood species, would be beneficial for a deeper understanding of size and system effects, as they may differ from the investigated boards. Hereby, hardwood species are of utmost importance as they gain more and more importance as a building material and their different size effects are already partially known. Using knots as surrogates for local growth characteristics might become an even greater challenge for hardwood species as their occurrence is less regular as in softwoods or at least different to them.
- (ii) Regarding the stochastic-numerical beam model for orthogonally laminated engineered timber products, a potential extension would involve the implementation of conventional CLT without edge bonding, as well as the consideration of additional failure modes such as rolling shear and tension perpendicular to the grain. This would also enable the analysis of the influence of the edge bonding of the boards on the bending strength for the application as beam as well as slab.
- (iii) Additionally, other loading situations can be implemented into the finite element software, e.g. point supported slabs. In this case the maximum bending moments only occur in a quite small and localised area and therefore a higher bending strength could be used. Similar calculations were already made by [Frese \[4\]](#) for multi-girder glulam systems.
- (iv) Furthermore, the stochastic-numerical model can be extended to model the tensile properties of various engineered timber products. Hereby, only the implementation within the finite element software needs to be adapted as the tensile properties parallel to the grain of the individual boards are already part of the model.
- (v) Finally, an implementation of the stochastic-numerical beam model into open-source software would be beneficial to increase the availability of the tool as well as to cut down on computation time.

Chapter 7: References

- [1] Ehlbeck, J.; Colling, F.; Görlacher, R. Einfluß keilgezinkter Lamellen auf die Biegefestigkeit von Brettschichtholz: Entwicklung eines Rechenmodells. *Holz als Roh- und Werkstoff* **1985**, *1985*, 333–337.
- [2] Colling, F. Tragfähigkeit von Biegeträgern aus Brettschichtholz in Abhängigkeit von den festigkeitsrelevanten Einflussgrößen. Dissertation; Universität Fridericiana zu Karlsruhe, Karlsruhe: 1990.
- [3] Fink, G. Influence of varying material properties on the load-bearing capacity of glued laminated timber. Dissertation; ETH Zurich: 2014.
- [4] Frese, M. Computergestützte Verfahren zur pragmatischen Beurteilung der Tragwiderstände von Brettschichtholz: Zusammenfassung exemplarischer Simulationsstudien. Habilitationsschrift; KIT Scientific Publishing, Karlsruhe: 2016.
- [5] Blaß, H.J.; Frese, M.; Glos, P.; Denzler, J.K.; Linsenmann, P.; Ranta-Maunus, A. *Zuverlässigkeit von Fichten-Brettschichtholz mit modifiziertem Aufbau*; Technische Informationsbibliothek u. Universitätsbibliothek; Universitätsverlag: Hannover, Karlsruhe: 2008, ISBN 9783866442511.
- [6] Tapia, C. Variation of mechanical properties in oak boards and its effect on glued laminated timber. Dissertation; Eric Cuvillier; Universität Stuttgart.
- [7] EN 14081-1: 2016. *Timber structures – Strength graded structural timber with rectangular cross section: Part 1: General requirements*. European Committee for Standardization.
- [8] EN 338: 2016. *Structural timber — Strength classes*. European Committee for Standardization.
- [9] DIN 4074-1: 2012. *Sortierung von Holz nach der Tragfähigkeit: Teil 1: Nadelschmittholz*. Deutsches Institut für Normung.
- [10] Ehlbeck, J.; Colling, F.; Görlacher, R. Einfluss keilgezinkter Lamellen Biegefestigkeit Brettschichtholztraeger: Eingangsdaten für das Rechenmodell. *Holz als Roh- und Werkstoff* **1985**, 369–373.
- [11] Isaksson, T. Modelling the variability of Bending Strength in Structural Timber: Length and Load Configuration Effects. Dissertation; Lund Institute of Technology, Lund: 1999.
- [12] Brandner, R. *Stochastic system actions and effects in engineered timber products and structures*. Zugl.: Graz, Techn. Univ., Diss., 2012; Verl. der Techn. Univ. Graz: Graz: 2013, ISBN 9783851252637.
- [13] Olsson, A.; Briggert, A.; Oscarsson, J. Increased yield of finger jointed structural timber by accounting for grain orientation utilizing the tracheid effect. *Eur. J. Wood Prod.* **2019**, *77*, 1063–1077, doi:10.1007/s00107-019-01465-0.
- [14] Schickhofer, G.; Augustin, M. *Project INTELLIWOOD: working package 3: ‘Strength correspondence’*. Report LR 9808/4: 2001.
- [15] Kastner, E.; Schickhofer, G.; Brandner, R.; Unterwieser, H. *COMET 2.1.6 seperate: Untersuchung der Auswirkung des längsweisen Auftrennens auf das mechanische Potenzial von Brettschichtholzlamellen und daraus aufgebauten Brettschichtholzträgern, hinsichtlich ihrer Festigkeit und Steifigkeit*, holz.bau forschungs gmbh: 2011.
- [16] EN 14080: 2013. *Timber structures – Glued laminated timber and glued solid timber – Requirements*. European Committee for Standardization.
- [17] EN 16351: 2021. *Timber structures – Cross laminated timber – Requirements*. European Committee for Standardization.
- [18] Fink, G.; Kohler, J. *Zerstörungsfreie Versuche zur Ermittlung des Elastizitätsmodules von Holzbrettern*, Institut für Baustatik und Konstruktion, Eidgenössische Technische Hochschule Zürich: 2012.

- [19] Briggert, A.; Olsson, A.; Oscarsson, J. Prediction of tensile strength of sawn timber: models for calculation of yield in strength classes. *Mater Struct* **2020**, *53*, doi:10.1617/s11527-020-01485-w.
- [20] Alpo Ranta-Maunus. *Strength of European timber: Part 1. Analysis of growth areas based on existing test results*, VTT Technical Research Centre of Finland: 2009. Available online: <https://cris.vtt.fi/en/publications/strength-of-european-timber-part-1-analysis-of-growth-areas-based>.
- [21] Alexandra Thiel. *KnotInterpreter*; holz.bau forschungs gmbh: 2019.
- [22] Wolfram Research, Inc. *Mathematica*; Wolfram Research, Inc.: Champaign, Illinois: 2021.
- [23] Burger, N. *Einfluß der Holzabmessungen auf die Festigkeit von Schnittholz unter Zugbeanspruchung in Faserrichtung*. Zugl.: München, Techn. Univ., Diss., 1998, Als Ms. gedr; Shaker: Aachen: 1998, ISBN 3826543769.
- [24] Alexandra Thiel. *KnotLogger*; holz.bau forschungs gmbh: 2019.
- [25] Ehlbeck, J.; Colling, F. *Biegefestigkeit von Brettschichtholz in Abhängigkeit von Dichte, Elastizitätsmodul, Festigkeit und Keilzinkungen der Lamellen, der Lage der Keilzinkungen sowie von der Trägerhöhe.: Teil A: Karlsruher Untersuchungen*, Versuchsanstalt für Stahl, Holz und Steine, Universität Karlsruhe: 1987.
- [26] Colling, F.; Dinort, R. Die Ästigkeit des in den Leimbaubetrieben verwendeten Schnittholzes. *Eur. J. Wood Prod.* **1987**, *45*, 23–26, doi:10.1007/BF02612040.
- [27] Köhler, J. Reliability of timber structures. Dissertation; ETH Zurich, Zürich: 2007.
- [28] Ditlevsen, O.; Källsner, B. System effects influencing the bending strength of timber beams. *IFIP 8th WG 7.5 Working Conference on Reliability and Optimization of Structural Systems*: 1998.
- [29] Källsner, B.; Ditlevsen, O. Lengthwise bending strength variation of structural timber. *IUFRO/S5.02 Timber Engineering Meeting*.
- [30] Stan. *Stan*; Stan Development Team: 2020.
- [31] Sieder, R.; Brandner, R. A new probabilistic approach to model the tensile properties of split spruce boards and its application in engineered timber products. *Proceedings of INTER 8th Meeting*: 2021.
- [32] Sieder, R.; Brandner, R. Tensile properties of lengthwise split boards and their application in engineered timber products. *Proceedings phd seminar Stuttgart* **2022**.
- [33] Rebonato, R.; Jaeckel, P. *The Most General Methodology to Create a Valid Correlation Matrix for Risk Management and Option Pricing Purposes*, The Journal of Risk: 2000.
- [34] Scherfler, J. Versuchstechnische Ermittlung des längsweisen Auftrennens auf die Zugeigenschaften von festigkeitssortierten Brettern. Masterprojekt; Technische Universität Graz, Graz: 2022.
- [35] Fink, G.; Frangi, A.; Köhler, J. *Modelling the bending strength of glued laminated timber - considering the natural growth characteristics*, International council for research and innovation in building and construction: 2013.
- [36] Brandner, R. Stochastic Modelling in Timber Engineering. Habilitation; Graz University of Technology, Graz: 2018.
- [37] EN 1194: 1999. *Timber structures - Glued laminated timber - Strength classes and determination of characteristic values*. European Committee for Standardization.
- [38] ON B 1995-1-1: 2019. *Eurocode 5: Bemessung und Konstruktion von Holzbauten: Teil 1-1: Allgemeines – Allgemeine Regeln und Regeln für den Hochbau*. Austrian Standards Institute.
- [39] EN 408: 2012. *Timber structures - Structural timber and glued laminated timber - Determination of some physical and mechanical properties*. European Committee for Standardization.

- [40] EN 1912: 2013. *Structural Timber - Strength classes - Assignment of visual grades and species*. European Committee for Standardization.
- [41] Brandner, R.; Schickhofer, G. Length Effects on Tensile Strength in Timber Members With and Without Joints. In *Materials and Joints in Timber Structures: Recent Developments of Technology*; Aicher, S., Reinhardt, H.-W., Garrecht, H., Eds.; Springer Netherlands: Dordrecht, s.l.: 2014; pp 751–760, ISBN 978-94-007-7810-8.
- [42] Viguier, J.; Boquet, J.-F.; Dopeux, J.; Bléron, L.; Dubois F; Aubert S. *Strength grading of split glulam beams*, International council for research and innovation in building and construction: 2014.
- [43] JCSS-3.05. *JCSS Probabilistic Model Code: Part 3.05: Resistance Models - Properties of timber*. Joint Committee on Structural Safety. Available online: <https://www.jcss-lc.org/publications/jcsspmc/timber.pdf> (accessed on 22 November 2022).
- [44] Fink, G.; Kohler, J. Probabilistic modelling of the tensile related material properties of timber boards and finger joint connections. *Eur. J. Wood Prod.* **2015**, *73*, 335–346, doi:10.1007/s00107-015-0895-z.
- [45] Brandner, R.; Schickhofer, G. Glued laminated timber in bending: new aspects concerning modelling. *Wood Sci Technol* **2008**, *42*, 401–425, doi:10.1007/s00226-008-0189-2.
- [46] Riberholt, H. *Nordic glulam – Mechanical properties*, SP Technical Research Institute of Sweden: 2008.
- [47] Blaß, H.J.; Frese, M. *Biegefestigkeit von Brettschichtholz-Hybridträgern mit Randlamellen aus Buchenholz und Kernlamellen aus Nadelholz*: 2006, ISBN 3866440723.
- [48] Vida, C.; Lukacevic, M.; Eberhardsteiner, J.; Füssl, J. Modeling approach to estimate the bending strength and failure mechanisms of glued laminated timber beams. *Engineering Structures* **2022**, *255*, 113862, doi:10.1016/j.engstruct.2022.113862.
- [49] Kandler, G.; Lukacevic, M.; Füssl, J. Experimental study on glued laminated timber beams with well-known knot morphology. *Eur. J. Wood Prod.* **2018**, *76*, 1435–1452, doi:10.1007/s00107-018-1328-6.
- [50] Ansys®. *Ansys Mechanical*; ANSYS, Inc.: 2020.
- [51] Brandner, R.; Flatscher, G.; Ringhofer, A.; Schickhofer, G.; Thiel, A. Cross laminated timber (CLT): overview and development. *Eur. J. Wood Prod.* **2016**, *74*, 331–351, doi:10.1007/s00107-015-0999-5.
- [52] Vida, C.; Hochreiner, G.; Füssl, J. *Size Effect of Large Glued Laminated Timber Beams – Contribution to the Ongoing Discussion*, International council for research and innovation in building and construction: 2022.
- [53] Tapia, C.; Aicher, S. *Size effect of glulam made of oak wood under consideration of the finite weakest link theory*, International council for research and innovation in building and construction: 2022.
- [54] Tapia Camú, C.; Aicher, S. *A-Stochastic-Finite-Element-Model-for-Glulam-Beams-of-Hardwoods*.
- [55] Frese, M.; Blaß, H.J. *Bending strength of spruce glulam new models for the characteristic bending strength*, International Council for Research and Innovation in Building and Construction: 2008.
- [56] Schickhofer, G. Development of Efficient Glued Laminated Timber. *Proceedings of INTER 29th Meeting 1996*.

- [57] Brandner, R.; Schickhofer, G. Probabilistic models for the modulus of elasticity and shear in serial and parallel acting timber elements. *Wood Sci Technol* **2015**, *49*, 121–146, doi:10.1007/s00226-014-0689-1.
- [58] Brandner, R.; Schickhofer, G. Glued laminated timber in bending: Thoughts, experiments, models and verification. *11th World Conference on Timber Engineering*: 2010.
- [59] ON EN 1995-1-1: 2019. *Eurocode 5: Bemessung und Konstruktion von Holzbauten: Teil 1-1: Allgemeines – Allgemeine Regeln und Regeln für den Hochbau*. Austrian Standards Institute.
- [60] AS 1720.1: 2010. *Timber structures, Part 1: Design methods*. Standards Australia.
- [61] Brandner, R.; Schickhofer, G. System effects of structural elements - determined for bending and tension **2006**.
- [62] EN 14374: 2005. *Timber structures – Structural laminated veneer lumber – Requirements*. European Committee for Standardization.
- [63] EAD 130320-00-0304. *EAD 130320-00-0304 Glued laminated timber made of solid hardwood*. EOTA - European Organisation for Technical Assessment.
- [64] Crocetti, R. *Strength of split glulam beams*, SP RISE Sweden: 2009.
- [65] Cleason, T. *Hallfasthet hos "klycbalkar"*, SP RISE Sweden: 2003.
- [66] Sieder, R.; Brandner, R. *FFG BRIDGE 1 Forschungsprojekt "Leistungsfähige, flexible Produktion und Anwendung von BSH und BSP-Trägern aus großformatigen Vollholz-Platten (flex GLT-CLT-beams)" AP3: Biege- und Schubkenngrößen von flex GLT\CLT beams sowie dazugehörige Kenngrößen des Grundmaterials und der Keilzinken: Prüf- und Forschungsbericht*, Institut für Holzbau und Holztechnologie Technische Universität Graz: 2022.
- [67] Frese, M.; Blaß, H.J. Bending strength of spruce glulam. *Eur. J. Wood Prod.* **2009**, *67*, 277–286, doi:10.1007/s00107-009-0316-2.
- [68] Colling, F. *Brettschichtholz unter Biegebeanspruchung: STEP 3: Holzbauwerke nach Eurocode 5: Grundlagen, Entwicklungen, Ergänzungen*, Düsseldorf: 1995.
- [69] draft_EAD 130801-00-0304. *EAD 130801-00-0304 Glued laminated timber from unidirectional laminated panels*. EOTA - European Organisation for Technical Assessment.
- [70] Flaig, M. *Biegeträger aus Brettsperrholz bei Beanspruchung in Plattenebene*. Zugl.: Karlsruhe, KIT, Diss., 2013, Print on demand; Technische Informationsbibliothek u. Universitätsbibliothek; KIT Scientific Publishing: Hannover, Karlsruhe: 2013, ISBN 9783731500520.
- [71] Brandner, R.; Ringhofer, A.; Sieder, R. Out-of-plane bending properties of cross laminated timber (CLT). *Construction and Building Materials* **2024**, *438*, 136991, doi:10.1016/j.conbuildmat.2024.136991.
- [72] Jöbstl, R.; Moosbrugger, T.; Bogensperger, T.; Schickhofer, G. *A contribution to the design and system effect of cross laminated timber (CLT)*, International Council for Research and Innovation in Building and Construction: 2006.
- [73] Unterwieser, H.; Schickhofer, G. Influence of moisture content of wood on sound velocity and dynamic MOE of natural frequency- and ultrasonic runtime measurement. *Eur. J. Wood Prod.* **2011**, *69*, 171–181, doi:10.1007/s00107-010-0417-y.
- [74] EN 384: 2016. *Structural timber — Determination of characteristic values of mechanical properties and density*. European Committee for Standardization.
- [75] EN 14358: 2016. *Timber structures – Calculation and verification of characteristic values*. European Committee for Standardization.

Annex A: List of Notations and Abbreviations

In the following all used notations and abbreviations are listed.

A-1 Latin Upper-case Letters

ARN.....	alternating renewal process
BD	beta distribution (2 parametric)
CDF.....	cumulative density function
CI	confidence interval
CLT	cross laminated timber
COV(X)	coefficient of variation of X
CW	clear wood
D_{FJ}	distance between finger joints
D_{IZ}	distance between intermediate knot/zone
D_{WZ}	distance between the centres of weak zone
E	modulus of elasticity
E(X).....	expected value of X
$E_{0,g,mean}$	mean modulus of elasticity parallel to the grain of glulam beams
$E_{c,0,ij}$	local deviation i within board j of the modulus of elasticity in compression parallel to the grain
$E_{DYN,b}$	dynamic modulus of boards
$E_{DYN,b,mean}$	mean dynamic modulus of elasticity of boards
$E_{DYN,F}$	dynamic modulus of elasticity based on eigen-frequency
$E_{DYN,ref}$	reference dynamic modulus of elasticity of boards
$E_{DYN,b,mean}$	mean dynamic modulus of elasticity of boards
$E_{glob,k}$	global modulus of elasticity of the beam at iteration k
E_{loc}	local modulus of elasticity of the beam in bending
$E_{m,b}$	modulus of elasticity in bending of boards
$E_{m,g}$	modulus of elasticity in bending of glue laminated product
$E_{m,g,05}$	5 %-quantile of the modulus of elasticity in bending of glue laminated product
$E_{m,g,flat}$	modulus of elasticity in bending of glulam with flatwise loaded lamellas
$E_{m,g,edge}$	modulus of elasticity in bending of glulam with edgewise loaded lamellas
E_S	modulus of elasticity of steel
$E_{t,0}$	modulus of elasticity in tension parallel to the grain
$E_{t,0,j}$	modulus of elasticity of board j in tension parallel to the grain
$E_{t,0,ij}$	local deviation i within board j of the modulus of elasticity in tension parallel to the grain
$E_{t,0,mean}$	mean modulus of elasticity in tension parallel to the grain
$E_{t,0,b,mean}$	mean modulus of elasticity of boards in tension parallel to the grain
$E_{t,0,loc,12,b}$	(local) modulus of elasticity in tension parallel to the grain of board at $u = 12\%$
$E_{t,CW}$	modulus of elasticity in tension parallel to the grain of clear wood
$E_{t,FJ}$	modulus of elasticity in tension parallel to the grain of finger joints
$E_{x y z}$	modulus of elasticity in $x y z$ direction
F_{test}	applied test load
$F_{max,k}$	maximum load at iteration k
F_{ult}	ultimate load carrying capacity of the beam
FEM	finite element method
FJ	finger joint
$G_{xy xz yz}$	shear modulus in $xy yz yz$ plane
GA_{eff}	effective shear stiffness of the beam
GI	board group GI (T14)

GII	board group GII (T24)
GD	gamma distribution
GLT	glulam; glued laminated timber
I_{eff}	effective moment of inertia of the beam
IZ	intermediate knot/zone
KZ	knot zone
L_{cell}	length of the cell to determine $tKAR$
$L_{\text{CW,FJ}}$	required length of the clear wood section to place a finger joint
L_{IZ}	length of an intermediate knot/zone
L_{KZ}	length of a knot zone
$L_{\text{KZ,new}}$	length of a knot zone of new model
L_{WZ}	length of a weak zone
$L_{\text{WZ},0.4 0.5}$	length of a weak zone determined by a $tKAR$ -value threshold of 0.4 or 0.5
LND	lognormal distribution (2 parametric)
ND	normal distribution
M_{ult}	ultimate moment carrying capacity of the beam
MC	monte carlo method
MLP	multi-layered panels
PDF	probability density function
R^2	coefficients of determination
$\text{Ref}_{\text{GI/GII}}$	reference value [mm]; [%]; [-]
SFEM	stochastic finite element method
SWP	solid wood panel
W_{eff}	effective section modulus of the beam
WD	Weibull distribution (2 parametric)
WZ	weak zone
X	reference property X
X_{pos}	position along board length direction (X -direction)
X_{ref}	reference value of property X
Y	property Y
Y_j	average property of board j
Y_{ref}	reference value of property Y
Z_{ij}	local deviation i within board j

A-2 Latin Lower-case Letters

d_{knot}	knot diameter
$d_{\text{knot},95}$	95 %-quantile of the knot diameter
$d_{\text{knot,mean}}$	mean knot diameter
$f_{\text{m,b}}$	bending strength of boards
$f_{\text{m,b,k}}$	characteristic bending strength of boards
$f_{\text{m,b,ref}}$	reference bending strength of boards
$f_{\text{m,FJ,k}}$	characteristic bending strength of finger joints
$f_{\text{m,g}}$	bending strength of glue laminated product
$f_{\text{m,g},05}$	5 %-quantile of the bending strength of glue laminated product
$f_{\text{m,g,flat}}$	bending strength of glulam with flatwise loaded lamellas
$f_{\text{m,g,edge}}$	bending strength of glulam with edgewise loaded lamellas
$f_{\text{m,g},05,\text{ref,model}}$	modelled characteristic (5 %-quantile) bending strength of glue laminated product

$f_{m,g,05,ref,sim test}$	simulated tested characteristic (5 %-quantile) bending strength of glue laminated product
$f_{m,s,05}$	5 %-quantile of the bending strength of resawn glulam
$f_{m,s,k}$	characteristic bending strength of resawn glulam
$f_{t,0}$	tensile strength parallel to the grain
$f_{t,0,b}$	tensile strength of boards parallel to the grain
$f_{t,0,b,k}$	characteristic tensile strength of boards parallel to the grain
$f_{t,0,b,ref}$	reference characteristic tensile strength of boards parallel to the grain
$f_{t,0,b,05,LN}$	lognormal 5 % quantile of the tensile strength of boards
$f_{t,0,FJ,k}$	characteristic tensile strength of finger joints
$f_{t,0,j}$	tensile strength parallel to the grain of board j
$f_{t,0,ij}$	local deviation i within board j of the tensile strength parallel to the grain
$f_{t,0,k}$	characteristic tensile strength of boards parallel to the grain
$f_{t,FJ}$	tensile strength of finger joints
$f_{t,FJ,ref}$	reference tensile strength of finger joints
$f_{t,FJ,05,LN}$	lognormal 5 % quantile of the tensile strength of finger joints
h_g	beam depth
$h_{g,A}$	beam depth of flex_GLT type A
$h_{g,B}$	beam depth of flex_GLT type B
$h_{g,C}$	beam depth of flex_CLT beams
$h_{g,D}$	beam depth of flex_CLT slabs
$h_{g,ref}$	reference beam depth
k	power coefficient
k_h	power coefficient for the beam depth
$k_{h,flexA,05}$	power coefficient for the beam depth of flex_GLT type A
$k_{h,flexB,05}$	power coefficient for the beam depth of flex_GLT type B
$k_{h,flexCLT-beams,05}$	power coefficient for the beam depth of flex_CLT beams
$k_{h,flexCLT-slabs,05}$	power coefficient for the beam depth of flex_CLT slabs
$k_{l,9b,05,GI GII}$	power coefficient for the board length with reference length $l_{b,ref} = 9 \cdot w_b$ and group GI GII
$k_{l,9b,05,L25 L40}$	power coefficient for the board length with reference length $l_{b,ref} = 9 \cdot w_b$ for strength class L25 L40; see Fink [3]
$k_{l,05,COV25 35}$	power coefficient for boards for a $COV(f_{t,0,b}) = \{25; 35\}$ %; see Brandner & Schickhofer [41]
$k_{l,EN1194}$	power coefficient for boards; see EN 1194 [37]
k_{sys}	factor for system effects of parallel acting members
$k_{sys,05,new}$	system factor of the bending strength of glulam with edgewise loaded lamellas
$k_{sys,flexA}$	system factor of the bending strength of flex_GLT type A
$k_{sys,flexB}$	system factor of the bending strength of flex_GLT type B
$k_{sys,flexCLT-beams}$	system factor of the bending strength of flex_CLT beams
$k_{sys,max}$	maximal achievable system factor
$k_{w,9b,05,GI GII}$	power coefficient for the board width at reference length $l_{b,ref} = 9 \cdot w_b$ and group GI GII
$k_{w,2 4m,05,GI GII}$	power coefficient for the board width at reference length $l_{b,ref} = \{2.0; 4.0\}$ m and group GI GII
$k_{w,05,S10 S13}$	power coefficient for the board width for strength class S10 S13; see Burger [23]
$k_{w,EN384}$	power coefficient for the board width; see EN 384 [74]
$k_{w,EN1194}$	power coefficient for the board width; see EN 1194 [37]
$k_{w,flexA,05}$	power coefficient for the beam width of flex_GLT type A

$k_{w,flexB,05}$	power coefficient for the beam width of flex_GLT type B
$k_{w,flexCLT-beams,05}$	power coefficient for the beam width of flex_CLT beams
$k_{w,flexCLT-slabs,05}$	power coefficient for the beam width of flex_CLT slabs
$k_{w,Flaig,05}$	power coefficient for the beam width of CLT beams; see Flaig [70]
l_b	board length
$l_{b,j}$	length of board j
$l_{b,ij}$	length of the board-segment i in board j
$l_{b,og}$	original board length
$l_{b,ref}$	reference board length
$l_{b,s}$	residual board length of the first board within MLP
$l_{e,x}$	element length in x-direction
$l_{e,t}$	element length in board thickness direction
$l_{e,w}$	element length in board width direction
$l_{e,w,f}$	element length in board width direction for flatwise loading
$l_{e,w,e}$	element length in board width direction for edgewise loading
l_g	length of the glue laminated product
l_{loc}	reference length for determination of the local of modulus of elasticity
l_{span}	free test span in bending test
n	number; amount
$n_{b,all}$	total number of boards in the bending tension zone
$n_{b,full}$	number of boards with full cross-section in the bending tension zone
$n_{b,split}$	number of split boards in the bending tension zone
n_{lay}	number of layers
$n_{lay,par}$	number of parallel acting layers
n_{par}	number of parallel acting members
t_b	board thickness
t_{lay}	layer thickness
t_{MLP}	thickness of MLP
$tKAR$	tensile knot-area-ratio
$tKAR_{100}$	tensile knot-area-ratio calculated based on a length of 100 mm
$tKAR_{150}$	tensile knot-area-ratio calculated based on a length of 150 mm
$tKAR_{200}$	tensile knot-area-ratio calculated based on a length of 200 mm
$tKAR_{IZ}$	tensile knot-area-ratio of an intermediate zone
$tKAR_{ij}$	local deviation i within board j of the tensile knot-area-ratio
$tKAR_{KZ}$	tensile knot-area-ratio of knot zone
$tKAR_{new}$	tensile knot-area-ratio of knot zone of new model
$tKAR_{max}$	maximum tensile knot-area-ratio of knot zone within a board
$tKAR_{WZ}$	tensile knot-area-ratio of a weak zone
u	moisture content
u_{ref}	reference moisture content $u_{ref} = 12 \%$
w_b	board width
$w_{b,res}$	residual board width
$w_{b,ref}$	reference board width
$w_{b,s}$	residual board width of first layer within MLP
$w_{cut,SWP}$	width of the cutting tool for the SWP
w_g	beam width
$w_{g,A}$	beam width of flex_GLT type A
$w_{g,B}$	beam width of flex_GLT type B

$w_{g,C}$	beam width of flex_CLT beams
$w_{g,D}$	beam width of flex_CLT slabs
$w_{glob,k}$	global deflection at iteration k
w_{lay}	layer width
$w_{loc,1}$	local deflection at the first iteration
w_{MLP}	width of MLP
$x_{05,emp}$	empirical 5 % quantile
$x_{05,LN}$	lognormal 5 % quantile
$x_{05,LN,ref}$	lognormal 5 % quantile at reference dimensions
$x_{05,ref}$	5 % quantile at reference dimensions
$x_{k,EN14358}$	characteristic value according to EN 14358 [75]
$x_{95,emp}$	empirical 95 % quantile

A-3 Greek Letters

β_{ij}	coefficients of regression model
ΔD_{WZ}	distance between two weak zones
$\Delta D_{WZ,GI GII}$	difference between distances of the weak zones for group GI or GII
Δ_{edge}	overlap of the board edges in neighbouring layers
$\Delta L_{WZ,GI GII}$	difference between lengths of the weak zone for group GI or GII
$\Delta L_{le/ri}$	additional length added to knot zone
$\Delta tKAR_{WZ,GI GII}$	difference between $tKAR$ -values of the weak zone for group GI or GII
Δw_b	allowed reduction in width
ε	error term; $\varepsilon \sim ND(0; \sigma_\varepsilon)$
ε_{mean}	mean of model residuals
η_s	separation ratio of boards; $\eta_s = w_{b,res}/w_b$
$\eta_{f,t,0,ij,k}$	degree of utilisation in tension parallel to the grain of elements at iteration k
η_w	board width ratio; $\eta_w = w_b/w_{b,ref}$
η_l	board length ratio; $\eta_l = l_b/l_{b,ref}$
ϱ	correlation
ϱ_{12}	density at reference moisture content $u_{ref} = 12 \%$
$\varrho_{12,b}$	density of boards at reference moisture content $u_{ref} = 12 \%$
ϱ_k	characteristic density of boards
ϱ_{equi}	equi-correlation
$\varrho_{equi,CW}$	equi-correlation of the clear wood section
$\varrho_{equi,IZ}$	equi-correlation of the intermediate zones
$\varrho_{equi,WZ}$	equi-correlation of the weak zones
$\mu_{E,DYN}$	location parameter of the dynamic modulus of elasticity
$\sigma_{E,DYN}$	dispersion parameter of the dynamic modulus of elasticity
$\sigma_z^2(X)$	total variance of property X
$\sigma_y^2(X)$	variance of board mean values of property X
$\sigma_\psi^2(X)$	variance of local deviation of property X
σ_ε	standard deviation of the error term
ζ_{05}	required strength ratio between tensile strength of boards and finger joints; see Brandner [12]
$\zeta_{Brandner}$	simplified required strength ratio between tensile strength of boards and finger joints; see Brandner & Schickhofer [58]
ζ_{new}	adapted required strength ratio between tensile strength of boards and finger joints

Ψ_{ij} local deviation i within board j

Annex B: Formulas

In the following additional formulas are listed for the hierarchical models for the used distributions. Additionally, formulas for the calculation of cross-section properties for beams built up of unidirectional and orthogonal layers are illustrated.

B-1 Hierarchical Models for Distributions & Statistical Values

B-1.1 Lognormal Distribution

$$Y_j \sim \text{LND}(\mu_{\text{LN},j}; \sigma_{\text{LN},j}^2) \quad (\text{B.1})$$

$$\mu_{\text{LN},j} = \ln \left(\frac{E(X)}{\sqrt{1 + \text{COV}(X)^2 \cdot \rho_{\text{equi}}(X)}} \right) \quad (\text{B.2})$$

$$\sigma_{\text{LN},j} = \sqrt{\ln(1 + \text{COV}(X)^2 \cdot \rho_{\text{equi}}(X))} \quad (\text{B.3})$$

$$Z_{ij} \sim \text{LND}(\mu_{\text{LN},ij}; \sigma_{\text{LN},ij}^2) \quad (\text{B.4})$$

$$\mu_{\text{LN},ij} = \ln \left(\frac{Y_j}{\sqrt{1 + \text{COV}(X)^2 \cdot (1 - \rho_{\text{equi}}(X))}} \right) \quad (\text{B.5})$$

$$\sigma_{\text{LN},ij} = \sqrt{\ln(1 + \text{COV}(X)^2 \cdot (1 - \rho_{\text{equi}}(X)))} \quad (\text{B.6})$$

with

- X random variable $X = \{L_{wz}; L_{iz}\}$ [mm]
- Y_j global mean of board j [mm]
- Z_{ij} local property i of board j [mm]
- $E(X)$ expected value of the random variable X [mm]
- $\text{COV}(X)$ coefficient of variation of the random variable X [%]
- $\rho_{\text{equi}}(X)$ equi-correlation coefficient of the random variable X [-]

B-1.2 Beta Distribution

$$Y_j \sim \text{BD}(\alpha_{\text{BD},j}; \beta_{\text{BD},j}) \quad (\text{B.7})$$

$$\alpha_{\text{BD},j} = \frac{1 - (1 + \text{COV}(X)^2 \cdot \rho_{\text{equi}}(X)) \cdot E(X)}{\text{COV}(X)^2 \cdot \rho_{\text{equi}}(X)} \quad (\text{B.8})$$

$$\beta_{\text{BD},j} = \frac{1 - E(X) \cdot (1 - E(X) - E(X) \cdot \text{COV}(X)^2 \cdot \rho_{\text{equi}}(X))}{E(X) \cdot \text{COV}(X)^2 \cdot \rho_{\text{equi}}(X)} \quad (\text{B.9})$$

$$Z_{ij} \sim \text{BD}(\alpha_{\text{BD},ij}; \beta_{\text{BD},ij}) \quad (\text{B.10})$$

$$\alpha_{\text{BD},ij} = \frac{1 - (1 + \text{COV}(X)^2 \cdot (1 - \rho_{\text{equi}}(X))) \cdot Y_j}{\text{COV}(X)^2 \cdot (1 - \rho_{\text{equi}}(X))} \quad (\text{B.11})$$

$$\beta_{\text{BD},ij} = (1 - X_j) \cdot \frac{(1 - Y_j - Y_j \cdot \text{COV}(X)^2 \cdot (1 - \rho_{\text{equi}}(X)))}{Y_j \cdot \text{COV}(X)^2 \cdot (1 - \rho_{\text{equi}}(X))} \quad (\text{B.12})$$

with

- X random variable $X = \{tKAR_{wz}; tKAR_{iz}\}$ [-]
- Y_j global mean of board j [-]
- Z_{ij} local property i of board j [-]
- $E(X)$ expected value of the random variable X [-]
- $\text{COV}(X)$ coefficient of variation of the random variable X [%]
- $\rho_{\text{equi}}(X)$ equi-correlation coefficient of the random variable X [-]

B-1.3 Gamma Distribution

$$Y_j \sim \text{GD}(\alpha_{\text{GD},j}; \beta_{\text{GD},j}) \quad (\text{B.13})$$

$$\alpha_{\text{GD},j} = \frac{1}{\text{COV}(X)^2 \cdot \rho_{\text{equi}}(X)} \quad (\text{B.14})$$

$$\beta_{\text{GD},j} = E(X) \cdot \text{COV}(X)^2 \cdot \rho_{\text{equi}}(X) \quad (\text{B.15})$$

$$Z_{ij} \sim \text{GD}(\alpha_{\text{BD},ij}; \beta_{\text{BD},ij}) \quad (\text{B.16})$$

$$\alpha_{\text{GD},ij} = \frac{1}{\text{COV}(X)^2 \cdot (1 - \rho_{\text{equi}}(X))} \quad (\text{B.17})$$

$$\beta_{\text{GD},ij} = Y_j \cdot \text{COV}(X)^2 \cdot (1 - \rho_{\text{equi}}(X)) \quad (\text{B.18})$$

with

X random variable $X = \{D_{Wz}; D_{Iz}\}$ [mm]

Y_j global mean of board j [mm]

Z_{ij} local property i of board j [mm]

$E(X)$ expected value of the random variable X [mm]

$\text{COV}(X)$ coefficient of variation of the random variable X [%]

$\rho_{\text{equi}}(X)$ equi-correlation coefficient of the random variable X [-]

B-1.4 Coefficient of determination

$$R^2 = 1 - \frac{SQR}{SQT} \quad (\text{B.19})$$

with

R^2 coefficient of determination [-]

SQR sum of squared residuals [-]

SQT total sum of squared deviation from the mean value of data [-]

B-2 Cross-Section Values

B-2.1 Beams with Unidirectional Layers

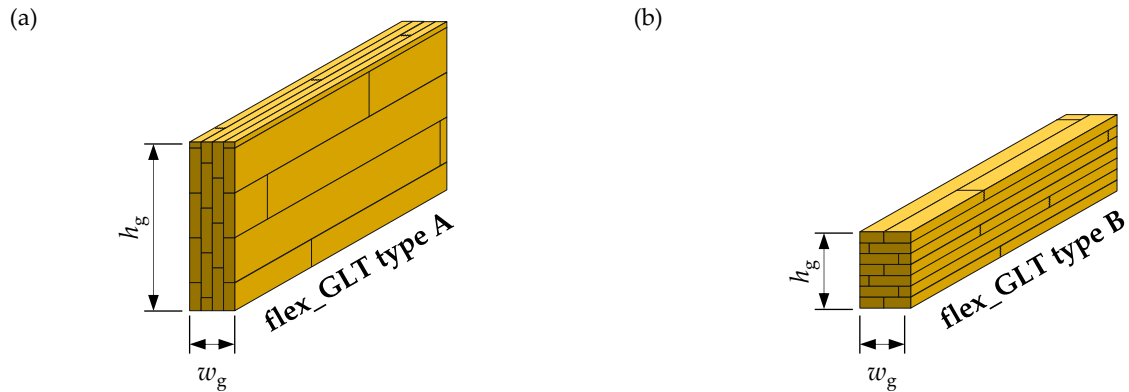


Figure Annex B-1: Beams with unidirectional layers (a) flex_GLT type A and (b) flex_GLT type B.

$$I_{\text{eff}} = \frac{w_g \cdot h_g^3}{12} \quad (\text{B.20})$$

$$EI_{\text{eff}} = E_0 \cdot \frac{w_g \cdot h_g^3}{12} \quad (\text{B.21})$$

$$W_{\text{eff}} = \frac{w_g \cdot h_g^2}{6} \quad (\text{B.22})$$

$$A_{\text{eff}} = w_g \cdot h_g \quad (\text{B.23})$$

$$GA_{\text{eff}} = \frac{5}{6} \cdot A_{\text{eff}} \cdot G_0 \quad (\text{B.24})$$

with

I_{eff} effective moment of inertia of the beam [mm⁴]

h_g depth of the beam [mm]

w_g width of the beam [mm]

EI_{eff} effective bending stiffness of the beam [Nmm²]

E_0 modulus of elasticity parallel to the grain of the beam in bending [Nmm²]

W_{eff} effective section modulus of the beam [mm³]

A_{eff} effective cross-section area of the beam [mm²]

GA_{eff} effective shear stiffness of the beam [N]

G_0 shear modulus [MPa]

B-2.2 Beams with Orthogonal Layers & Edgewise Loaded Boards

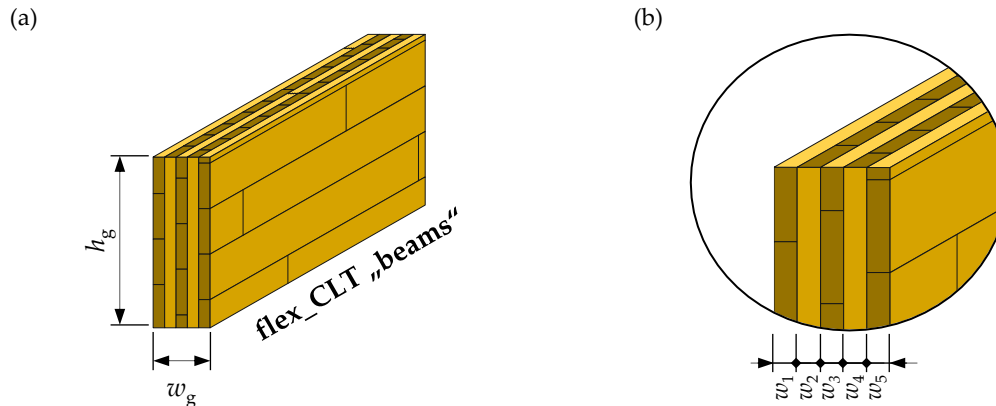


Figure Annex B-2: Beams with orthogonal layers and edgewise loaded boards; (a) overview and (b) detail concerning the layer widths.

$$E_i = \begin{cases} E_{0,\text{ref}} = 11,500 & \dots \text{ for layers parallel to the span} \\ E_{90,\text{ref}} = 0 & \dots \text{ for other layers} \end{cases} \quad (\text{B.25})$$

$$n_i = \frac{E_i}{E_{0,\text{ref}}} \quad (\text{B.26})$$

$$w_{g,\text{eff}} = \sum_{i=1}^{n_{\text{lay}}} [w_i \cdot n_i] \quad (\text{B.27})$$

$$EI_{\text{eff}} = \sum_{i=1}^{n_{\text{lay}}} [E_i \cdot I_i] \quad (\text{B.28})$$

$$I_{\text{eff}} = \frac{EI_{\text{eff}}}{E_{0,\text{ref}}} = \frac{w_{g,\text{eff}} \cdot h_g^3}{12} \quad (\text{B.29})$$

$$W_{\text{eff}} = \frac{w_{g,\text{eff}} \cdot h_g^2}{6} \quad (\text{B.30})$$

$$A_{\text{eff}} = w_{g,\text{eff}} \cdot h_g \quad (\text{B.31})$$

$$GA_{\text{eff}} = \frac{5}{6} \cdot A_{\text{eff}} \cdot G_0 \quad (\text{B.32})$$

with

- E_i modulus of elasticity of layer i [MPa]
- n_i ratio between the modulus of elasticity of layer i and that of the layer parallel to the span [-]
- $w_{g,\text{eff}}$ effective width of the beam [mm]
- w_i width of layer i [mm]
- n_{lay} number of layers [-]
- EI_{eff} effective bending stiffness of the beam [Nm²]
- I_{eff} effective moment of inertia of the beam [mm⁴]
- h_g depth of the beam [mm]
- W_{eff} effective section modulus of the beam [mm³]
- A_{eff} effective cross-section area of the beam [mm²]
- GA_{eff} effective shear stiffness of the beam [N]
- G_0 shear modulus [MPa]

B-2.3 Slabs with Orthogonal Layers & Flatwise Loaded Boards

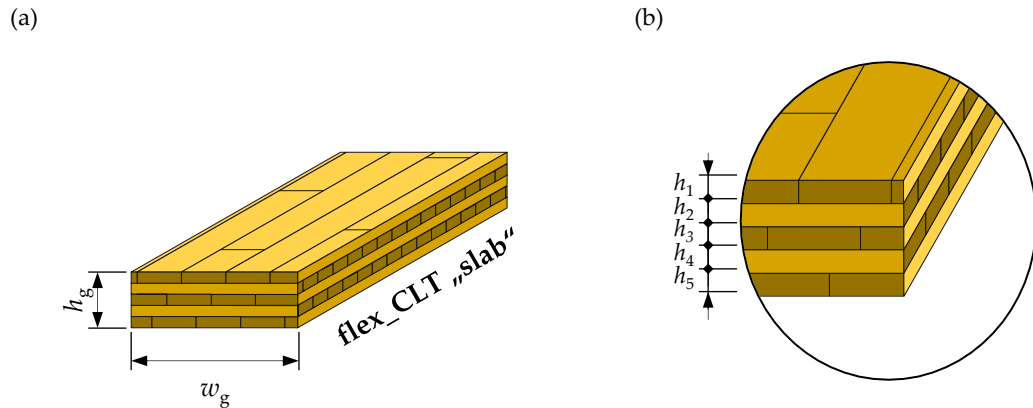


Figure Annex B-3: Slabs with orthogonal layers and flatwise loaded boards; (a) overview and (b) detail layer depths.

$$E_i = \begin{cases} E_{0,\text{ref}} = 11,500 & \dots \text{ for layers parallel to the span} \\ E_{90,\text{ref}} = 0 & \dots \text{ for other layers} \end{cases} \quad (\text{B.33})$$

$$n_i = \frac{E_i}{E_{0,\text{ref}}} \quad (\text{B.34})$$

$$h_{g,\text{eff}} = \sum_{i=1}^{n_{\text{lay}}} [h_i \cdot n_i] \quad (\text{B.35})$$

$$EI_{\text{eff}} = \sum_{i=1}^{n_{\text{lay}}} [E_i \cdot (I_i + A_i \cdot e_i^2)] \quad (\text{B.36})$$

$$I_{\text{eff}} = \frac{EI_{\text{eff}}}{E_{0,\text{ref}}} \quad (\text{B.37})$$

$$W_{\text{eff}} = \frac{I_{\text{eff}} \cdot 2}{h_g} \quad (\text{B.38})$$

$$A_{\text{eff}} = h_{g,\text{eff}} \cdot w_g \quad (\text{B.39})$$

$$GA_{\text{eff}} = \frac{\sum_{i=1}^{n_{\text{lay}}} [G_i \cdot A_i]}{\kappa} \quad (\text{B.40})$$

$$G_i = \begin{cases} G_{0,\text{ref}} = 650 & \dots \text{ for layers parallel to the span} \\ G_{90,\text{ref}} = 100 & \dots \text{ for other layers to the span} \end{cases} \quad (\text{B.41})$$

$$\kappa = \frac{\sum_{i=1}^{n_{\text{lay}}} [G_i \cdot h_i]}{EI_{\text{eff}}} \cdot \sum_{i=1}^{n_{\text{lay}}} \left[\frac{h_i}{60 \cdot G_i} \cdot \left[60 \cdot S_{0,i}^2 + 20 \cdot E_i \cdot S_{0,i} \cdot h_i \cdot (h_i + 3 \cdot z_{0,i}) + \right] \right] \quad (\text{B.42})$$

$$S_{0,i} = \sum_{j=1}^{i-1} \left[\frac{E_j \cdot h_j \cdot (h_j - 2 \cdot z_{0,j})}{2} \right] \quad (\text{B.43})$$

with

E_imodulus of elasticity of layer i [MPa]

n_iratio between the modulus of elasticity of layer i and that of the layer parallel to the span [-]

$h_{g,eff}$	effective depth of beam [mm]
h_i	depth of layer i [mm]
n_{lay}	number of layers [-]
EI_{eff}	effective bending stiffness of the beam [Nmm ²]
I_{eff}	effective moment of inertia of the beam [mm ⁴]
W_{eff}	effective section modulus area of the beam [mm ³]
A_{eff}	effective cross-section area of the beam [mm ²]
GA_{eff}	effective shear stiffness of the beam [N]
G_i	shear modulus of layer i [MPa]
κ	shear correction factor [-]
$S_{0,i}$	static moment at layer i [mm ³]
$z_{0,i/j}$	distance between the centre of gravity of the cross-section and the upper edge of the layer i [mm]

Annex C: Plots

In the following, additional plots are illustrated for a complete picture of all data used without sacrificing readability in the main part.

C-1 Probabilistic Board Model

C-1.1 Influence of the Board Thickness on the Model Parameters

Length of the Weak Zone (L_{WZ})

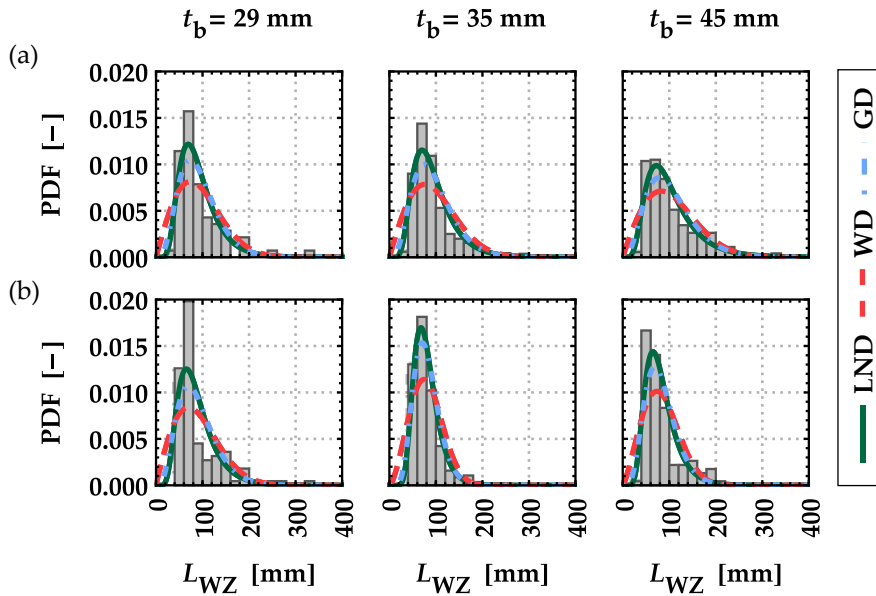


Figure Annex C-1: Histograms of the length of the weak zones L_{WZ} of boards featuring a width of $w_b = 150$ mm and a thickness of $t_b = \{29; 35; 45\}$ mm allocated to (a) group GI (T14) and (b) group GII (T24) together with calibrated density functions {LND; WD; GD}.

Total Knot Area Ratio at the Weak Zone ($tKAR_{WZ}$)

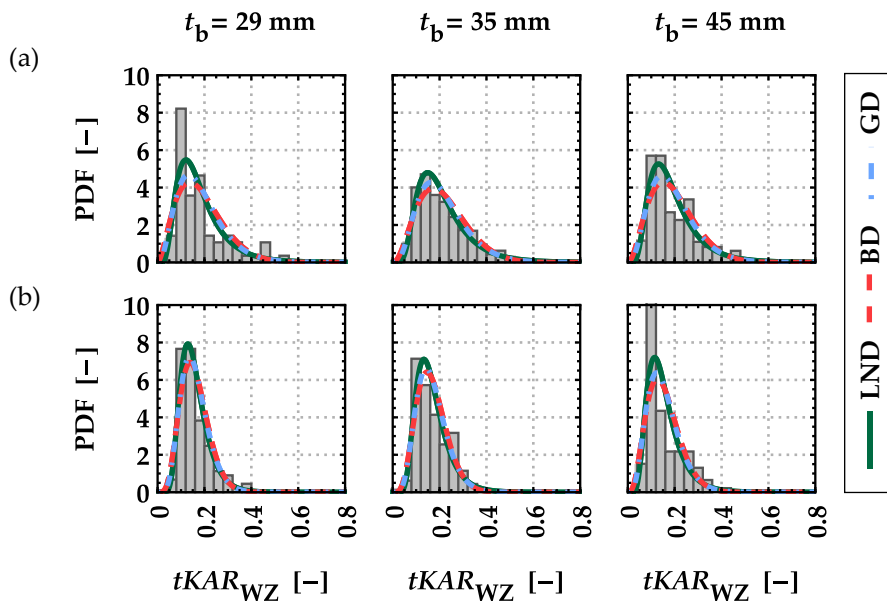


Figure Annex C-2: Histograms of the length of the total knot area ratio at weak zones $tKAR_{WZ}$ of boards featuring a width of $w_b = 150$ mm and a thickness of $t_b = \{29; 35; 45\}$ mm allocated to (a) group GI (T14) and (b) group GII (T24) together with calibrated density functions {LND; BD; GD}.

Distance between Weak Zones (D_{WZ})

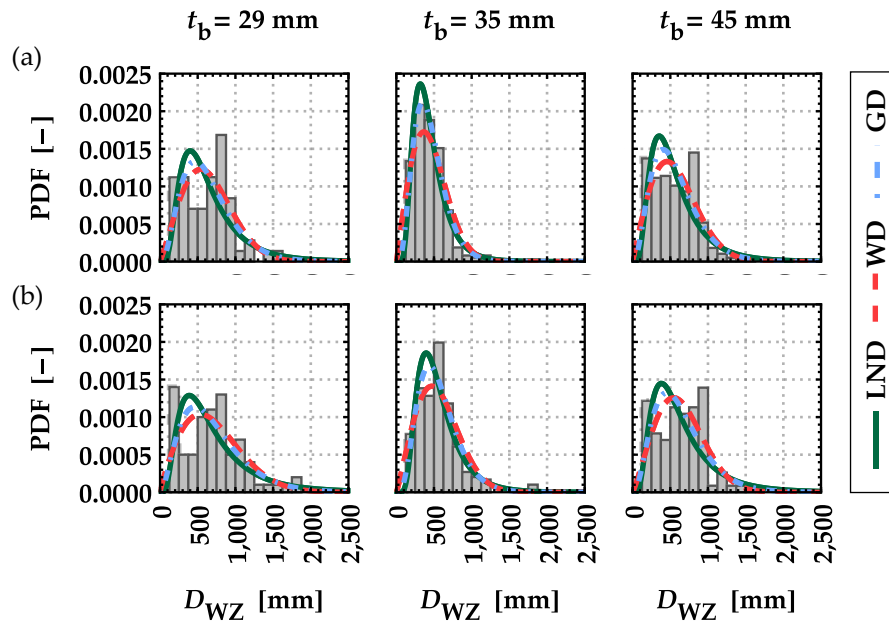


Figure Annex C-3: Histograms of the length of the distance between weak zones D_{WZ} of boards featuring a width of $w_b = 150$ mm and a thickness of $t_b = \{29; 35; 45\}$ mm allocated to (a) group GI (T14) and (b) group GII (T24) together with calibrated density functions {LND; WD; GD}.

Length of the Intermediate Zones (L_{IZ})

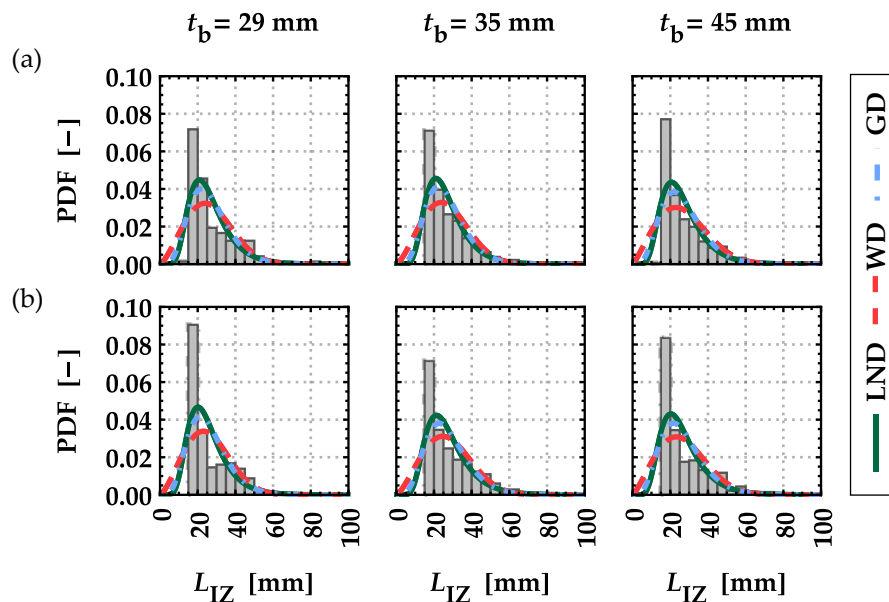


Figure Annex C-4: Histograms of the length of the intermediate knot zones L_{IZ} of boards featuring a width of $w_b = 150$ mm and a thickness of $t_b = \{29; 35; 45\}$ mm allocated to (a) group GI (T14) and (b) group GII (T24) together with calibrated density functions {LND; WD; GD}.

Total Knot Area Ratio at the Intermediate Zone ($tKAR_{IZ}$)

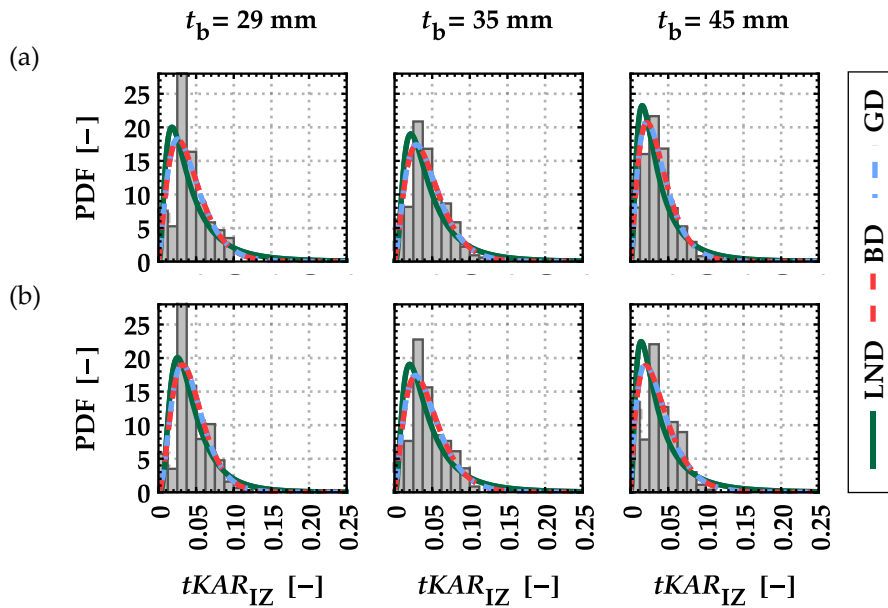


Figure Annex C-5: Histograms of the length of the total knot area ratio at intermediate zones $tKAR_{IZ}$ of boards featuring a width of $w_b = 150$ mm and a thickness of $t_b = \{29; 35; 45\}$ mm allocated to (a) group GI (T14) and (b) group GII (T24) together with calibrated density functions {LND; BD; GD}.

Distance between Intermediate Zones (D_{IZ})

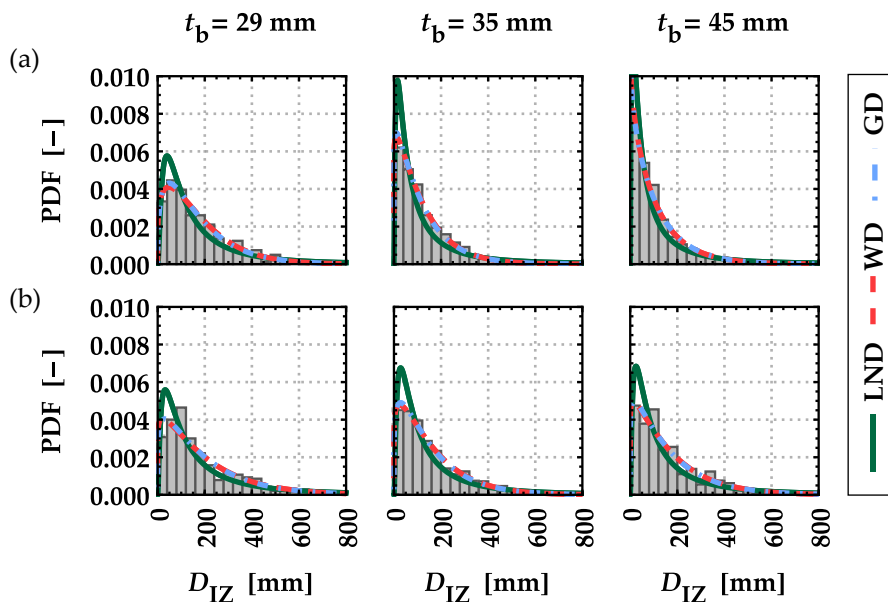


Figure Annex C-6: Histograms of the length of the distance between intermediate zones D_{IZ} of boards featuring a width of $w_b = 150$ mm and a thickness of $t_b = \{29; 35; 45\}$ mm allocated to (a) group GI (T14) and (b) group GII (T24) together with calibrated density functions {LND; WD; GD}.

C-1.2 Influence of the Board Width on the Model Parameters

Length of the Weak Zone (L_{WZ})

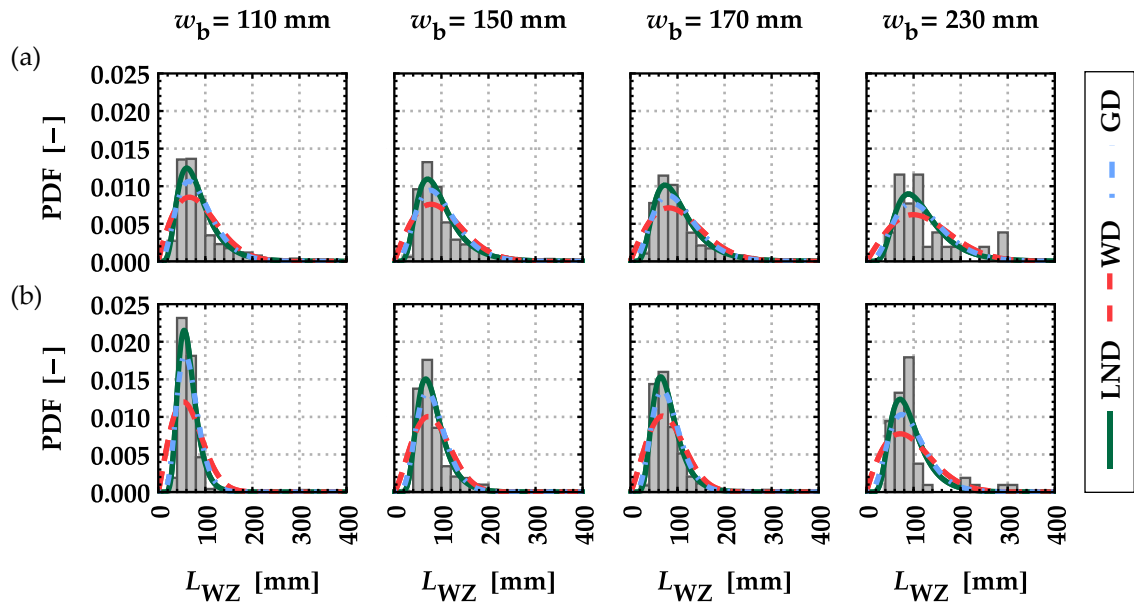


Figure Annex C-7: Histograms of the length of the weak zones L_{WZ} of boards featuring a width of $w_b = \{110; 150; 170; 230\}$ mm allocated to (a) group GI (T14) and (b) group GII (T24) together with calibrated density functions {LND; WD; GD}.

Total Knot Area Ratio at the Weak Zone ($tKAR_{WZ}$)

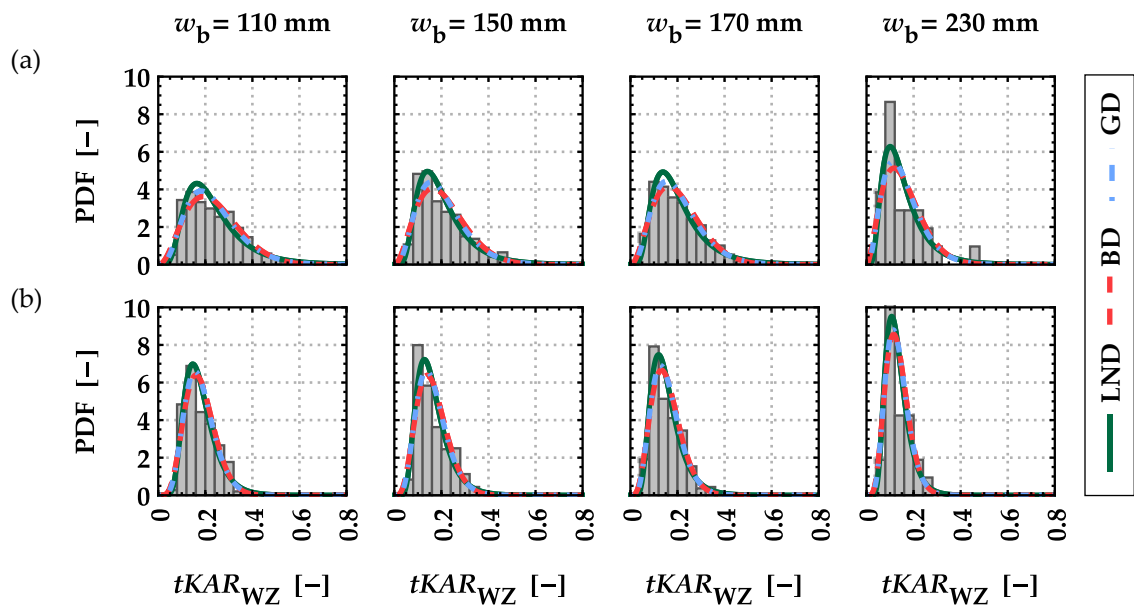


Figure Annex C-8: Histograms of the total knot area ratio at weak zones $tKAR_{WZ}$ of boards featuring a width of $w_b = \{110; 150; 170; 230\}$ mm allocated to (a) group GI (T14) and (b) group GII (T24) together with calibrated density functions {LND; BD; GD}.

Distance between Weak Zones (D_{WZ})

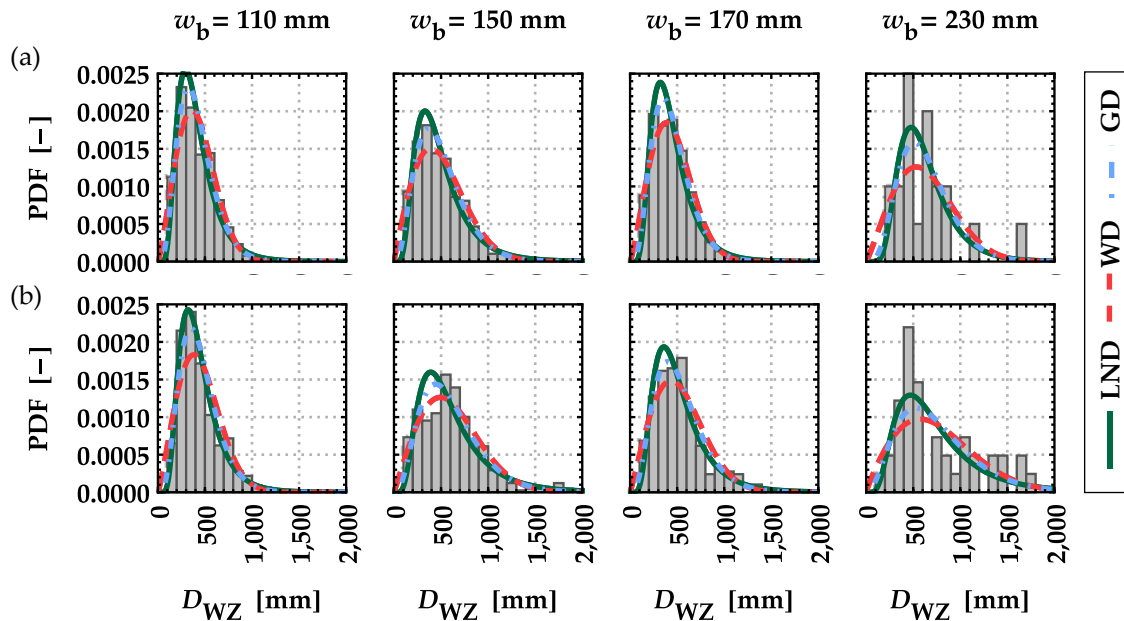


Figure Annex C-9: Histograms of the distance between weak zones D_{WZ} of boards featuring a width of $w_b = \{110; 150; 170; 230\}$ mm allocated to (a) group GI (T14) and (b) group GII (T24) together with calibrated density functions {LND; WD; GD}.

Length of the Intermediate Zones (L_{IZ})

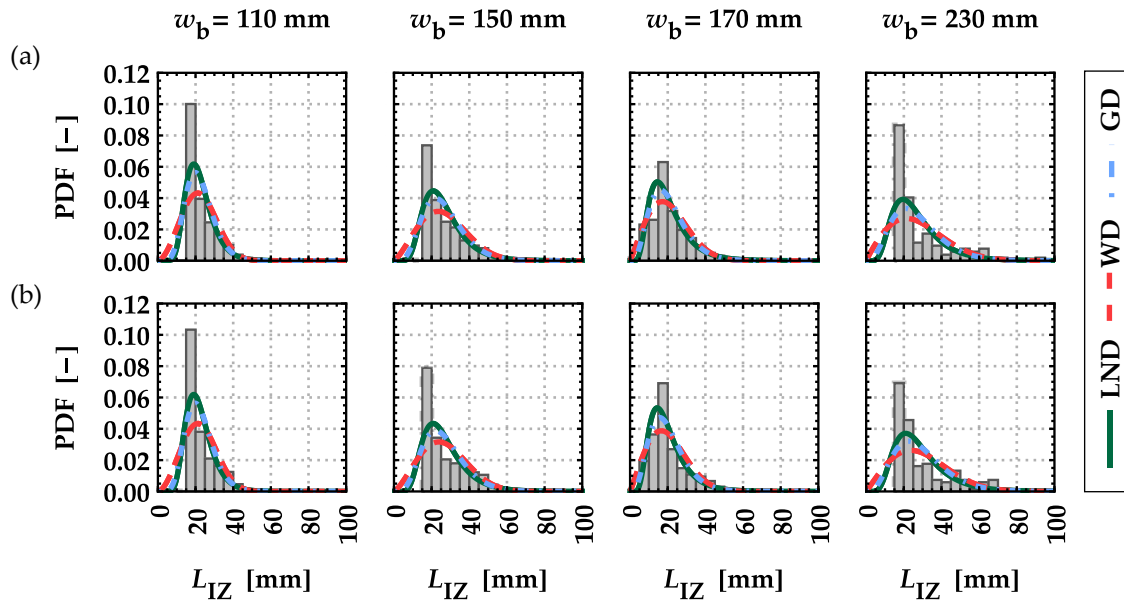


Figure Annex C-10: Histograms of the length of the intermediate zones L_{IZ} of boards featuring a width of $w_b = \{110; 150; 170; 230\}$ mm allocated to (a) group GI (T14) and (b) group GII (T24) together with calibrated density functions {LND; WD; GD}.

Total Knot Area Ratio at the Intermediate Zone ($tKAR_{IZ}$)

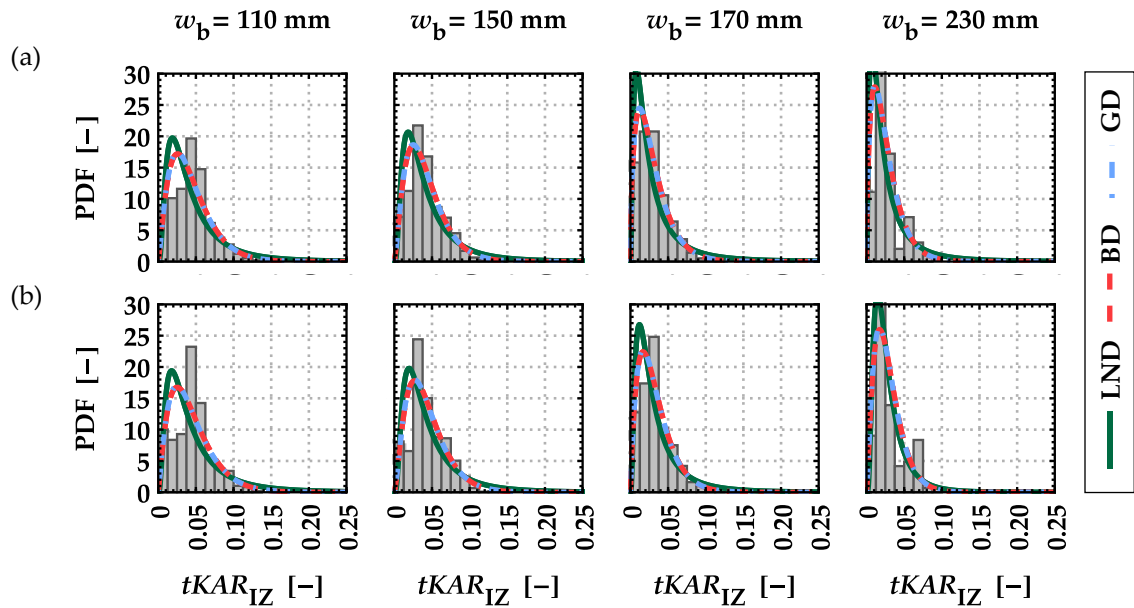


Figure Annex C-11: Histograms of the total knot area ratio at intermediate zones $tKAR_{IZ}$ of boards featuring a width of $w_b = \{110; 150; 170; 230\}$ mm allocated to (a) group GI (T14) and (b) group GII (T24) together with calibrated density functions {LND; BD; GD}.

Distance between Intermediate Zones (D_{IZ})

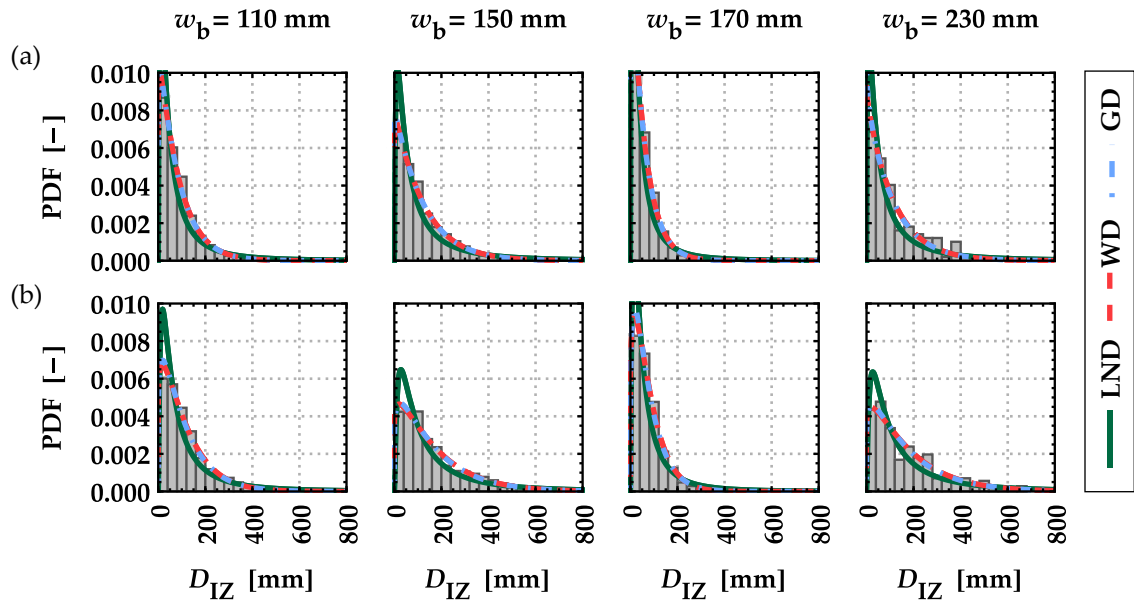


Figure Annex C-12: Histograms of the distance between intermediate zones D_{IZ} of boards featuring a width of $w_b = \{110; 150; 170; 230\}$ mm allocated to (a) group GI (T14) and (b) group GII (T24) together with calibrated density functions {LND; WD; GD}.

C-1.3 Influence of lengthwise Splitting on the Model Parameters

Length of the Weak Zone (L_{WZ})

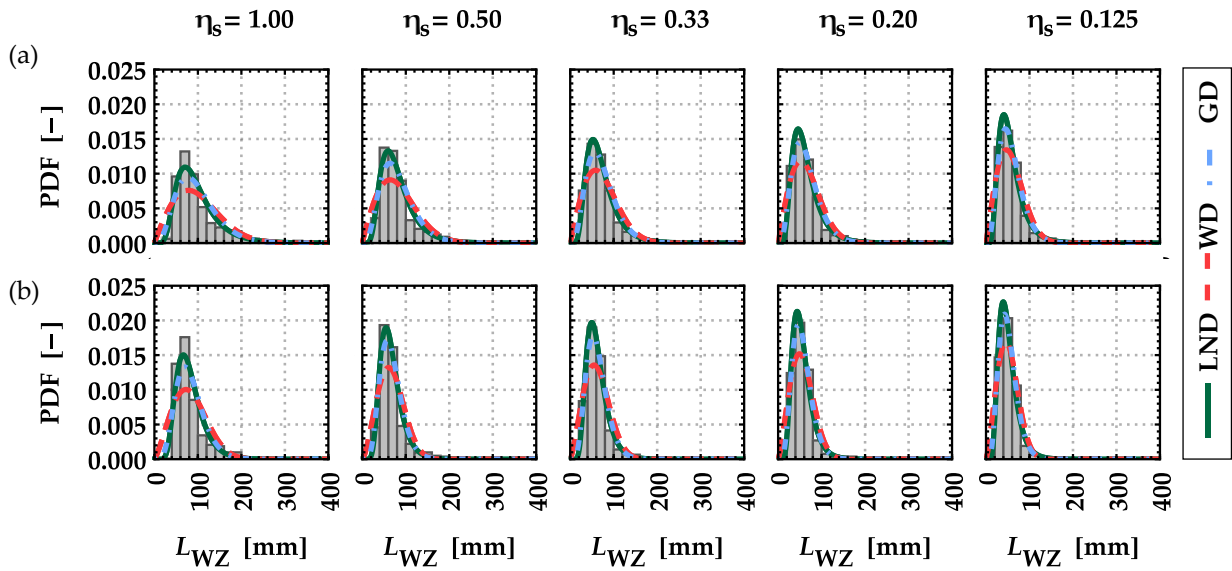


Figure Annex C-13: Histograms of the length of the weak zones L_{WZ} of boards featuring a width of $w_b = 150$ mm and a separation ratio of $\eta_s = \{1.00; 0.50; 0.33; 0.20; 0.125\}$ allocated to (a) group GI (T14) and (b) group GII (T24) together with calibrated density functions {LND; WD; GD}.

Total Knot Area Ratio at the Weak Zone ($tKAR_{WZ}$)

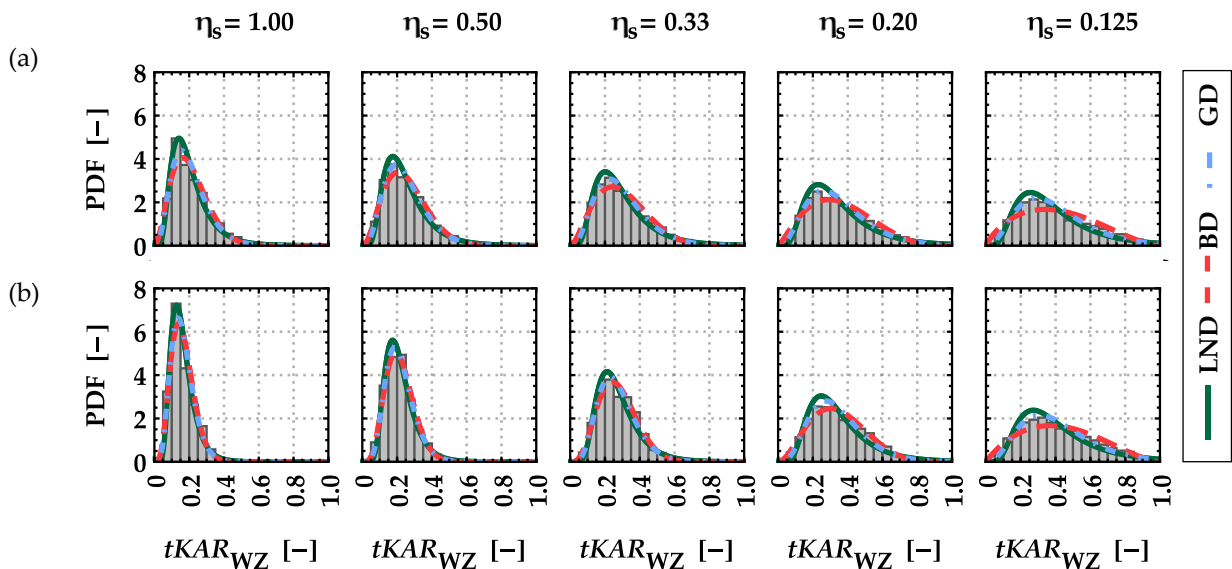


Figure Annex C-14: Histograms of the total knot area ratio at weak zones $tKAR_{WZ}$ of boards featuring a width of $w_b = 150$ mm and a separation ratio of $\eta_s = \{1.00; 0.50; 0.33; 0.20; 0.125\}$ allocated to (a) group GI (T14) and (b) group GII (T24) together with calibrated density functions {LND; BD; GD}.

Distance between Weak Zones (D_{WZ})

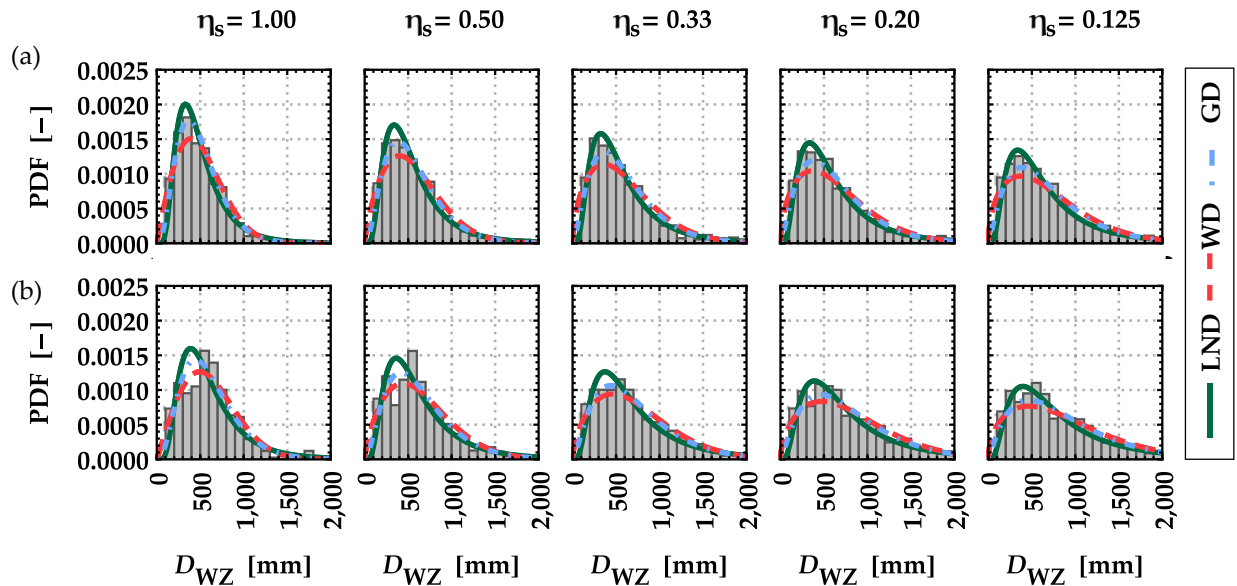


Figure Annex C-15: Histograms of the distance between weak zones D_{WZ} of boards featuring a width of $w_b = 150$ mm and a separation ratio of $\eta_s = \{1.00; 0.50; 0.33; 0.20; 0.125\}$ allocated to (a) group GI (T14) and (b) group GII (T24) together with calibrated density functions {LND; WD; GD}.

Length of the Intermediate Zones (L_{IZ})

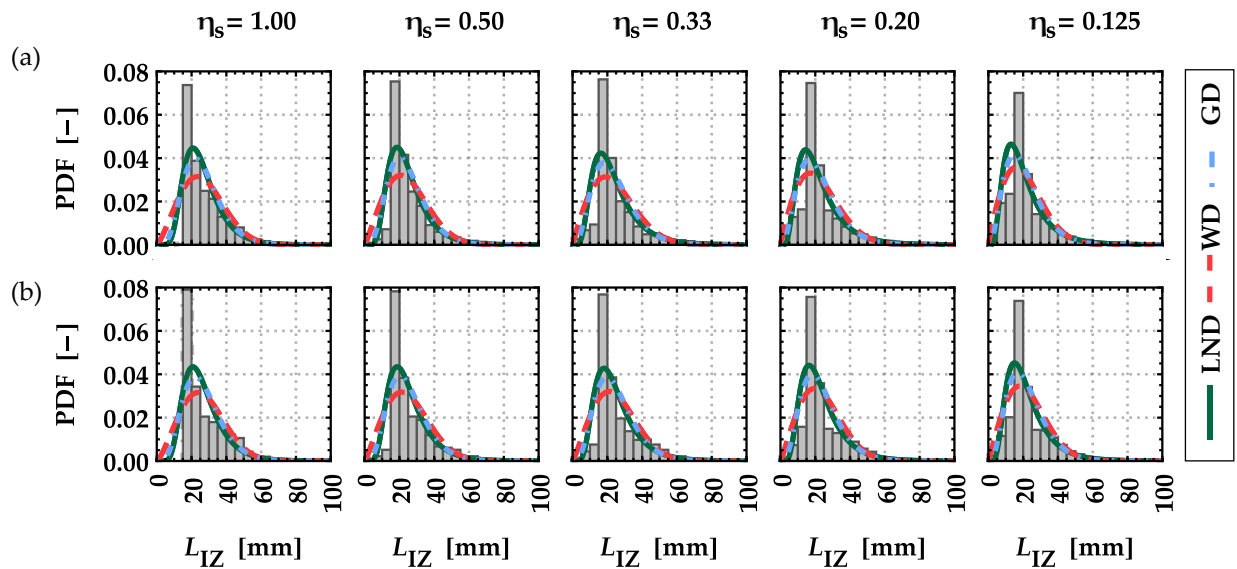


Figure Annex C-16: Histograms of the length of the intermediate zones L_{IZ} of boards featuring a width of $w_b = 150$ mm and a separation ratio of $\eta_s = \{1.00; 0.50; 0.33; 0.20; 0.125\}$ allocated to (a) group GI (T14) and (b) group GII (T24) together with calibrated density functions {LND; WD; GD}.

Total Knot Area Ratio at the Intermediate Zone ($tKAR_{IZ}$)

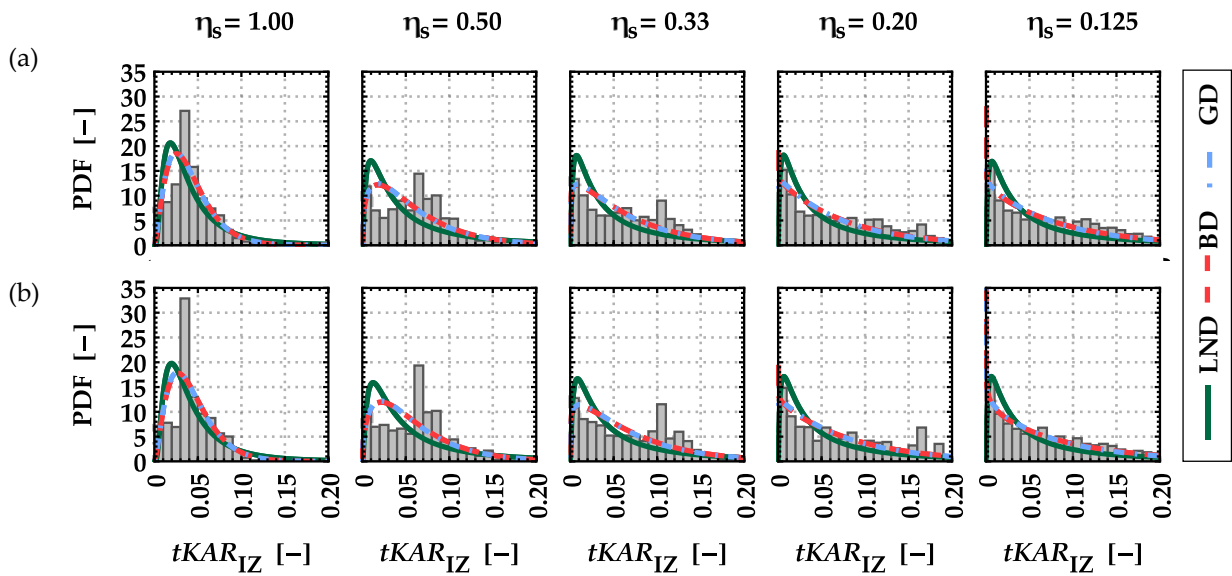


Figure Annex C-17: Histograms of the total knot area ratio at intermediate zones $tKAR_{IZ}$ of boards featuring a width of $w_b = 150$ mm and a separation ratio of $\eta_s = \{1.00; 0.50; 0.33; 0.20; 0.125\}$ allocated to (a) group GI (T14) and (b) group GII (T24) together with calibrated density functions {LND; BD; GD}.

Distance between Intermediate Zones (D_{IZ})

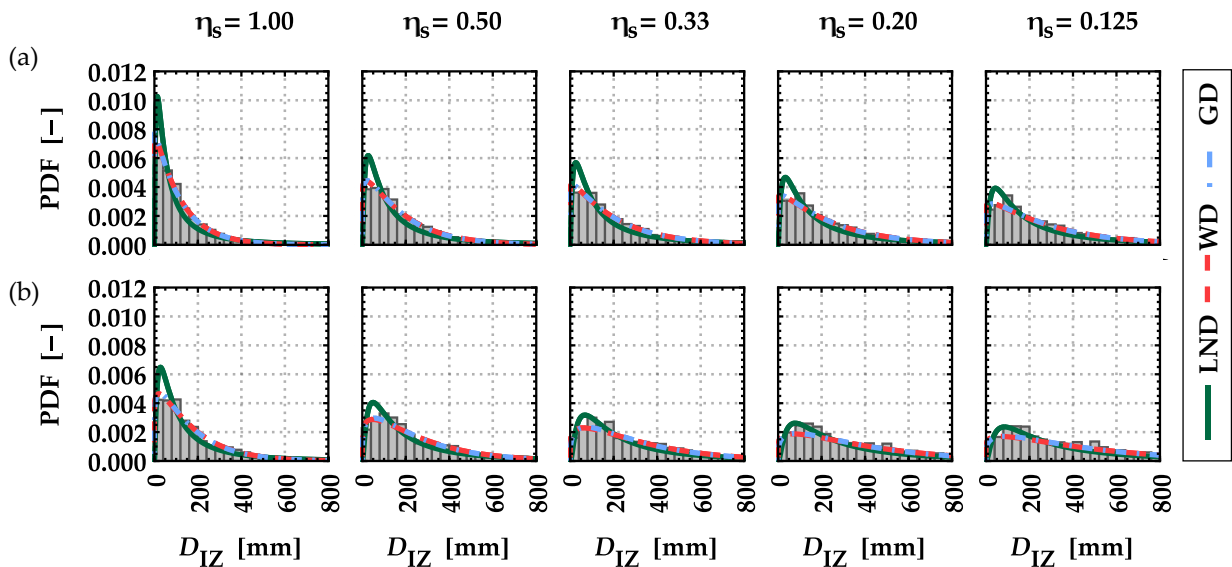


Figure Annex C-18: Histograms of the distance between intermediate zones D_{IZ} of boards featuring a width of $w_b = 150$ mm and a separation ratio of $\eta_s = \{1.00; 0.50; 0.33; 0.20; 0.125\}$ allocated to (a) group GI (T14) and (b) group GII (T24) together with calibrated density functions {LND; WD; GD}.

C-1.4 Correlation of Model Parameters

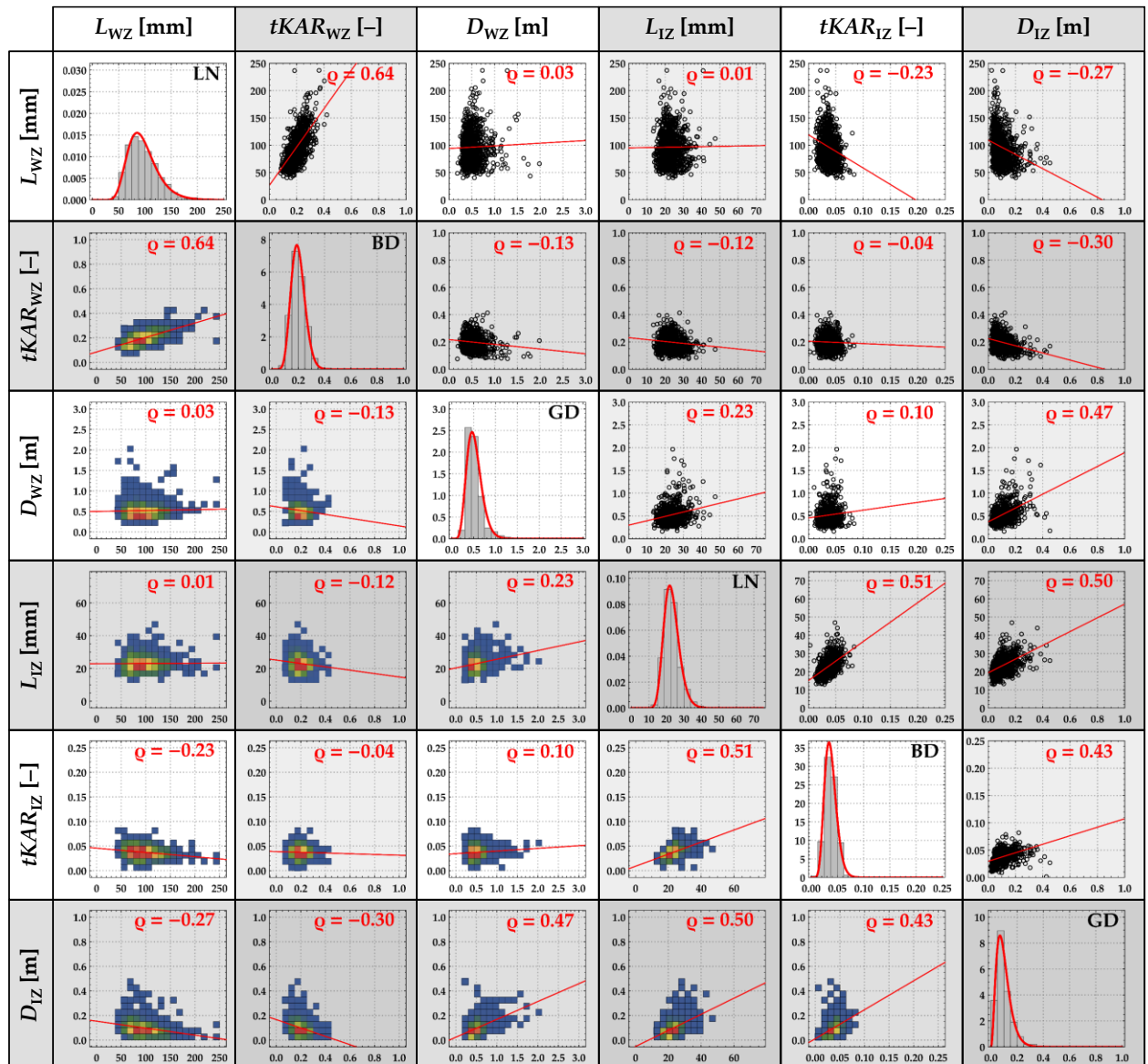


Figure Annex C-19: Correlations and linear trendlines together with histograms and calibrated density functions of global (mean) board properties of $\{L_{wz}; tKAR_{wz}; D_{wz}; L_{lIZ}; tKAR_{lIZ}; D_{lIZ}\}$ of all boards in the databases given a separation ratio of $\eta_s = 1.00$.

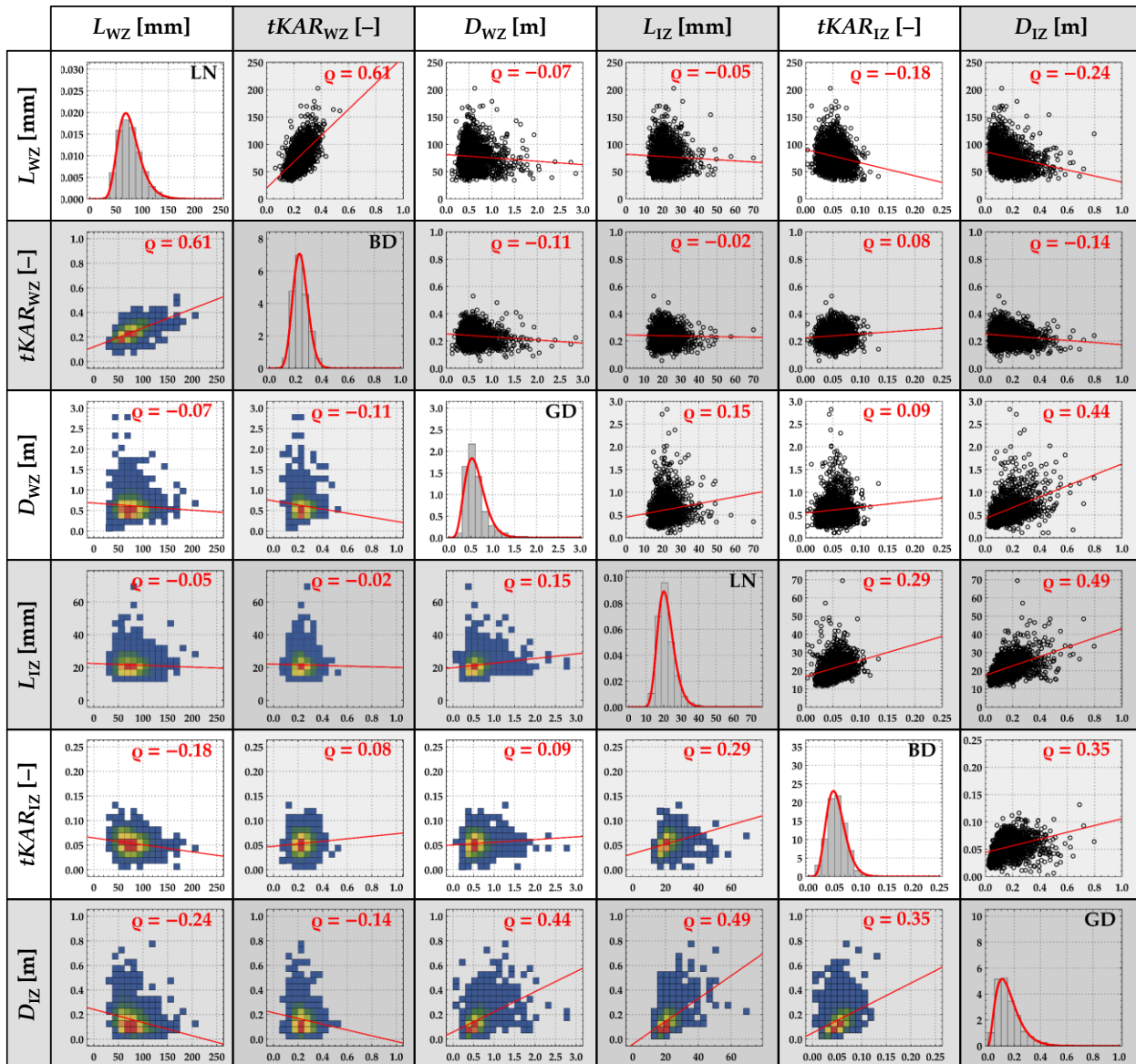


Figure Annex C-20: Correlations and linear trendlines together with histograms and calibrated density functions of global (mean) board properties of $\{L_{WZ}; tKAR_{WZ}; D_{WZ}; L_{IZ}; tKAR_{IZ}; D_{IZ}\}$ of all boards in the databases given a separation ratio of $\eta_s = 0.50$.

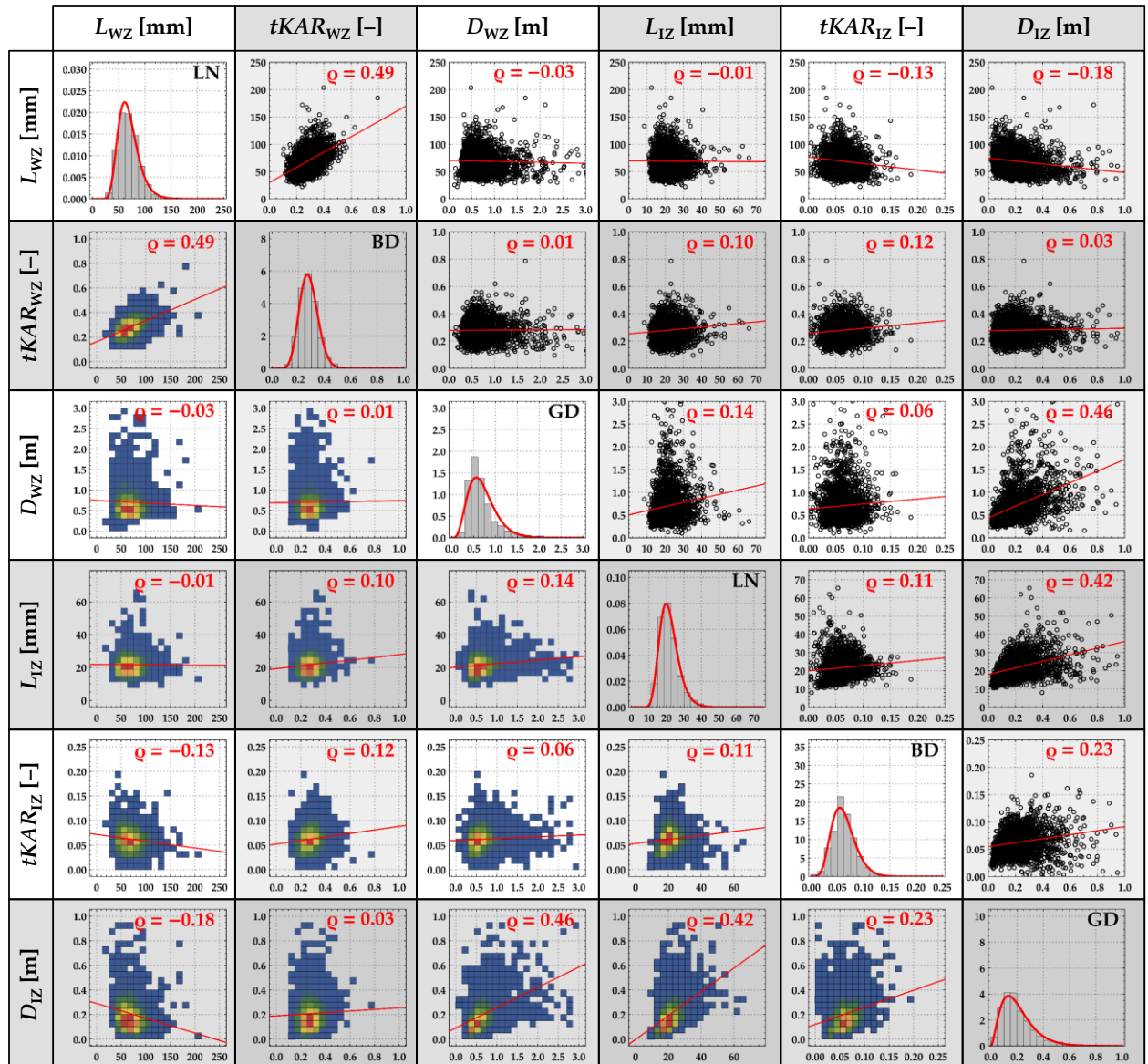


Figure Annex C-21: Correlations and linear trendlines together with histograms and calibrated density functions of global (mean) board properties of $\{L_{Wz}; tKAR_{Wz}; D_{Wz}; L_{Iz}; tKAR_{Iz}; D_{Iz}\}$ of all boards in the databases given a separation ratio of $\eta_s = 0.33$.

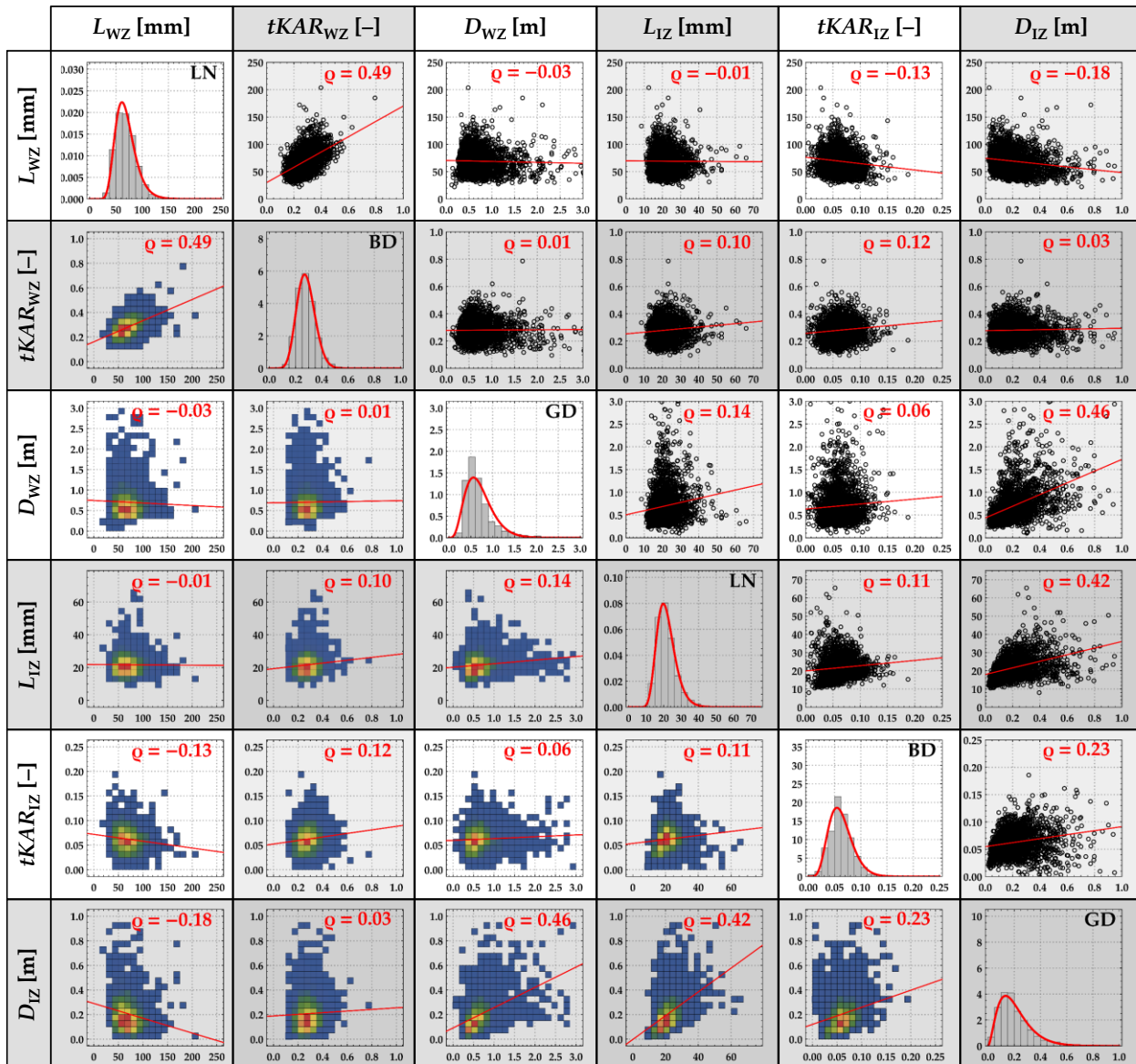


Figure Annex C-22: Correlations and linear trendlines together with histograms and calibrated density functions of global (mean) board properties of $\{L_{WZ}; tKAR_{WZ}; D_{WZ}; L_{IZ}; tKAR_{IZ}; D_{IZ}\}$ of all boards in the databases given a separation ratio of $\eta_s = 0.20$.

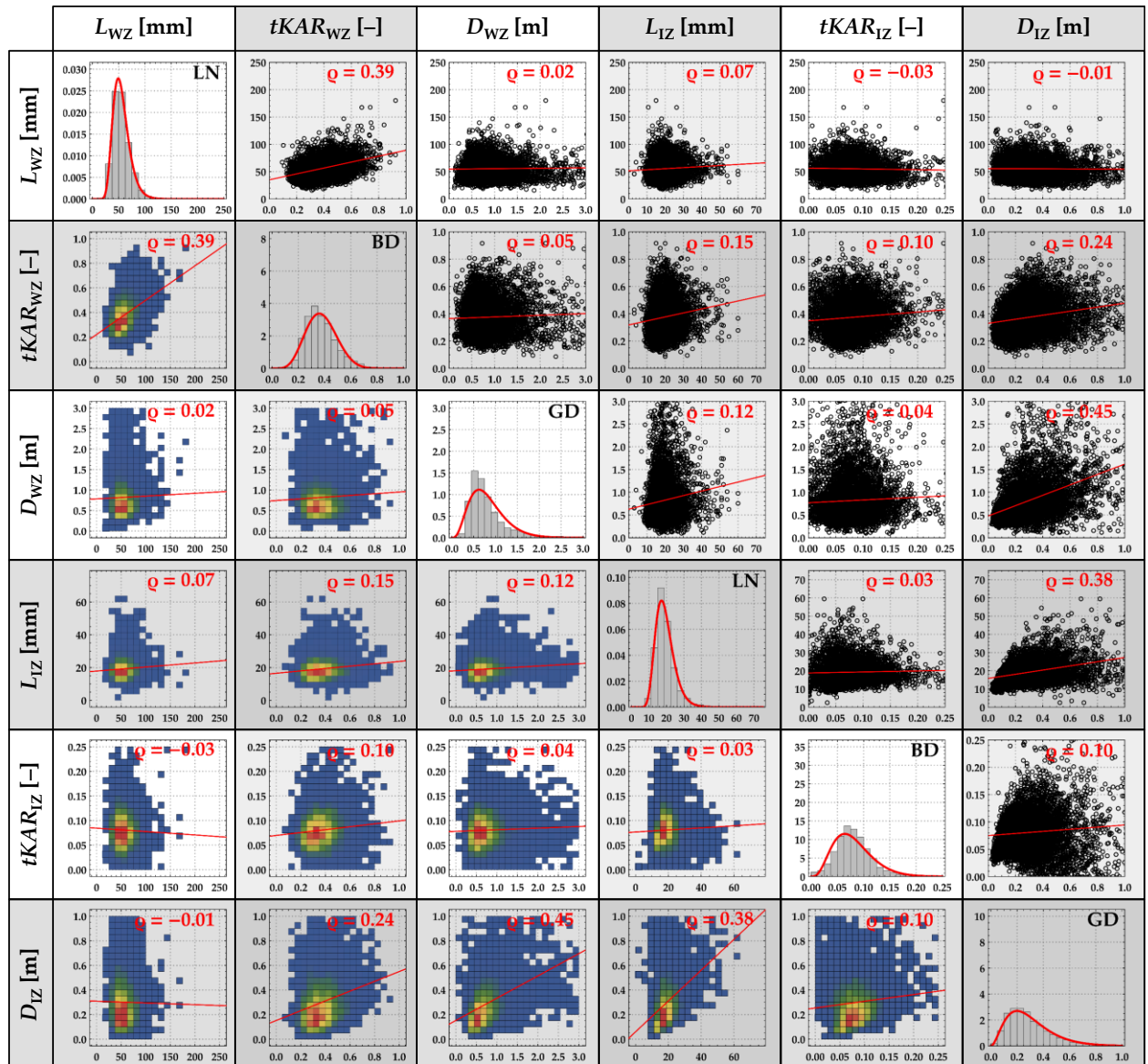


Figure Annex C-23: Correlations and linear trendlines together with histograms and calibrated density functions of global (mean) board properties of $\{L_{WZ}; tKAR_{WZ}; D_{WZ}; L_{IZ}; tKAR_{IZ}; D_{IZ}\}$ of all boards in the databases given a separation ratio of $\eta_s = 0.125$.

Annex D: Tables

In the following, tabulated results from different chapters are provided. The data presents also the basis for the figures in the main part.

D-1 Probabilistic Board Model

D-1.1 Influence of the Board Thickness on the Model Parameters

Table Annex D-1: Statistics of the weak zones $\{L_{wz}; tKAR_{wz}; D_{wz}\}$ of boards featuring dimension of $w_b = 150$ mm and $t_b = \{29; 35; 45\}$ mm allocated to group GI (T14) and GII (T24).

Thickness t_b [mm]		GI (T14)			GII (T24)		
		29	35	45	29	35	45
#boards		13	80	56	27	46	23
L_{wz}	#	70	678	362	111	284	114
	min [mm]	39	33	34	41	40	37
	max [mm]	329	366	345	329	249	209
	mean [mm]	92.5	95.7	104.9	88.8	80.2	82.6
	COV [%]	55.4	54.3	50.9	55.8	48.0	46.1
	$\chi_{05,emp}$ [mm]	50	46	45	45	49	46
	$\chi_{95,emp}$ [mm]	195	202	203	181	176	166
$tKAR_{wz}$	#	70	680	364	111	284	115
	min [-]	0.05	0.05	0.05	0.07	0.04	0.07
	max [-]	0.52	0.70	0.58	0.39	0.35	0.44
	mean [-]	0.19	0.21	0.19	0.16	0.17	0.15
	COV [%]	59.2	50.5	53.6	40.5	39.3	48.8
	$\chi_{05,emp}$ [-]	0.08	0.09	0.08	0.09	0.09	0.08
	$\chi_{95,emp}$ [-]	0.46	0.43	0.41	0.30	0.28	0.31
D_{wz}	#	57	599	309	80	237	92
	min [mm]	160	132	131	147	136	142
	max [mm]	1,592	1,865	1,927	1,842	1,806	1,510
	mean [mm]	612	513	571	672	616	640
	COV [%]	50.4	64.5	53.0	55.7	59.6	49.0
	$\chi_{05,emp}$ [mm]	175	167	176	176	189	163
	$\chi_{95,emp}$ [mm]	1,168	1,023	1,050	1,452	1,311	1,160

Table Annex D-2: Statistics of the intermediate zones $\{L_{IZ}; tKAR_{IZ}; D_{IZ}\}$ of boards featuring dimension of $w_b = 150$ mm and $t_b = \{29; 35; 45\}$ mm allocated to group GI (T14) and GII (T24).

Thickness t_b [mm]		GI (T14)			GII (T24)		
		29	35	45	29	35	45
#boards		13	80	56	27	46	23
L_{IZ}	#	145	1,101	947	274	567	273
	min [mm]	14	15	13	15	15	15
	max [mm]	80	90	94	72	82	74
	mean [mm]	26.5	26.4	26.7	25.5	27.5	26.6
	COV [%]	44.5	43.5	48.2	44.3	44.7	47.5
	$\chi_{05,emp}$ [mm]	15	15	15	15	15	15
	$\chi_{95,emp}$ [mm]	49	48	53	47	51	51
$tKAR_{IZ}$	#	137	943	794	252	471	214
	min [-]	0.001	0.001	0.000	0.002	0.000	0.002
	max [-]	0.097	0.141	0.130	0.116	0.130	0.107
	mean [-]	0.042	0.045	0.037	0.044	0.045	0.039
	COV [%]	51.0	52.5	60.7	47.6	53.9	63.5
	$\chi_{05,emp}$ [-]	0.004	0.007	0.007	0.007	0.009	0.004
	$\chi_{95,emp}$ [-]	0.086	0.088	0.084	0.085	0.089	0.084
D_{IZ}	#	20	1,701	1,259	357	805	365
	min [mm]	10	10	10	10	10	10
	max [mm]	730	916	870	1,084	1,137	874
	mean [mm]	162	120	114	185	157	165
	COV [%]	73.7	99.6	106.9	85.2	98.0	93.7
	$\chi_{05,emp}$ [mm]	17	14	15	17	14	15
	$\chi_{95,emp}$ [mm]	387	362	367	528	487	460

D-1.2 Influence of the Board Width on the Model Parameters

Table Annex D-3: Statistics of the weak zones $\{L_{wz}; tKAR_{wz}; D_{wz}\}$ of boards featuring a width of $w_b = \{110; 150; 170; 230\}$ mm allocated to group GI (T14) and GII (T24).

Width w_b [mm]		GI (T14)				GII (T24)			
		110	150	170	230	110	150	170	230
#boards		123	149	488	6	46	96	48	12
L_{wz}	#	1,111	1,110	4,246	26	367	509	341	53
	min [mm]	30	33	27	52	32	37	33	45
	max [mm]	347	366	441	293	330	329	316	314
	mean [mm]	85.8	98.5	104.2	122.1	65.0	82.6	80.3	94.1
	COV [%]	57.1	54.8	55.5	54.6	49.2	45.6	46.8	58.4
	$\chi_{05,emp}$ [mm]	39	46	44	54	41	48	44	46
	$\chi_{95,emp}$ [mm]	191	204	225	292	98	161	144	223
$tKAR_{wz}$	#	1,114	680	4,249	26	367	284	341	53
	min [-]	0.05	0.05	0.04	0.05	0.06	0.04	0.05	0.06
	max [-]	0.78	0.70	0.70	0.45	0.44	0.44	0.39	0.28
	mean [-]	0.24	0.21	0.20	0.16	0.18	0.16	0.15	0.13
	COV [%]	48.3	52.2	50.0	58.2	36.3	41.7	41.9	38.9
	$\chi_{05,emp}$ [-]	0.09	0.08	0.08	0.05	0.09	0.08	0.08	0.07
	$\chi_{95,emp}$ [-]	0.45	0.43	0.40	0.31	0.29	0.29	0.27	0.23
D_{wz}	#	991	599	3,760	20	321	237	291	41
	min [mm]	123	131	129	270	127	136	137	161
	max [mm]	1,458	1,927	1,794	1,664	1,376	1,842	1,636	1,789
	mean [mm]	411	498	444	631	442	607	525	752
	COV [%]	47.1	54.2	47.2	50.6	48.4	52.2	51.1	57.4
	$\chi_{05,emp}$ [mm]	164	175	178	270	189	185	182	282
	$\chi_{95,emp}$ [mm]	775	972	819	1,125	863	1,144	1,050	1,639

Table Annex D-4: Statistics of the intermediate zones $\{L_{IZ}; tKAR_{IZ}; D_{IZ}\}$ of boards featuring a width of $w_b = \{110; 150; 170; 230\}$ mm allocated to group GI (T14) and GII (T24).

Width w_b [mm]		GI (T14)				GII (T24)			
		110	150	170	230	110	150	170	230
#boards		123	149	488	6	46	96	48	12
L_{IZ}	#	2,588	1,101	15,583	104	819	567	1,386	136
	min [mm]	7	13	3	15	13	15	3	15
	max [mm]	78	94	108	90	66	82	75	81
	mean [mm]	22.3	26.5	20.7	27.4	22.3	26.8	20.1	29.1
	COV [%]	37.1	45.7	50.8	56.3	37.2	45.4	51.3	53.2
	$\chi_{05,emp}$ [mm]	15	15	9	15	15	15	9	15
	$\chi_{95,emp}$ [mm]	39	50	41	60	38	49	42	65
$tKAR_{IZ}$	#	2,419	943	12,992	73	775	471	990	115
	min [-]	0.001	0.001	0.001	0.001	0.001	0.001	0.001	0.001
	max [-]	0.152	0.141	0.124	0.086	0.136	0.130	0.122	0.096
	mean [-]	0.044	0.041	0.030	0.026	0.044	0.043	0.033	0.029
	COV [%]	56.1	54.5	65.9	67.9	55.5	53.3	62.3	68.0
	$\chi_{05,emp}$ [-]	0.007	0.007	0.006	0.005	0.006	0.008	0.005	0.006
	$\chi_{95,emp}$ [-]	0.091	0.083	0.068	0.063	0.091	0.086	0.071	0.072
D_{IZ}	#	3,579	1,701	19,340	124	1,140	805	1,674	179
	min [mm]	10	10	10	10	10	10	10	10
	max [mm]	716	916	574	417	689	1,137	406	814
	mean [mm]	85	121	59	115	111	168	76	175
	COV [%]	96.5	96.7	98.2	91.4	87.4	92.7	84.6	89.6
	$\chi_{05,emp}$ [mm]	12	13	11	12	12	12	12	14
	$\chi_{95,emp}$ [mm]	244	351	165	340	309	471	199	519

D-1.3 Influence of lengthwise Splitting on the Model Parameters

Table Annex D-5: Statistics of the weak zones $\{L_{wz}; tKAR_{wz}; D_{wz}\}$ of boards featuring a width of $w_b = 150$ mm and a separation ratio of $\eta_s = \{1.00; 0.50; 0.33; 0.20; 0.125\}$ allocated to group GI (T14) and GII (T24).

Separation ratio η_s [-]		GI (T14)					GII (T24)				
		1.00	0.50	0.33	0.20	0.125	1.00	0.50	0.33	0.20	0.125
#boards		149	294	430	675	1039	96	175	247	370	515
L_{wz}	#	1,110	1,837	2,400	3,400	4,844	509	815	1,004	1,353	1,725
	min [mm]	33	23	15	16	15	37	18	18	18	15
	max [mm]	366	389	334	322	264	329	209	236	212	179
	mean [mm]	98.5	81.7	72.3	64.5	57.4	82.6	66.6	62.0	55.6	50.9
	COV [%]	54.8	55.2	53.1	52.8	51.7	45.6	42.0	44.5	44.3	43.4
	$\chi_{05,emp}$ [mm]	46	37	31	27	24	48	37	31	26	23
	$\chi_{95,emp}$ [mm]	204	173	150	133	114	161	127	112	98	87
$tKAR_{wz}$	#	1,114	1,834	2,403	3,401	4,846	510	816	1,002	1,354	1,729
	min [-]	0.05	0.04	0.03	0.02	0.03	0.04	0.06	0.07	0.07	0.07
	max [-]	0.70	0.81	0.93	0.98	1.00	0.44	0.59	0.74	1.00	1.00
	mean [-]	0.21	0.25	0.30	0.35	0.40	0.16	0.22	0.27	0.34	0.41
	COV [%]	52.2	49.0	50.0	51.2	52.4	41.7	38.2	40.0	44.9	50.0
	$\chi_{05,emp}$ [-]	0.08	0.10	0.11	0.12	0.13	0.08	0.10	0.12	0.14	0.14
	$\chi_{95,emp}$ [-]	0.43	0.49	0.58	0.71	0.82	0.29	0.38	0.47	0.63	0.81
D_{wz}	#	965	1,538	1,971	2,725	3,805	409	634	747	983	1,214
	min [mm]	131	118	119	117	113	136	116	116	121	117
	max [mm]	1,927	2,305	2,792	3,302	3,304	1,842	2,611	2,477	3,061	3,665
	mean [mm]	498	562	595	644	690	607	640	726	808	871
	COV [%]	54.2	60.5	68.7	71.0	73.0	52.2	61.6	64.9	67.9	72.0
	$\chi_{05,emp}$ [mm]	175	171	163	164	163	185	167	174	179	183
	$\chi_{95,emp}$ [mm]	972	1,202	1,478	1,556	1,727	1,144	1,408	1,676	1,956	2,241

Table Annex D-6: Statistics of the intermediate zones $\{L_{Iz}; tKAR_{Iz}; D_{Iz}\}$ of boards featuring a width of $w_b = 150$ mm and a separation ratio of $\eta_s = \{1.00; 0.50; 0.33; 0.20; 0.125\}$ allocated to group GI (T14) and GII (T24).

Separation ratio η_s [-]		GI (T14)					GII (T24)				
		1.00	0.50	0.33	0.20	0.125	1.00	0.50	0.33	0.20	0.125
#boards		149	294	430	675	1039	96	175	247	370	515
L_{Iz}	#	2,193	3,026	3,819	4,928	6,626	1,114	1,278	1,396	1,549	1,853
	min [mm]	13	3	3	3	3	15	3	3	3	3
	max [mm]	94	99	99	98	86	82	90	81	81	90
	mean [mm]	26.5	24.7	23.9	22.3	20.7	26.8	25.1	24.9	23.5	22.2
	COV [%]	45.7	49.3	54.2	55.5	55.1	45.4	48.8	49.2	50.4	52.0
	$\chi_{05,emp}$ [mm]	15	14	10	8	6	15	15	12	10	9
	$\chi_{95,emp}$ [mm]	50	51	51	48	45	49	51	51	48	46
$tKAR_{Iz}$	#	1,874	2,578	3,308	4,320	5,872	937	1,060	1,175	1,314	1,567
	min [-]	0.001	0.001	0.001	0.001	0.001	0.001	0.001	0.001	0.001	0.001
	max [-]	0.141	0.190	0.241	0.285	0.371	0.130	0.173	0.220	0.262	0.329
	mean [-]	0.041	0.059	0.064	0.072	0.079	0.043	0.059	0.068	0.077	0.084
	COV [%]	54.5	60.8	71.3	79.3	82.7	53.3	60.0	69.6	78.8	87.6
	$\chi_{05,emp}$ [-]	0.006	0.003	0.003	0.002	0.002	0.007	0.004	0.003	0.003	0.002
	$\chi_{95,emp}$ [-]	0.083	0.120	0.143	0.174	0.200	0.086	0.122	0.140	0.183	0.238
D_{Iz}	#	3,162	4,572	5,792	7,650	10,436	1,527	1,920	2,157	2,536	3,067
	min [mm]	1	1	1	1	1	1	1	1	1	1
	max [mm]	916	1,507	1,508	1,945	2,456	1,137	1,556	2,021	2,270	3,185
	mean [mm]	121	181	211	251	288	168	254	319	394	443
	COV [%]	96.7	94.9	98.3	98.7	99.2	92.7	88.9	90.8	90.7	92.7
	$\chi_{05,emp}$ [mm]	10	11	11	14	20	12	22	34	42	49
	$\chi_{95,emp}$ [mm]	351	510	626	740	845	471	694	904	1,138	1,305

D-1.4 Boards in Full Cross-Section Width

Table Annex D-7: Statistics of the tensile strength $f_{t,0,b}$ and modulus of elasticity in tension $E_{t,0,b}$ parallel to the grain calculated from $1.5 \cdot 10^4$ virtually generated boards for each width and group, considering a test length of $l_b = 9 \cdot w_b$ according to **EN 408 [39]**.

Width w_b [mm]		GI (T14)				GII (T24)			
		100	150	200	250	100	150	200	250
$f_{t,0,b}$	min [MPa]	6.1	6.3	5.8	6.8	12.2	12.3	13.3	14.5
	max [MPa]	76.6	74.6	74.7	75.2	115.9	101.2	105.9	106.1
	mean [MPa]	27.8	27.4	27.7	27.6	40.4	40.2	40.4	40.1
	COV [%]	34.8	31.6	30.0	29.3	30.1	28.1	27.0	26.6
	$\chi_{05,LN}$ [MPa]	14.4	15.3	15.9	16.0	23.6	24.4	25.1	25.2
$E_{t,0,b}$	min [MPa]	6,206	6,101	6,486	6,543	6,958	7,484	7,829	7,617
	max [MPa]	19,135	17,915	19,676	20,909	25,920	25,784	24,958	25,151
	mean [MPa]	10,454	10,442	10,485	10,486	12,988	13,008	13,062	12,992
	COV [%]	15.3	14.9	14.9	14.8	17.2	17.3	17.1	17.2
	$\chi_{05,LN}$ [MPa]	8,062	8,114	8,149	8,169	9,713	9,721	9,799	9,737

Table Annex D-8: Statistics of the tensile strength $f_{t,0,b}$ and modulus of elasticity in tension $E_{t,0,b}$ parallel to the grain calculated from $1.5 \cdot 10^4$ virtually generated boards for each width and group, considering a test length of $l_b = \{2.0; 4.0\}$ m.

Width w_b [mm]		GI (T14)				GII (T24)				
		100	150	200	250	100	150	200	250	
$l_b = 2.0$ m	$f_{t,0,b}$	min [MPa]	4.7	6.5	6.5	6.8	11.2	11.5	13.8	10.4
		max [MPa]	74.2	68.0	69.1	70.1	92.1	109.6	98.0	101.4
		mean [MPa]	23.4	25.6	27.3	28.0	35.8	38.2	39.7	40.4
		COV [%]	33.7	31.6	30.0	29.7	28.6	28.0	26.8	26.3
		$\chi_{05,LN}$ [MPa]	12.5	14.3	15.7	16.2	21.5	23.4	24.8	25.5
	$E_{t,0,b}$	min [MPa]	6,113	5,889	6,359	6,222	7,520	6,972	7,245	7,228
		max [MPa]	19,774	18,821	18,155	19,783	27,851	26,414	25,611	25,850
		mean [MPa]	10,429	10,454	10,495	10,487	12,991	13,014	13,025	13,003
		COV [%]	15.2	15.1	15.1	15.0	17.0	17.5	17.1	17.0
		$\chi_{05,LN}$ [MPa]	8,074	8,105	8,142	8,143	9,758	9,703	9,767	9,759
$l_b = 4.0$ m	$f_{t,0,b}$	min [MPa]	4.9	5.1	5.0	5.9	9.2	11.4	12.0	11.3
		max [MPa]	56.6	62.9	61.3	57.5	78.3	103.9	94.4	105.1
		mean [MPa]	20.3	22.8	24.3	25.3	32.5	35.2	36.8	37.7
		COV [%]	32.8	31.2	29.6	28.9	27.4	27.4	26.3	26.6
		$\chi_{05,LN}$ [MPa]	11.1	12.8	14.1	14.8	19.9	21.8	23.2	23.6
	$E_{t,0,b}$	min [MPa]	6,464	6,313	6,242	6,326	7,630	7,691	7,641	7,517
		max [MPa]	19,448	19,402	19,363	18,765	24,041	26,392	29,764	27,987
		mean [MPa]	10,419	10,456	10,463	10,477	12,947	13,014	13,018	13,051
		COV [%]	14.9	15.0	14.9	14.9	16.8	17.2	17.0	17.3
		$\chi_{05,LN}$ [MPa]	8,103	8,131	8,145	8,150	9,741	9,746	9,778	9,765

Table Annex D-9: Statistics of the tensile strength $f_{t,0,b}$ and modulus of elasticity in tension $E_{t,0,b}$ parallel to the grain calculated from $1.5 \cdot 10^4$ virtually generated boards from both groups featuring a board widths $w_b = \{100; 150; 200; 250\}$ mm and group, considering a test length of $l_b = \{0.90; 1.35; 2.00; 2.25; 4.00\}$ m.

Length l_b [m]		GI (T14)					GII (T24)					
		0.90	1.35	2.00	2.25	4.00	0.90	1.35	2.00	2.25	4.00	
$w_b = 100$ mm	$f_{t,0,b}$	min [MPa]	6.8	6.3	6.5	6.0	5.1	12.9	12.3	11.5	9.0	11.4
		max [MPa]	95.5	74.6	68.0	69.9	62.9	106.2	101.2	109.6	96.9	103.9
		mean [MPa]	29.7	27.4	25.6	25.1	22.8	42.5	40.2	38.2	37.6	35.2
		COV [%]	32.3	31.6	31.6	31.3	31.2	28.1	28.1	28.0	27.7	27.4
		$\chi_{05,LN}$ [MPa]	16.3	15.3	14.3	14.0	12.8	25.8	24.4	23.4	23.0	21.8
	$E_{t,0,b}$	min [MPa]	5,798	6,101	5,889	6,291	6,313	7,353	7,484	6,972	7,404	7,691
		max [MPa]	19,987	17,915	18,821	18,996	19,402	25,525	25,784	26,414	24,876	26,392
		mean [MPa]	10,477	10,442	10,454	10,446	10,456	13,009	13,008	13,014	12,994	13,014
		COV [%]	15.3	14.9	15.1	15.0	15.0	17.2	17.3	17.5	17.0	17.2
		$\chi_{05,LN}$ [MPa]	8,085	8,114	8,105	8,109	8,131	9,733	9,721	9,703	9,757	9,746
$w_b = 150$ mm	$f_{t,0,b}$	min [MPa]	6.8	6.3	6.5	6.0	5.1	12.9	12.3	11.5	9.0	11.4
		max [MPa]	95.5	74.6	68.0	69.9	62.9	106.2	101.2	109.6	96.9	103.9
		mean [MPa]	29.7	27.4	25.6	25.1	22.8	42.5	40.2	38.2	37.6	35.2
		COV [%]	32.3	31.6	31.6	31.3	31.2	28.1	28.1	28.0	27.7	27.4
		$\chi_{05,LN}$ [MPa]	16.3	15.3	14.3	14.0	12.8	25.8	24.4	23.4	23.0	21.8
	$E_{t,0,b}$	min [MPa]	5,798	6,101	5,889	6,291	6,313	7,353	7,484	6,972	7,404	7,691
		max [MPa]	19,987	17,915	18,821	18,996	19,402	25,525	25,784	26,414	24,876	26,392
		mean [MPa]	10,477	10,442	10,454	10,446	10,456	13,009	13,008	13,014	12,994	13,014
		COV [%]	15.3	14.9	15.1	15.0	15.0	17.2	17.3	17.5	17.0	17.2
		$\chi_{05,LN}$ [MPa]	8,085	8,114	8,105	8,109	8,131	9,733	9,721	9,703	9,757	9,746
$w_b = 200$ mm	$f_{t,0,b}$	min [MPa]	7.5	6.6	6.5	5.2	5.0	14.7	13.9	13.8	15.1	12.0
		max [MPa]	81.8	75.5	69.1	67.6	61.3	115.6	105.3	98.0	102.4	94.4
		mean [MPa]	31.2	29.1	27.3	26.6	24.3	43.9	41.9	39.7	39.2	36.8
		COV [%]	30.6	30.0	30.0	29.8	29.6	27.6	27.4	26.8	26.4	26.3
		$\chi_{05,LN}$ [MPa]	17.7	16.7	15.7	15.3	14.1	27.0	25.8	24.8	24.7	23.2
	$E_{t,0,b}$	min [MPa]	6,099	5,895	6,359	6,087	6,242	7,362	6,987	7,245	7,479	7,641
		max [MPa]	19,971	18,572	18,155	18,915	19,363	25,731	25,119	25,611	26,823	29,764
		mean [MPa]	10,513	10,490	10,495	10,471	10,463	13,050	13,036	13,025	13,013	13,018
		COV [%]	15.3	15.0	15.1	14.9	14.9	17.1	17.3	17.1	17.1	17.0
		$\chi_{05,LN}$ [MPa]	8,130	8,142	8,142	8,139	8,145	9,782	9,749	9,767	9,767	9,778
$w_b = 250$ mm	$f_{t,0,b}$	min [MPa]	6.7	6.3	6.8	6.8	5.9	13.9	13.7	10.4	14.5	11.3
		max [MPa]	81.6	74.3	70.1	75.2	57.5	120.6	112.2	101.4	106.1	105.1
		mean [MPa]	31.9	29.9	28.0	27.6	25.3	44.8	42.5	40.4	40.1	37.7
		COV [%]	30.3	29.7	29.7	29.3	28.9	27.2	27.1	26.3	26.6	26.6
		$\chi_{05,LN}$ [MPa]	18.3	17.2	16.2	16.0	14.8	27.7	26.4	25.5	25.2	23.6
	$E_{t,0,b}$	min [MPa]	6,088	6,365	6,222	6,543	6,326	7,393	7,585	7,228	7,617	7,517
		max [MPa]	17,979	22,000	19,783	20,909	18,765	28,564	24,782	25,850	25,151	27,987
		mean [MPa]	10,516	10,496	10,487	10,486	10,477	13,050	13,028	13,003	12,992	13,051
		COV [%]	15.3	15.2	15.0	14.8	14.9	17.2	17.3	17.0	17.2	17.3
		$\chi_{05,LN}$ [MPa]	8,126	8,130	8,143	8,169	8,150	9,770	9,731	9,759	9,737	9,765

D-1.5 Boards in Split Condition

Table Annex D-10: Statistics of the tensile strength $f_{t,0,b}$ and modulus of elasticity in tension $E_{t,0,b}$ parallel to the grain calculated from $1.5 \cdot 10^4$ virtually generated and lengthwise split boards from both groups featuring a dimension $w_b = \{100; 150; 200; 250\}$ mm and $l_b = 2.0$ m.

Length $l_b = 2.0$ m		GI (T14)						GII (T24)						
		1.00	0.67	0.50	0.33	0.25	0.13	1.00	0.67	0.50	0.33	0.25	0.13	
$w_b = 100$ mm	$f_{t,0,b}$	min [MPa]	4.7	4.4	4.0	3.5	3.2	2.5	10.6	9.8	7.1	7.4	6.2	4.2
		max [MPa]	70.8	75.8	73.0	69.7	74.0	100.8	97.2	102.0	123.1	110.0	123.2	130.3
		mean [MPa]	23.2	22.2	20.9	18.6	16.8	13.6	35.8	35.1	33.7	31.1	28.9	24.8
		COV [%]	33.5	35.6	39.8	43.6	49.5	63.8	29.2	30.5	32.8	36.4	40.2	51.7
		$\chi_{05,LN}$ [MPa]	12.5	11.4	9.9	8.3	6.8	4.6	21.4	20.4	18.8	16.3	14.2	10.1
	$E_{t,0,b}$	min [GPa]	6.1	6.0	5.9	5.8	5.7	4.9	7.3	6.9	6.9	7.0	6.5	6.3
		max [GPa]	18.4	21.3	22.9	23.2	24.1	30.4	24.8	29.7	35.5	32.8	36.2	42.9
		mean [GPa]	10.4	10.5	10.5	10.5	10.5	10.6	13.0	13.1	13.1	13.1	13.2	13.3
		COV [%]	15.1	16.3	17.3	18.4	19.8	24.2	17.2	18.9	20.2	21.3	23.2	29.0
		$\chi_{05,LN}$ [GPa]	8.1	8.0	7.8	7.7	7.6	7.1	9.7	9.5	9.4	9.2	9.0	8.3
$w_b = 150$ mm	$f_{t,0,b}$	min [MPa]	5.1	5.5	4.7	3.5	3.5	2.5	11.1	11.6	8.5	7.6	6.8	4.9
		max [MPa]	64.4	64.8	77.8	74.5	89.3	79.6	90.4	91.7	107.1	106.2	124.7	138.0
		mean [MPa]	25.6	24.9	22.9	20.2	18.4	15.3	38.3	37.7	36.1	32.8	31.0	28.1
		COV [%]	31.4	33.0	36.8	42.2	46.1	56.3	27.4	29.1	31.7	35.3	38.5	46.3
		$\chi_{05,LN}$ [MPa]	14.3	13.5	11.5	9.2	7.9	5.6	23.6	22.5	20.6	17.4	15.7	12.4
	$E_{t,0,b}$	min [GPa]	5.8	6.3	5.9	5.9	5.8	5.3	7.2	7.1	6.7	6.8	6.4	6.5
		max [GPa]	20.2	19.1	20.7	22.0	25.8	30.4	25.3	25.9	32.0	32.9	32.9	39.7
		mean [GPa]	10.5	10.5	10.5	10.5	10.5	10.5	13.0	13.1	13.1	13.2	13.1	13.3
		COV [%]	15.3	16.1	17.1	18.7	19.7	22.7	17.1	18.5	19.8	21.5	22.9	27.2
		$\chi_{05,LN}$ [GPa]	8.1	8.0	7.9	7.7	7.6	7.2	9.8	9.6	9.4	9.2	9.0	8.5
$w_b = 200$ mm	$f_{t,0,b}$	min [MPa]	5.8	6.5	4.6	3.7	3.7	2.9	13.2	11.7	10.8	7.6	7.6	4.7
		max [MPa]	78.2	76.5	72.3	86.5	85.8	92.0	109.7	111.9	108.5	110.6	120.7	131.2
		mean [MPa]	27.3	26.5	24.4	21.1	19.4	16.3	39.8	39.3	36.8	33.6	32.1	28.9
		COV [%]	30.2	31.3	34.8	41.6	44.6	55.7	27.1	28.7	30.8	35.2	38.0	46.3
		$\chi_{05,LN}$ [MPa]	15.6	14.9	12.7	9.7	8.5	6.0	24.7	23.8	21.4	18.1	16.4	12.8
	$E_{t,0,b}$	min [GPa]	6.2	6.1	6.3	5.6	5.5	5.2	7.3	7.3	7.0	6.7	6.6	6.1
		max [GPa]	19.7	20.1	20.2	24.4	24.1	28.7	27.5	30.2	27.8	35.7	35.9	39.2
		mean [GPa]	10.5	10.5	10.5	10.5	10.5	10.5	13.0	13.1	13.1	13.1	13.2	13.2
		COV [%]	15.0	16.0	16.9	18.9	19.7	23.4	17.3	18.6	19.7	22.1	23.4	27.6
		$\chi_{05,LN}$ [GPa]	8.1	8.1	7.9	7.7	7.6	7.2	9.7	9.6	9.4	9.1	9.0	8.4
$w_b = 250$ mm	$f_{t,0,b}$	min [MPa]	5.7	6.4	5.6	4.2	3.5	2.8	12.8	13.6	10.2	8.3	7.1	5.1
		max [MPa]	73.0	76.6	86.3	73.7	79.8	112.2	99.1	116.3	120.2	119.1	124.5	155.1
		mean [MPa]	28.1	27.5	25.7	22.6	19.8	17.0	40.6	40.2	38.4	34.9	32.4	29.3
		COV [%]	29.6	31.1	33.2	38.6	44.4	55.3	26.3	28.3	30.1	34.4	38.3	46.0
		$\chi_{05,LN}$ [MPa]	16.3	15.5	13.9	11.1	8.7	6.3	25.6	24.4	22.6	19.1	16.6	13.1
	$E_{t,0,b}$	min [GPa]	6.4	6.4	5.7	5.7	5.3	5.3	7.5	7.1	7.0	6.7	6.6	6.1
		max [GPa]	19.3	21.2	21.7	23.0	24.0	37.6	25.1	29.2	29.0	31.0	42.7	42.6
		mean [GPa]	10.5	10.5	10.5	10.5	10.5	10.5	13.0	13.1	13.1	13.1	13.2	13.3
		COV [%]	15.1	16.2	16.9	18.3	19.9	23.6	17.0	19.1	19.8	21.7	23.6	28.3
		$\chi_{05,LN}$ [GPa]	8.1	8.0	7.9	7.8	7.5	7.2	9.8	9.5	9.4	9.1	8.9	8.4

Table Annex D-11: Statistics of the tensile strength $f_{t,0,b}$ and modulus of elasticity in tension $E_{t,0,b}$ parallel to the grain calculated from $1.5 \cdot 10^4$ virtually generated and lengthwise split boards from both groups featuring dimension $w_b = \{100; 150; 200; 250\}$ mm and $l_b = 4.0$ m.

Length $l_b = 2.0$ m		GI (T14)						GII (T24)						
		1.00	0.67	0.50	0.33	0.25	0.13	1.00	0.67	0.50	0.33	0.25	0.13	
Separation ratio η_s [-]														
$w_b = 100$ mm	$f_{t,0,b}$	min [MPa]	4.6	4.7	3.3	3.3	2.8	2.4	8.9	8.7	4.9	6.3	5.7	4.1
		max [MPa]	57.3	62.8	54.6	55.5	63.5	56.4	92.9	96.7	97.9	91.6	103.1	139.2
		mean [MPa]	20.4	19.4	17.8	15.5	13.6	10.5	32.7	31.8	30.1	27.3	25.0	20.6
		COV [%]	32.9	34.7	38.0	41.6	45.5	53.7	27.8	30.1	31.9	35.3	38.0	48.2
		$\chi_{05,LN}$ [MPa]	11.1	10.2	8.8	7.2	6.0	4.2	20.0	18.7	17.1	14.6	12.7	8.9
	$E_{t,0,b}$	min [GPa]	6.1	6.0	5.9	5.8	5.7	4.9	7.3	6.9	6.9	7.0	6.5	6.3
		max [GPa]	18.4	21.3	22.9	23.2	24.1	30.4	24.8	29.7	35.5	32.8	36.2	42.9
		mean [GPa]	10.4	10.5	10.5	10.5	10.5	10.6	13.0	13.1	13.1	13.1	13.2	13.3
		COV [%]	15.1	16.3	17.3	18.4	19.8	24.2	17.2	18.9	20.2	21.3	23.2	29.0
		$\chi_{05,LN}$ [GPa]	8.1	8.0	7.8	7.7	7.6	7.1	9.7	9.5	9.4	9.2	9.0	8.3
$w_b = 150$ mm	$f_{t,0,b}$	min [MPa]	6.4	5.2	4.0	3.4	3.0	2.6	11.8	11.3	9.4	7.4	6.5	5.4
		max [MPa]	63.4	66.9	63.5	69.9	60.1	67.9	98.6	91.5	98.6	86.5	114.4	101.1
		mean [MPa]	22.7	21.9	19.8	17.2	15.2	12.1	35.0	34.4	32.7	28.9	27.3	23.8
		COV [%]	30.9	32.9	36.0	40.2	42.9	50.6	27.2	28.8	30.9	34.5	36.8	43.0
		$\chi_{05,LN}$ [MPa]	12.8	12.0	10.1	8.2	7.0	5.0	21.7	20.7	19.0	15.6	14.4	11.1
	$E_{t,0,b}$	min [GPa]	5.8	6.3	5.9	5.9	5.8	5.3	7.2	7.1	6.7	6.8	6.4	6.5
		max [GPa]	20.2	19.1	20.7	22.0	25.8	30.4	25.3	25.9	32.0	32.9	32.9	39.7
		mean [GPa]	10.5	10.5	10.5	10.5	10.5	10.5	13.0	13.1	13.1	13.2	13.1	13.3
		COV [%]	15.3	16.1	17.1	18.7	19.7	22.7	17.1	18.5	19.8	21.5	22.9	27.2
		$\chi_{05,LN}$ [GPa]	8.1	8.0	7.9	7.7	7.6	7.2	9.8	9.6	9.4	9.2	9.0	8.5
$w_b = 200$ mm	$f_{t,0,b}$	min [MPa]	5.4	5.0	4.2	3.8	3.1	2.7	12.9	9.3	9.8	7.2	6.0	5.3
		max [MPa]	63.3	69.3	63.3	56.0	61.8	65.0	95.5	96.3	109.8	102.9	101.3	132.1
		mean [MPa]	24.5	23.7	21.3	18.0	16.2	12.9	36.7	36.2	33.7	30.0	28.1	24.5
		COV [%]	29.9	31.5	34.5	39.2	41.6	51.3	26.2	27.9	30.2	34.3	36.3	43.4
		$\chi_{05,LN}$ [MPa]	14.1	13.3	11.3	8.7	7.6	5.2	23.2	22.2	19.9	16.4	14.7	11.6
	$E_{t,0,b}$	min [GPa]	6.2	6.1	6.3	5.6	5.5	5.2	7.3	7.3	7.0	6.7	6.6	6.1
		max [GPa]	19.7	20.1	20.2	24.4	24.1	28.7	27.5	30.2	27.8	35.7	35.9	39.2
		mean [GPa]	10.5	10.5	10.5	10.5	10.5	10.5	13.0	13.1	13.1	13.1	13.2	13.2
		COV [%]	15.0	16.0	16.9	18.9	19.7	23.4	17.3	18.6	19.7	22.1	23.4	27.6
		$\chi_{05,LN}$ [GPa]	8.1	8.1	7.9	7.7	7.6	7.2	9.7	9.6	9.4	9.1	9.0	8.4
$w_b = 250$ mm	$f_{t,0,b}$	min [MPa]	5.5	5.6	5.2	4.0	3.4	2.7	12.5	11.6	12.0	8.2	7.5	5.5
		max [MPa]	67.5	67.7	65.5	63.8	66.2	72.7	101.6	102.5	105.1	122.6	111.5	105.8
		mean [MPa]	25.2	24.7	22.7	19.2	16.5	13.6	37.7	37.1	35.0	31.1	28.5	25.1
		COV [%]	29.2	30.8	33.0	37.2	42.0	50.3	26.4	27.9	29.7	33.5	37.0	43.3
		$\chi_{05,LN}$ [MPa]	14.8	14.0	12.3	9.7	7.7	5.6	23.7	22.8	20.8	17.3	14.9	11.8
	$E_{t,0,b}$	min [GPa]	6.4	6.4	5.7	5.7	5.3	5.3	7.5	7.1	7.0	6.7	6.6	6.1
		max [GPa]	19.3	21.2	21.7	23.0	24.0	37.6	25.1	29.2	29.0	31.0	42.7	42.6
		mean [GPa]	10.5	10.5	10.5	10.5	10.5	10.5	13.0	13.1	13.1	13.1	13.2	13.3
		COV [%]	15.1	16.2	16.9	18.3	19.9	23.6	17.0	19.1	19.8	21.7	23.6	28.3
		$\chi_{05,LN}$ [GPa]	8.1	8.0	7.9	7.8	7.5	7.2	9.8	9.5	9.4	9.1	8.9	8.4

D-2 Input Parameters for the Load-Bearing Models

Table Annex D-12: Statistics of the tensile strength $f_{t,0,b}$ and modulus of elasticity in tension $E_{t,0,b}$ parallel to the grain calculated from $1.5 \cdot 10^4$ virtually generated boards for each width and group, considering a test length of $l_b = 2.0$ m.

Width w_b [mm]		GI (T14)				GII (T24)				
		100	150	200	250	100	150	200	250	
$l_b = 2.0$ m	$f_{t,0,b}$	mean [MPa]	23.2	25.6	27.3	28.1	35.8	38.3	39.8	40.6
		COV [%]	33.5	31.4	30.2	29.6	29.2	27.4	27.1	26.3
		$\chi_{05,LN}$ [MPa]	12.5	14.3	15.6	16.3	21.4	23.6	24.7	25.6
	$E_{t,0,b}$	mean [MPa]	10,398	10,481	10,474	10,486	12,973	13,036	13,019	13,030
		COV [%]	15.1	15.3	15.0	15.1	17.2	17.1	17.3	17.0

Table Annex D-13: Statistics of the tensile strength $f_{t,0,b}$ and modulus of elasticity in tension $E_{t,0,b}$ parallel to the grain calculated from $1.5 \cdot 10^4$ virtually generated boards for the separation ratios $\eta_s = \{0.50; 0.33\}$ and each group, considering a board width of $w_b = 150$ mm and a test length of $l_b = 2.0$ m.

Separation ratio η_s [-]		GI (T14)		GII (T24)		
		0.50	0.33	0.50	0.33	
$w_b = 150$ mm	$f_{t,0,b}$	mean [MPa]	22.9	20.2	36.1	32.8
		COV [%]	36.8	42.2	31.7	35.3
		$\chi_{05,LN}$ [MPa]	11.5	9.2	20.6	17.4
	$E_{t,0,b}$	mean [GPa]	10.5	10.5	13.1	13.2
		COV [%]	17.1	18.7	19.8	21.5

Table Annex D-14: Statistics of the tensile strength $f_{t,FJ}$ parallel to the grain calculated from $1.5 \cdot 10^4$ virtually generated finger joints for each width and group.

Width w_b [mm]		GI (T14)				GII (T24)			
		100	150	200	250	100	150	200	250
$f_{t,FJ}$	mean [MPa]	29.3				36.0			
	COV [%]	19.4				20.7			
	$\chi_{05,LN}$ [MPa]	20.9				25.1			

Table Annex D-15: Statistics of the bending strength $f_{m,b}$ and modulus of elasticity in bending $E_{m,b}$ parallel to the grain calculated from 10^3 virtually tested boards for each width and group, considering a test length (with constant moment) of $l_b = 2.0$ m.

Width w_b [mm]		GI (T14)				GII (T24)				
		100	150	200	250	100	150	200	250	
$l_b = 2.0$ m	$f_{m,b}$	mean [MPa]	30.9	31.8	31.5	31.6	47.5	48.1	46.5	46.5
		COV [%]	32.8	30.9	29.9	29.4	28.9	27.5	25.7	25.7
		$\chi_{05,LN}$ [MPa]	16.6	18.0	18.1	17.8	28.5	29.5	29.5	29.5
	$E_{m,b}$	mean [MPa]	10,408	10,437	10,485	10,467	12,921	13,030	12,955	12,955
		COV [%]	16.2	15.2	15.6	15.4	17.9	17.3	17.2	17.2

D-3 Unidirectional Laminated Engineered Timber Products

D-3.1 Glulam – Flatwise Loaded Lamellas

Table Annex D-16: Statistics of the bending strength $f_{m,g}$ and modulus of elasticity in bending $E_{m,g}$ parallel to the grain calculated from 10^3 virtually tested glulam beam for different dimensions.

Dim. $w_g \times h_g$ [mm ²]		GI (T14)				GII (T24)			
		100×280	150×280	200×280	150×600	150×920	150×280	150×600	150×920
$f_{m,g}$	min [MPa]	16.0	14.8	19.6	15.7	17.1	26.1	24.2	24.1
	max [MPa]	50.5	55.4	57.0	39.7	33.5	77.9	54.5	47.9
	mean [MPa]	30.4	32.0	33.3	26.5	24.5	44.9	37.1	34.3
	COV [%]	19.5	18.7	18.5	13.0	11.0	17.4	12.6	10.0
	$\chi_{05,LN}$ [MPa]	21.5	23.0	24.1	21.2	20.2	33.3	29.9	28.9
	$\chi_{05,LN,ref}$ [MPa]	19.9	21.3	22.3	21.2	21.1	30.8	29.9	30.2
$E_{m,g}$	min [MPa]	8,218	8,387	8,371	9,021	9,366	10,277	10,978	11,618
	max [MPa]	14,055	14,379	13,282	12,028	12,275	17,677	15,421	15,143
	mean [MPa]	10,424	10,459	10,472	10,438	10,469	12,953	12,950	12,981
	COV [%]	7.4	7.0	7.3	4.6	3.6	7.9	5.3	4.1
	$\chi_{05,LN}$ [MPa]	9,214	9,302	9,264	9,661	9,858	11,360	11,850	12,129

D-3.2 Flex_GLT – type A – Edgewise Loaded Lamellas

Table Annex D-17: Statistics of the bending strength $f_{m,g}$ and modulus of elasticity in bending $E_{m,g}$ parallel to the grain calculated from 10^3 virtually tested flex_GLT type A beams from group GI (T14) – 1.

Width w_g [mm]		GI (T14)							
		90	120	120	120	120	120	150	150
Board Width w_b [mm]		100	100	150	100	150	100	200	100
Depth h_g [mm]		360	150	225	360	600	600	210	210
$E_{m,g}$	mean [MPa]	10,471	10,526	10,499	10,487	10,495	10,485	10,561	10,510
	COV [%]	4.8	5.6	5.4	4.3	3.9	3.3	5.4	4.5
$f_{m,g}$	mean [MPa]	23.9	29.7	27.0	23.7	22.2	21.6	29.3	27.4
	COV [%]	13.9	15.7	14.9	13.1	11.9	11.6	14.7	12.7
	$\chi_{05,LN}$ [MPa]	18.7	22.5	20.8	18.9	18.1	17.7	22.7	22.0
	$\chi_{05,LN,corr}^1$ [MPa]	17.4	18.6	18.1	17.6	18.1	17.7	19.6	19.0

¹ corr. to reference depth $h_{g,ref} = 600$ mm with $k_h = (h_g/h_{g,ref})^{0.14}$

Table Annex D-18: Statistics of the bending strength $f_{m,g}$ and modulus of elasticity in bending $E_{m,g}$ parallel to the grain calculated from 10^3 virtually tested flex_GLT type A beams from group GI (T14) – 2.

		GI (T14)							
Width w_g [mm]		150	150	150	150	240	240	270	600
Board Width w_b [mm]		200	150	100	100	100	150	100	100
Depth h_g [mm]		360	360	360	600	150	225	360	150
$E_{m,g}$	mean [MPa]	10,506	10,545	10,502	10,489	10,553	10,543	10,499	10,555
	COV [%]	4.6	4.2	3.9	3.1	3.9	3.9	2.6	2.4
$f_{m,g}$	mean [MPa]	24.8	24.5	24.1	21.5	29.2	26.8	23.8	28.6
	COV [%]	13.0	12.1	11.7	10.0	11.6	10.9	9.0	7.7
	$\chi_{05,LN}$ [MPa]	19.8	19.8	19.7	18.1	24.0	22.2	20.5	25.1
	$\chi_{05,LN,corr}^1$ [MPa]	18.4	18.5	18.3	18.1	19.7	19.3	19.0	20.7

¹ corr. to reference depth $h_{g,ref} = 600$ mm with $k_h = (h_g/h_{g,ref})^{0.14}$

Table Annex D-19: Statistics of the bending strength $f_{m,g}$ and modulus of elasticity in bending $E_{m,g}$ parallel to the grain calculated from 10^3 virtually tested flex_GLT type A beams from group GII (T24) – 1.

		GII (T24)					
Width w_g [mm]		90	120	120	120	120	120
Board Width w_b [mm]		100	100	150	100	150	100
Depth h_g [mm]		360	150	225	360	600	600
$E_{m,g}$	mean [MPa]	13,010	13,026	13,043	12,996	12,998	12,980
	COV [%]	5.3	6.2	6.0	4.9	4.5	4.0
$f_{m,g}$	mean [MPa]	34.2	41.8	37.9	33.5	31.5	31.1
	COV [%]	12.6	14.0	13.1	11.8	11.0	10.3
	$\chi_{05,LN}$ [MPa]	27.5	32.8	30.3	27.4	26.0	26.1
	$\chi_{05,LN,corr}^1$ [MPa]	25.6	27.0	26.4	25.5	26.0	26.1

¹ corr. to reference depth $h_{g,ref} = 600$ mm with $k_h = (h_g/h_{g,ref})^{0.14}$

Table Annex D-20: Statistics of the bending strength $f_{m,g}$ and modulus of elasticity in bending $E_{m,g}$ parallel to the grain calculated from 10^3 virtually tested flex_GLT type A beams from group GII (T24) – 2.

		GII (T24)					
Width w_g [mm]		150	150	150	240	240	600
Board Width w_b [mm]		100	100	100	100	150	100
Depth h_g [mm]		210	360	600	150	225	150
$E_{m,g}$	mean [MPa]	13,029	13,022	12,970	13,061	13,078	13,082
	COV [%]	5.4	4.3	3.4	4.4	4.3	2.9
$f_{m,g}$	mean [MPa]	38.2	33.8	31.3	40.5	37.2	39.7
	COV [%]	11.9	10.6	9.0	10.1	10.0	7.3
	$\chi_{05,LN}$ [MPa]	31.1	28.2	26.8	34.1	31.4	35.1
	$\chi_{05,LN,corr}^1$ [MPa]	26.9	26.2	26.8	28.1	27.4	28.9

¹ corr. to reference depth $h_{g,ref} = 600$ mm with $k_h = (h_g/h_{g,ref})^{0.14}$

Table Annex D-21: Test results of the tensile tests on boards, finger joints and bending tests on six series of flex_GLT type A from Sieder & Brandner [66].

	Boards	FJ	Flex_A-i	Flex_A-ii	Flex_A-iii	Flex_A-iv	Flex_A-v	Flex_A-vi
Width w_b w_g [mm]	100	100	210	150	90	150	270	150
Thickness depth t_b h_g [mm]	30	30	150	210	360	360	360	600
number of tests	53	70	7	7	7	7	7	7

		Boards	FJ	Flex_A-i	Flex_A-ii	Flex_A-iii	Flex_A-iv	Flex_A-v	Flex_A-vi
Width w_b w_g [mm]		100	100	210	150	90	150	270	150
Thickness depth t_b h_g [mm]		30	30	150	210	360	360	360	600
u	mean [%]	8.5	11.3	7.6	8.3	7.5	7.3	7.6	7.6
	COV [%]	8.4	4.2	2.9	3.3	4.3	2.2	2.2	3.9
Q_{12}	mean [kg/m ³]	451	435	449	471	438	468	461	464
	COV [%]	10.5	8.1	2.9	2.6	1.1	1.7	1.8	1.5
	$\chi_{05,LN}$ [kg/m ³]	378	380	428	451	430	455	447	452
$E_{t,0,b}$ $E_{m,g}$	mean [MPa]	13,129	–	12,123	13,302	12,595	13,365	13,705	13,222
	COV [%]	20.7	–	7.1	6.6	5.8	5.5	5.1	6.6
$f_{t,0,b}$ $f_{m,FJ} / f_{m,g}$	mean [MPa]	31.4	43.2	44.1	45.7	36.7	42.9	40.2	37.5
	COV [%]	43.2	11.6	8.8	23.2	8.5	9.9	6.8	16.6
	$\chi_{05,LN}$ [MPa]	14.9	35.4	38.0	30.2	31.8	36.4	35.9	28.2
	$\chi_{05,LN,corr}$ [MPa]	16.0 ¹	–	31.3 ²	26.1 ²	29.6 ²	33.9 ²	33.4 ²	28.2 ²

¹ corr. to reference length $l_{b,ref} = 2$ m with $k_{l,05} = (l_b/l_{b,ref})^{0.15}$

² corr. to reference depth $h_{g,ref} = 600$ mm with $k_h = (h_g/h_{g,ref})^{0.14}$

D-3.3 Flex_GLT – type B – Flatwise Loaded Lamellas

Table Annex D-22: Statistics of the bending strength $f_{m,g}$ and modulus of elasticity in bending $E_{m,g}$ parallel to the grain calculated from 10^3 virtually tested flex_GLT type B beams from group GI (T14).

		GI (T14)							
Width w_g [mm]		100	150	150	150	210	225	250	500
Board Width w_b [mm]		100	100	100	100	100	150	100	100
Depth h_g [mm]		360	210	360	600	150	210	360	360
$E_{m,g}$	mean [MPa]	10,506	10,509	10,514	10,495	10,460	10,484	10,496	10,500
	COV [%]	4.8	5.3	4.0	3.0	5.7	5.4	3.3	2.4
$f_{m,g}$	mean [MPa]	28.7	32.7	28.9	25.6	35.8	33.9	28.6	28.1
	COV [%]	14.2	14.4	11.7	9.4	15.3	14.3	10.6	8.2
	$\chi_{05,LN}$ [MPa]	22.5	25.5	23.6	21.8	27.4	26.5	23.8	24.4
	$\chi_{05,LN,corr}^1$ [MPa]	20.9	22.0	22.0	21.8	22.6	22.9	22.2	22.8

¹ corr. to reference depth $h_{g,ref} = 600$ mm with $k_h = (h_g/h_{g,ref})^{0.14}$

Table Annex D-23: Statistics of the bending strength $f_{m,g}$ and modulus of elasticity in bending $E_{m,g}$ parallel to the grain calculated from 10^3 virtually tested flex_GLT type B beams from group GII (T24).

		GII (T24)					
Width w_g [mm]		100	150	150	150	210	225
Board Width w_b [mm]		100	100	100	100	100	150
Depth h_g [mm]		360	210	360	600	150	210
$E_{m,g}$	mean [MPa]	13,040	12,972	13,008	13,000	13,004	12,973
	COV [%]	5.5	6.0	4.7	3.4	6.3	6.2
$f_{m,g}$	mean [MPa]	39.6	45.1	40.0	35.7	50.1	47.3
	COV [%]	13.5	14.3	11.6	9.7	14.0	13.3
	$x_{05,LN}$ [MPa]	31.4	35.3	32.8	30.2	39.5	37.7
	$x_{05,LN,corr}^1$ [MPa]	29.2	30.5	30.5	30.2	32.5	32.5

¹ corr. to reference depth $h_{g,ref} = 600$ mm with $k_h = (h_g/h_{g,ref})^{0.14}$

Table Annex D-24: Test results of the tensile test on boards, finger joints and bending test on two series of flex_GLT type B from Sieder & Brandner [66].

		Boards	FJ	Flex_B-i	Flex_B-ii
Width w_b w_g [mm]		100	100	210	150
Thickness depth t_b h_g [mm]		30	30	150	360
number of tests		53	70	7	7
u	mean [%]	8.5	11.3	8.3	7.4
	COV [%]	8.4	4.2	2.5	2.9
Q_{12}	mean [kg/m ³]	451	435	472	455
	COV [%]	10.5	8.1	3.5	2.3
	$x_{05,LN}$ [kg/m ³]	378	380	446	439
$E_{t,0,b}$ $E_{m,g}$	mean [MPa]	13,129	–	13,617	13,761
	COV [%]	20.7	–	4.7	5.4
$f_{t,0,b}$ $f_{m,FJ} / f_{m,g}$	mean [MPa]	31.4	43.2	45.0	40.6
	COV [%]	43.2	11.6	17.3	16.7
	$x_{05,LN}$ [MPa]	14.9	35.4	33.9	30.7
	$x_{05,LN,corr}$ [MPa]	16.0 ¹	–	27.9 ²	28.5 ²

¹corr. to reference length $l_{b,ref} = 2$ m with $k_{l,05} = (l_b/l_{b,ref})^{0.15}$

²corr. to reference depth $h_{g,ref} = 600$ mm with $k_h = (h_g/h_{g,ref})^{0.14}$

D-4 Orthogonally Engineered Timber Products

D-4.1 Flex_CLT – beams

Table Annex D-25: Statistics of the bending strength $f_{m,g}$ and modulus of elasticity in bending $E_{m,g}$ parallel to the grain calculated from 10^3 virtually tested flex_CLT beams from group GI (T14) – 1.

		GI (T14)						
Width w_g [mm]		090	090	090	090	090	090	090
Board Width w_b [mm]		100	150	200	200	150	100	200
Depth h_g [mm]		150	225	300	360	360	360	600
$E_{m,g}$	mean [MPa]	10,641	10,644	10,613	10,637	10,608	10,636	10,630
	COV [%]	7.9	7.1	7.2	6.9	6.6	5.7	5.9
$f_{m,g}$	mean [MPa]	30.8	28.8	27.4	26.5	26.3	26.1	24.6
	COV [%]	22.1	19.5	17.1	17.1	16.0	15.1	13.9
	$\chi_{05,LN}$ [MPa]	20.6	20.2	20.3	19.6	19.9	20.1	19.3
	$\chi_{05,LN,corr}^1$ [MPa]	19.8	19.6	19.8	19.3	19.6	19.8	19.3

¹ corr. to reference depth $h_{g,ref} = 600$ mm with $k_h = (h_g/h_{g,ref})^{0.03}$

Table Annex D-26: Statistics of the bending strength $f_{m,g}$ and modulus of elasticity in bending $E_{m,g}$ parallel to the grain calculated from 10^3 virtually tested flex_CLT beams from group GI (T14) – 2.

		GI (T14)					
Width w_g [mm]		090	090	150	150	150	270
Board Width w_b [mm]		150	100	100	100	100	100
Depth h_g [mm]		600	600	150	360	600	360
$E_{m,g}$	mean [MPa]	10,612	10,618	10,714	10,696	10,670	10,745
	COV [%]	5.3	4.8	6.2	4.8	3.8	3.6
$f_{m,g}$	mean [MPa]	24.6	24.5	31.3	27.1	25.6	27.6
	COV [%]	13.1	11.2	17.3	11.5	9.2	9.3
	$\chi_{05,LN}$ [MPa]	19.6	20.2	22.9	22.2	21.8	23.6
	$\chi_{05,LN,corr}^1$ [MPa]	19.6	20.2	22.0	21.9	21.8	23.2

¹ corr. to reference depth $h_{g,ref} = 600$ mm with $k_h = (h_g/h_{g,ref})^{0.03}$

Table Annex D-27: Statistics of the bending strength $f_{m,g}$ and modulus of elasticity in bending $E_{m,g}$ parallel to the grain calculated from 10^3 virtually tested flex_CLT beams from group GII (T24).

		GII (T24)								
Width w_g [mm]		090	090	090	090	150	150	150	270	090
Board Width w_b [mm]		100	150	100	100	100	100	100	100	100
Depth h_g [mm]		150	225	360	600	150	360	600	360	150
$E_{m,g}$	mean [MPa]	13,195	13,191	13,136	13,164	13,266	13,191	13,240	13,268	13,195
	COV [%]	8.8	8.5	6.6	5.2	7.0	5.3	4.5	4.2	8.8
$f_{m,g}$	mean [MPa]	42.3	41.5	36.2	33.8	44.4	37.2	34.6	37.6	42.3
	COV [%]	19.3	17.9	12.8	10.1	15.5	10.7	9.2	8.6	19.3
	$\chi_{05,LN}$ [MPa]	30.1	30.6	29.1	28.5	34.0	31.0	29.5	32.5	30.1
	$\chi_{05,LN,corr}^1$ [MPa]	28.9	29.8	28.6	28.5	32.6	30.5	29.5	32.0	28.9

¹ corr. to reference depth $h_{g,ref} = 600$ mm with $k_h = (h_g/h_{g,ref})^{0.03}$

Table Annex D-28: Test results of the tensile test on boards, finger joints and bending test on six series of flex_CLT beams from [Sieder & Brandner \[66\]](#).

		Boards	FJ	Flex_CLT beam-i	Flex_CLT beam-ii
Width w_b w_g [mm]		100	100	150	150
Thickness depth t_b h_g [mm]		30	30	210	360
number of tests		53	70	7	7
u	mean [%]	8.5	11.3	9.2	8.0
	COV [%]	8.4	4.2	2.4	2.5
Q_{12}	mean [kg/m ³]	451	435	462	466
	COV [%]	10.5	8.1	1.5	1.5
	$x_{05,LN}$ [kg/m ³]	378	380	451	455
$E_{t,0,b}$ $E_{m,g}$	mean [MPa]	13,129	–	12,420	14,080
	COV [%]	20.7	–	5.9	8.2
$f_{t,0,b}$ $f_{m,FJ} / f_{m,g}$	mean [MPa]	31.4	43.2	42.5	48.7
	COV [%]	43.2	11.6	13.0	8.7
	$x_{05,LN}$ [MPa]	14.9	35.4	34.0	42.3
	$x_{05,LN,corr}$ [MPa]	16.0 ¹	–	33.0 ²	41.6 ²

¹corr. to reference length $l_{b,ref} = 2$ m with $k_{l,05} = (l_b/l_{b,ref})^{0.15}$

²corr. to reference depth $h_{g,ref} = 600$ mm with $k_h = (h_g/h_{g,ref})^{0.03}$

D-4.2 Flex_CLT – slabs

Table Annex D-29: Statistics of the bending strength $f_{m,g}$ and modulus of elasticity in bending $E_{m,g}$ parallel to the grain calculated from 10^3 virtually tested flex_CLT slabs from group GI (T14) – 1.

		GI (T14)					
Depth h_g [mm]		090	090	150	150	150	150
Width w_g [mm]		600	1200	200	200	200	600
Board with w_b [mm]		150	150	100	150	200	100
# of Layers m_{lay} [-]		3	3	5	5	5	5
$E_{m,g}$	mean [MPa]	10,241	10,253	10,421	10,570	10,660	10,425
	COV [%]	8.4	8.1	6.6	7.9	8.1	4.0
$f_{m,g}$	mean [MPa]	41.6	40.2	33.1	36.5	38.6	32.1
	COV [%]	17.0	12.4	21.0	23.5	23.4	12.1
	$\chi_{05,LN}$ [MPa]	30.9	32.3	22.9	23.7	25.4	26.0
	$\chi_{05,LN,corr}^1$ [MPa]	28.8	30.1	22.9	23.7	25.4	26.0

¹ corr. to reference depth $h_{g,ref} = 150$ mm with $k_{h_i} = (h_g/h_{g,ref})^{0.14}$
Table Annex D-30: Statistics of the bending strength $f_{m,g}$ and modulus of elasticity in bending $E_{m,g}$ parallel to the grain calculated from 10^3 virtually tested flex_CLT slabs from group GI (T14) – 2.

		GI (T14)					
Depth h_g [mm]		150	150	150	200	210	210
Width w_g [mm]		1200	1200	1200	600	200	1200
Board with w_b [mm]		100	150	200	150	150	150
# of Layers m_{lay} [-]		5	5	5	5	7	7
$E_{m,g}$	mean [MPa]	10,448	10,569	10,681	10,498	10,591	10,646
	COV [%]	3.0	3.6	3.8	4.8	7.1	3.4
$f_{m,g}$	mean [MPa]	31.4	34.6	36.5	33.3	35.2	34.1
	COV [%]	9.4	10.1	10.8	13.4	18.6	8.5
	$\chi_{05,LN}$ [MPa]	26.8	29.1	30.3	26.3	25.2	29.5
	$\chi_{05,LN,corr}^1$ [MPa]	26.8	29.1	30.3	27.4	26.4	30.9

¹ corr. to reference depth $h_{g,ref} = 150$ mm with $k_{h_i} = (h_g/h_{g,ref})^{0.14}$
Table Annex D-31: Statistics of the bending strength $f_{m,g}$ and modulus of elasticity in bending $E_{m,g}$ parallel to the grain calculated from 10^3 virtually tested flex_CLT slabs from group GII (T24).

		GII (T24)					
Depth h_g [mm]		150	090	150	150	150	210
Width w_g [mm]		200	600	600	600	600	600
Board with w_b [mm]		150	150	100	150	200	150
# of Layers m_{lay} [-]		5	3	5	5	5	7
$E_{m,g}$	mean [MPa]	12,857	12,350	12,831	12,858	12,972	13,051
	COV [%]	8.3	8.9	4.6	5.4	5.7	5.1
$f_{m,g}$	mean [MPa]	51.5	58.8	44.6	48.7	51.7	46.6
	COV [%]	20.3	15.1	10.8	13.2	14.1	11.0
	$\chi_{05,LN}$ [MPa]	36.4	45.3	37.1	38.9	40.7	38.7
	$\chi_{05,LN,corr}^1$ [MPa]	36.4	42.2	37.1	38.9	40.7	40.5

¹ corr. to reference depth $h_{g,ref} = 150$ mm with $k_{h_i} = (h_g/h_{g,ref})^{0.14}$

Monographic Series TU Graz
Timber Engineering & Technology

- Vol. 1** Gerhard Schickhofer
**Starrer und nachgiebiger Verbund bei geschichteten,
flächenhaften Holzstrukturen**
2013
ISBN 978-3-85125-262-0
- Vol. 2** Reinhard Brandner
**Stochastic System Actions and Effects in
Engineered Timber Products and Structures**
2013
ISBN 978-3-85125-263-7
- Vol. 3** Ulrich Hübner
**Mechanische Kenngrößen von Buchen-, Eschen- und
Robinienholz für lastabtragende Bauteile**
2014
ISBN 978-3-85125-314-6
- Vol. 4** Andreas Meisel
**Historische Dachwerke - Beurteilung,
realitätsnahe statische Analyse und Instandsetzung**
2015
ISBN 978-3-85125-433-4

Monographic Series TU Graz
Timber Engineering & Technology

- Vol. 5** Andreas Ringhofer
**Axially Loaded Self-Tapping Screws in Solid Timber
and Laminated Timber Products**
2017
ISBN 978-3-85125-555-3
- Vol. 6** Georg Flatscher
**Evaluation and approximation of timber connection
properties for displacement-based analysis of
CLT wall systems**
2017
ISBN 978-3-85125-557-7
- Vol. 7** Harald Krenn
**Die Stahlblech-Holz-Laschenverbindung mit
schrägen Schrauben**
2018
ISBN 978-3-85125-622-2
- Vol. 8** Raimund Sieder
**Influence of Lengthwise Split Boards on the
Mechanical Properties of Engineered Timber Products**
2026
ISBN 978-3-99161-063-2

Influence of Lengthwise Split Boards on the Mechanical Properties of Engineered Timber Products

The bending strength and elastic properties of engineered timber products such as glulam (GLT) and cross laminated timber (CLT) are commonly described via load-bearing models based on the tensile properties parallel to the grain of boards and finger joints. These models assume that strength-graded boards remain unsplit in the final product. In practice, however, products can be lengthwise split (e.g. resawn glulam) or may include a significant share of split lamellas, as in CLT beams or slabs. After splitting, the assigned strength class no longer applies. Lengthwise split lamellas also occur in the novel products flex_GLT and flex_CLT. The first part covers the develops a probabilistic board model capable of describing knot distributions and tensile properties not only for full-section but also for lengthwise split boards. Combined with a newly developed stochastic-numerical beam model, the load-bearing behaviour of beams containing such split lamellas can be calculated. The model covers products with uni- or orthogonally oriented lamellas and is validated by tests. System and size effects as well as the influence of split lamellas are analysed. Finally, load bearing models and minimal geometric requirements for the newly developed flex_GLT-CLT products are presented.

MONOGRAPHIC SERIES TU GRAZ
TIMBER ENGINEERING & TECHNOLOGY

Verlag der Technischen Universität Graz
www.tugraz-verlag.at

ISBN 978-3-99161-063-2
ISSN 1990-357X

